

AD-A220 845

FORCE IDENTIFICATION FROM STRUCTURAL RESPONSE

DTIC
ELECTE
APR 24 1990
S D
cc D

BY

TIMOTHY JOHN KREITINGER

DISTRIBUTION STATEMENT A

Approved for public release
Distribution Unlimited

ABSTRACT OF DISSERTATION

Submitted in Partial Fulfillment of the
Requirements for the Degree of

Doctor of Philosophy in Engineering

The University of New Mexico
Albuquerque, New Mexico

December, 1989

04 23 066

REPORT DOCUMENTATION PAGE

Form Approved
OMB No. 0704-0188


1a. REPORT SECURITY CLASSIFICATION UNCLASSIFIED			1b. RESTRICTIVE MARKINGS NONE		
2a. SECURITY CLASSIFICATION AUTHORITY			3. DISTRIBUTION/AVAILABILITY OF REPORT APPROVED FOR PUBLIC RELEASE; DISTRIBUTION UNLIMITED.		
2b. DECLASSIFICATION/DOWNGRADING SCHEDULE					
4. PERFORMING ORGANIZATION REPORT NUMBER(S)			5. MONITORING ORGANIZATION REPORT NUMBER(S) AFIT/CI/CIA-90-009D		
6a. NAME OF PERFORMING ORGANIZATION AFIT STUDENT AT Univ of New Mexico		6b. OFFICE SYMBOL (If applicable)	7a. NAME OF MONITORING ORGANIZATION AFIT/CIA		
6c. ADDRESS (City, State, and ZIP Code)			7b. ADDRESS (City, State, and ZIP Code) Wright-Patterson AFB OH 45433-6583		
8a. NAME OF FUNDING/SPONSORING ORGANIZATION		8b. OFFICE SYMBOL (If applicable)	9. PROCUREMENT INSTRUMENT IDENTIFICATION NUMBER		
8c. ADDRESS (City, State, and ZIP Code)			10. SOURCE OF FUNDING NUMBERS		
			PROGRAM ELEMENT NO.	PROJECT NO.	TASK NO.
			WORK UNIT ACCESSION NO.		
11. TITLE (Include Security Classification) (UNCLASSIFIED) Force Identification from Structural Response					
12. PERSONAL AUTHOR(S) Timothy John Kreithinger					
13a. TYPE OF REPORT THESIS/DISSERTATION		13b. TIME COVERED FROM _____ TO _____		14. DATE OF REPORT (Year, Month, Day) 1990	
				15. PAGE COUNT 153	
16. SUPPLEMENTARY NOTATION APPROVED FOR PUBLIC RELEASE IAW AFR 190-1 ERNEST A. HAYGOOD, 1st Lt, USAF Executive Officer, Civilian Institution Programs					
17. COSATI CODES			18. SUBJECT TERMS (Continue on reverse if necessary and identify by block number)		
FIELD	GROUP	SUB-GROUP			
19. ABSTRACT (Continue on reverse if necessary and identify by block number)					
20. DISTRIBUTION/AVAILABILITY OF ABSTRACT <input checked="" type="checkbox"/> UNCLASSIFIED/UNLIMITED <input type="checkbox"/> SAME AS RPT. <input type="checkbox"/> DTIC USERS					
21. ABSTRACT SECURITY CLASSIFICATION UNCLASSIFIED					
22a. NAME OF RESPONSIBLE INDIVIDUAL ERNEST A. HAYGOOD, 1st Lt, USAF			22b. TELEPHONE (Include Area Code) (513) 255-2259		22c. OFFICE SYMBOL AFIT/CI


Timothy John Kreitinger
Candidate

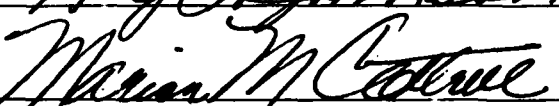
Civil Engineering
Department

This dissertation is approved, and it is acceptable in quality
and form for publication on microfilm:

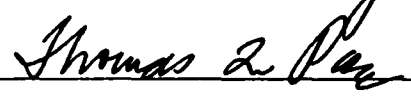
Approved by the Dissertation Committee:

 , Chairperson











Accepted:


Asst. Dean, Graduate School

December 18, 1989

Date

*To Diane JaeSuk, my wife,
Gloria, Angela, and Kimberly, my daughters
for their love, patience, and understanding.*

ACKNOWLEDGMENTS

The work reported herein was conducted at the Civil Engineering Structural Laboratory, University of New Mexico, Albuquerque, New Mexico. It represents a partial completion of requirements for the degree of Doctor of Philosophy in Civil Engineering.

We may all learn through our senses by just being alive; but, the environment bestowed on me during the past few years was my good fortune. I want to express many thanks to colleagues, technicians, and professors at the University of New Mexico. In particular, I want to thank Professor Ming Wang, who enthusiastically advised me and exhibited unlimited amounts of confidence and patience in my educational development. I wish to thank Dr. Thomas Paez, Dr. Tom Priddy and Dan Gregory of Sandia National Laboratories, Albuquerque, New Mexico, for their valuable discussions during this research. Also gratefully acknowledged is the participation of the other committee members: Prof. Marion Cottrell and Prof. Roy Johnson, Department of Civil Engineering; Prof. Dick Metzler, Department of Mathematics, all from the UNM; and Dr. Raymond Bennett, of the Weapons Laboratory, Albuquerque, New Mexico. Also, thanks to Mr. Garfield and Mr. Bushfield, Technicians at the UNM, for wide tolerances of patience, undivided attention, and time.

Finally, I acknowledge the United States Air Force for sponsoring my educational endeavor and Sandia National Laboratories for partial funding of this research.

FORCE IDENTIFICATION FROM STRUCTURE RESPONSE

Timothy J. Kreitinger

B.S., Civil Engineering, North Dakota State University, 1980

M.S., Civil Engineering, University of New Mexico, 1986

Ph.D., Civil Engineering, University of New Mexico, 1989

Force identification is a type of system identification procedure which determines applied forces from system response measurements. To identify the force, one can consider the system model and parameters which are known, and then use the response that is measured to determine the unknown forces. In this research, a more direct way to identify the unknown force without knowing the model of the system is proposed. However, to postulate the system model and its parameters is difficult to justify, especially when considering a nonlinear system where the model poses a great deal of unknowns or inherent characteristics of the mathematical problem. The approach called the sum of weighted acceleration technique, SWAT, is a method that can predict input forces with measured linear and nonlinear structural responses. SWAT uses measured accelerations multiplied by effective or optimal weights to estimate the input force. The effective weights are the coefficients of an equivalent mass at each acceleration location. Once the effective weights are determined, the unknown input forces can be predicted by using a mathematical formulation, which is the goal of force identification. The approach of SWAT was validated in the time and frequency domain. For practical applications, the approach of SWAT was

extended to a finite element approach for further validation of larger elastic structures. The results show that the force calculated from SWAT accurately predicts the force which was inputted to the structure.

Presented by: [illegible]



Accession For	
NTIS GRA&I	<input checked="" type="checkbox"/>
DTIC TAB	<input type="checkbox"/>
Unannounced	<input type="checkbox"/>
Justification	
By	
Distribution /	
Availability Codes	
Dist	Avail and/or Special
A-1	

TABLE OF CONTENTS

	Page
ACKNOWLEDGMENTS	iv
ABSTRACT	v
LIST OF FIGURES	x
LIST OF TABLES	xvii
NOMENCLATURE	xviii
CHAPTER 1. INTRODUCTION	1
1.0 Introduction	1
1.1 Literature Review	3
1.1.1 System Identification Overview	4
1.1.2 Force Identification Overview	9
1.2 Objective	14
CHAPTER 2. FORCE IDENTIFICATION FOR LUMPED MASS SYSTEMS	15
2.0 Model	15
2.1 Time Domain Approach	18
2.2 Frequency Domain Approach	24
2.3 Experimental Setup	29
2.4 Results	31
CHAPTER 3. FORCE IDENTIFICATION OF CONTINUOUS MASS SYSTEMS	35
3.0 Model	35
3.1 Experimental Setup	35
3.2 Results	37
CHAPTER 4. FORCE IDENTIFICATION OF NONLINEAR SYSTEMS	46
4.0 Nonlinear Model	46
4.1 Force Mapping	46
4.2 Displacement and Velocity for Acceleration Data	55

4.3	Nonlinear Test Setup	57
4.4	Nonlinear Test Results	58
CHAPTER 5.	ANALYTICAL APPROACHES	71
5.0	Introduction	71
5.1	An Analytical Method Based on Mode Shapes	72
5.2	Weighted Residuals and the Finite Element Method	78
5.3	Application of the Finite Element Method to Beams	84
5.4	Experimental Results	86
CHAPTER 6.	PROCEDURES AND INSTRUMENTATION FOR DYNAMIC TESTING	95
6.0	Introduction	95
6.1	Description of Equipment	95
6.2	Methodology and Testing Procedures	97
6.3	Simulation of Digital Random Signal	101
6.4	Experimental Tests	109
CHAPTER 7.	SUMMARY AND CONCLUSIONS	114
7.0	Summary	114
7.1	Conclusions	115
APPENDICES		
APPENDIX 1.	DATA RECORDS FOR LUMPED MASS SYSTEMS	117
A1.0	Introduction	117
A1.1	Symmetric Records	117
A1.2	Antisymmetric Records	127
APPENDIX 2.	RECURSIVE LEAST SQUARE ALGORITHM	143
REFERENCES	146
VITA	153

LIST OF FIGURES

Figure		Page
2.1	Free-Free Lumped Mass System	16
2.2	Frequency Domain Records of Acceleration and Force	26
2.3	Symmetric Lump Mass Test Setup	28
2.4	Antisymmetric Lump Mass Test Setup	28
2.5	Comparison of Forces for Test Run 2 (Symmetric Test Specimen)	30
2.6	Comparison of Forces for Test Run 4 (Symmetric Test Specimen)	30
2.7	Comparison of Forces for Test Run 7 (Symmetric Test Specimen)	31
2.8	Comparison of Forces for Test Run 2 (Antisymmetric Test Specimen)	32
2.9	Comparison of Forces for Test Run 4 (Antisymmetric Test Specimen)	32
2.10	Comparison of Forces for Test Run 7 (Antisymmetric Test Specimen)	33
3.1	Free-Free Beam Configuration	36
3.2	Acceleration #1 Record for Continuous Beam	38
3.3	Modulus of Acceleration #1 Record for Continuous Beam	38
3.4	Acceleration #2 Record for Continuous Beam	39
3.5	Modulus of Acceleration #2 Record for Continuous Beam	39
3.6	Acceleration #3 Record for Continuous Beam	40
3.7	Modulus of Acceleration #3 Record for Continuous Beam	40
3.8	Acceleration #4 Record for Continuous Beam	41

3.9	Modulus of Acceleration #4 Record for Continuous Beam	41
3.10	Acceleration #5 Record for Continuous Beam	42
3.11	Modulus of Acceleration #5 Record for Continuous Beam	42
3.12	Force Record for Continuous Beam	43
3.13	Modulus of Force Record for Continuous Beam	43
3.14	Random Excitation Loading Comparison for a Continuous Beam. (Time Domain Approach.)	44
3.15	Random Excitation Loading Comparison for a Continuous Beam. (Frequency Domain Approach.)	44
3.16	Impact Loading Force Comparison for a Continuous Beam	45
4.1	Force-Map for a Linear System (K and D are Constants)	47
4.2	Force-Map for Cubic Stiffness	49
4.3	Force-Map with Cubic Damping	50
4.4	Force-Map with Both Cubic Damping and Stiffness	51
4.5	Force Mapping Setup for Linear System	52
4.6	Modulating Sinusoid Wave, Frequency is 30 Hz	52
4.7	F_r versus Velocity and Displacement	53
4.8	Nonlinear Setup	54
4.9	F_r versus Velocity and Displacement for the Nonlinear Setup	54
4.10	Test Specimen Number 1	60
4.11	Test Specimen Number 2	61
4.12	Test Specimen Number 3	61
4.13	Acceleration at the End, $a_1(t)$, for Test Specimen #1, Run #1	62
4.14	Modulus of Acceleration at the End, $a_1(t)$, for Test Specimen #1, run #1	62

4.15	Acceleration at the Center, $a_2(t)$, for Test Specimen #1, Run #1	63
4.16	Modulus of Acceleration at the Center, $a_2(t)$, for Test Specimen #1, run #1	63
4.17	Measured Force for Test Specimen #1, Run #1	64
4.18	Modulus of Force for Test Specimen #1, Run #1	64
4.19	Predicted and Measured Force for Test Specimen #1, Run #2.	65
4.20	Acceleration at the End, $a_1(t)$, for Test Specimen #2, Run #1	65
4.21	Modulus of Acceleration at the End, $a_1(t)$, for Test Specimen #2, run #1	66
4.22	Acceleration at the Joint, $a_2(t)$, for Test Specimen #2, Run #1	66
4.23	Modulus of Acceleration at the Joint, $a_2(t)$, for Test Specimen #2, run #1	67
4.24	Acceleration at the Center, $a_3(t)$, for Test Specimen #2, Run #1	67
4.25	Modulus of Acceleration at the Center, $a_3(t)$, for Test Specimen #2, run #1	68
4.26	Measured Force for Test Specimen #2, Run #1	68
4.27	Modulus of Force for Test Specimen #2, Run #1	69
4.28	Predicted and Measured Force for Test Specimen #2, Run #2.	69
4.29	Predicted and Measured Force for Test Specimen #3	70
5.1	Nodal Basis Functions for a Bar	85
5.2	Case 1 - Free-Free Beam Configuration of Accelerometers (A Strategic Location)	88
5.3	Case 1 - Free-Free Beam. Predicted Force Calculated from the Effective Weights Determined from the Mode Shape Approach	89

5.4	Case 1 - Free-Free Beam. Predicted Force Calculated from the Effective Weights Determined from the Mode Shape Approach	89
5.5	Case 1 - Free-Free Beam. Predicted Force Calculated from the Effective Weights Determined from the Finite Element Approach.	90
5.6	Case 1 - Free-Free Beam. Predicted Force Calculated from the Effective Weights Determined from the Finite Element Approach	90
5.7	Case 2 - Free-Free Beam Configuration of Accelerometers (A Routine Location)	92
5.8	Case 2 - Free-Free Beam. Predicted Force Calculated from the Effective Weights Determined from the Mode Shape Approach	92
5.9	Case 2 - Free-Free Beam. Predicted Force Calculated from the Effective Weights Determined from the Finite Element Approach	93
5.10	Case 3 - Plate Configuration	93
5.11	Case 3 - Predicted and Measured Forces for the Plate	94
6.1	Vibration Systems with Microcomputer	96
6.2	Step 1 to Determine $H(w)$	98
6.3	Step 2, Determine Input Signal for a Desired Response	100
6.4	Ensemble of Sample Function for a Random Process	103
6.5	Typical Narrow-Banded Spectra Density Curve	104
6.6	Narrow-Band Random Vibration Signal	104
6.7	Typical Wide-Banded Spectral Density Curve	105
6.8	Wide-Band Random Vibration Signal	105
6.9	Sine Waveform Spectral Density Curve	106
6.10	Spectral Density Notation Used in Equation (6.19)	110
6.11	Force Identification Specimen	111
6.12	Spectral Density Curve with Bandwidth of 5 to 30 Hz	111
6.13	Desired and Measured Response	112

6.14	Modulus of $H^1(\omega)$ for Force Identification Setup . . .	112
6.15	Input Signal for Desired Signal of Figure 6.12 . . .	113
6.16	Modulus of Acceleration for Mass 2	113
A1.1	Acceleration Record of Mass 1 for Symmetric Test Specimen of Test Run 1.	118
A1.2	Modulus of Acceleration Record of Mass 1 for Symmetric Test Specimen of Test Run 1	118
A1.3	Acceleration Record of Mass 2 for Symmetric Test Specimen of Test Run 1.	119
A1.4	Modulus of Acceleration Record of Mass 2 for Symmetric Test Specimen of Test Run 1	119
A1.5	Force Record for Symmetric Test Specimen of Test Run 1	120
A1.6	Modulus of Force Record for Symmetric Test Specimen of Test Run 1	120
A1.7	Acceleration Record of Mass 1 for Symmetric Test Specimen of Test Run 3.	121
A1.8	Modulus of Acceleration Record of Mass 1 for Symmetric Test Specimen of Test Run 3	121
A1.9	Acceleration Record of Mass 2 for Symmetric Test Specimen of Test Run 3.	122
A1.10	Modulus of Acceleration Record of Mass 2 for Symmetric Test Specimen of Test Run 3	122
A1.11	Force Record for Symmetric Test Specimen of Test Run 3	123
A1.12	Modulus of Force Record for Symmetric Test Specimen of Test Run 3	123
A1.13	Acceleration Record of Mass 1 for Symmetric Test Specimen of Test Run 5.	124
A1.14	Modulus of Acceleration Record of Mass 1 for Symmetric Test Specimen of Test Run 5	124
A1.15	Acceleration Record of Mass 2 for Symmetric Test Specimen of Test Run 5.	125
A1.16	Modulus of Acceleration Record of Mass 2 for Symmetric Test Specimen of Test Run 5	125

A1.17	Force Record for Symmetric Test Specimen of Test Run 5	126
A1.18	Modulus of Force Record for Symmetric Test Specimen of Test Run 5	126
A1.19	Acceleration Record of Mass 1 for Antisymmetric Test Specimen of Test Run 1	128
A1.20	Modulus of Acceleration Record of Mass 1 for Antisymmetric Test Specimen of Test Run 1	128
A1.21	Acceleration Record of Mass 2 for Antisymmetric Test Specimen of Test Run 1	129
A1.22	Modulus of Acceleration Record of Mass 2 for Antisymmetric Test Specimen of Test Run 1	129
A1.23	Acceleration Record of Mass 3 for Antisymmetric Test Specimen of Test Run 1	130
A1.24	Modulus of Acceleration Record of Mass 3 for Antisymmetric Test Specimen of Test Run 1	130
A1.25	Acceleration Record of Mass 4 for Antisymmetric Test Specimen of Test Run 1	131
A1.26	Modulus of Acceleration Record of Mass 4 for Antisymmetric Test Specimen of Test Run 1	131
A1.27	Force Record for Antisymmetric Test Specimen of Test Run 1	132
A1.28	Modulus of Force Record for Antisymmetric Test Specimen of Test Run 1	132
A1.29	Acceleration Record of Mass 1 for Antisymmetric Test Specimen of Test Run 3	133
A1.30	Modulus of Acceleration Record of Mass 1 for Antisymmetric Test Specimen of Test Run 3	133
A1.31	Acceleration Record of Mass 2 for Antisymmetric Test Specimen of Test Run 3	134
A1.32	Modulus of Acceleration Record of Mass 2 for Antisymmetric Test Specimen of Test Run 3	134
A1.33	Acceleration Record of Mass 3 for Antisymmetric Test Specimen of Test Run 3	135
A1.34	Modulus of Acceleration Record of Mass 3 for Antisymmetric Test Specimen of Test Run 3	135

A1.35	Acceleration Record of Mass 4 for Antisymmetric Test Specimen of Test Run 3	136
A1.36	Modulus of Acceleration Record of Mass 4 for Antisymmetric Test Specimen of Test Run 3 . . .	136
A1.37	Force Record for Antisymmetric Test Specimen of Test Run 3	137
A1.38	Modulus of Force Record for Antisymmetric Test Specimen of Test Run 3	137
A1.39	Acceleration Record of Mass 1 for Antisymmetric Test Specimen of Test Run 5	138
A1.40	Modulus of Acceleration Record of Mass 1 for Antisymmetric Test Specimen of Test Run 5 . . .	138
A1.41	Acceleration Record of Mass 2 for Antisymmetric Test Specimen of Test Run 5	139
A1.42	Modulus of Acceleration Record of Mass 2 for Antisymmetric Test Specimen of Test Run 5 . . .	139
A1.43	Acceleration Record of Mass 3 for Antisymmetric Test Specimen of Test Run 5	140
A1.44	Modulus of Acceleration Record of Mass 3 for Antisymmetric Test Specimen of Test Run 5 . . .	140
A1.45	Acceleration Record of Mass 4 for Antisymmetric Test Specimen of Test Run 5	141
A1.46	Modulus of Acceleration Record of Mass 4 for Antisymmetric Test Specimen of Test Run 5 . . .	141
A1.47	Force Record for Antisymmetric Test Specimen of Test Run 5	142
A1.48	Modulus of Force Record for Antisymmetric Test Specimen of Test Run 5	142

LIST OF TABLES

Table		Page
1.1	Structural System Identification Procedures	6
3.1	Effective Weights for a Continuous Beam	37
5.1	Effective Weights for Each Case	88
A1.1	Symmetric Lumped Mass Specimen's Reference for Plots of the Test Runs 1, 3, and 5	117
A1.2	Antisymmetric Lumped Mass Specimen's Reference for Plots of the Test Runs 1, 3, and 5	127

NOMENCLATURE

$[M]$	- Mass matrix.
$[C]$	- Damping matrix.
$[K]$	- Stiffness matrix.
(\ddot{X})	- Acceleration vector.
(\dot{X})	- Velocity vector.
(X)	- Displacement vector.
(F)	- Force vector.
B	- Arbitrary constant.
m_i	- Lumped mass.
\ddot{x}_i	- Acceleration.
f_i	- Force at a point.
F_R	- Resulting force.
a_i	- Acceleration.
w_i	- Effective weight.
ϵ	- Error term.
s_{ij}	- Positive or negative one.
M_T	- Total mass of the structure.
d_i	- Distance from the centroid to an accelerometer.
(W)	- Effective weight vector.
$[A]$	- Acceleration matrix.
(F_R)	- Resulting force vector.
T	- Total time.

t	- Time.
ω	- Frequency.
M	- Mass.
D	- Generalized damping.
K	- Generalized stiffness.
F	- Forcing Function.
F_r	- Force transmitted across a location.
t^*	- Surface traction.
b	- Body force.
r	- Position vector.
r^*	- Position vector on a surface.
ρ	- Mass density.
u	- Displacement vector.
$\underline{\sigma}$	- Symmetric Cauchy stress tensor.
$\nabla \cdot ()$	- Divergence operator.
$\underline{\underline{E}}$	- Elasticity tensor.
$\underline{\underline{e}}$	- Strain tensor.
φ_i	- Eigenfunction.
r_c	- Position vector to the center of mass.
\underline{R}	- Rotation tensor.
M^e	- Mass of an element.
h	- Length of an element.
$H(\omega)$	- Transfer function.
G_{xx} & G_{xy}	- Autospectrum or cross-spectrum.

- R_{xx} - Autocorrelation function.
- μ_x - Mean value.
- $S(\omega)$ - Spectral density function.

CHAPTER 1.

INTRODUCTION

1.0. Introduction.

In structural analysis, an engineer needs to evaluate the response of a complex structure which is subjected to dynamic loads, such as a conventional (nonnuclear) blast, a nuclear blast or an earthquake. This assessment generally involves an analytical simulation of an environmental load, an analytical structural model, and a method for determining structural response. However, another type of system identification procedure based on structural response can also be used. This technique involves finding the input forces to a given structure when a given structural response is known.

System identification uses mathematical models which approximate an engineer's materials or structures. Engineers analyze structural systems through mathematical models for static and dynamic loads for the purpose of design, evaluation, control, etc. Engineering approaches to problems are broadly categorized as direct or inverse problems according to the amount of knowledge available to develop a model. The direct problem assumes that the differential equations and mechanical properties are defined for a system. In a direct problem, an engineer uses a model to analytically determine structural responses from simulated environmental loads. This approach is widely used in the engineering fields; however, its usefulness is limited by the mathematical model's degree of realistic representation. Without sufficient data to develop a complete model, a second method, called an inverse or system identification problem, can be used to model the

structure response. This method estimates model response by techniques using data from measured structural response to known or unknown applied excitations. System identification problems deal with improving the model of a system before direct problem procedures are applied. When total prior knowledge is lacking about a system and only input-output data are available, both the parametric form and parameters must be determined. This is referred to as the black box problem. When the form of the model is known or assumed, such as differential equations or state models, only the specific parameter values must be determined. This is referred to as the gray box problem. Solving the black box problem would be the most generalized modeling technique, but not the most realistic or cost effective means. System identification problems in nature are generally unstable or ill-conditioned; therefore, use of any prior knowledge is usually the preferred method of developing a model.

The gray box, parameter estimation, or parameter identification method in structural engineering has seen more activity in the last decade as shown in the literature review. The basic idea of parameter identification is to fit input-output data to a parametric form by minimizing the error between the real data and the data predicted from the model.

Models that predict the input forces for a structure, when given the structural response data, are usually formulated under the class of gray box problems. For complex structures, the process of developing models which determine force directly from structural properties is not an easy task. The equations tend to be ill-conditioned, which means small changes in the data can lead to large changes in the solution. The

forward problem, determining the response of a structure when given the force which was applied, has smoothing properties which are lost in the inverse problem. These smoothing properties encourage using system identification techniques for estimating forces. For this type of problem, force identification is defined as the process of determining a model which computes loads from measurements of the system.

Force identification is needed for a number of present and future structural problems. As force identification is perfected, its application to structural problems will increase. An example is the design of weapon systems such as water entry and earth penetrators. This is done by identifying the interactive forces between the weapon's structure and the target, and applying them to the structural design process. Force identification would have applications in controlling the movement of (1) tall buildings due to wind loads, (2) vehicles moving through space, and (3) large space antennas and platforms. Also, there are applications for force identification in aiding the evaluation of damage for structures that encounter earthquakes, blast loads, and other forces. The platforms in space or contaminated areas could be monitored with minimum visual inspection. Another benefit is the determination of equivalent dynamic loading, which is useful in vibration testing. This list does not include all engineering disciplines, but will still continue to increase as new developments occur.

1.1. Literature Review.

The investigation described in this report established mathematical models and procedures to identify input forces to structures. Force

identification is generally under the broad heading of system identification; therefore, for continuity this literature review is divided into two sections. The first section is on system identification in general, and the second section specifically relates to force identification.

1.1.1. System Identification Overview.

As the previous section stated, system identification is a process of estimating a model by techniques using input-output data. System identification started evolving in structural engineering in the early 1970's, but has been rapidly developing in control theory since the 1960's. Even today, researchers and engineers are expanding the techniques and passing information from one discipline to the other. Two symposia (Eykhoff, 1981; Bekey and Sardis, 1982) sponsored by the International Federation of Automatic Control in recent years were dedicated to system identification. Early surveys on system identification in general by Bekey (1970) and Åström and Eykhoff (1971) still provide a good introduction to system identification. In particular, Åström and Eykhoff provided 230 references on the topic at the time of the publication. A later book by Eykhoff (1974) provides a more detailed discussion on system identification techniques. Another survey by Rodeman and Yao (1973) provides one of the first structural reviews. They presented modal and non-modal models, but their main emphasis was identifying parameters for modal models. This is not surprising since modal analysis has been used for structural analysis since the 1940's. Modal analysis is the process of analyzing a structure using modal properties such as damping, natural frequencies,

and mode shapes. An early paper by Kennedy and Pancu (1947) introduced separating frequency response functions by circle fitting. Their motivation was to analyze, identify and describe normal modes of vibrations for airplanes from vibrational measurements. Bishop and Gladwell (1963) investigated further into the theory of resonance testing with more discussion on damping of the structure system. These papers are two of the most noted papers through the years that show the development of modal analysis. Ibáñez (1973) presented the identification of dynamic properties such as damping, eigenfrequencies, mode shapes and nonlinear effects with system identification techniques. Collins, et al. (1974) experimentally determined natural frequencies and mode shapes to modify the structural parameters of a finite element model. Recently, Luk and Mitchell (1983) summarized system identification for a modal analysis method which experimentally determines the system parameters of a structure. A recent book by Ewins (1984) provides an introduction to present day modal testing. The papers described below show that the modal model is still used as part of a system identification process for structures. Juang and Pappa (1987) discussed relating modal testing and system identification and postulated that combining the two would lead to control of large space antennas and platforms.

Two structural identification surveys by Hart and Yao (1977) and Kozin and Natke (1986) presented system identification by dividing the techniques into time domain and frequency domain. Hart and Yao provided time and frequency domain technology trees and grouped three standard approaches for modal parameter estimation defined in Table 1.1.

Ljung and Glover (1981) compared frequency domain and time domain

Table 1.1 - Structural System Identification Procedures
(Hart and Yao, 1977).

Method	Modal Measurements	Structural Parameters
Least Squares	Deterministic	Deterministic
Weighted Least Squares	Stochastic	Deterministic
Statistical Structural Identification	Stochastic	Stochastic

methods in system identification on how they differ and how they complement each other. A structural identification example in which both domains were used was McVerry (1980), who used an output-error approach in the frequency domain to identify the parameters of the lower modes of a linear time invariant model from recorded earthquake response. Then a complementary study in the time domain was presented by Beck and Jennings (1980). They both used system identification techniques of least squares. In both domains the basic methods of system identification are (Juang and Pappa, 1987):

Least Squares

- Ordinary least squares
- Stochastic approximation
- Extended Kalman-Bucy filtering
- Instrumental Variable Method

- Generalized least squares
- Extended least squares (pseudolinear regression)
- Square root filtering

Maximum likelihood estimation

Bayesian approach

Minimum realization

Ladder or lattice filtering

From the previous list, least squares techniques have a number of subheadings. Hsia's book (1977) discusses least square techniques. The least square techniques have been used in structural identification with favorable results. Caravani and Thomson (1974) used a frequency domain algorithm to estimate the viscous-damping for multi-degree structures. Bendat (1976) used a least square technique to identify frequency response functions for multiple input-output data. Caravani, Watson, and Thomson (1971) used a recursive least square time domain approach to identify structural damping and stiffness parameters. Paez, et al. (1982) and Wang, et al. (1982,1983) presented methods which used both a time and frequency domain least-squares parameter identification for linear differential equations up to the third order and time varying linear models. The models were used to represent a hysteretic system which was used for damage assessment. They found the frequency domain approach more suited to identify the parameters of these models. Gersh, et al. (1973,1974a,1974b) were concerned about estimating the natural frequency and damping parameters. They estimated the parameters using an auto-regressive moving average time series with a two-stage least square method and the maximum likelihood procedures.

There are a wide variety of techniques to attack the unstable

characteristics of system identification problems. One of the reasons for the unstable characteristics is the noise in the measured data. Maine and Iliff (1981) discussed this problem of noise as they presented a maximum likelihood technique. Adding constraints and bounds to least square methods (Hanson, 1986) helps to stabilize the system identification problem. Craig and Blair (1985) used a generalized multiple input, multiple output modal parameter estimation algorithm for multiple input forces to be applied simultaneously and for an arbitrary number of acceleration response measurements. The modal parameters were obtained through eigenvalue techniques. Subbayyan and Nagarajan (1977) use a modified parameter algorithm for linear multi-variable discrete time systems by the use of a gradient estimation approach to improve convergence. Shinozuka, Yun, and Imai (1980) used an auto-regressive and moving average model with instrumental variable and maximum likelihood methods.

Distefano and Pena-Pardo (1976) determined an optimal linear model for a structure frame. The parameters were calculated by nonlinear fitting methods. This paper showed a common example of determining a linear model to estimate nonlinear behavior. Nonlinearity is always present to some degree in engineering problems. Since linear theory is thoroughly developed, it is customary to model nonlinear systems by linear models when possible.

There is a vast area of nonlinear modeling that needs to be explored. Tomlinson (1986) presented a review on the detection, identification, and quantifications of nonlinearity in modal analysis. Two other surveys by Mertens, et al. (1986) and Natke, et al. (1988) discussed how to detect nonlinearity in mechanical systems.

The actual identification of nonlinear models is more complex than linear models. Singh and Subramanian (1980) attacked the problem from a frequency response identification. Distefano and Rath (1975) presented methods of identification for the determination of nonlinear parameters associated with third-order damping and stiffness terms. Their application was for seismic conditions. Billings (1980) presented a survey on nonlinear system identification. The significant trend in nonlinear identification is to use nonparametric models. This is when the model for the system is not defined or assumed. An example is the functional series method. Wellstrad (1981) presented a nonparametric method of spectral and impulse response estimation. Masri, et al. (1982) present a nonparametric identification technique for multi-degree models based on state variables. They applied the model to a steel frame. Another structure nonparametric investigation was by Paez (1987) and Hunter and Paez (1988). They demonstrated the computing of higher order transfer functions for a cubic stiffness nonlinearity. Chouychai and Vinh (1986) considered using impact testing on structures to determine the Volterra series for analyzing nonlinear structures.

Nonparametric models require more input-output data to obtain a model. Barker and Davy (1970), Barrett (1980), Fakhouri (1980) and Lawrence (1981) presented methods to estimate the Volterra functional series.

1.1.2. Force Identification Overview.

Force identification is the process of determining input excitations using measured responses for a system. This definition encompasses simple to complex systems. For a simple force transducer, a linear

relationship is normally used for a correlation of the response to the input force. For complex systems the relationship between the response and the input may be ill-posed. One example is small perturbations in the response measurements caused by large changes in the input forces. Further, complex systems usually require more than one measured response to identify the input forces.

This field of force identification has broad implications. In its present stage of development it is not generalized, even though research in the last ten years has increased. Some of the literature in this field is mentioned below.

Stevens (1987) presented an overview for the force identification problem for linear vibration. He discussed the major difficulty associated with discrete and continuous systems.

Different approaches and problems are being studied. Doyle (1984a, 1984b) used strain response on a beam to determine the contact forces. The formulation used Bernoulli-Euler beam theory. The formulation was extended to include shear effects in the beam. This had little effect on experimental test results. A follow-on paper by Doyle (1987) used a formulation using phases of response to accurately locate in space and time the origin of a dispersing pulse.

Simonian (1981a, 1981b) used a dynamic programming filter to predict wind loads on a structure. The filter was used to identify the structure and wind force parameters. The method used an optimal state estimation. This was an attempt to apply nonlinear filtering methods to large structural dynamic models. The results were satisfactory for the range of frequencies considered, allowing the identification of variable parameters so important for nonlinear systems. The biggest drawback for

this method is the amount of calculation that is needed to obtain the results.

Hillary and Ewins (1984) investigated, both analytically and experimentally, the sinusoidal loads on a cantilever beam which was to be extended to turbine blades. They worked in the frequency domain using acceleration and strain gages on this beam. Their results showed that the strain-related model was less ill-conditioned than the acceleration model and that the predicted forces were less accurate at the fundamental modes.

Fabunmi (1985, 1986, 1987) studied the effects of structural modes for the determination of vibration force. Acceleration measurements from cantilever and free-free beams were used to predict multi-input forces. He found that, in areas of a fundamental mode of vibration, only one excitation could be identified accurately. To help relieve this problem, he suggested elimination of the degrees of freedom at which the fundamental modes of vibration have large deflections.

Bateman and Soloman (1987) used a deconvolution technique in the frequency domain for determining the input forces to a structure. This technique was for earth penetrators. Laboratory experiments were conducted with a bar 76.0 mm in diameter and 1.524 m long. The results of the tests were reasonable but there was concern on how the frequency response function calibrated at loads lower than actual field data (ten times less) would affect predicted input forces. Also, the results indicated that the placement of the accelerometers may greatly influence the success of the technique.

Michaels and Pao (1985, 1986) investigated analytically and experimentally an iterative deconvolution method to determine the

orientation and time histories of applied forces to an elastic glass plate. The procedure involves determining the coefficients of a linear combination of Green's functions of the plate. Chung and Shase (1985) furthered this study by introducing uniform loads and loads inside the medium to the elastic plate.

Elliott, Juang, and Robinson (1988) used a singular value decomposition technique to reduce noise contaminating the input measured strain matrix. This improved the ill-conditioning of the inverse problem due to this noise. The method was used to predict acoustic forces on a plate.

Gregory, et al. (1985, 1986) explored analytically and experimentally the sum of weighted acceleration signals for free-free beams and a weapon system that was instrumented. The results showed the predicted force was captured for a band-limited range of input forces.

Hu (1980) used the equivalent linearization method in the frequency domain to identify the input forces from known structural responses and system parameters. He encountered a major difficulty, though, when he introduced high levels of nonlinear displacement responses in his analysis.

Ibáñez (1974) applied inverse method to a prior model to determine the input force that would best excite the modes of the structure. When the structure parameters were identified, the new model was used to identify the input forces.

Imregun and Ewins (1987) investigated determining equivalent forces from structural responses. Equivalent forces allow complex excitation of a structure to be replaced by simpler forces in dynamic testing.

Whitson (1984) and Jordan and Whitson (1984) presented a theory and

an application of a Timoshenko transformation technique to identify impact forces in a heat exchanger tubing system. The technique used acceleration measurements at remote locations and required the distances from the remote location to the location of the input force. This distance could be estimated from the analysis of the dispersion in beam acceleration.

Kreitinger and Wang (1988) applied the sum of the weighted acceleration to nonlinear structures. They compared two structures, one linear and one nonlinear, similar in design. The results showed the method captured the basic nonlinear phenomenon but the amplitude showed discrepancies.

Priddy, Gregory, and Coleman (1988) discussed strategic placement of accelerometers to measure responses for determining input forces. They showed that for linear systems the weighting coefficients for sum of the weight acceleration method can be determined with the knowledge of the mode shapes of the structure.

Smallwood and Gregory (1987) applied a constrained least squares method for determining the coefficients for sum of the weighted acceleration method.

Trujillo (1978) presented a state variable form of the differential equations and solved for the input excitations. Two example problems, heat conduction and structural dynamics, were presented using the formulation developed.

Wang and Kreitinger (1987) presented a lump mass formulation of a free-free beam to predict the input forces to the structure. The lump mass was determined from a least square time domain method and a frequency domain method. The predicted force and measured force showed

very close correlation.

Yoshikawa and Sugie (1981) presented an inverse method to reproduce the input to a system which can determine parts of the input.

Natke (1987) presented a frequency domain method for identifying the input forces.

1.2. Objectives.

The first objective of this study is to explore the sum of weighted acceleration technique, SWAT, in both the time and the frequency domains. SWAT is an approach to identify the force input to a structure. An additional objective is to validate SWAT as to whether the approach can be used for nonlinear cases as well as linear cases. The above objectives use experimental test data to verify the proposed approach. A final objective is to extend the approach to a more general scheme which is applicable for more complex structures.

CHAPTER 2.

FORCE IDENTIFICATION OF LUMPED MASS SYSTEMS

2.0. Model.

A force transducer is usually based on a linear relationship between the forces applied and the output measured. One such transducer is a force transducer which uses strain gages. The strain gage transducer is calibrated by applying a known force and correlating this force with the voltage output that is measured. The strain gage transducer is modeled as a single degree of freedom system. The approach which is discussed in this chapter and others to follow is a method which models a structure system as a force transducer. This approach can be applied to the simple transducer which was described above as well as complicated multi-degree-of-freedom systems. This accomplishment allows the determination of input forces to the structure. The common outputs which are measured from structures are accelerations, velocities, and displacements. The strain gage transducer indirectly measures the displacement through measuring voltages, which are then correlated to the force that is applied. The approach called sum of weighted acceleration technique, SWAT, which is described in this report provides the use of acceleration as the output measurements of the structure to determine the force.

For real structures, one degree of freedom is not always the best choice for modeling a structure as a force transducer. The research conducted for this report explored force identification of multi-degree-of-freedom systems. The first application of SWAT which is described in this chapter was to linear lumped mass systems. The equations for a

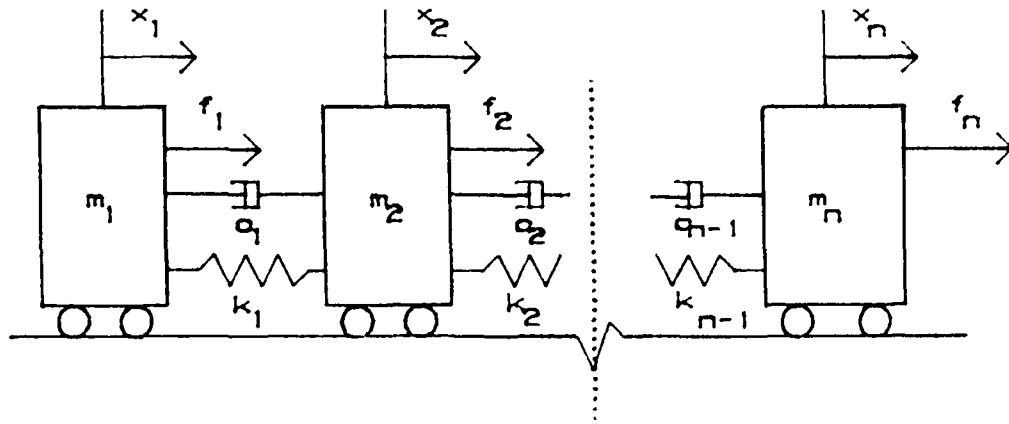


Figure 2.1 Free-Free Lumped Mass System.

free-free lump mass system shown in Figure 2.1 is represented in matrix form by

$$[M] \{\ddot{X}\} + [C] \{\dot{X}\} + [K] \{X\} = \{F\}, \quad (2.1)$$

where $[M]$ is the mass matrix (diagonal for a lumped mass system), $[C]$ is the damping matrix, $[K]$ is the stiffness matrix, $\{F\}$ is the force vector and $\{\ddot{X}\}$, $\{\dot{X}\}$, $\{X\}$ are the acceleration, velocity and displacement vectors respectively.

For this system, the mass matrix is diagonal and the stiffness and damping matrices are singular. When a matrix is singular, it has at least one eigenvalue of zero and corresponding eigenvectors of the form

$$B \begin{Bmatrix} 1 \\ 1 \\ \vdots \\ 1 \end{Bmatrix}, \quad (2.2)$$

where B is an arbitrary constant. For the above mechanical system, this represents rigid body motion. The transpose of the vector in Equation (2.2) with $B=1$ is

$$(1 \ 1 \ 1 \ \dots \ 1). \quad (2.3)$$

The multiplication of Equation (2.3) and Equation (2.1) yields the results

$$m_1 \ddot{x}_1 + m_2 \ddot{x}_2 + \dots + m_n \ddot{x}_n = f_1 + f_2 + \dots + f_n, \quad (2.4)$$

where m_i , $i=1\dots n$, are the lumped masses on the diagonal of $[M]$, and f_i the point forces. The damping and the stiffness terms cancel out. Let F_R equal the resulting force on the system, then

$$F_R = f_1 + f_2 + \dots + f_n = m_1 \ddot{x}_1 + m_2 \ddot{x}_2 + \dots + m_n \ddot{x}_n \quad (2.5)$$

Note, this does not imply $f_1 = m_1 \ddot{x}_1$, $f_2 = m_2 \ddot{x}_2$, etc. Equation (2.5) can be rewritten as

$$F_R = \sum_{i=1}^n m_i a_i \quad (2.6)$$

where n is the number of degrees-of-freedom, and $a_i = \ddot{x}_i$, $i=1, \dots, n$, the acceleration of the i^{th} mass, m_i . When m_i is known for a lumped mass system, the force can be calculated with the measurements of the acceleration. The next two sections discuss and describe time and frequency domain approaches which take acceleration signals that are multiplied by a coefficient to predict an external force that excites a mechanical system. The technique (method) discussed here involves using the least square system identification approach to determine the optimal distribution factors associated with an equivalent mass at each acceleration location and then verifying these predictions through experiments. In order to assess this approach, several specimens with different configurations were constructed. These specimens were tested by applying random forces and measuring both the forces which were applied and the acceleration at selected locations. The force exciting the specimen was predicted by summing the coefficients, which were determined by the time and frequency domain approaches, multiplied by the coefficients' respective acceleration records. The force that was predicted was compared with the force that was measured. The results of this chapter demonstrate good experimental verification.

2.1 Time Domain Approach.

This chapter essentially describes two methods: time domain and frequency domain. The first method, time domain, uses a linear combination of time histories of accelerations and the external force which was applied to determine the unknown parameters. The sum of the products of mass times acceleration for each sub-section of a structure system provides the prediction of the external force. This can be

written as:

$$F_R(t) = \sum_{i=1}^n (w_i a_i(t)) \quad (2.7)$$

where the w_i was changed from m_i in Equation (2.6) and are the unknown coefficients to be determined. These coefficients are considered effective weights associated with each acceleration measurement. This equation is different from Equation (2.6) by changing the name of m_i to w_i . In this model, w_i may be negative for a system that is not truly lumped. For a truly lumped mass system, the values of the weighting factors can be readily estimated; however, for a system where the masses are more uniformly distributed, good estimates for the effective weights are not obvious. Consequently, the appropriate number and the location of the measurements to be used for identifying the force that is applied must be determined first. In general, the values of the effective weights are frequency dependent (Smallwood and Gregory, 1987). From the modal analysis viewpoint, the structure must be represented by at least the number of vibration modes to be captured in measuring the external forces plus two. The exception for SWAT is the case when gauges are placed at the nodes of vibration for the highest vibration mode (Priddy, et al. 1988). Then the structure can be represented by the number of vibration modes plus one.

The time domain approach uses a least-square technique. From system identification, which was discussed in chapter one, a parametric model is chosen and the parameters are determined from the input/output measurements. The model chosen for this force identification procedure

is Equation (2.7) and the effective weights are the parameters to be determined. Thus, if the system under consideration is linear and all field measurements are noise free, Equation (2.7) can be assumed true. However, some noise will inevitably be present; thus the data which are measured will not satisfy Equation (2.7). Therefore, an error term $\epsilon(t)$, must be introduced to satisfy the equality and then Equation (2.7) can be rewritten as

$$\epsilon(t) = F_R(t) - \sum_{i=1}^n (w_i a_i(t)). \quad (2.8)$$

The square error of Equation (2.8) is defined as follows:

$$\epsilon^2 = \int_0^T \left[F_R(t) - \sum_{i=1}^n (w_i a_i(t)) \right]^2 dt \quad (2.9)$$

The effective weights w_i , then, are those values which satisfy the sequence of the equations and n is the number of acceleration measurements. To minimize the error, the partial derivative of ϵ with respect to w_i is set equal to zero.

$$\frac{\partial \epsilon^2}{\partial w_i} = 0, \quad i = 1 \dots n \quad (2.10)$$

Although many different solution schemes are available, the scheme used for this study is shown by the discretization of the above equations and solve Equation (2.10) for w_i , $i = 1, \dots, n$. In this case there are more

equations then the unknowns w_i , $i = 1, \dots, n$. The solution of the set of equation (matrix notation)

$$\{ F_R \} = [A] \{ W \} \quad (2.11)$$

is

$$\{ W \} = ([A]^T [A])^{-1} [A]^T \{ F_R \}, \quad (2.12)$$

where

$$\{ W \} = \{ w_1 \ w_2 \ w_3 \ \dots \ w_n \}_{1 \times n}^T,$$

$$[A] = \{ a_{1k} \ a_{2k} \ a_{3k} \ \dots \ a_{nk} \}_{m \times 4}, \ k = 1, \dots, m,$$

$$\{ F_R \} = \left\{ \begin{matrix} F_{R1} \\ F_{R2} \\ \vdots \\ F_{Rk} \end{matrix} \right\}_{m \times 1}, \ k = 1, \dots, m.$$

In this form, k represents each time increment where the data are taken. For example, $a_{1k} = a_1(k\Delta t)$ and $m\Delta t = T$; thus, T is the total time duration and Δt is the time increment. Once the effective weights w_i are determined, the same values can be used to determine the forces exerted on the structure.

Additionally, the least square method chosen here was a recursive estimation (Hsia, 1977). This allowed a huge amount of data to be

processed through the personal computer with limited memory. The experimental data from the laboratory were digitized. The least square algorithm is developed by introducing a subscript to $\{F_R\}$ and $[A]$ for k equations.

$$\{F_R\}_k = [A]_k \{W\} \quad (2.13)$$

Also, denote $\{W\}$ in Equation (2.12) as $\{W\}_k$,

$$\{W\}_k = ([A]_k^T [A]_k)^{-1} [A]_k^T \{F_R\}_k. \quad (2.14)$$

Suppose a new equation, the $(k+1)^{th}$, is obtained as

$$F_R(k+1) = w_1 a_1(k+1) + w_2 a_2(k+1) + \dots + w_n a_n(k+1) \quad (2.15)$$

Then defining

$$\{a\}_{k+1}^T = \{a_1(k+1), a_2(k+1), \dots, a_n(k+1)\} \quad (2.16)$$

yields

$$F_R(k+1) = \{a\}_{k+1}^T \{W\}_{k+1}. \quad (2.17)$$

Now the system of $k+1$ equations can be written as

$$\{F_R\}_{k+1} = [A]_{k+1} \{W\}_{k+1}. \quad (2.18)$$

The new least-square estimator is

$$\{W\}_{k+1} = ([A]_{k+1}^T [A]_{k+1})^{-1} [A]_{k+1}^T (F_R)_{k+1} \quad (2.19)$$

Now let $P(k)$ be given by

$$P(k) = ([A]_k^T [A]_k)^{-1} \quad (2.20)$$

and therefore

$$P(k+1) = ([A]_{k+1}^T [A]_{k+1})^{-1} \quad (2.21)$$

Recall that if A , C , and $A+BCD$ are nonsingular matrices, then

$$(A + BCD)^{-1} = A^{-1} - A^{-1}B(C^{-1} + DA^{-1}B)^{-1}DA^{-1}. \quad (2.22)$$

Using the relationship of Equation (2.22) and rearranging Equation (2.21)

$$\begin{aligned} P(k+1) &= [P(k)^{-1} + (a)_{k+1}(a)_{k+1}^T]^{-1} \\ &= P(k) \cdot P(k)(a)_{k+1}[1 + (a)_{k+1}^T P(k)(a)_{k+1}]^{-1} (a)_{k+1}^T P(k) \end{aligned} \quad (2.23)$$

In view of Equation (2.19), it can be seen

$$\{W\}_{k+1} = P(k)([A]_k^T (F_R)_k + (a)_{k+1} F_R(k+1)) \quad (2.24)$$

This algorithm was incorporated into a program shown in Appendix 2.

With this algorithm and experimental data, the effective weights for a structure can be determined. After the effective weights are determined, SWAT will provide the means to predict future input forces to a structure. Experimental data from mechanical systems were used in this approach and are described and shown in Sections 2.3 and 2.4 and Appendix 1.

2.2 Frequency Domain Approach.

A second technique explored to determine the effective weights was in the frequency domain. This technique obtained the equations needed to solve for the effective weights by applying physical constraints to the effective weights and using statistical averaging of the force and acceleration time histories in the frequency domain.

A first physical constraint is the sum of effective weights is equal to the total mass, M_T , of the structure.

$$M_T = \sum_{i=1}^n w_i \quad (2.25)$$

A second physical constraint is the sum of the moment around the centroid is equal to zero.

$$\sum_{i=1}^n w_i d_i = 0 \quad (2.26)$$

where d_i , $i=1, \dots, n$, are the distances from the centroid to the acceleration measuring point for the i^{th} effective weight.

The other equations are obtained by averaging the data in the frequency domain. First, the digitized experimental data is transformed into the frequency domain with the discrete Fourier transform. Second, the modulus of the force and accelerations are computed. At the modes of vibration the values from the modulus are taken to form the additional equations. This is represented by

$$\begin{aligned}
 |F(\omega_1)| &= s_{11}|a_1(\omega_1)|w_1 + s_{12}|a_2(\omega_1)|w_2 + \dots + s_{1n}|a_n(\omega_1)|w_n \\
 |F(\omega_2)| &= s_{21}|a_1(\omega_2)|w_1 + s_{22}|a_2(\omega_2)|w_2 + \dots + s_{2n}|a_n(\omega_2)|w_n \\
 &\vdots \\
 |F(\omega_m)| &= s_{m1}|a_1(\omega_m)|w_1 + s_{m2}|a_2(\omega_m)|w_2 + \dots + s_{mn}|a_n(\omega_m)|w_n
 \end{aligned} \tag{2.27}$$

where $| \ |$ is the modulus, ω_i , $i=1\dots n$, are the natural frequencies, and s_{ij} are signs determined by the mode shapes of the structure. If a structure does not significantly excite any of the modes of vibration, then any effective weights that meet the physical constraints would predict the input force accurately. But as the modes of vibrations are excited, they must be represented by the effective weights. The number of modes that can be represented is $n-2$ for a beam except when the gauges are placed at the nodes of vibration of the highest mode of vibration. In this case, one extra mode of vibration is captured. This is the band-limited characteristic of this technique.

For an example, the use of a beam where only the first two modes of vibration are excited would require four acceleration measurements on the structure. The first equation is

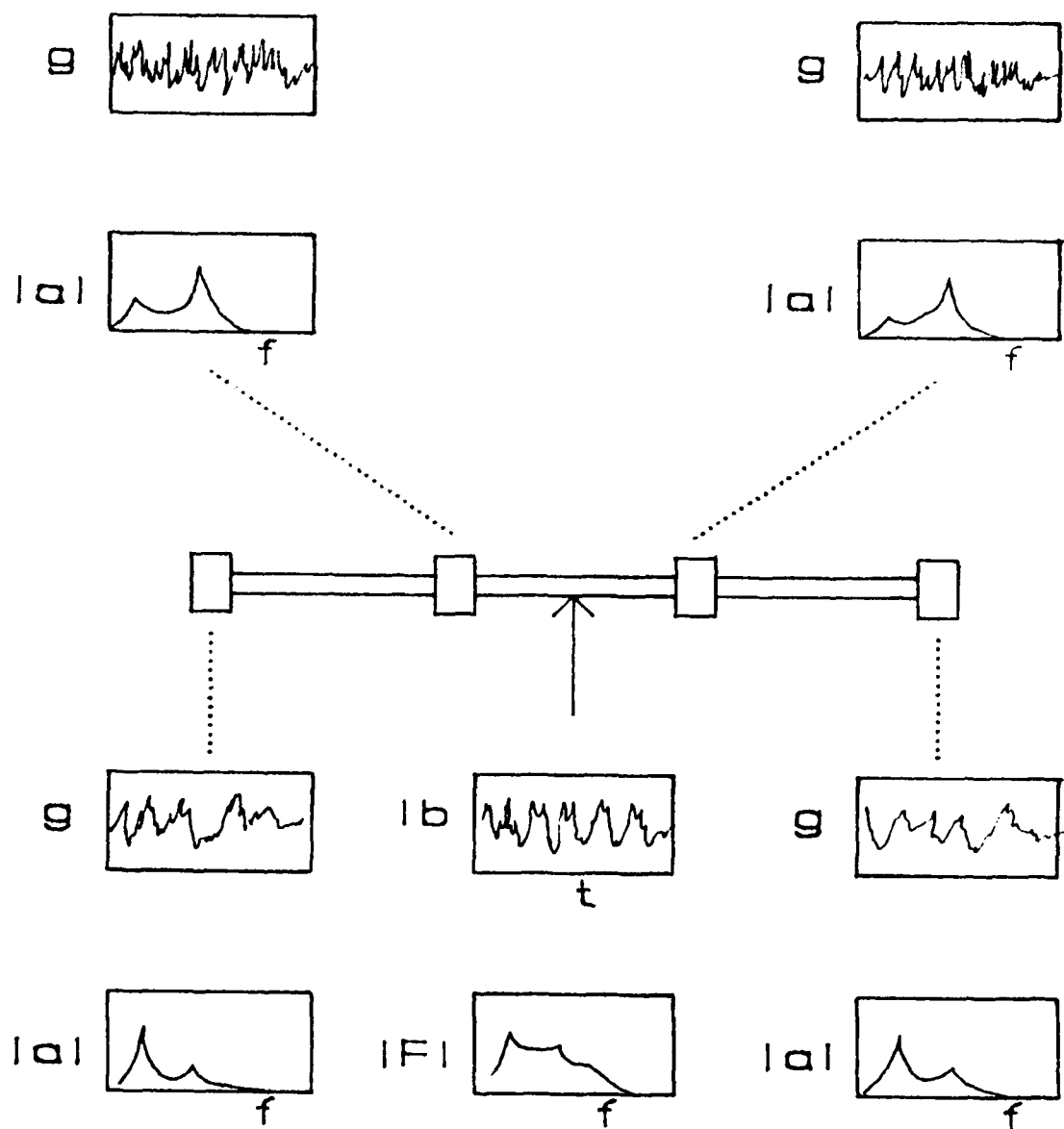


Figure 2.2. Frequency Domain Records of Accelerations and Force.

$$\sum_{i=1}^4 w_i = M_T \quad (2.28)$$

where M_T is the total mass of the structure. The second equation is

$$\sum_{i=1}^4 w_i d_i = 0 \quad (2.29)$$

where d_i , $i = 1, \dots, 4$ are the distance from the centroid to the placement of the acceleration gauge associated with w_i . The moduli of the acceleration records and the force record in the frequency domain would be in the form shown in Figure 2.2. The third and fourth equations would be obtained from these records as

$$|F(\omega_1)| = -s_{11}|a_1(\omega_1)|w_1 + s_{12}|a_2(\omega_1)|w_2 + s_{13}|a_3(\omega_1)|w_3 + s_{14}|a_4(\omega_1)|w_4 \quad (2.30a)$$

$$|F(\omega_2)| = -s_{21}|a_1(\omega_2)|w_1 + s_{22}|a_2(\omega_2)|w_2 + s_{23}|a_3(\omega_2)|w_3 + s_{24}|a_4(\omega_2)|w_4 \quad (2.30b)$$

where $|F(\omega_i)|$ is the value of the modulus of the force at ω_i . The signs, s_{ij} , are determined by the mode shapes of the structure.

The above equations can be represented in matrix form as

$$\begin{bmatrix} 1 & 1 & 1 & 1 \\ d_1 & d_2 & d_3 & d_4 \\ s_1|a_1(\omega_1)| & s_2|a_2(\omega_1)| & s_3|a_3(\omega_1)| & s_4|a_4(\omega_1)| \\ s_5|a_1(\omega_2)| & s_6|a_2(\omega_2)| & s_7|a_3(\omega_2)| & s_8|a_4(\omega_2)| \end{bmatrix} \begin{Bmatrix} m_1 \\ m_2 \\ m_3 \\ m_4 \end{Bmatrix} = \begin{Bmatrix} M_T \\ 0 \\ |F(\omega_1)| \\ |F(\omega_2)| \end{Bmatrix}$$

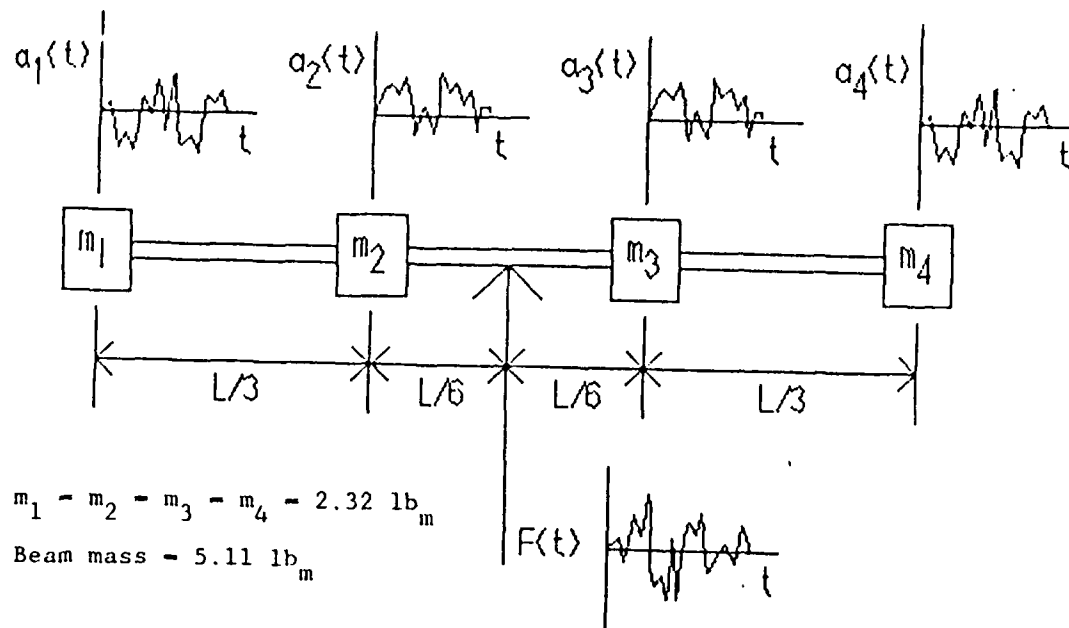


Figure 2.3. Symmetric Lumped Mass Test Setup.

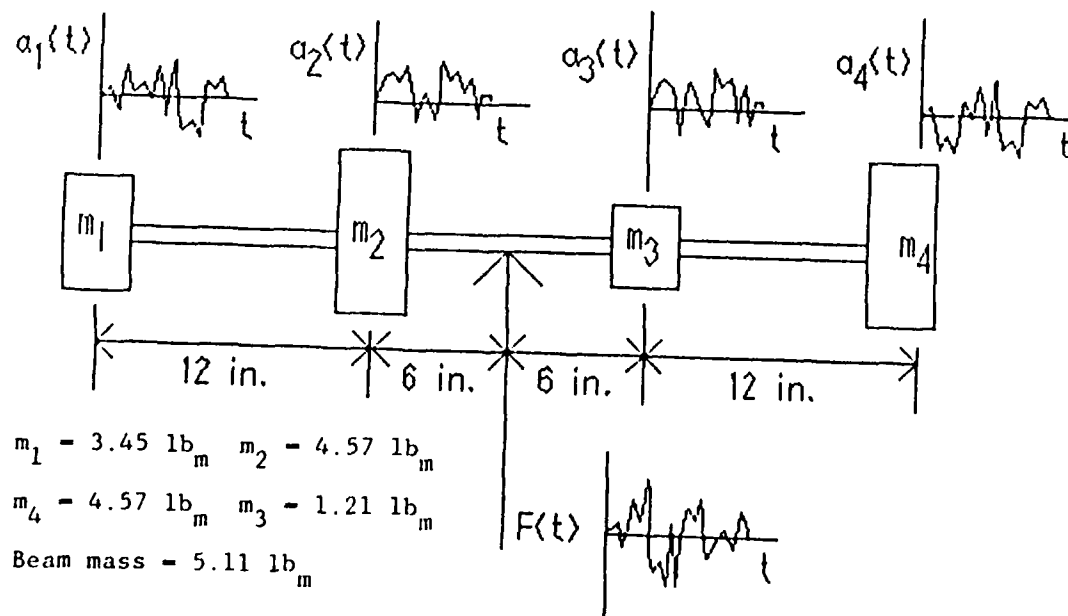


Figure 2.4. Antisymmetric Lumped Mass Test Setup.

2.3 Experimental Setup.

Once the approaches to determine the effective weights were developed, several experiments were performed in the laboratory to confirm their accuracy. A specimen made of steel with a size of 37" x 1" x 1/4" was chosen as the test structure with two different configurations of mass, which were added to the beam, as shown in Figures 2.3 and 2.4. Four rectangular masses were added along the length of this beam to form a symmetric and an anti-symmetric configuration. The beam was excited by a 2000-lb electrodynamic shaker through a drive rod and force transducer connection. The force was exerted to the test structure's center of mass. The specimen shown in Figure 2.3 is symmetric about the centroid. The force is applied in the center and measured with a force transducer. The acceleration is measured at each of the masses. The natural frequencies were 22 Hz and 169 Hz. The second setup was an antisymmetric specimen (see Figure 2.4). The masses were balanced to position the centroid in the center, allowing the same beam for both setups. The first two natural frequencies for this beam were 23 Hz and 135 Hz.

Response data were recorded and digitized through an ISAAC-2000 data acquisition system with a 2000 data point sampling rate per second per channel. Data reduction was performed by using an IBM-XT and Micro-VAX II computers. Also, the identification algorithms to determine the effective weights were run on the IBM-XT and Micro-Vax II computers. The following section presents results of the two examples.

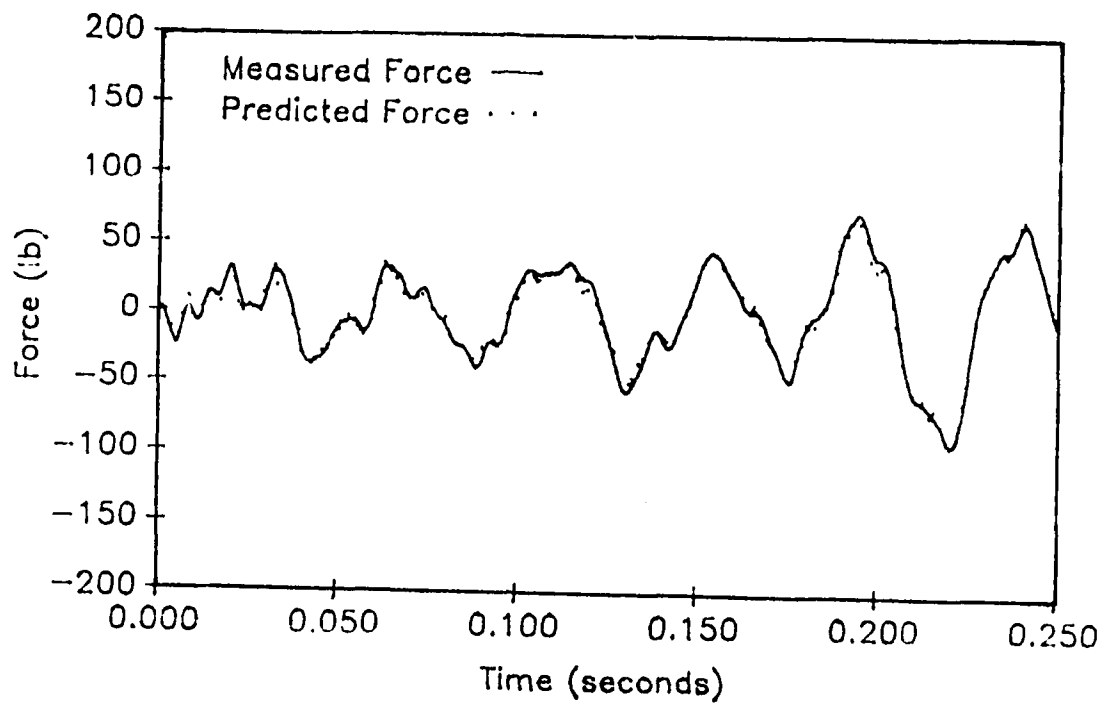


Figure 2.5. Comparison of Forces for Test Run 2 (Symmetric Test Specimen).

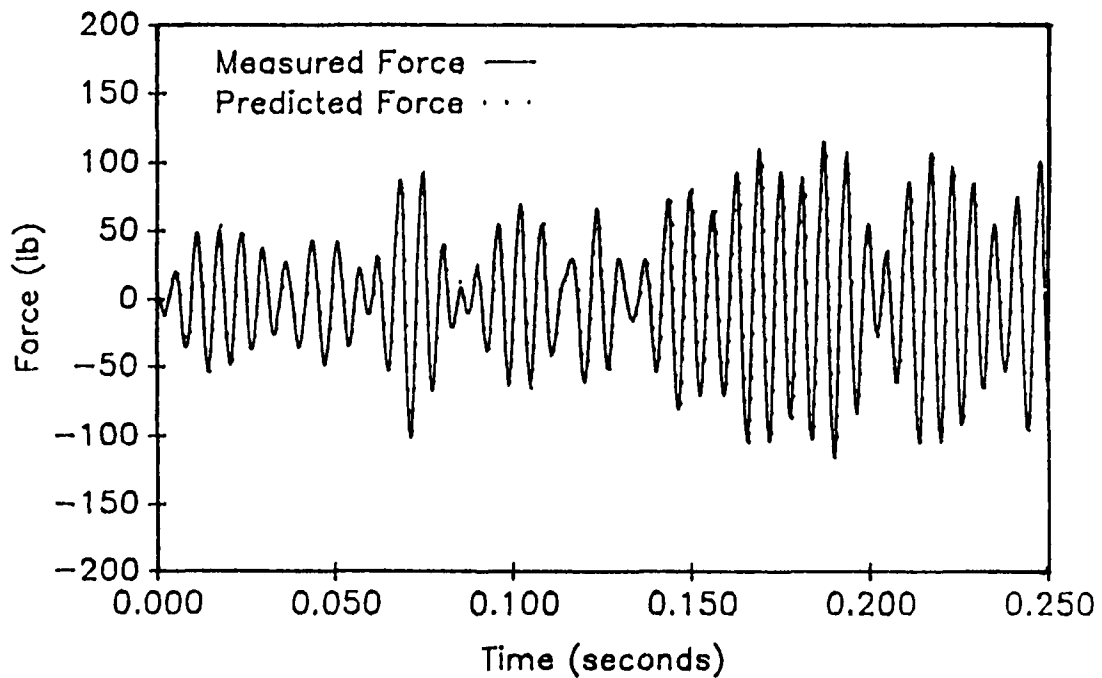


Figure 2.6. Comparison of Forces for Test Run 4 (Symmetric Test Specimen).

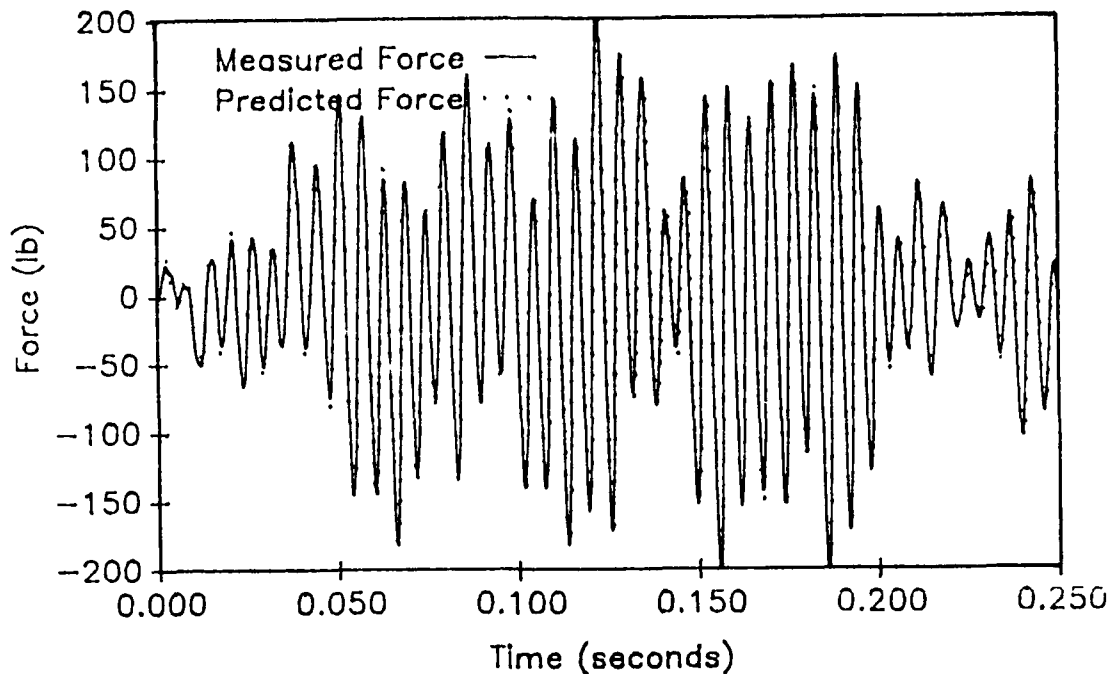


Figure 2.7. Comparison of Forces for Test Run 7 (Symmetric Test Specimen).

2.4 Results.

The first configuration which is shown in Figure 2.3 had four equal masses distributed along the beam. The test specimen was symmetric. Seven test runs, with random force applied at the centroid, were conducted to investigate how the bandwidth of the excitation would affect the results. The first two vibration modes were at 22 Hz and 169 Hz. The test runs consist of random excitation with bandwidth of frequency of the following:

2 test runs at 0-50 Hz

2 test runs at 110-200 Hz

3 test runs at 0-200 Hz

The bandwidth is the range of frequency where the input force shows

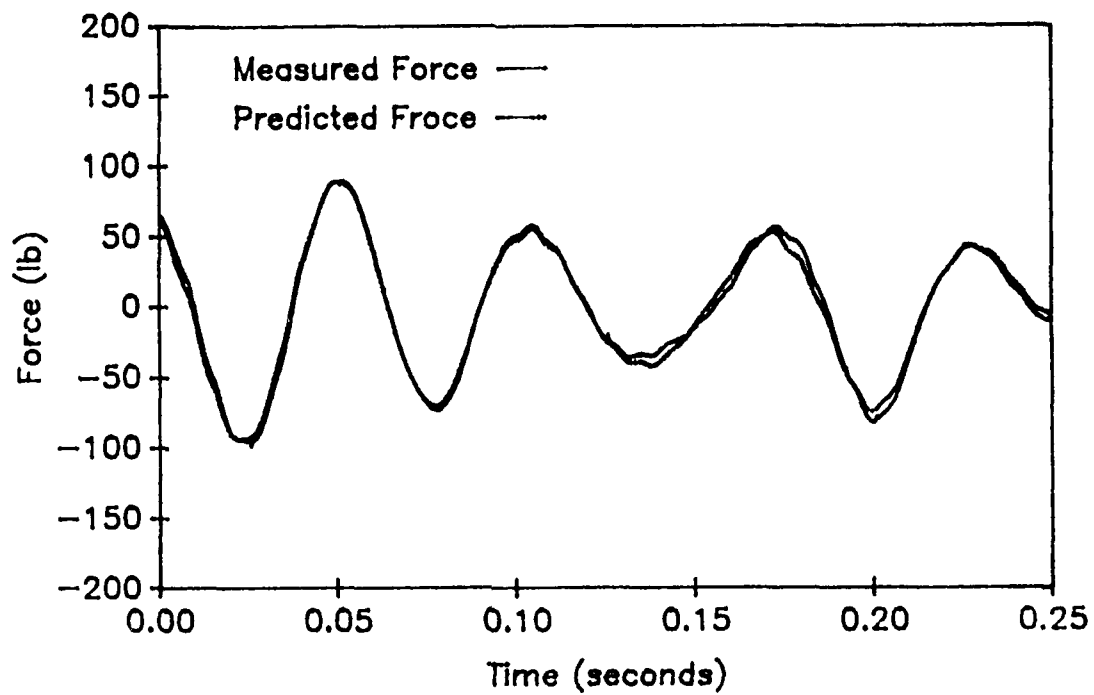


Figure 2.8. Comparison of Forces for Test Run 2 (Antisymmetric Test Specimen).

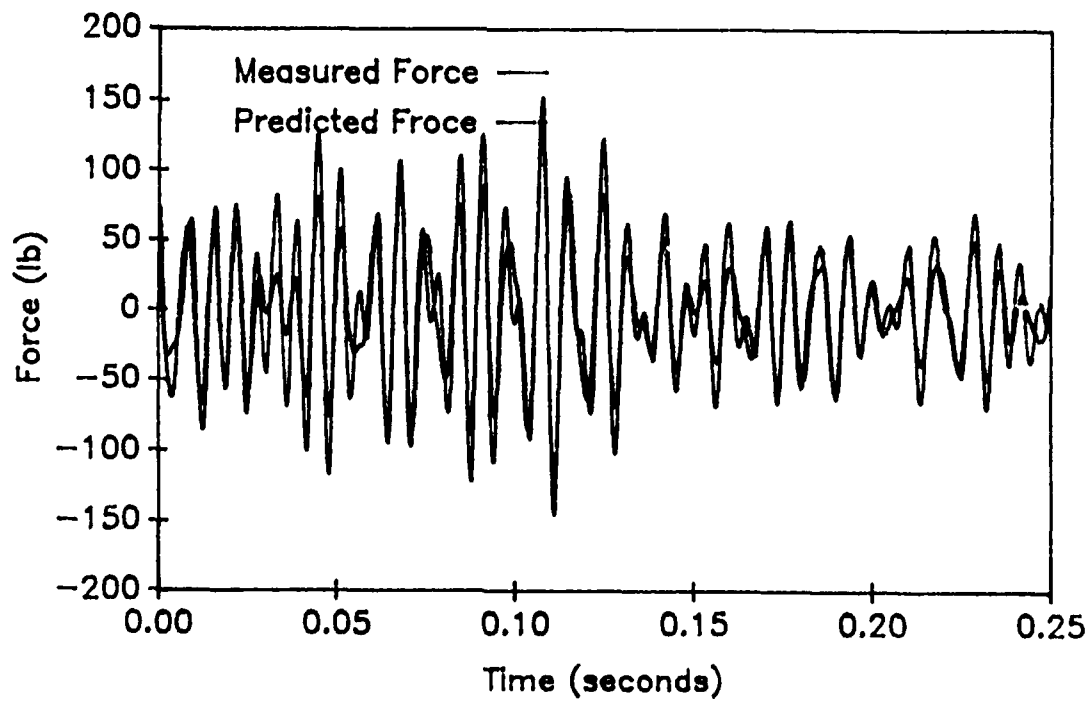


Figure 2.9. Comparison of Forces for Test Run 4 (Antisymmetric Test Specimen).

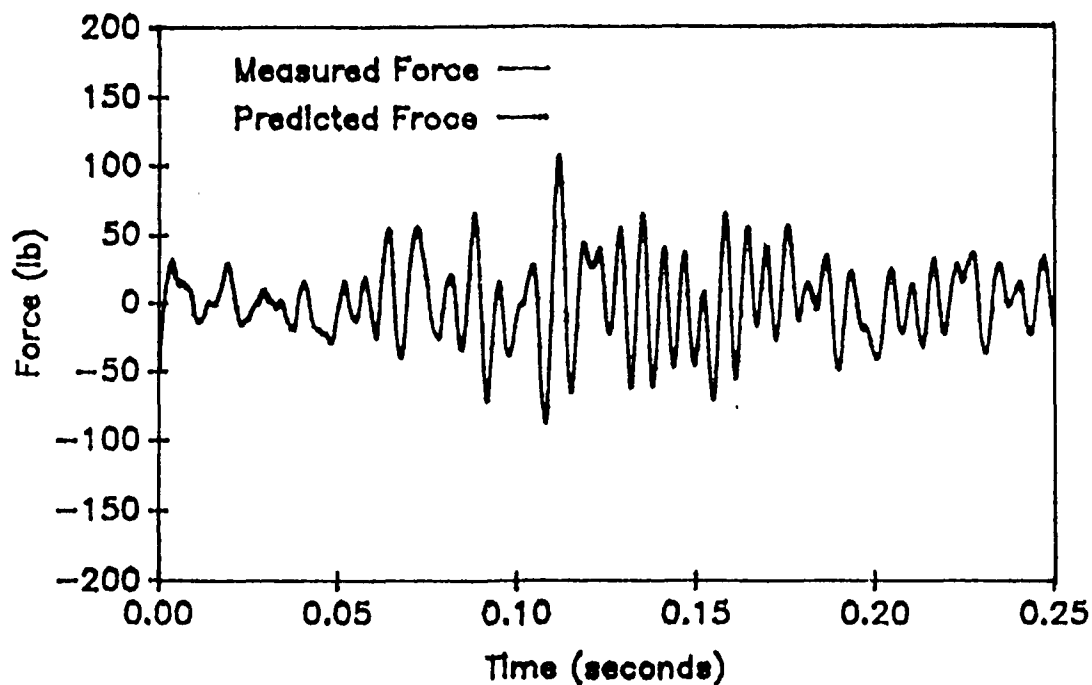


Figure 2.10. Comparison of Forces for Test Run 7 (Antisymmetric Test Specimen).

power in the frequency domain. The bandwidths were chosen to include specific vibration modes. The 0-50 Hz bandwidth included only the first mode, the 110-200 Hz bandwidth included only the second mode, and the 0-200 Hz bandwidth included both of the vibration modes. A total of four measurements at each lumped mass location were taken. The force was applied at the center, which was clamped for this symmetric specimen. Therefore, the acceleration records opposite the center were equal. For this test specimen, n of Equation (2.7) was equal to four. The experimental data are shown in Appendix 1. The effective weights were determined using both the time and frequency domain approaches which were described in Sections 2.1 and 2.2. Figure 2.5 shows the

force that was measured and the force that was predicted using Equation (2.7) with effective weights. This figure is test run 2. Figure 2.6 compares the force for test run 4 which used a 110-200 Hz bandwidth of force excitation. Figure 2.7 compares the two forces for test run 7 which used a 0-200 Hz bandwidth of force excitation.

The second configuration (see Figure 2.4) was excited with random vibration with the following test runs:

2 test runs at 0-50 Hz

2 test runs at 110-200 Hz

3 test runs at 0-200 Hz

Again, the bandwidths were chosen to include specific vibration modes. The 0-50 Hz bandwidth included only the first mode of vibration, 110-200 Hz bandwidth included only the second mode of vibration, and the 0-200 Hz bandwidth included both of the vibration modes. Since this was an antisymmetric specimen, all four acceleration measurements were used to determine the effective weights. Figure 2.8 compares the measured force to the predicted force using Equation (2.7) with effective weights. Figure 2.9 compares the force for test run 4. Finally, Figure 2.10 compares the forces for test run 7.

CHAPTER 3.

FORCE IDENTIFICATION OF CONTINUOUS SYSTEMS

3.0. Model.

From the previous chapter's results, the sum of the weighted acceleration technique, SWAT, can adequately predict external forces for lumped mass structures. The prediction of the input forces used the following equation

$$F_R = \sum_{i=1}^n w_i a_i \quad (3.1)$$

where the effective weights were determined using mathematical techniques with experimental data. This chapter demonstrates and discusses applying SWAT to continuous structures. Experimental verification compares the predicted force which was determined by SWAT to the force which was measured for a structure.

3.1 Experimental Setup

The structure selected for a continuous system was a beam which was made of steel. The beam's dimensions were .5" X 1" X 80.75". The beam was suspended with rubber bands to simulate a free-free beam. A total of five accelerometers were mounted along the beam as shown in Figure 3.1. Both random force loadings and impact loadings were applied. The random excitation produced data to determine the effective weights. Comparisons of forces for both types of loadings were made of the predicted and measured forces.

The modulus of elasticity for steel is 29×10^6 psi. The mass per

All Dimensions in Inches.

Mass = 11.38 lb.

O - Location of an accelerometer.

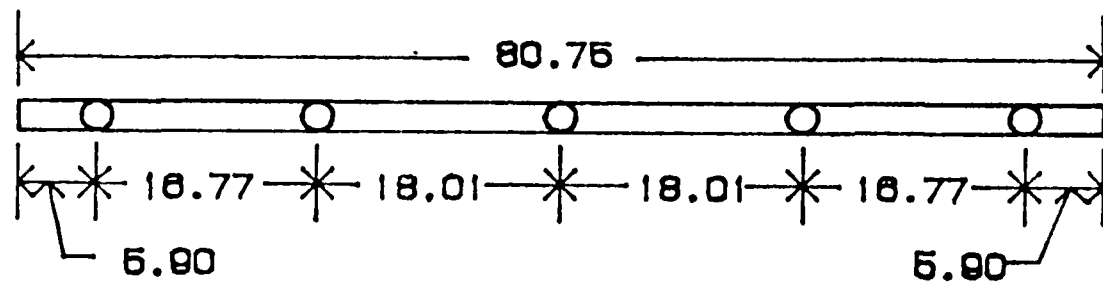


Figure 3.1. Free-Free Beam Configuration.

unit length of this beam is 0.14 lb/in. The area moment of inertia of the beam is $I = 1.04 \times 10^{-2} \text{ in}^4$. From these values the first three theoretical natural frequencies are approximately:

Natural Frequencies (Hertz)

1	16
2	43
3	85

The effective weights were determined from the time and frequency approaches discussed in Chapter 2 using a random input. Two tests with random excitation inputs were recorded. The first data were used to determine the effective weights for the beam. A comparison of forces which were predicted using SWAT and measured are shown in the results.

3.2. Results.

The first test's acceleration records for the continuous beam are shown in Figures 3.2 through 3.11. The force loadings were applied at the center of the beam. The first test loading's time history and modulus is shown in Figures 3.12 and 3.13, respectively.

The first test's acceleration and force data were used to determine the effective weights. The effective weights that were determined are shown in Table 3.1.

Table 3.1. Effective Weights for a Continuous Beam.

	Determined From Time Domain Approach	Determined From Frequency Domain Approach
w_1	2.31	2.40
w_2	2.60	2.55
w_3	1.49	1.60
w_4	2.86	2.41
w_5	2.45	2.50

The comparison of the force measured and predicted for a random excitation is shown in Figure 3.14. The force which was predicted was calculated using SWAT with the effective weights determined by the time domain approach. Figure 3.15 compares the force measured to the force which was calculated using SWAT, with the effective weights determined by the frequency domain approach. Finally, the force for an impact loading is compared with the force determined using the effective weights in Figure 3.16.

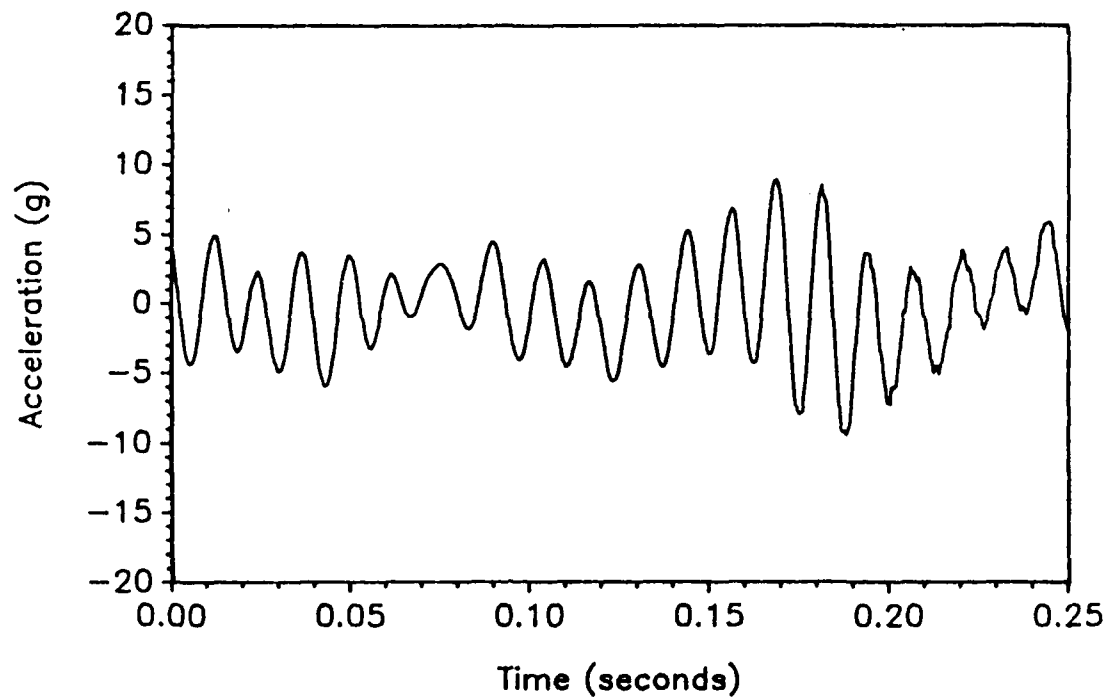


Figure 3.2. Acceleration #1 Record for Continuous Beam.

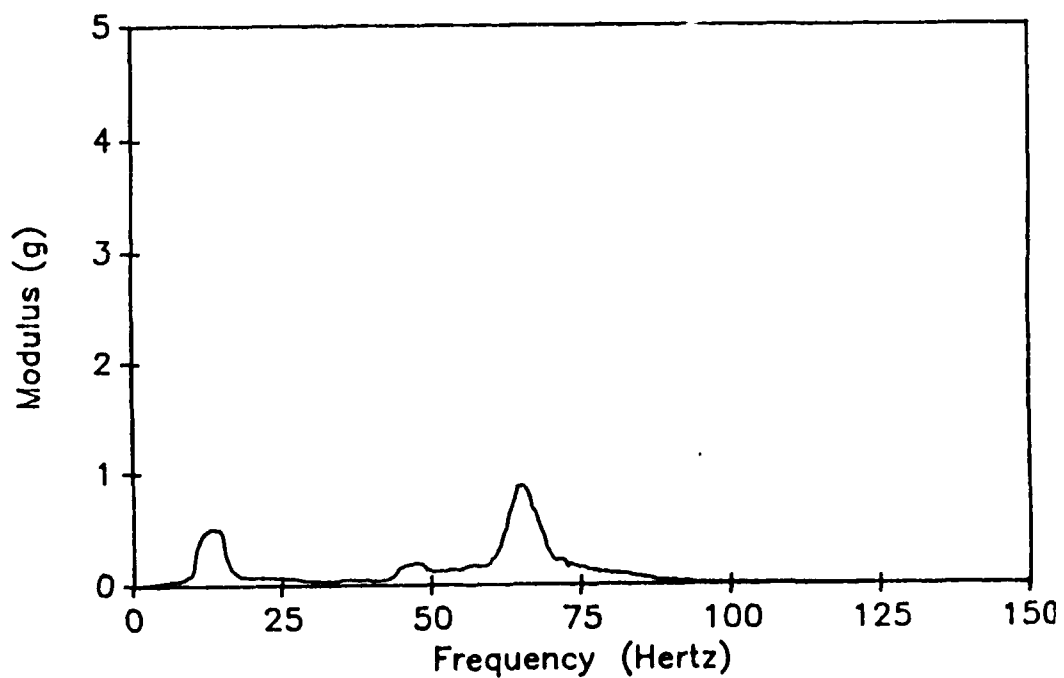


Figure 3.3. Modulus of Acceleration #1 Record for Continuous Beam.

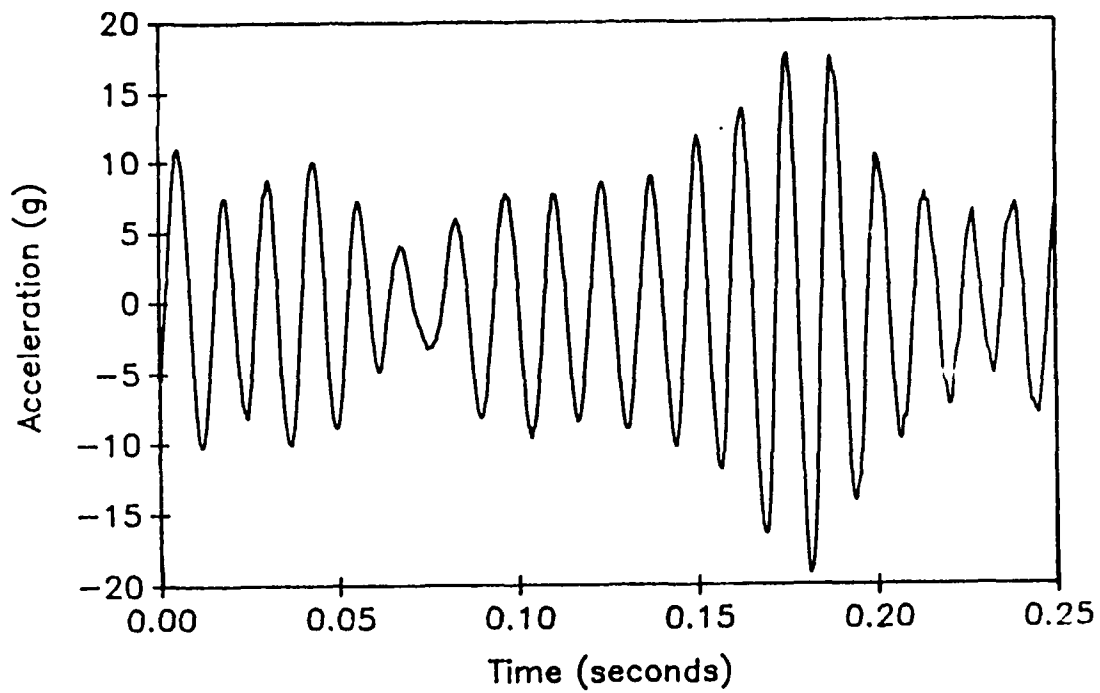


Figure 3.4. Acceleration #2 Record for Continuous Beam.

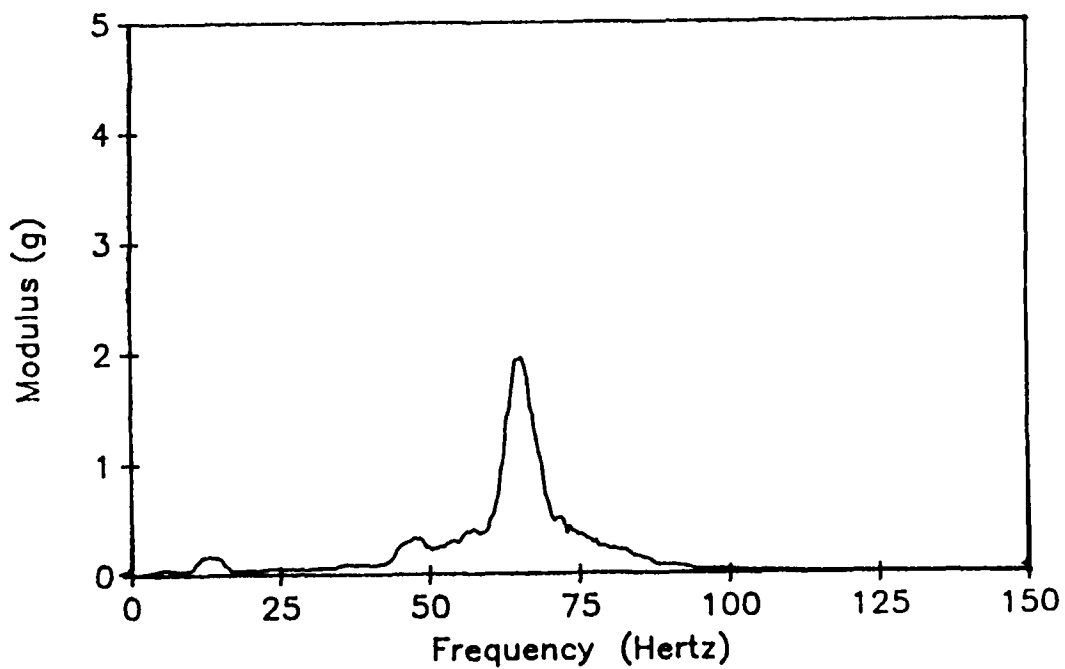


Figure 3.5. Modulus of Acceleration #2 Record for Continuous Beam.

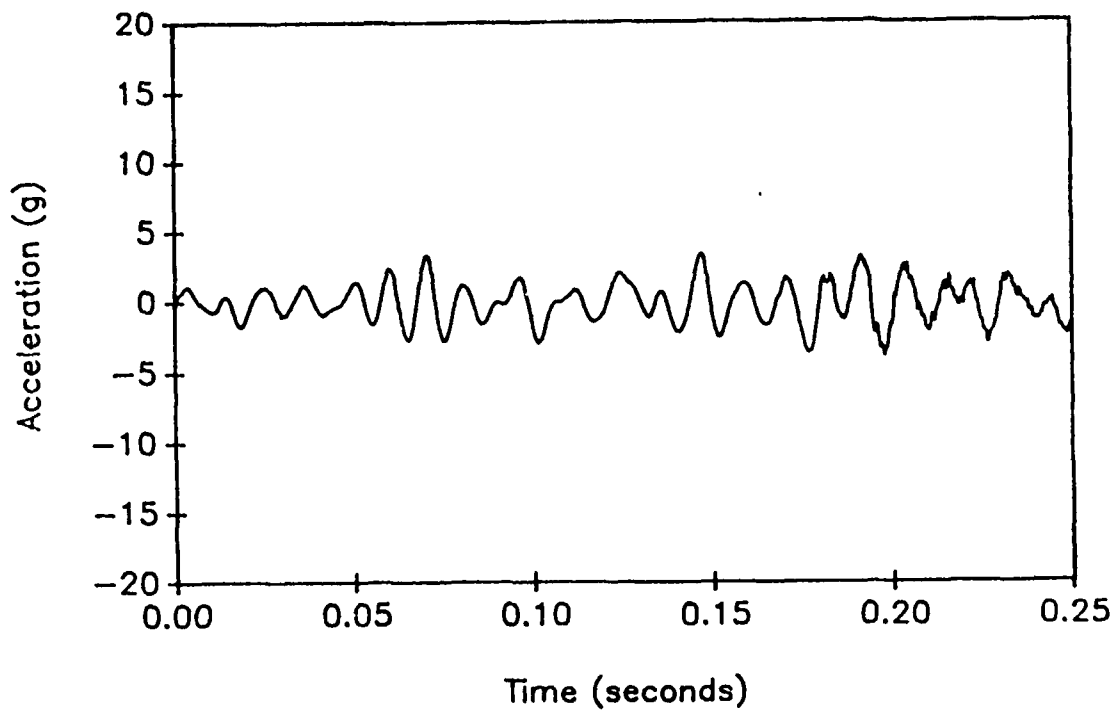


Figure 3.6. Acceleration #3 Record for Continuous Beam.

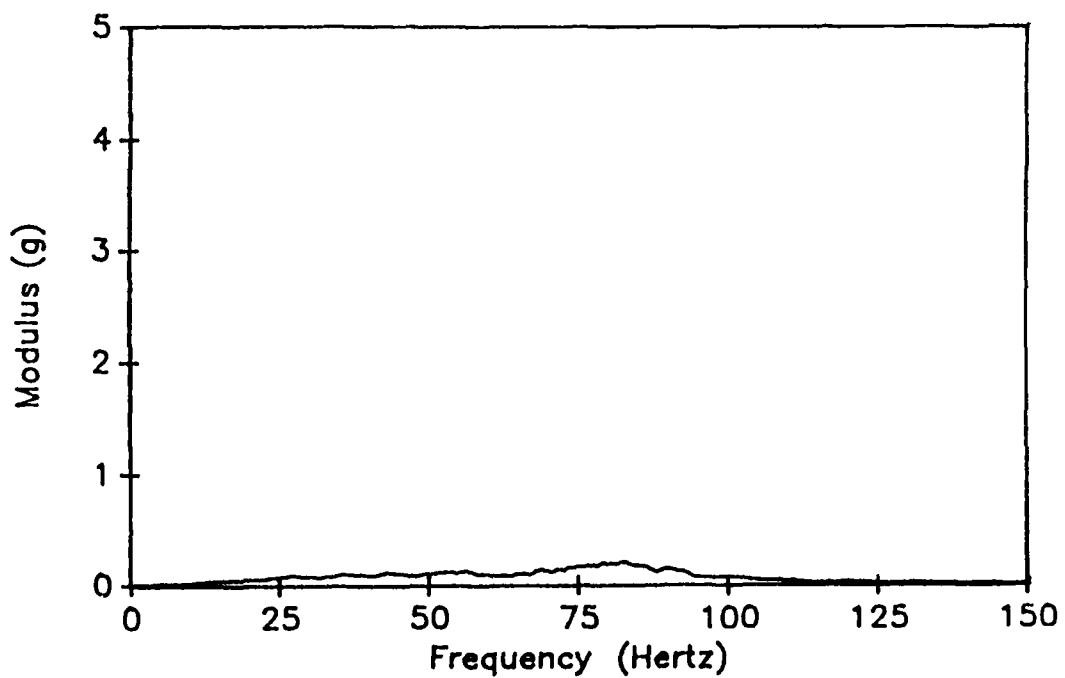


Figure 3.7. Modulus of Acceleration #3 Record for Continuous Beam.

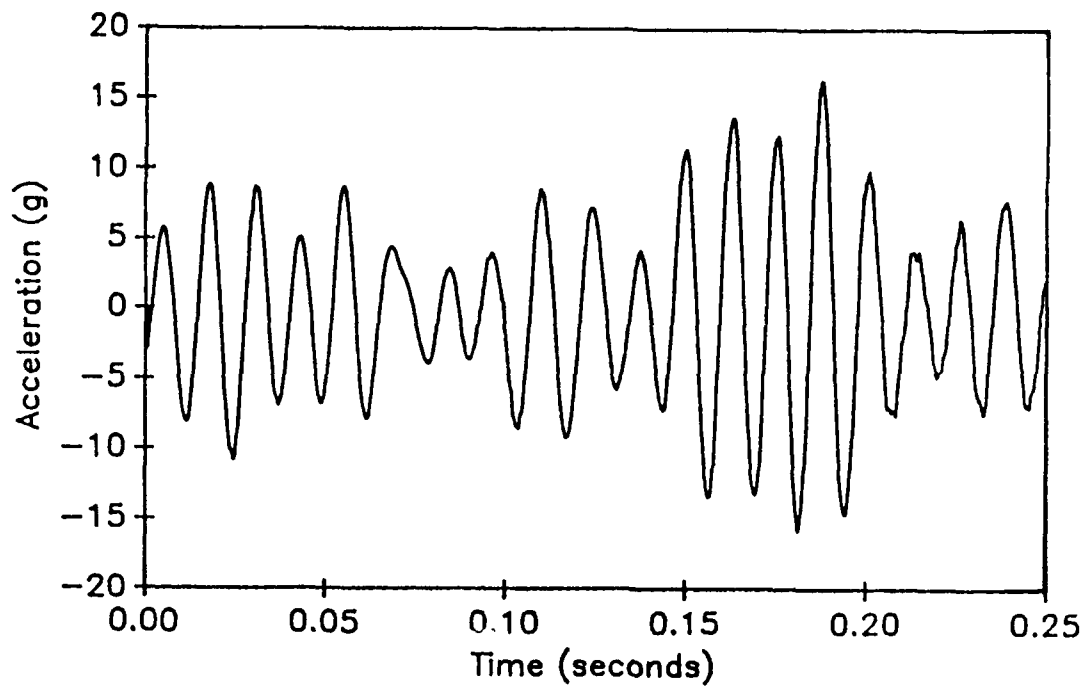


Figure 3.8. Acceleration #4 Record for Continuous Beam.

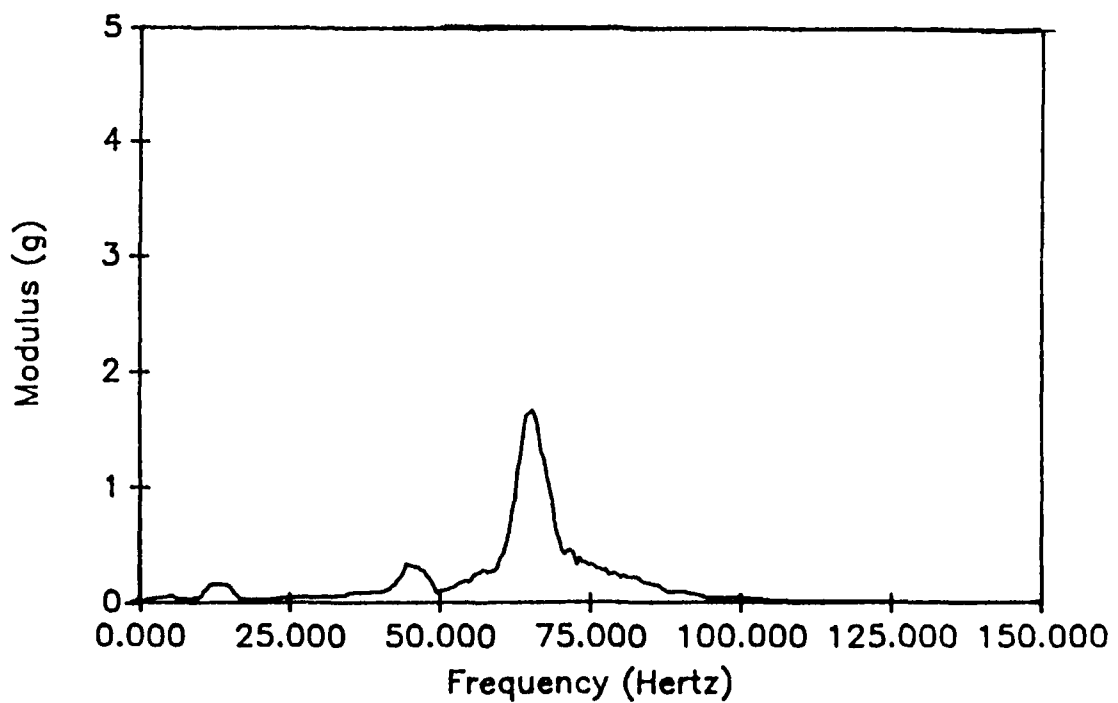


Figure 3.9. Modulus of Acceleration #4 Record for Continuous Beam.

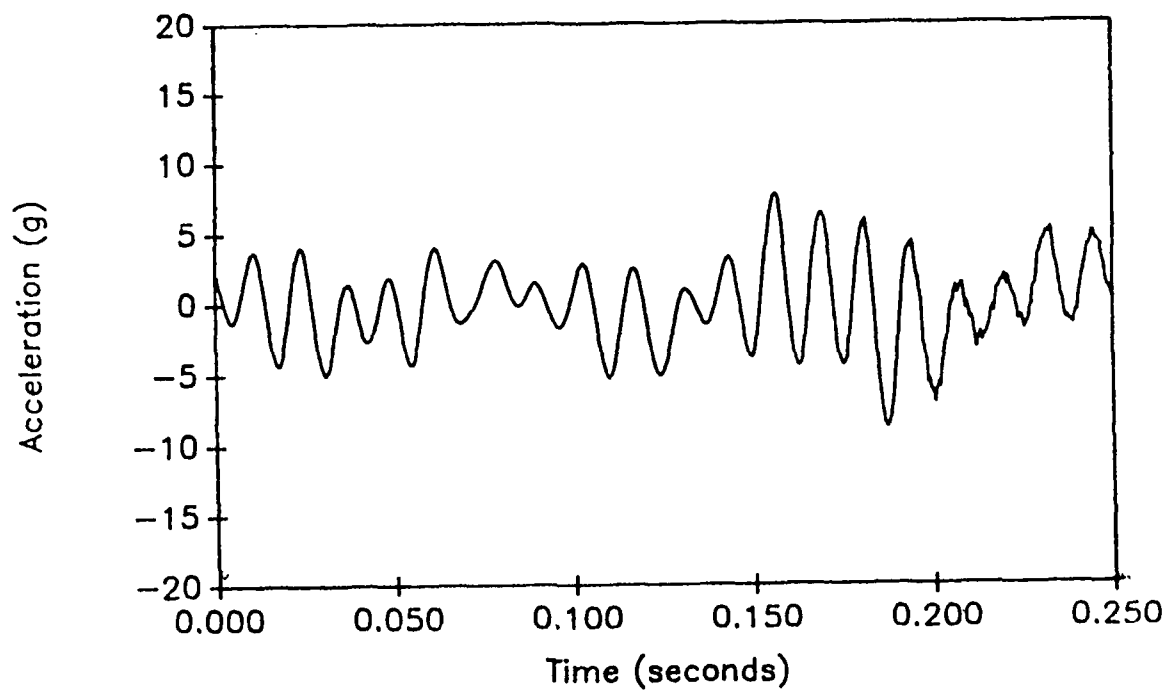


Figure 3.10. Acceleration #5 Record for Continuous Beam.

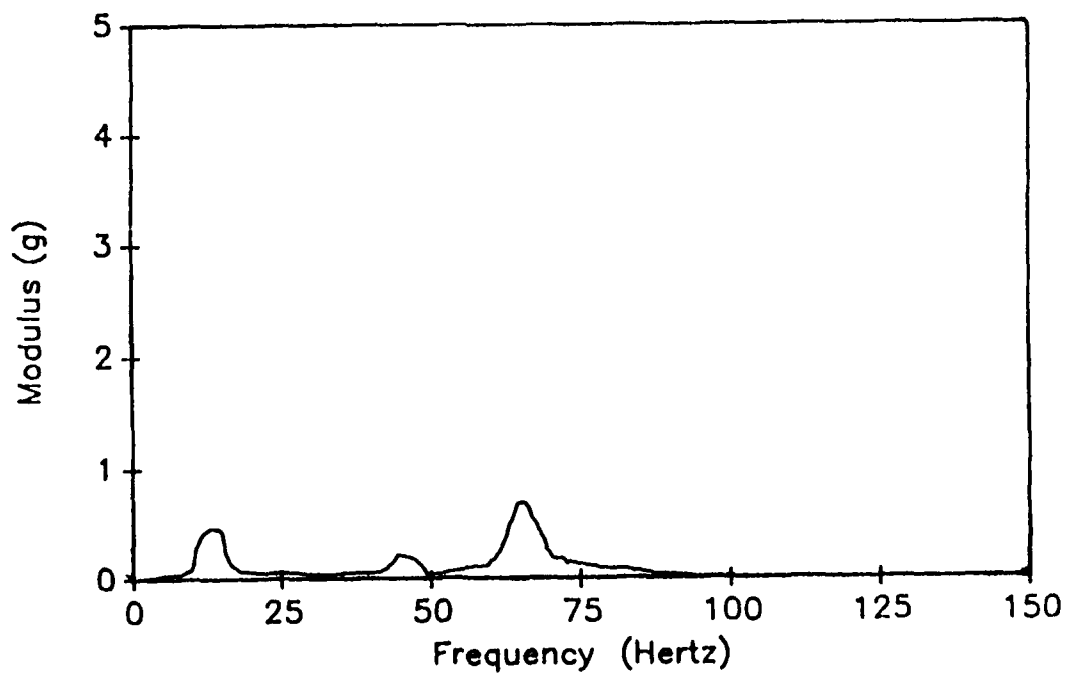


Figure 3.11. Modulus of Acceleration #5 Record for Continuous Beam.

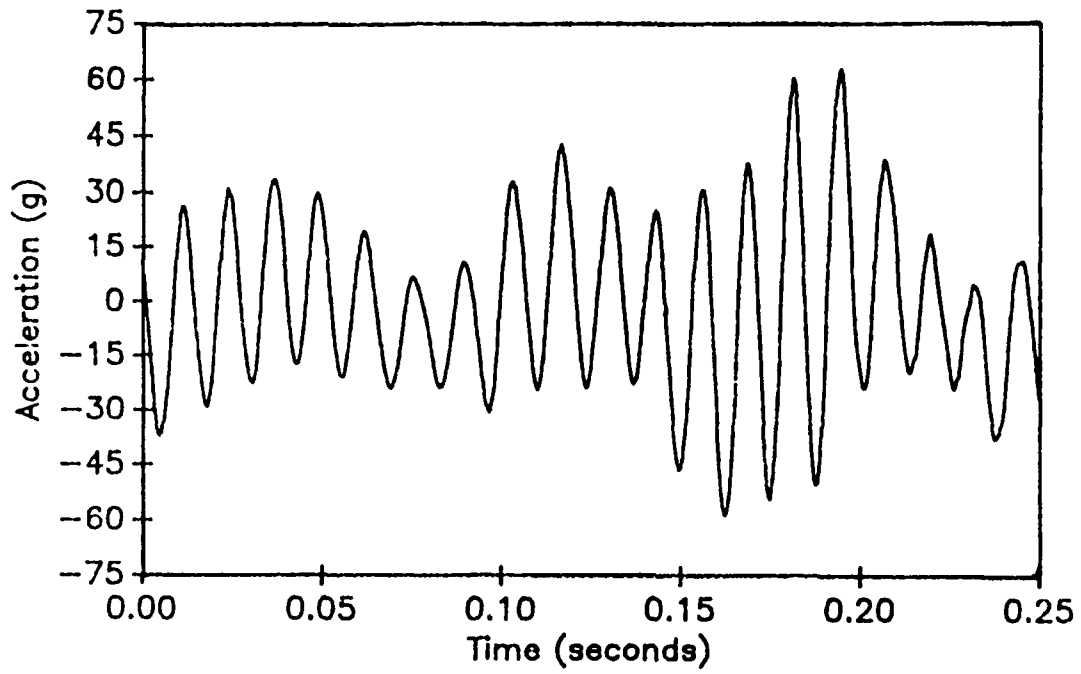


Figure 3.12. Force Record for Continuous Beam.

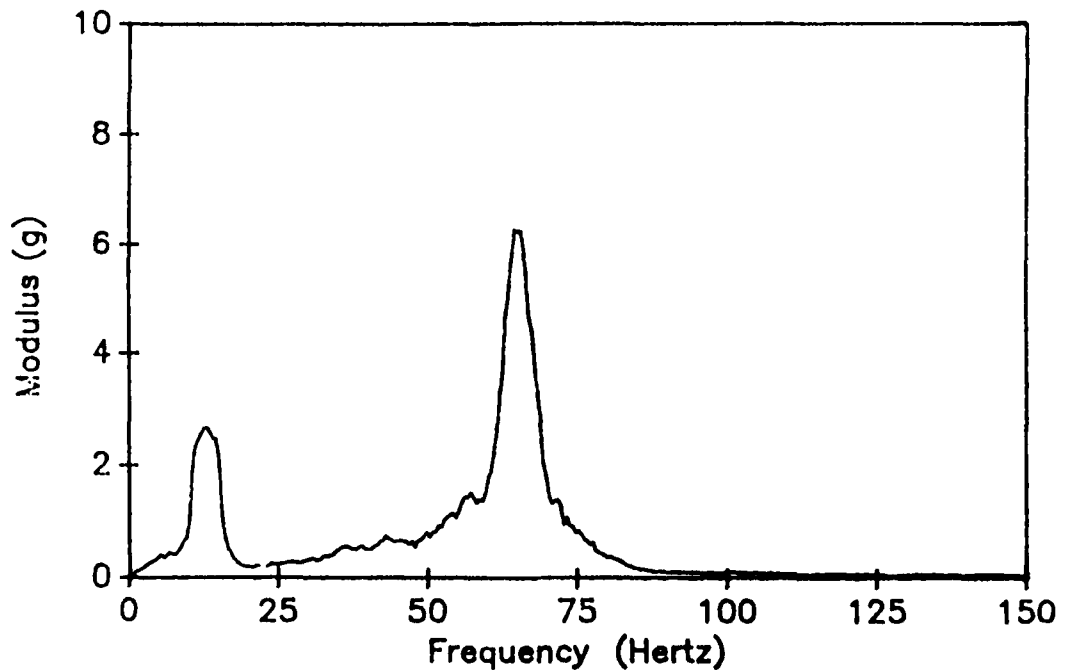


Figure 3.13. Modulus of Force Record for Continuous Beam.

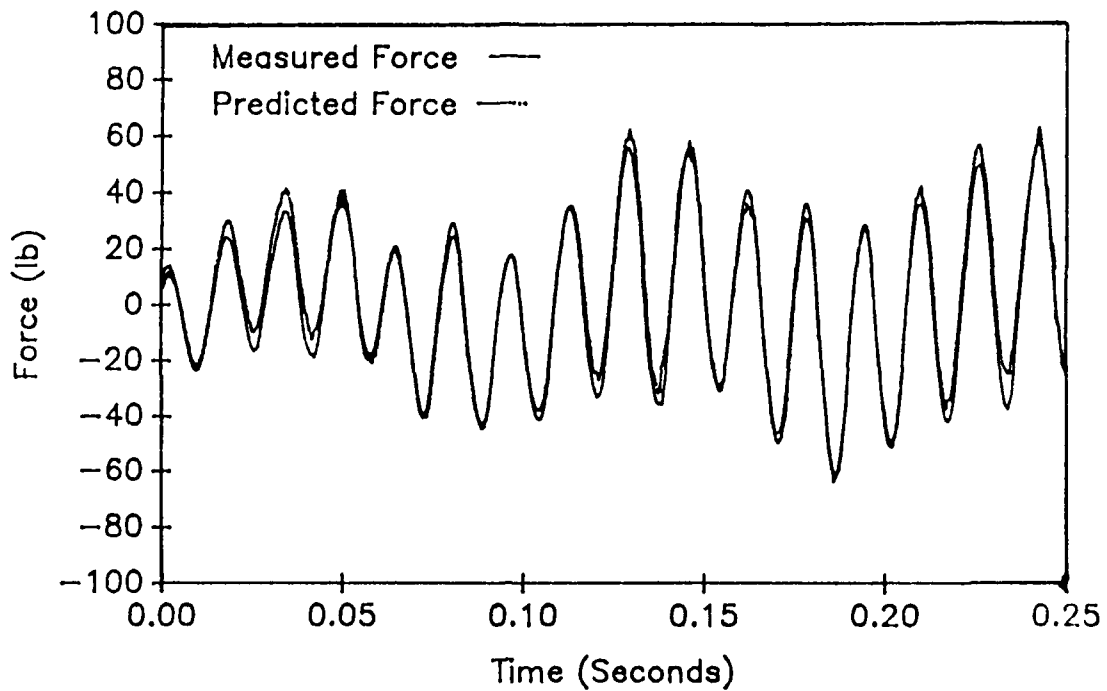


Figure 3.14. Random Excitation Loading Comparison for a Continuous Beam. (Time Domain Approach.)

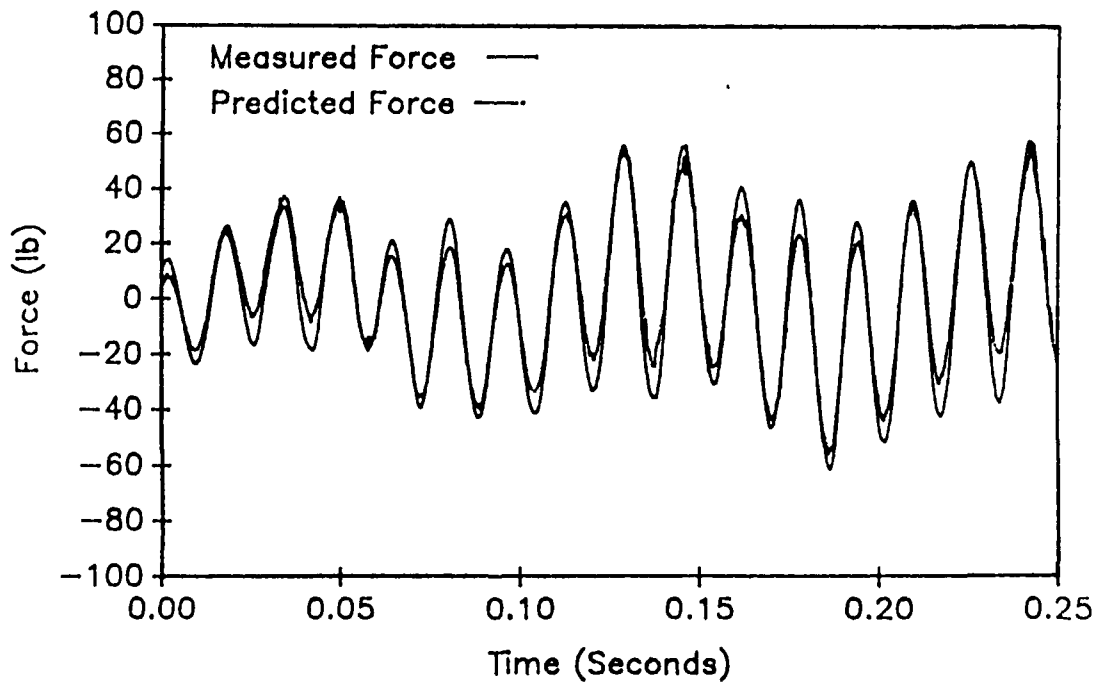


Figure 3.15. Random Excitation Loading Comparison for a Continuous Beam. (Frequency Domain Approach.)

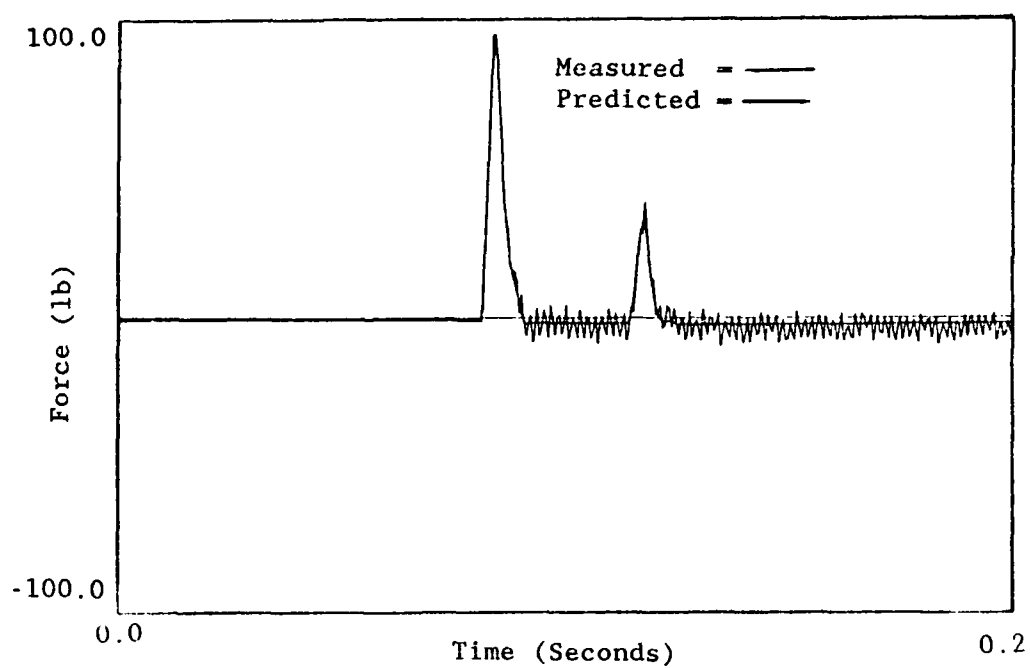


Figure 3.16. Impact Loading Force Comparison for a Continuous Beam.

CHAPTER 4.

FORCE IDENTIFICATION OF NONLINEAR SYSTEMS

4.0. Nonlinear Model.

All structures have some degree of nonlinearity. A structure can be modeled by a linear model; but, when a more exact description of the structure is needed, a nonlinear model may be needed. This chapter describes the application of the sum of the weighted acceleration technique which was used in previous chapters for linear specimens.

The force-mapping technique allows the non-linearity or linearity to be shown in a three-dimensional graph. The determination of the nonlinearity for a test specimen with a nonlinear joint was explored using the force-mapping technique. The three-dimensional plot of the displacement, velocity and force is shown in this chapter. The same type of joint was added to a second test specimen and used with the sum of the weighted acceleration method. The force which was measured is compared with the force that was predicted.

4.1. Force Mapping.

When nonlinear structures are studied for dynamic response, it is important for the engineer to know what types of nonlinearity the structure has. The force-mapping technique described by Crawley and O'Donnel (1986a) is a vital method to determine the type of nonlinearity exhibited by a structure. The method involves graphing the force versus velocity and displacement into a three-dimensional plot.

The graph is a picture of the state of a joint or the system between selected coordinates. The dynamics of a system can be represented by a

second order equation of motion

$$M\ddot{x} + D(x, \dot{x})\dot{x} + K(x, \dot{x})x = F(t) \quad (4.1)$$

where the generalized damping, D , and stiffness, K , can vary as a function of the state. Let

$$F_r(x, \dot{x}) = F(t) - M\ddot{x} = B(x, \dot{x})\dot{x} + K(x, \dot{x})x \quad (4.2)$$

where F_r represents the force transmitted by the joint entirely as a function of the instantaneous state of the system.

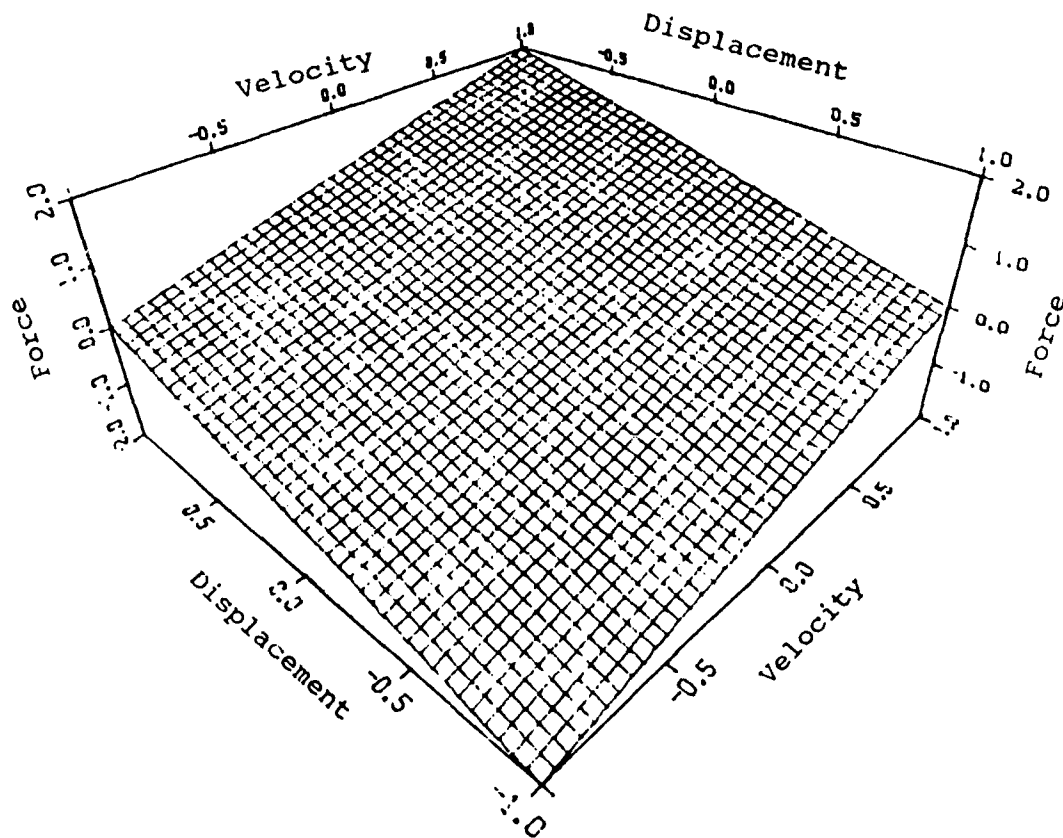


Figure 4.1. Force-Map for a Linear System (K and D are Constants).

Equation (4.2) is the mathematical representation for the forcing-mapping technique when F_r is plotted versus displacement and velocity. If the system is linear, that is $D(x, \dot{x})$ and $K(x, \dot{x})$ are constant, the plot of $F_r(x, \dot{x})$ would be an inclined plane of the type shown in Figure 4.1. The slope of F_r and velocity would be D and the slope of F_r and displacement would be K . Deviation from the linear plot is an indication of nonlinearity for a system. The shape of F_r shows the type of nonlinearity.

F_r can be composed of superposition of the linear and nonlinear combination for the plot. For an example (Crawley, et al. 1986b)

$$F_r = C + K_1 x + D_1 \dot{x} + \dots + K_n x^n + D_n \dot{x}^n + K_{DB} + D_{DB} + F_F \text{sign}(\dot{x}) + g|x| \text{sign}(\dot{x}) \quad (4.3)$$

with

$$K_{DB} = \begin{bmatrix} k_{DB}(x-x_{DB}) \\ 0 \\ k_{DB}(x+x_{DB}) \end{bmatrix}, \quad D_{DB} = \begin{bmatrix} d_{DB}(\dot{x}) \\ 0 \\ d_{DB}(\dot{x}) \end{bmatrix}, \quad \begin{matrix} x_{DB} \leq x \\ x_{DB} \leq x \leq x_{DB} \\ x_{DB} \leq -x_{DB} \end{matrix}$$

where the first three terms represent a constant preload, a linear spring and a linear damper. The next two terms represent higher order springs and dampers, the sixth and seventh terms dead-band springs and dampers, the eighth classical Coulomb friction, and the last, classical material hysteresis damping and displacement dependent friction.

A system with a cubic stiffness which is represented by

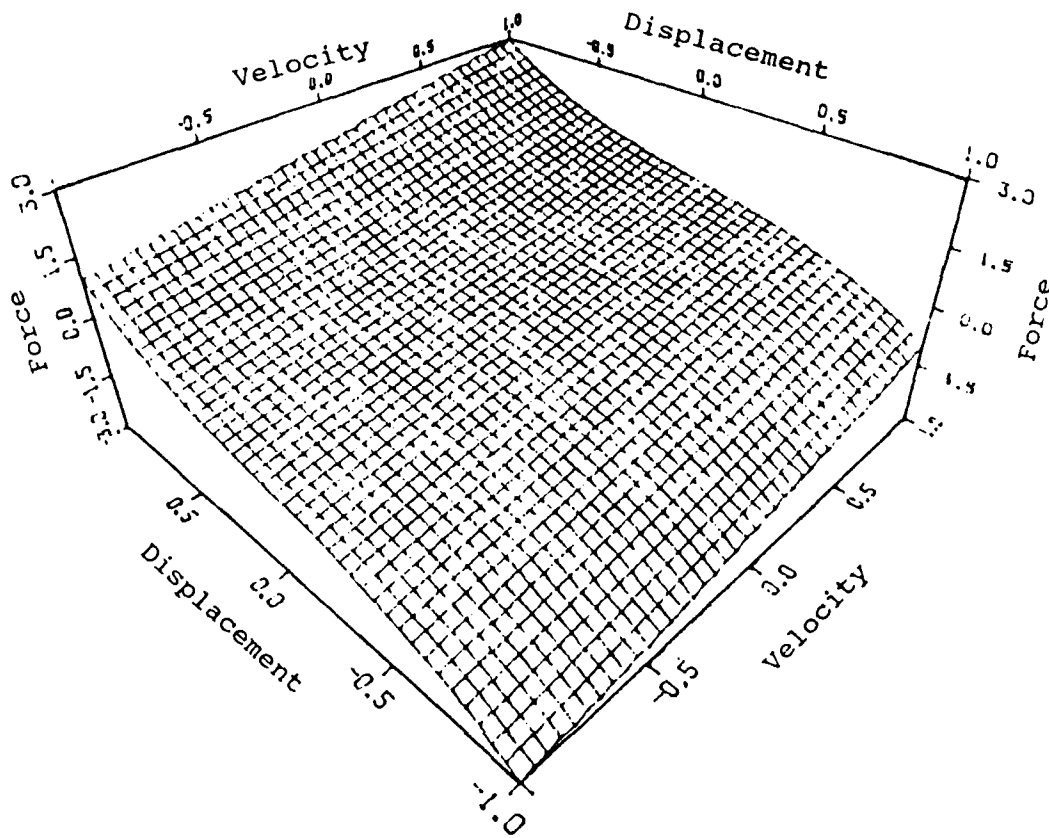


Figure 4.2. Force Map for Cubic Stiffness.

$$M\ddot{x} + D\dot{x} + K_1x + K_2x^3 = F(t) \quad (4.4)$$

is mapped in Figure 4.2. A second system with a cubic damping which is represented by

$$M\ddot{x} + D_1\dot{x} + D_2\dot{x}^3 + Kx = F(t) \quad (4.5)$$

is mapped in Figure 4.3. A third system with both cubic stiffness and damping is represented by

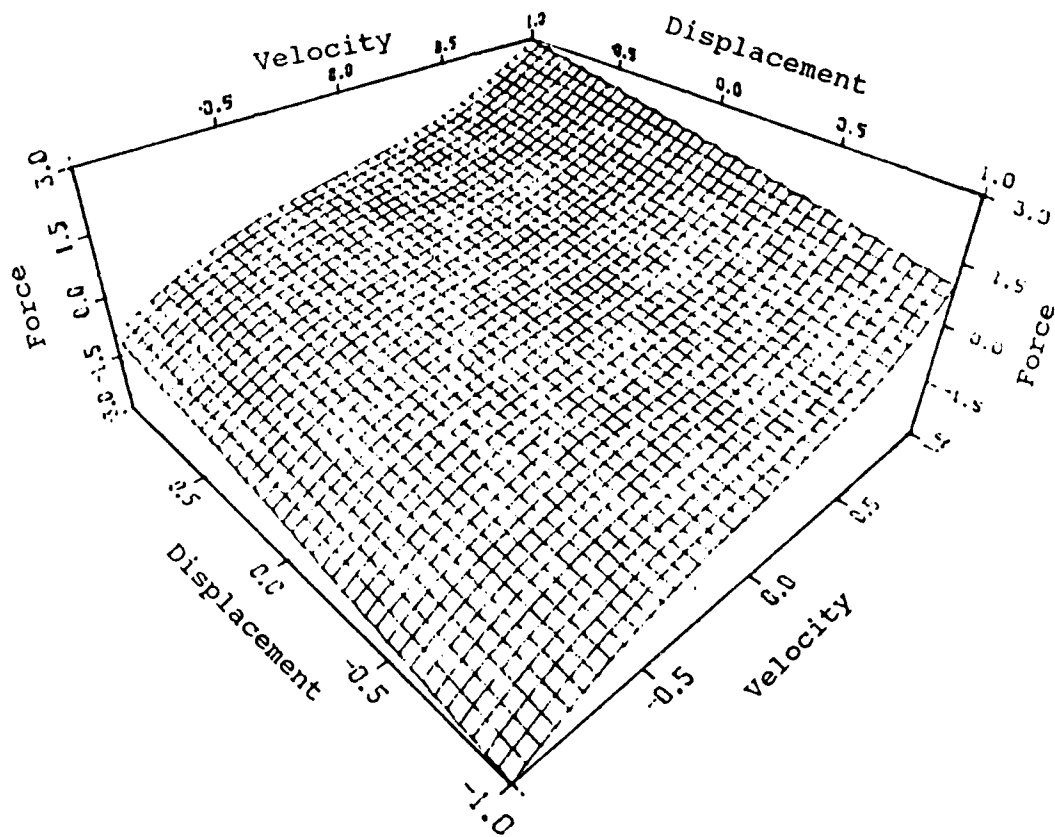


Figure 4.3. Force Map with Cubic Damping.

$$M\ddot{x} + B_1\dot{x} + B_2\dot{x}^3 + K_1x + K_2x^3 = F(t) \quad (4.6)$$

and is mapped in Figure 4.4.

When implementing this method, it is desirable to be able to span the range of the velocity and displacement plane so the measurements are dense enough to plot F_r . One procedure is to use a modulated sinusoidal wave that is monotonically increased in amplitude from zero to some final value.

Crawley and O'Donnell (1986b) demonstrated the technique by computer

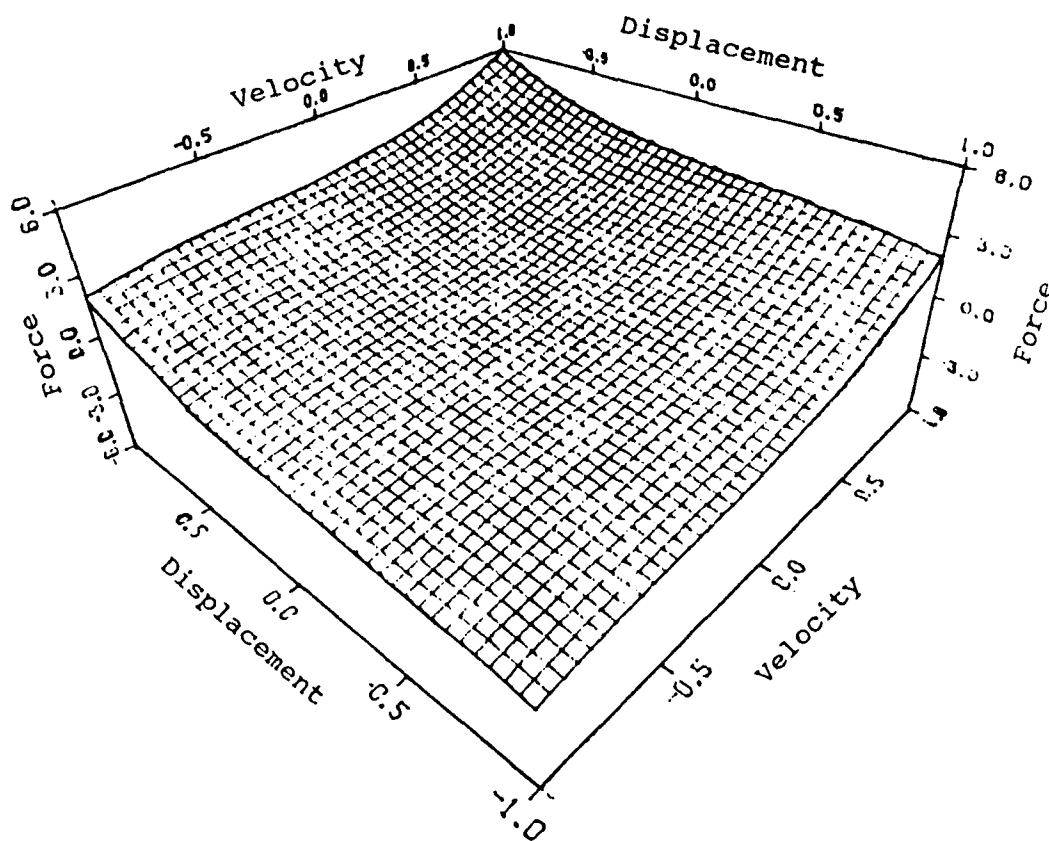


Figure 4.4. Force Map with Both Cubic Damping and Stiffness.

simulated spring mass damped system including a cubic spring, and experimentally for a pinned clevis joint and for a pinned clevis joint with sleeve. The acceleration, displacement and force were measured in their experimental tests. From the acceleration and displacement the velocity was obtained.

To verify and work out the details of this method, an experiment with a linear and a nonlinear test were conducted. The linear experiment setup is shown in Figure 4.5. The specimen was a 1" X 1/4" X 48" steel bar. It was attached to a large mass (assumed fixed in space)

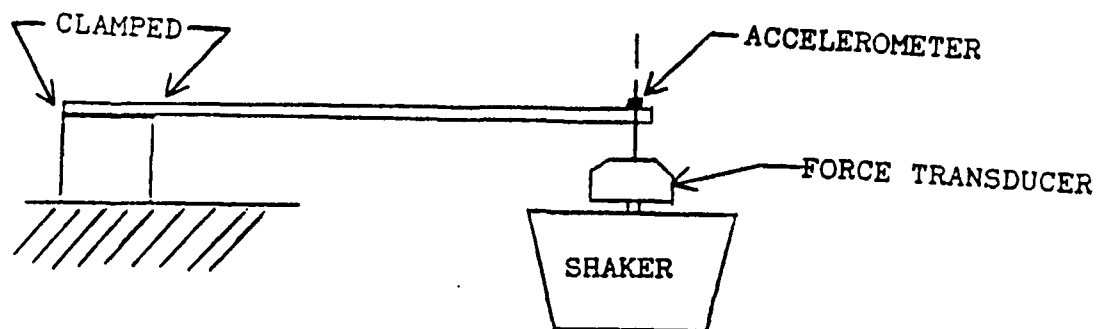


Figure 4.5 Force Mapping Setup for Linear System.

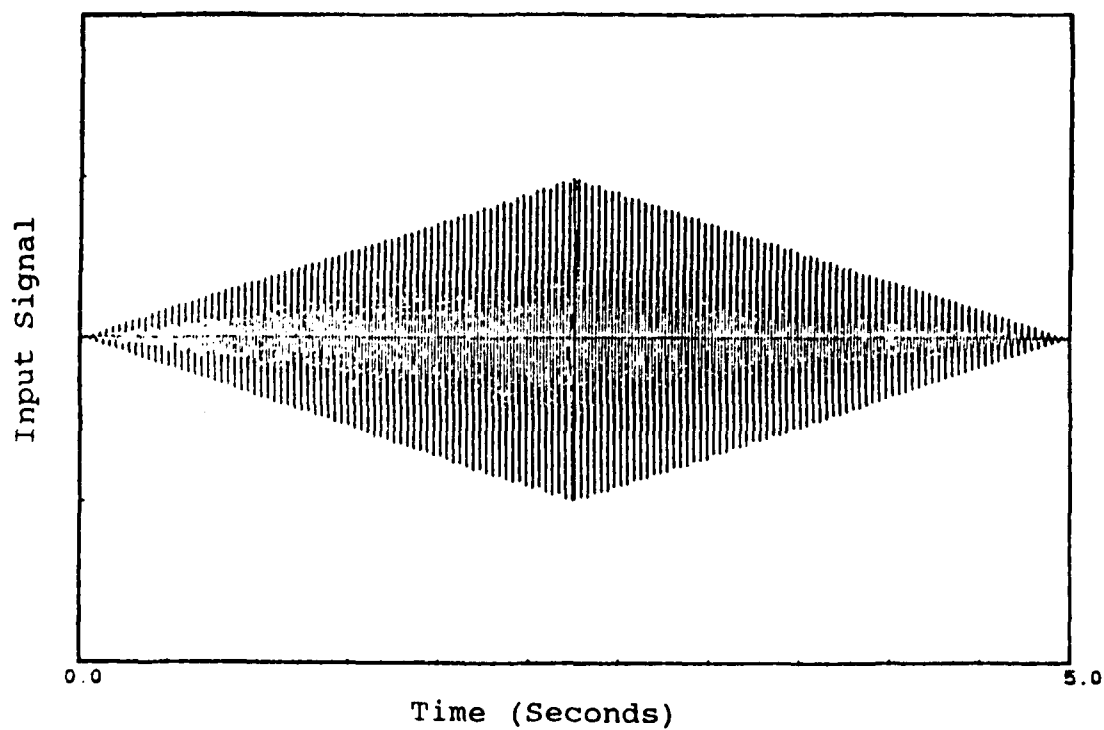


Figure 4.6. Modulating Sinusoidal Wave, Frequency is 30 Hz.

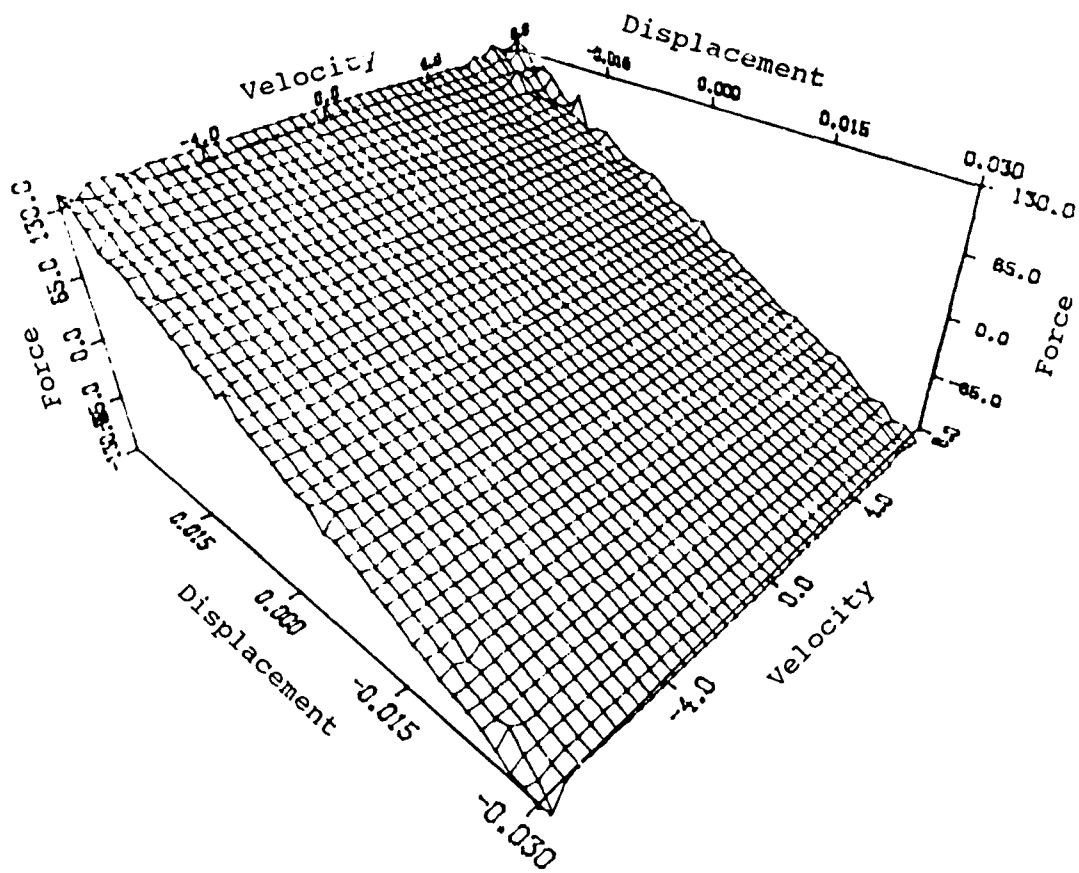


Figure 4.7. F_r versus Velocity and Displacement.

at one end and a dynamic shaker at the other end. The force applied was a modulating 30-Hz sinusoidal wave increasing from 0 to 5 seconds and then decreasing from 5 to 10 seconds at a linear rate shown in Figure 4.6. The results were plotted in a three-dimensional plot shown in Figure 4.7.

The results were comparable with Crawley and O'Donnell (1986b), but had the added feature of double integration of the acceleration to obtain the velocity and displacement.

A second experiment used a nonlinear joint between the fixed mass

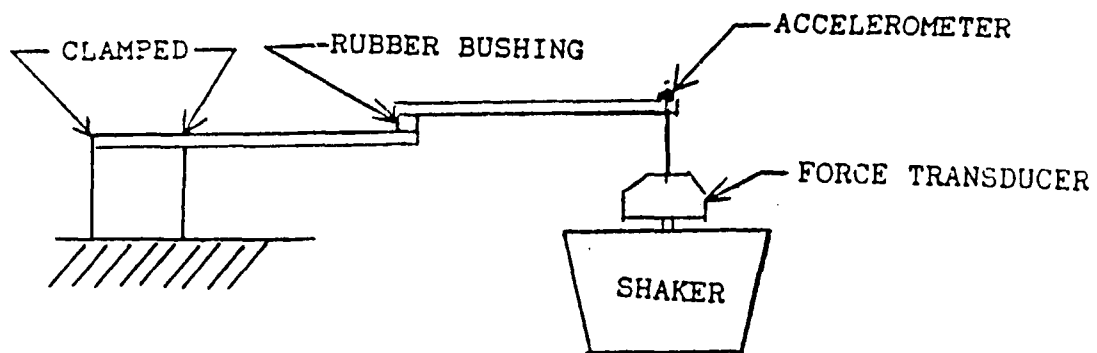


Figure 4.8. Nonlinear Setup.

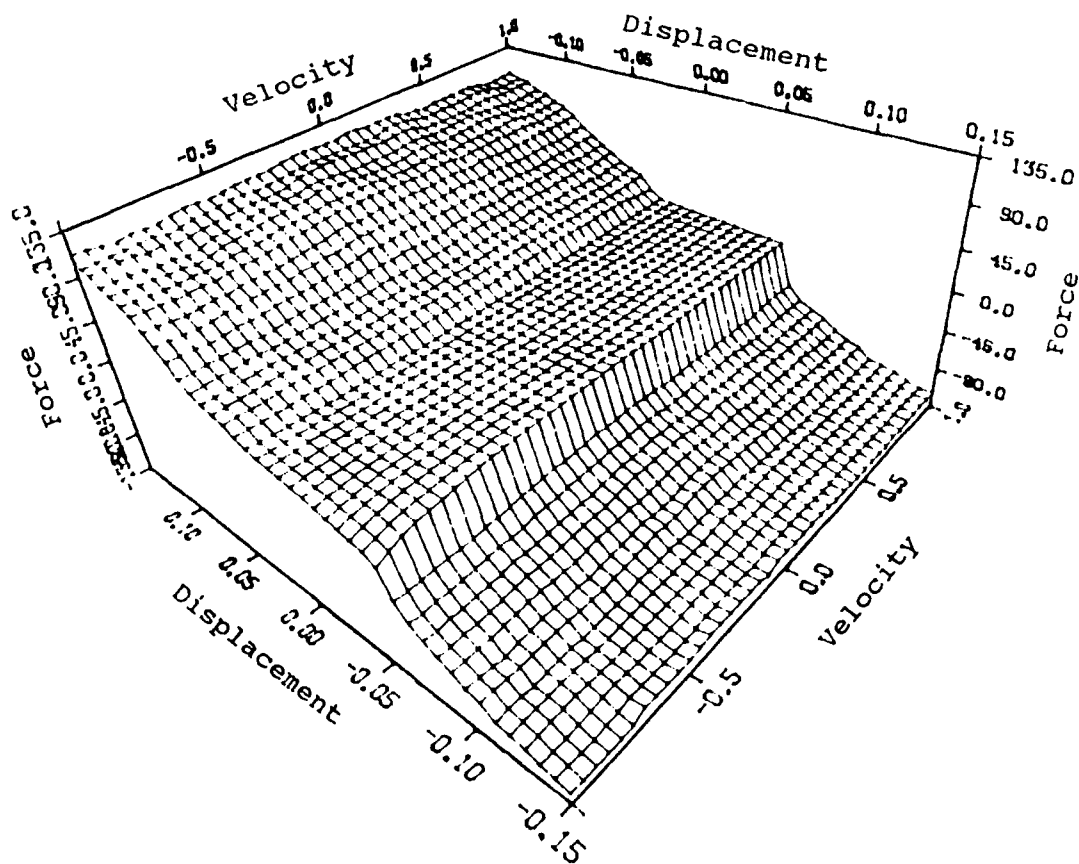


Figure 4.9 F_r versus Velocity and Displacement for the Nonlinear Setup.

and the end that was excited as shown in Figure 4.8. The results of this test are shown in Figure 4.9.

The critical step for the force mapping technique is to obtain the velocity, displacement, and force records. One of the most common measurements for a dynamic structure is acceleration. If true velocity and displacement could be acquired from the acceleration, it would facilitate the force mapping technique. The problems and method of double integration will be discussed in the next section.

4.2 Displacement and Velocity from Acceleration Data

Since the acceleration is commonly the only dynamic measurement taken from a structure, it is desirable to obtain displacement and velocity from the acceleration record. When double integrating the acceleration data, the displacement and velocity produced are not 100 percent accurate. Double integrating of acceleration records is an art that can be learned only by practice. Different methods create different results. Trujillo and Carter (1982) proposed a minimization problem to solve for the velocity and displacement. The method has advantages if all three measurements are taken; it can correct all three to each other by minimizing the error. This method can be used with a minimum of information of the acceleration record, initial and final velocity and displacement values. The fewer the data, the more unrealistic the results could become. The general error equation is

$$E = h \sum_{i=1}^n [(a_i - a_i^*)^2 + \lambda_1 (v_i - v_i^*)^2 + \lambda_2 (d_i - d_i^*)^2] + \lambda_3 v_N^2 + \lambda_4 (d_N - d_N^*)^2 + \lambda_5 e_N^2 \quad (4.7)$$

where

a_i - Estimated Acceleration

a_i^* - Measured Acceleration

v_i - Estimated Velocity

v_i^* - Measured Velocity

d_i - Estimated Displacement

d_i^* - Measured Displacement

λ_i - Weight Factors

e_N - Error average

The weight factors were investigated by Trujillo and Carter (1982). They showed that when the terminal velocity was a small value, increasing the weight factors had negligible effects. The results for minimum data requirements, that is acceleration, initial and final velocity and displacement, have not proven effective in the tests of force mapping because the data are affected by a low frequency noise that obscures the displacement plot.

A second procedure by Stephens and Yao (1985) showed a comprehensive method to double integrate the acceleration. The procedure involves an intuitive feeling of the results. It considers filtering out high and low frequencies of the acceleration that are not supposed to be present. These frequencies are considered to be noise. Second, the acceleration record must be processed to eliminate spikes and linear trends if present. Considering these different problems of double integration of acceleration, an engineer can obtain reasonable results. The engineer's intuition or data processing is used to determine noise problems in the original acceleration record. For example, the problem in the force mapping experimentation was that the acceleration record contained

linear trends and low frequency noise. Low frequency noise has a devastating effect on the displacement. The main problem of eliminating noise is that by eliminating the noise, the desired record can be distorted. It is not uncommon to have 60-Hz noise problems because most equipment runs off a 60-Hz cycle AC current. It is hard to filter off the 60-Hz noise without interfering with frequencies near 60 Hz. Therefore one technique is not a solution to all noise problems.

4.3. Nonlinear Test Setup.

The previous chapters showed that SWAT can adequately predict external forces in linear elastic structures. To verify the SWAT for nonlinear structures, three different test specimens were constructed and randomly excited by an electrodynamic shaker through a drive rod and force transducer connection.

The first two specimens were similar in detail except that a nonlinear joint was added to one. This was to compare a linear and a nonlinear system. (See Figures 4.10 and 4.11, respectively.)

The dimensions for test specimen #1 were

$$L = 21.5 \text{ inches (546.1 mm)}$$

$$m_1 = m_3 = 2.34 \text{ lb (1.04 kg)}$$

$$m_2 = 6.52 \text{ lb (2.90 kg)}$$

$$m_{\text{bar}} = 3.06 \text{ lb (1.39 kg)}$$

$$M_T = 14.26 \text{ lb (6.35 kg)}.$$

The dimensions for test specimen #2 were

$$L = 21.5 \text{ inches (546.1 mm)}$$

$$D = 9.5 \text{ inches (241.30 mm)}$$

$$m_1 = m_3 = 2.34 \text{ lb (1.04 kg)}$$

$$m_2 = 6.52 \text{ lb (2.90 kg)}$$

$$m_{\text{bar}} = 3.39 \text{ lb (1.54 kg)}$$

$$M_T = 14.57 \text{ lb (6.61 kg)}.$$

Each of these two specimens was excited for two test runs with an input signal of a bandwidth of 0-20 Hz. Measurements were recorded for half of the structure due to symmetry. The first test run for each of these two specimens was the same input excitation. The measured accelerations and forces from the first run was used to determine the effective weights. In the second test run the effective weights multiplied by their corresponding accelerations were then compared with the measured force.

Finally, a more complex nonlinear structure was used to verify results. The third test specimen, shown in Figure 4.12, used the acceleration measurements at the four lumped masses to determine four effective weights.

4.4. Nonlinear Test Results.

The results from the first two test specimens are described in detail. Test specimen #1 was considered linear. Figures 4.13 through 4.18 show the raw measurements with their respective transform. The equations formed were

$$\begin{bmatrix} 1.0 & 1.0 & 1.0 \\ -21.5 & 0.0 & 21.5 \\ 8.89 & .48 & 8.89 \end{bmatrix} \begin{Bmatrix} w_1 \\ w_2 \\ w_3 \end{Bmatrix} = \begin{Bmatrix} 14.26 \\ 0.0 \\ 58.73 \end{Bmatrix} \quad (4.8)$$

The third equation was determined from the modulus values. Since $w_1 = w_3$ due to symmetry, Equation (4.8) is rearranged as

$$\begin{bmatrix} 1.0 & 1.0 \\ 8.89 & .48 \end{bmatrix} \begin{Bmatrix} 2w_1 \\ w_3 \end{Bmatrix} = \begin{Bmatrix} 14.26 \\ 58.73 \end{Bmatrix} \quad (4.9)$$

Solving Equation (4.9) yields

$$2w_1 = 6.17 \text{ lb (2.80 kg)} \quad w_1 = 3.09 \text{ lb (1.40 kg)}$$

$$w_2 = 8.09 \text{ lb (3.67 kg)}$$

A comparison of the predicted and measured forces for the second test run is shown in Figure 4.19. The two forces are practically identical.

As shown in Figures 4.20 through 4.27, the test for specimen #2 has similar results. Taking the values from the data and applying the two constraint equations, the reduced equations are

$$\begin{bmatrix} 1.0 & 1.0 \\ 8.51 & .48 \end{bmatrix} \begin{Bmatrix} 2w_1 \\ w_3 \end{Bmatrix} = \begin{Bmatrix} 14.57 \\ 18.53 \end{Bmatrix} \quad (4.10)$$

Solving Equation (4.10) yields

$$2w_1 = 1.44 \text{ lb (0.65 kg)} \quad w_1 = 0.72 \text{ lb (0.33 kg)}$$

$$w_2 = 13.13 \text{ lb (5.96 kg)}$$

The predicted force using these effective weights for the second test run was compared with the measured force shown in Figure 4.28. The comparison shows good correlation between the waveforms.

For test specimen #3, the same technique was applied to determine the effective weights. The four effective weights calculated were

$$w_1 = 4.02 \text{ lb (1.83 kg)}$$

$$w_2 = 5.10 \text{ lb (2.32 kg)}$$

$$w_3 = 6.58 \text{ lb (2.99 kg)}$$

$$w_4 = 5.06 \text{ lb (2.30 kg)}$$

This specimen was more complex and excited with a wider and stronger excitation. However, even with these changed parameters, the waveform was captured with the effective weights multiplied by their associated accelerations. Figure 4.29 shows the predicted and measured force for an independent test run.

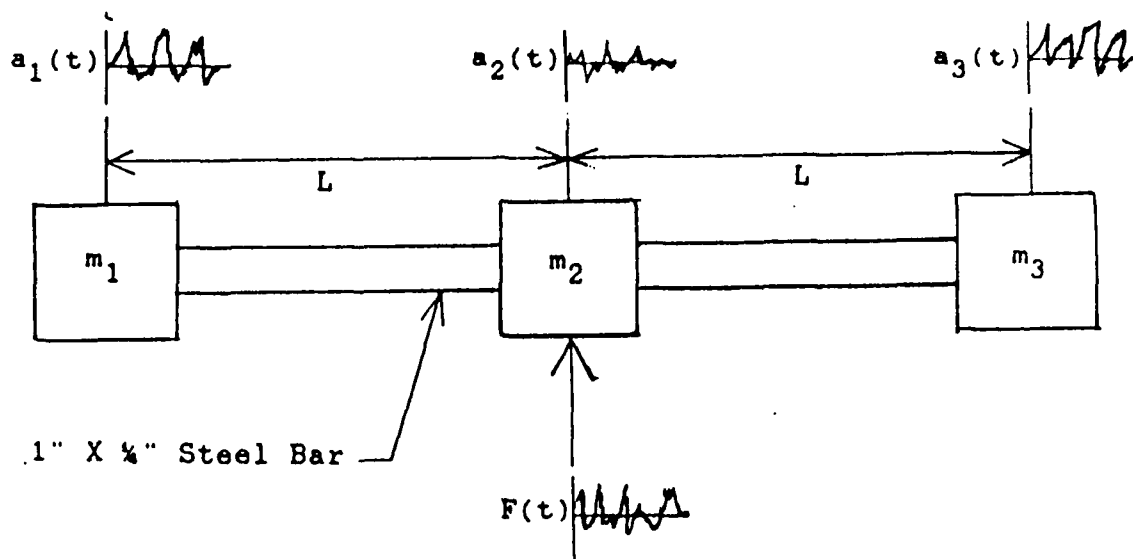


Figure 4.10. Test Specimen Number 1.

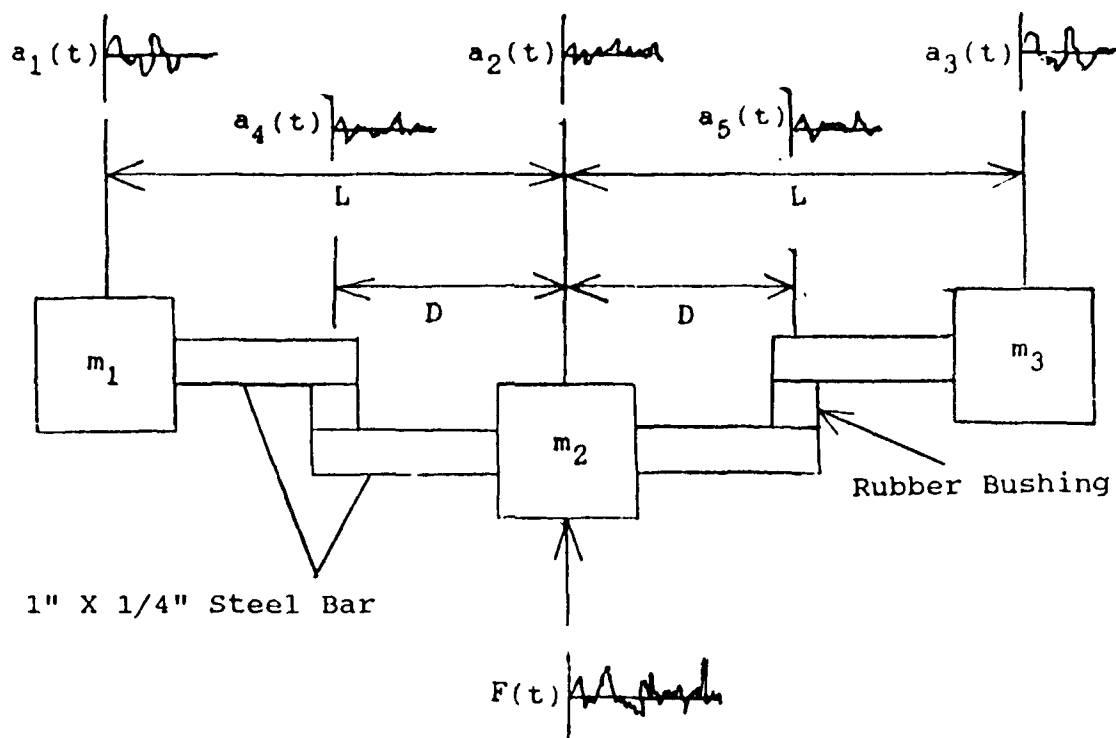


Figure 4.11. Test Specimen Number 2.

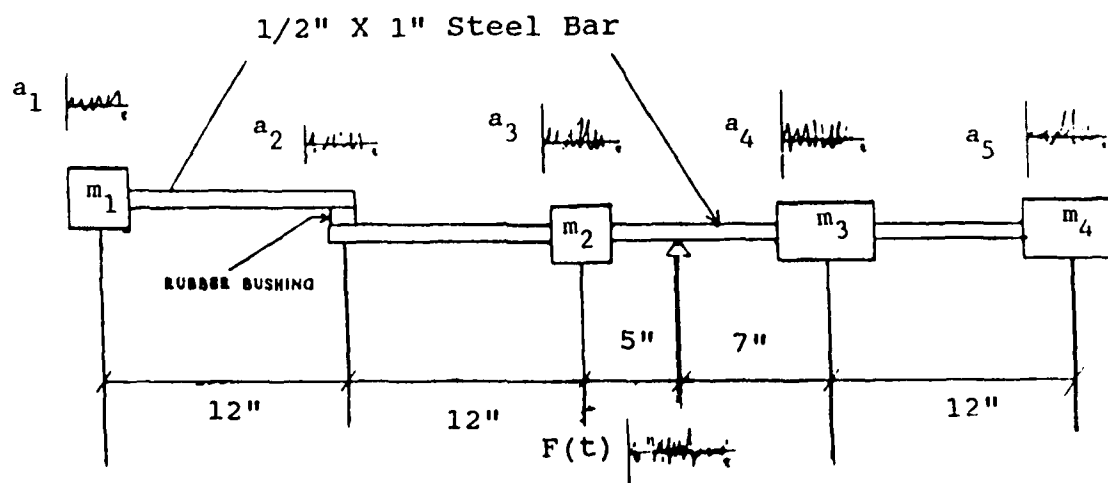


Figure 4.12. Test Specimen Number 3.

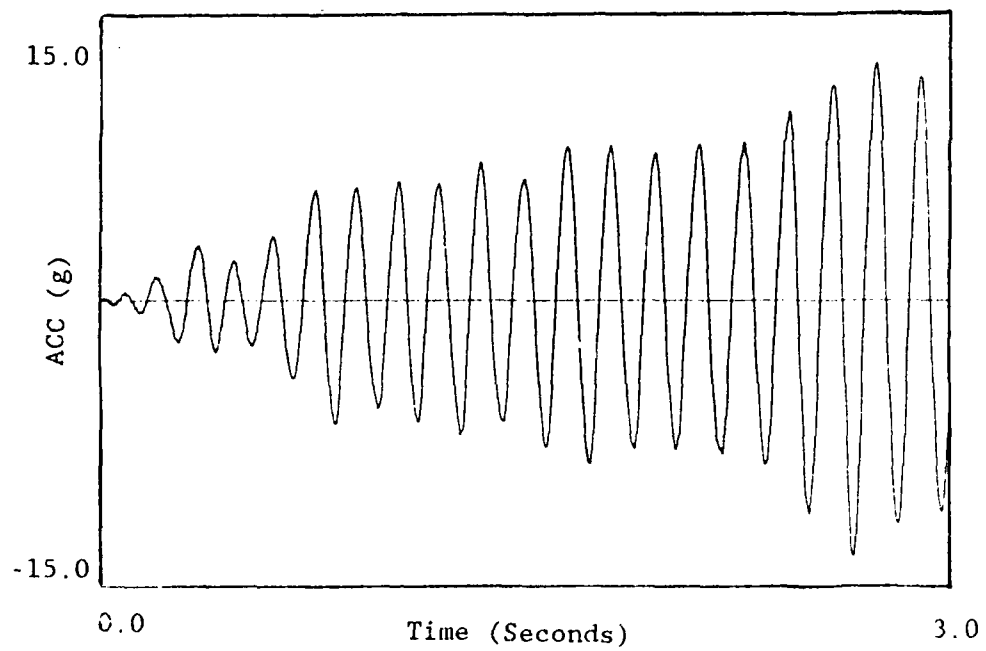


Figure 4.13. Acceleration at the End, $a_1(t)$, for Test Specimen #1, Run #1.

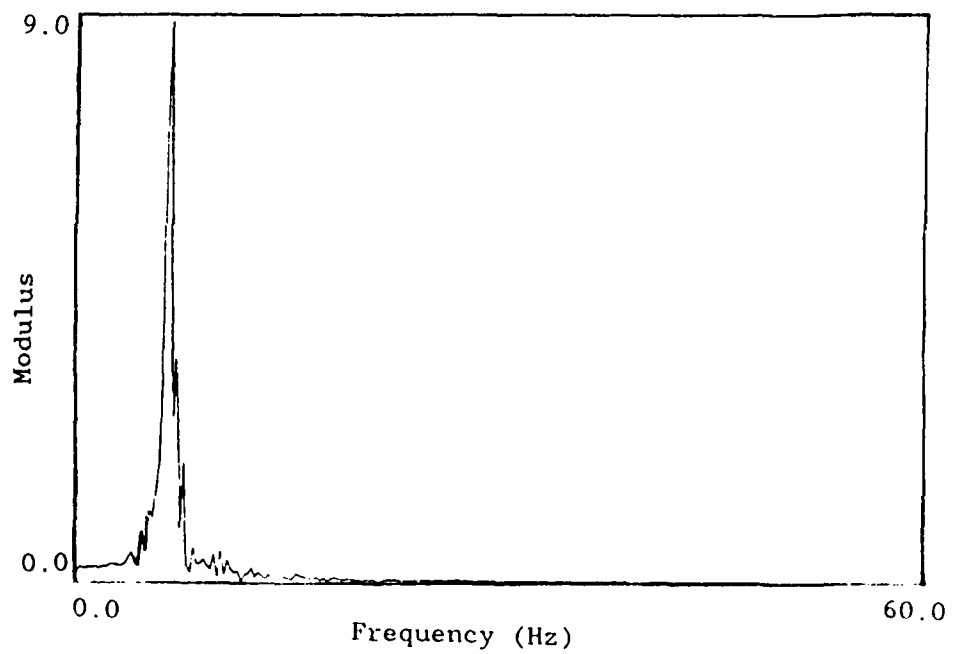


Figure 4.14. Modulus of Acceleration at the End, $a_1(t)$, for Test Specimen #1, Run #1.

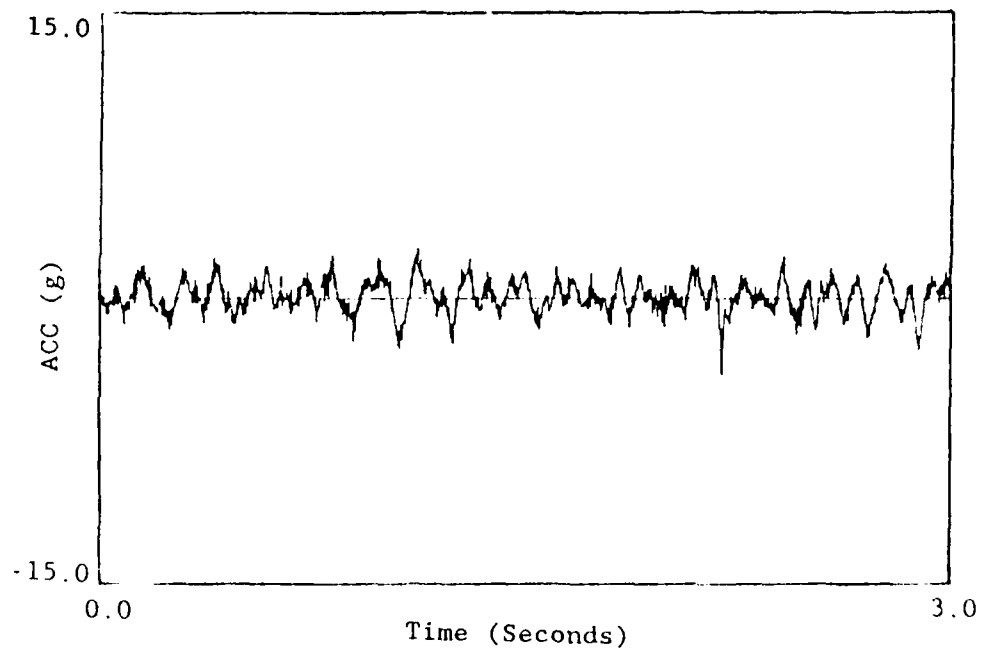


Figure 4.15. Acceleration at the Center, $a_2(t)$, for Test Specimen #1, Run #1.

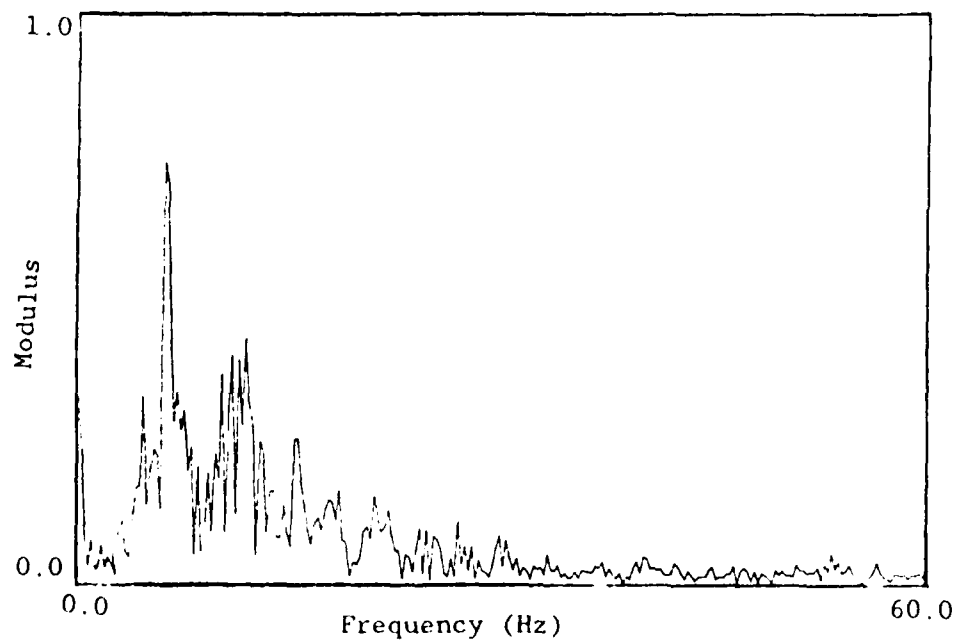


Figure 4.16. Modulus of Acceleration at the Center, $a_2(t)$, for Test Specimen #1, Run #1.

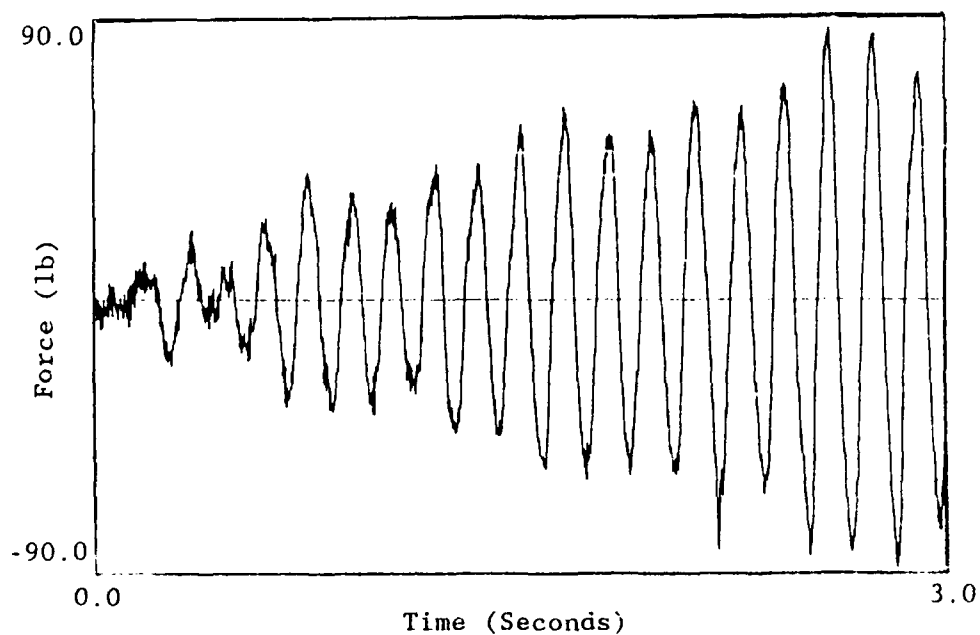


Figure 4.17. Measured Force for Test Specimen #1, Run #1.

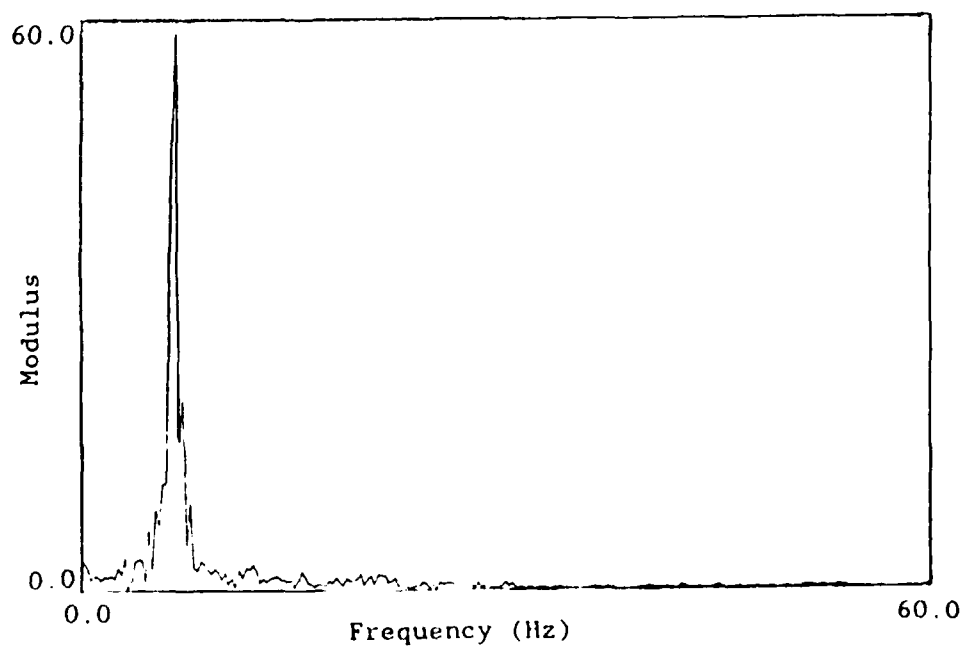


Figure 4.18. Modulus of Force for Test Specimen #1, Run #1.

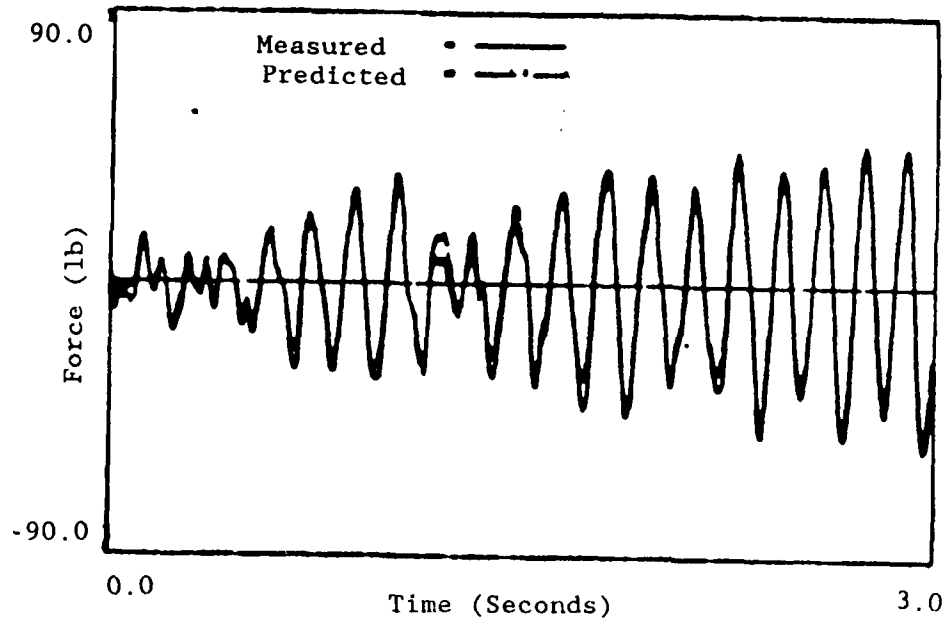


Figure 4.19. Predicted and Measured Force for Test Specimen #1, Run #2.

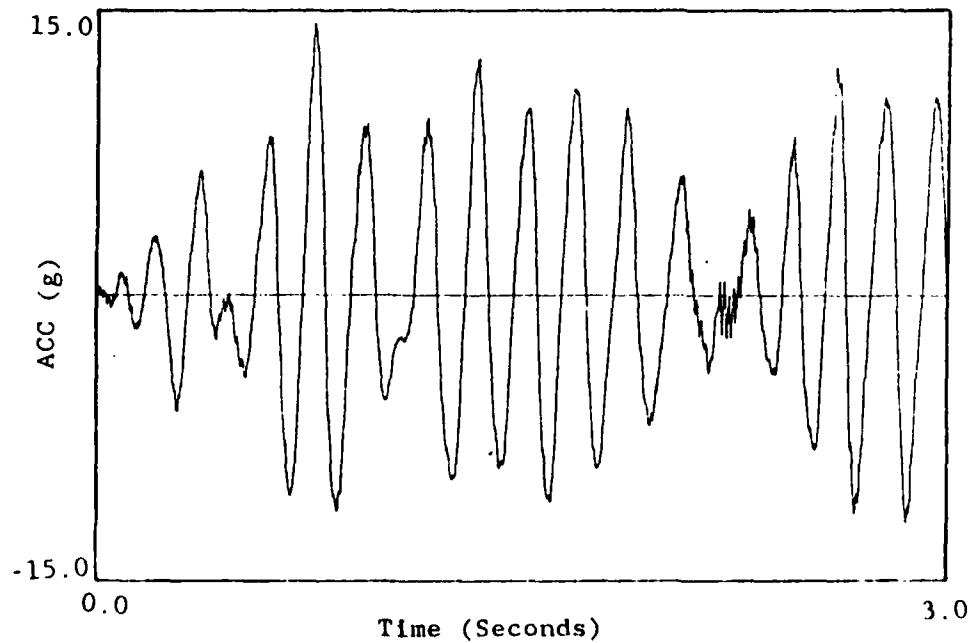


Figure 4.20. Acceleration at the End, $a_1(t)$, for Test Specimen #2, Run #1.

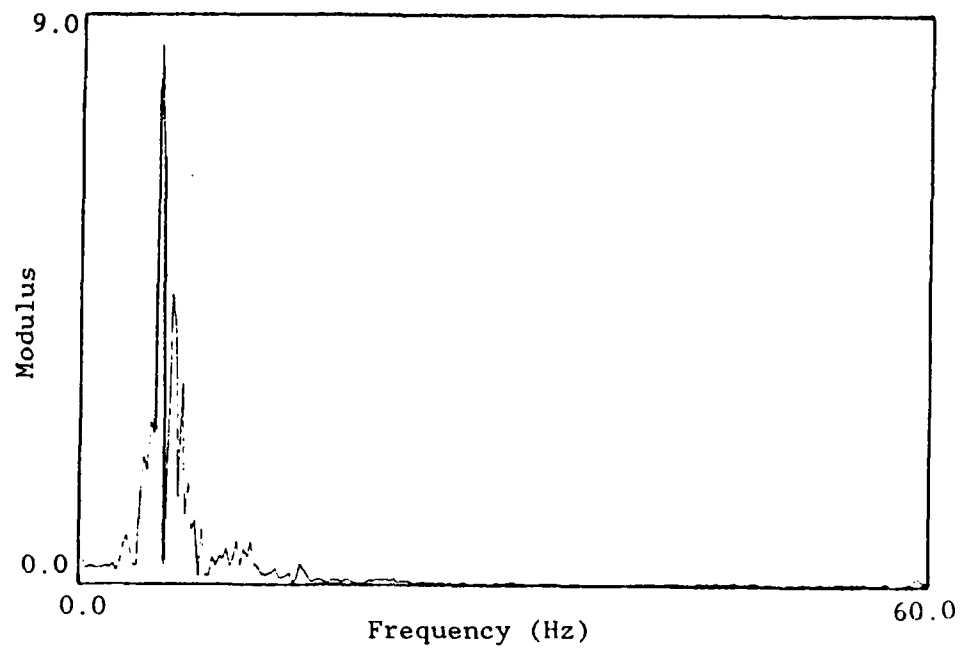


Figure 4.21. Modulus of Acceleration at the End, $a_1(t)$, for Test Specimen #2, Run #1.

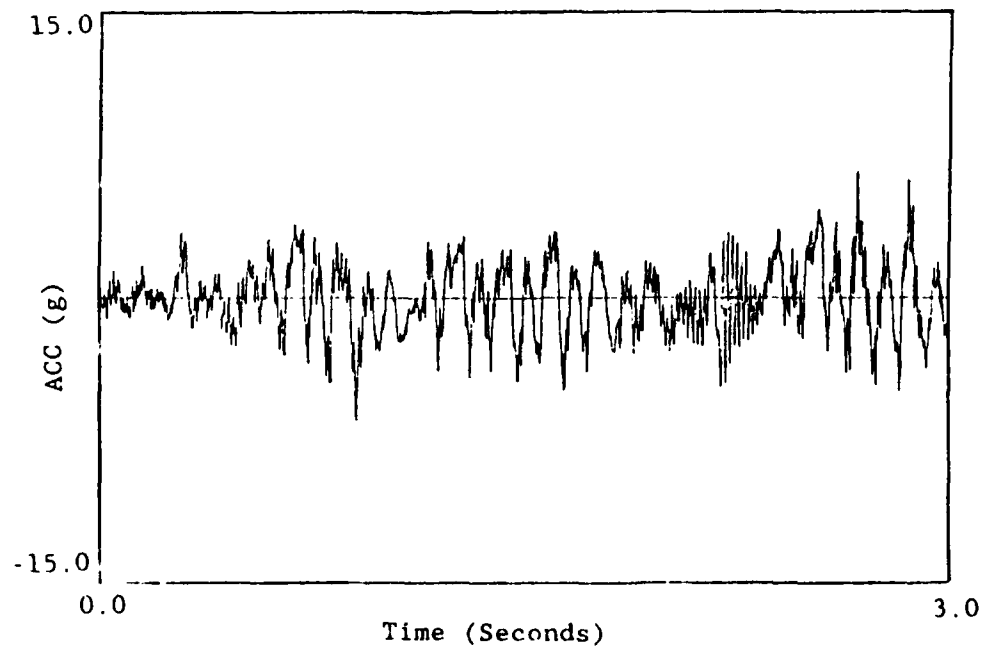


Figure 4.22. Acceleration at the Joint, $a_2(t)$, for test specimen #2, Run #1.

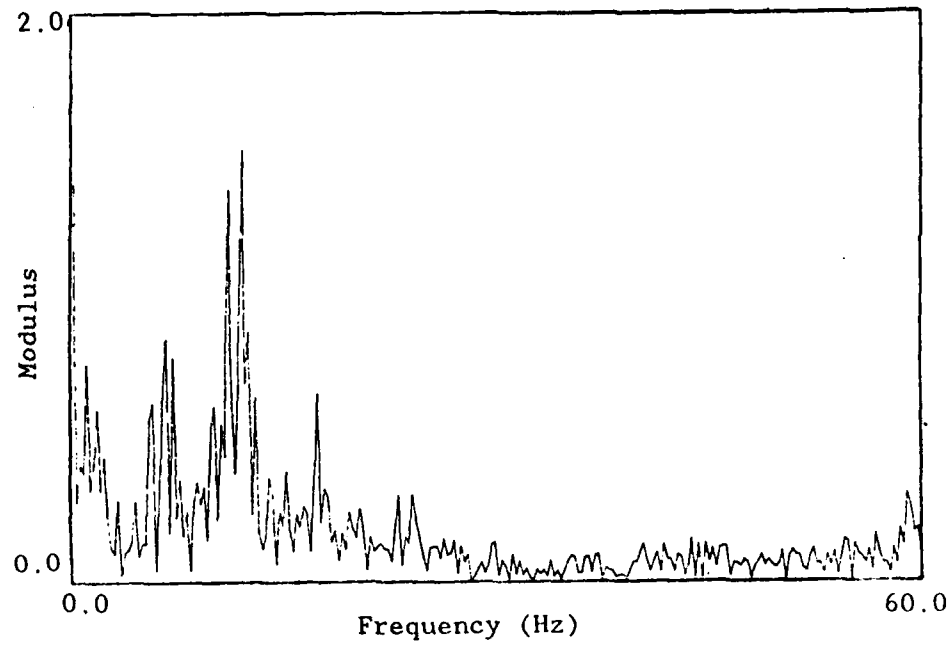


Figure 4.23. Modulus of Acceleration at the Joint, $a_2(t)$, for Test Specimen #2, Run #1.

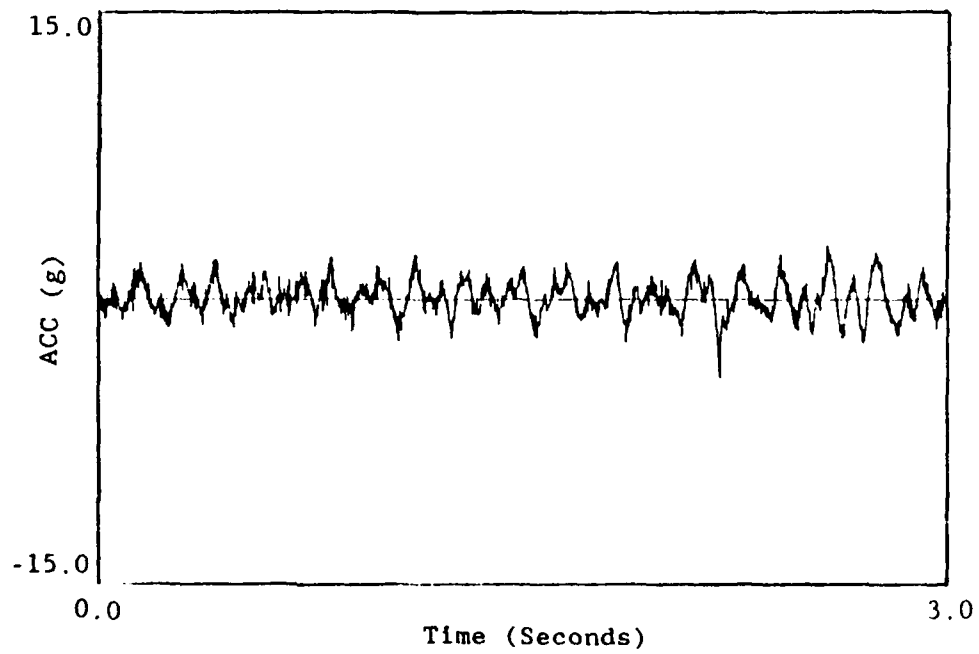


Figure 4.24. Acceleration at the Center, $a_3(t)$, for Test Specimen #2, Run #1.

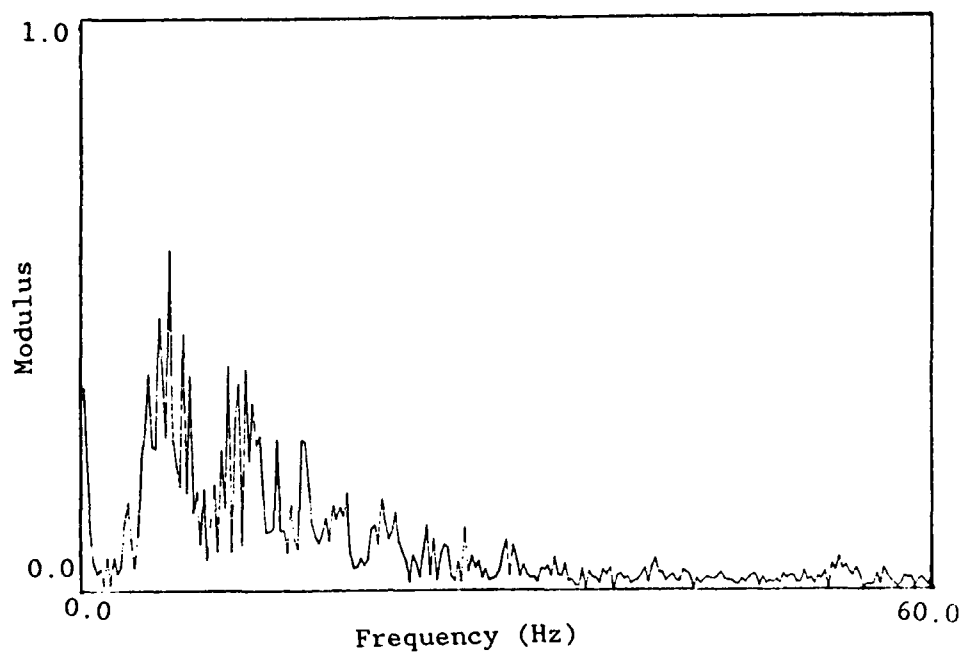


Figure 4.25. Modulus of Acceleration at the Center, $a_3(t)$, for Test Specimen #2, Run #1.

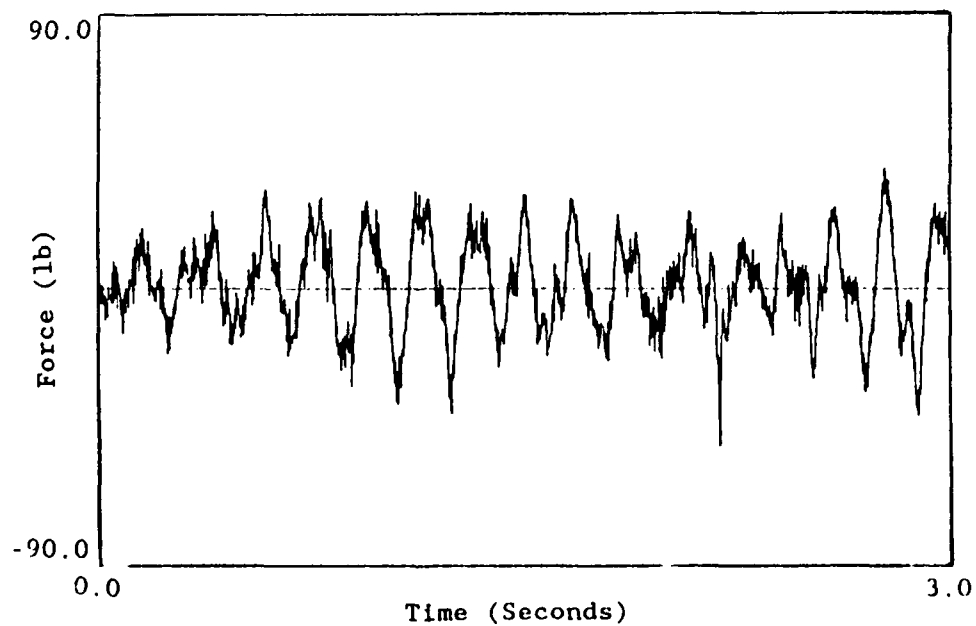


Figure 4.26. Measured Force for Test Specimen #2, Run #1.

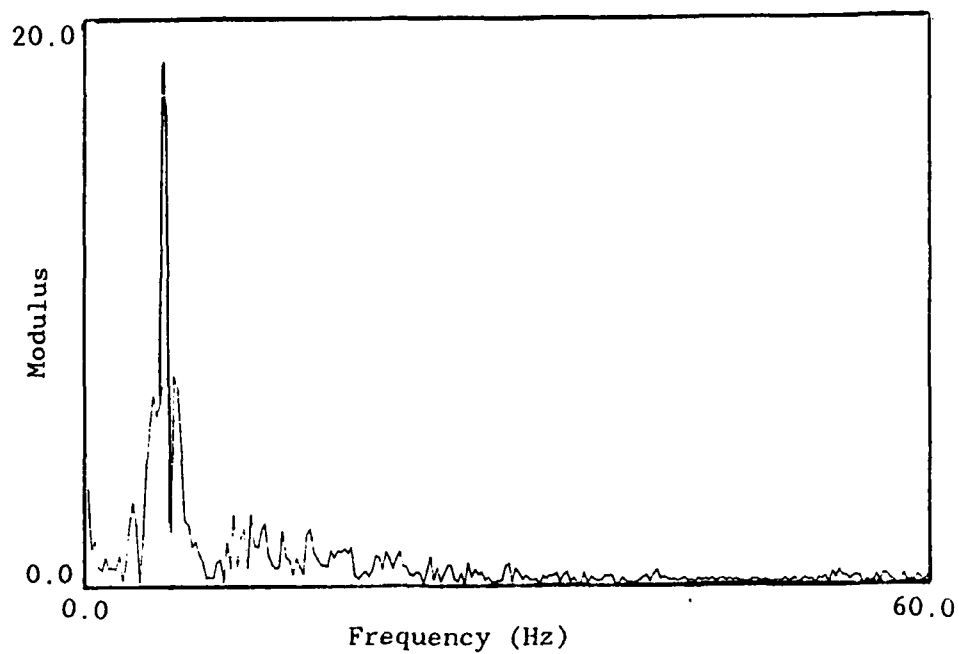


Figure 4.27. Modulus of Force for Test Specimen #2, Run #1.

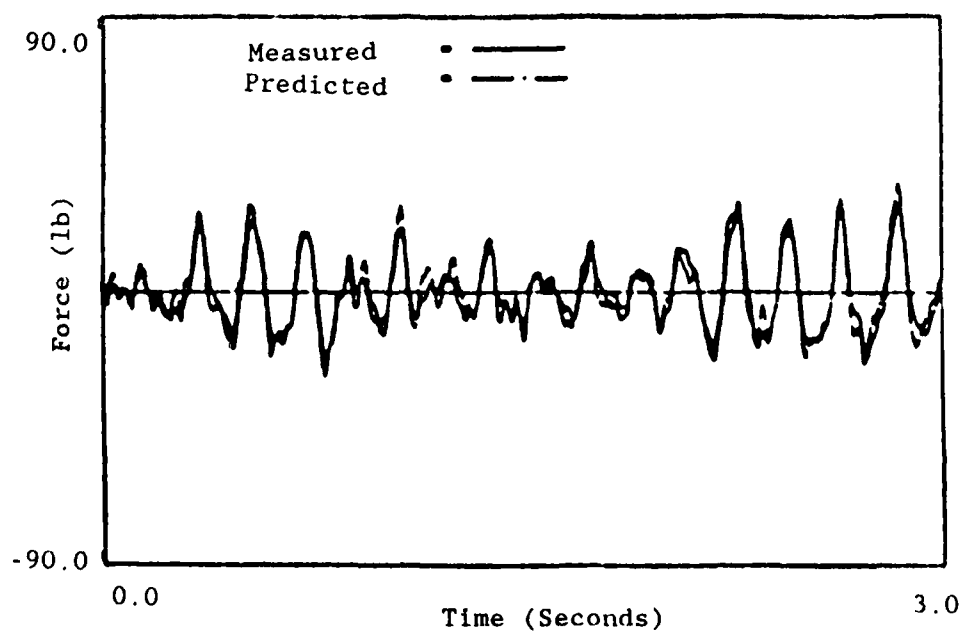


Figure 4.28. Predicted and Measured Force for Test Specimen #2, Run #2.

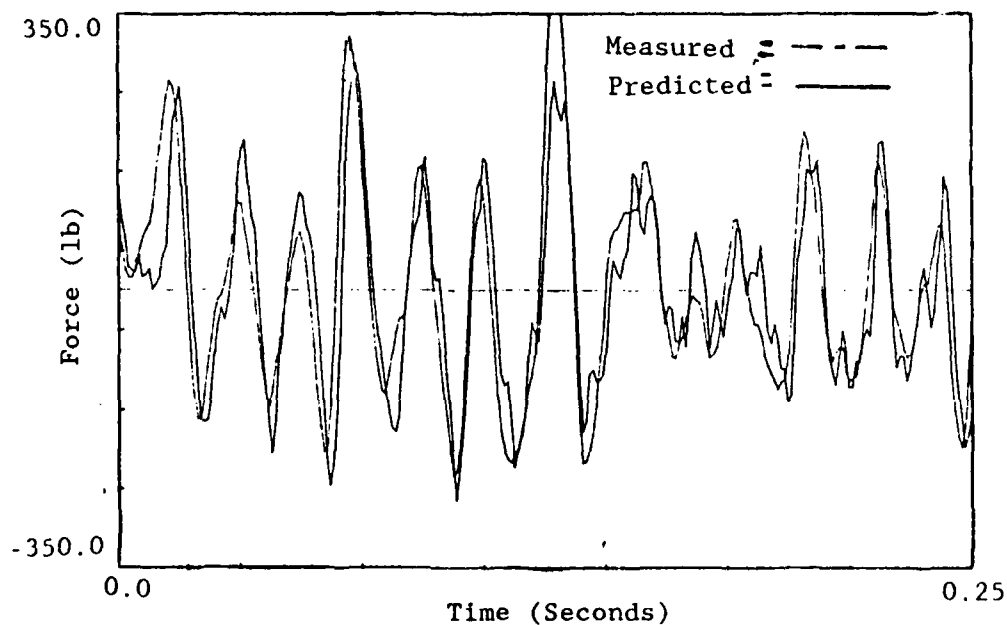


Figure 4.29. Predicted and Measured Force for Test Specimen #3.

CHAPTER 5.

ANALYTICAL APPROACHES

5.0 Introduction.

This chapter further expands on the idea of sum of weighted acceleration technique, SWAT, by presenting alternative formulations for the determination of the effective weights. For models of linear systems, the weighting coefficients or effective weights can be determined analytically with knowledge of the mode shapes of the structure rather than experimentally determining the weights. These approaches allow estimation of effective weights without experimental data, which is valuable for large complex structures where known forces can not be easily applied. These mathematical formulations provide advantages for determining the effective weights analytically rather than through the use of the known forces on the actual or prototypical structure. Results indicate the procedures have a wide range of applicability which is of considerable importance for large multi-degree-of-freedom structures.

The first methods used in the previous chapters to obtain w_i were experimental in that known forces were applied to specific structures and the w_i were obtained by minimizing the difference (in some norm) between the predicted and known forcing functions. Then the actual situation in which the forcing function is not known could be predicted using Equation 5.1.

$$F_R = \sum_{i=1}^n w_i a_i \quad (5.1)$$

Since many structures are too complicated to perform the tests necessary to experimentally determine the weighting coefficients, alternative analytical approaches could prove to be valuable for engineering applications. The next sections provide derivations and preliminary evaluations of schemes which appear to be useful.

5.1 An Analytical Method Based on Mode Shapes.

A method described by Priddy et al. (1988) uses mode shapes in analytical expressions for determining the effective weights. Since the finite element procedure can be used to obtain mode shapes, this procedure can be considered quite general. Therefore, for the sake of completeness, a derivation is given which is different from that given by Priddy et al. (1988) and which may provide additional insight into the method.

Suppose an elastic body is subjected to a surface traction \mathbf{t}^* and a body force \mathbf{b} of the following type:

$$\mathbf{t}^* = \mathbf{F}(t) \chi^*(\mathbf{r}^S) \quad (5.2a)$$

$$\mathbf{b} = \mathbf{F}(t) \chi(\mathbf{r}) \quad (5.2b)$$

in which $\chi(\mathbf{r})$ and $\chi^*(\mathbf{r}^S)$ are known functions, defined over the volume and surface, respectively. In other words, the forcing function is assumed to be separable with the spatial distribution known and one unknown time dependent coefficient described by the vector \mathbf{F} . The position vector \mathbf{r} assumes the value \mathbf{r}^S on the surface. Since the method of weighted accelerations is applicable only if there are no

displacement prescribed boundary conditions, χ^* is defined (perhaps zero) over the complete surface.

If ρ denotes the mass density, \mathbf{u} the displacement vector and $\underline{\sigma}$ the symmetric Cauchy stress tensor, then the equation of motion is

$$\rho \ddot{\mathbf{u}} = \nabla \cdot \underline{\sigma} + \mathbf{b} \quad (5.3)$$

in which $\nabla \cdot ()$ denotes the divergence operator and a dot denotes a derivative with respect to the time. For a linearly elastic body, the constitutive equation is

$$\underline{\sigma} = \underline{\mathbb{E}} : \underline{\epsilon} \quad (5.4)$$

in which $\underline{\mathbb{E}}$ is the elasticity tensor and $\underline{\epsilon}$ the strain tensor. For small deformations, the strain is the symmetric part of the displacement gradient:

$$\underline{\epsilon} = (\nabla \mathbf{u})_{\text{symm}} \quad (5.5)$$

A modal solution to Equation (5.3) is given by

$$\mathbf{u} = \sum_{i=1}^{\infty} \eta_i(t) \boldsymbol{\varphi}_i(\mathbf{r}) \quad (5.6)$$

in which $\boldsymbol{\varphi}_i$ denote the eigenfunctions. The first two eigenfunctions represent rigid body translation

$$\varphi_1 = c \qquad c \cdot c = 1 \qquad (5.7)$$

in which c is independent of r , and rigid body rotation

$$\varphi_2 = \underline{R} \cdot (r - r_c) \qquad (5.8)$$

The position vector to the center of mass is denoted by r_c and \underline{R} is a rotation tensor, also independent of r , and orthogonal:

$$\underline{R}^T \cdot \underline{R} = \underline{I} \qquad (5.9)$$

in which the superscript T denotes the transpose and \underline{I} the identity tensor. The functions φ_i with $i \geq 3$ represent deformation modes of vibration associated with natural frequencies ω_i .

The first step in the procedure of Priddy et al. (1988) is to note that the total mass of the body is given by

$$M = \int_D \rho \, dv \qquad (5.10)$$

in which D denotes the domain of volume integration and dv a volume element. It is also known that the modes are orthogonal to each other. In particular, consider the orthogonality of the second mode to the first one, i.e.,

$$\int_D c \cdot \varphi_2 \, dv = 0 \qquad (5.11)$$

Since \mathbf{c} and $\underline{\mathbf{R}}$ are independent of \mathbf{r} , and because the resulting expression must hold for arbitrary values of \mathbf{c} and $\underline{\mathbf{R}}$, the result of substituting Equation (5.8) in Equation (5.11) is that

$$\int_D (\mathbf{r} - \mathbf{r}_c) dv = 0 \quad (5.12)$$

which is, of course, another identity.

The orthogonality of \mathbf{c} with the other modes yields

$$\int_D \mathbf{c} \cdot \boldsymbol{\varphi}_i dv = 0 \quad i = 3, 4, \dots \quad (5.13)$$

but since \mathbf{c} is constant and arbitrary it follows that

$$\int_D \boldsymbol{\varphi}_i dv = 0 \quad i = 3, 4, \dots \quad (5.14)$$

Equations (5.10), (5.12) and (5.14) prove to be the key ones for obtaining the weighting coefficients.

If these integrals are computed using numerical quadrature, then a typical integral of a function $G(\mathbf{r})$ is approximated as follows:

$$\int_D G(\mathbf{r}) dv = \sum_{i=1}^n w_i G(\mathbf{r}_i) \quad (5.15)$$

in which \mathbf{r}_i is the position vector of the integration point and w_i is the weight. The number of integration points is denoted by n . Numerous

schemes exist (e.g., Gaussian quadrature) for which specific values are assigned to w_i and rules are given for choosing r_i . However, here the w_i 's are left unassigned for the moment, and the points r_i are defined to be those points where accelerometers are placed. Then the result of utilizing Equation (5.15) in Equations (5.10), (5.12) and (5.14) is the following:

$$\sum_{j=1}^n \rho w_j = M$$

$$\sum_{j=1}^n (r_j - r_c) w_j = 0 \quad (5.16)$$

$$\sum_{j=1}^n \varphi_{ij} w_j = 0 \quad i = 3, 4, \dots$$

in which

$$\varphi_{ij} = \varphi_i(r_j) \quad (5.17)$$

Now Equation (5.16) is used as the governing set of equations for obtaining the weighting coefficients w_j . In three dimensions, only $n-6$ deformable modes can be accommodated with the scheme.

To derive the equation that is actually used to obtain the resultant force $F(t)$, integrate each term in Equation (5.3) over the domain:

$$\int_D \rho \ddot{\mathbf{u}} \, dv = \int_D \nabla \cdot \underline{\sigma} \, dv + \int_D \mathbf{b} \, dv \quad (5.18)$$

The Gauss-Green theorem yields

$$\int_D \nabla \cdot \underline{\sigma} \, dv = \int_{\partial D} \boldsymbol{\eta} \cdot \underline{\sigma} \, ds = \int_{\partial D} \mathbf{t} \, ds \quad (5.19)$$

in which ∂D denotes the surface and ds an area element. Then the use of Equations (5.2a) and (5.2b) results in

$$\int_D \rho \ddot{\mathbf{u}} \, dv = \mathbf{F}(t) \, \psi \quad (5.20)$$

in which

$$\psi = \int_D \chi \, dv + \int_{\partial D} \chi^S \, ds \quad (5.21)$$

is a constant vector which is presumably known. Suppose the scale factor is absorbed in F so that

$$\psi = 1 \quad (5.22)$$

If numerical quadrature is used, then Equation (5.20) becomes

$$\sum_{i=1}^n \rho \ddot{\mathbf{u}}_i w_i = \mathbf{F}(t) \quad (5.23)$$

which is the general form of the method of weighted accelerations.

As reported by Priddy et al. (1988), very good results have been obtained using this approach to obtain the weighting coefficients. However, it seems that other orthogonality relations may serve equally well, and there may even be a possibility that alternative schemes may be viable in which it is not necessary to obtain the mode shapes at all. The next section indicates how the finite element approach might be applied directly.

5.2 Weighted Residuals and the Finite Element Method.

The finite element method can be considered as a systematic procedure for developing compact nodal basis functions for use in a weak formulation such as the method of weighted residuals. To illustrate that various analytical approaches can be used to obtain suitable factors for use in the procedure involving the sum of weighted accelerations, the more general approach involving weak formulations is given in this section. Then the specialization to finite elements is made.

To illustrate the concepts in as simple a manner as possible, consider the one-dimensional model problem of motion in a bar of length, L . Since the method of weighted accelerations applies only to unsupported bodies, the boundaries defined by $x=0$ and $x=L$ are free. Acceleration time histories $a_i(t)$ are presumed to be available from accelerometers placed at the n points x_i , $i=1 \dots n$. Consider a forcing function that is separable in space and time

$$f(x,t) = F(t) \chi(x) \quad \int_0^L \chi(x) dx = 1 \quad (5.24)$$

in which the spatial distribution, $\chi(x)$, is assumed known but the temporal part, $F(t)$, is unknown. The normalization on χ is done for future convenience. The procedure states that with a suitable choice of scalar weight variables, w_i , the force is given by the formula

$$F(t) = \sum_{i=1}^n w_i a_i(t) \quad (5.25)$$

Normally the weight variables are obtained by performing an experiment in which the forcing function is known and then adjusting the variables by the method of least squares so that the function $F(t)$ is as close as possible to the measured function. Then the weight variables are used in the actual problem in which the forcing function is desired but unknown.

The governing differential equation for an elastic bar with unit cross-sectional area is

$$(ku,_{xx})_{,x} + F(t)\chi(x) = \rho \ddot{u} \quad 0 < x < L \quad (5.26)$$

in which k is the elastic stiffness.

Label the points at which the accelerometers are placed, x_j , as nodes. Introduce nodal basis functions $N_i(x)$ which are defined to have the value one at associated nodes and zero at all other nodes. Lagrange polynomials are examples of such basis functions which are complete

polynomials and, hence, will automatically represent rigid body modes in the following representation for u :

$$u = \sum_{i=1}^n u_i(t) N_i(x) \quad (5.27)$$

Let $q(x)$ denote a weight function with continuity of at least C^0 . A weak form of the equation of motion is obtained by multiplying each term in Equation (5.26) by q and integrating over the domain. With the use of Equation (5.27), an integration by parts, and the use of the free end boundary conditions, the result is:

$$\sum_{i=1}^n \int_0^L \rho q(x) N_i(x) dx \ddot{u}_i + \sum_{i=1}^n \int_0^L k q, x N_i, x dx u_i = F(t) \int_0^L q(x) \chi(x) dx \quad (5.28)$$

If a representation similar to Equation (5.27) is used for q :

$$q = \sum_{i=1}^n q_i N_i(x) \quad (5.29)$$

then with q_i considered to be arbitrary, Equation (5.28) becomes

$$[M] (\ddot{u}) + [K] (u) = F(t) (f) \quad (5.30)$$

in which standard matrix notation has been used. The column vector (u)

consists of the time dependent components $u_i(t)$ while components of the remaining matrices are:

$$\begin{aligned} K_{ij} &= \int_0^L k N_{i,x} N_{j,x} dx & M_{ij} &= \int_0^L \rho N_i N_j dx \\ f_i &= \int_0^L x N_i dx \end{aligned} \quad (5.31)$$

Let $\{R\}$ denote the rigid body mode. Since the associated stiffness eigenvalue is zero, it follows that

$$\langle R \rangle [K] = \langle 0 \rangle \quad \langle R \rangle = \langle 1, 1, \dots, 1 \rangle \quad (5.32)$$

in which $\langle R \rangle$ is the transpose of $\{R\}$. Also, because the basis functions must represent complete polynomials up to the first order for convergence to be assured, these basis functions will automatically satisfy the relation

$$\sum_{i=1}^n N_i(x) = 1 \quad (5.33)$$

With the use of Equation (5.33) and the normalizing result of Equation (5.24), it follows that

$$\langle R \rangle \{f\} = 1 \quad (5.34)$$

Thus the inner product of $\langle R \rangle$ with each term in Equation (5.30) yields

$$\langle W \rangle \{\ddot{u}\} = F(t) \quad (5.35)$$

where

$$\langle W \rangle = \langle R \rangle [M] \quad (5.36)$$

and Equation (5.35) is identical in form to Equation (5.25) which is the method of weighted accelerations.

Under rigid body motion

$$\{\ddot{u}\} = \ddot{u}_c \{R\} \quad (5.37)$$

in which \ddot{u}_c denotes the rigid body acceleration which is also the acceleration of the center of mass. Because of the use of nodal basis functions, it can be shown that

$$\langle R \rangle [M] \{R\} = M \quad (5.38)$$

where M is the total mass of the body. Then for rigid body motion Equation (5.35) reduces to

$$P(t) = M \ddot{u}_c \quad (5.39)$$

as it should.

The result of the formulation is that once nodal basis functions are chosen, the mass matrix can be constructed from Equation (5.31) and the weighting parameters from Equation (5.36). In particular, for the first

node, the result is

$$w_1 = \int_0^L \rho N_1 [N_1 + N_2 + \dots] dx \quad (5.40)$$

The use of Equation (5.33) yields

$$w_1 = \int_0^L \rho N_1 dx \quad (5.41)$$

with a similar expression for each of the other weighting parameters.

With reference to Figure 5.1a which represents a bar on which three accelerometers are placed, Lagrange polynomials (See Figure 5.1b) represent one possible choice for nodal basis functions:

$$\begin{aligned} N_1 &= \frac{(x - x_2)(x - x_3)}{(x_1 - x_2)(x_1 - x_3)} & N_2 &= \frac{(x - x_1)(x - x_3)}{(x_2 - x_1)(x_2 - x_3)} \\ N_3 &= \frac{(x - x_1)(x - x_2)}{(x_3 - x_1)(x_3 - x_2)} \end{aligned} \quad (5.42)$$

from which weight factors can be determined.

Alternatively, the points x_1 , x_2 , and x_3 can be used to define the two elements shown in Figure 5.1c. Finite elements also define nodal basis functions, which are shown in Figure 5.1c, for elements that provide C^0 continuity. The effect of using basis functions based on finite elements is that one-half the mass of each element is assigned to

each of the two nodes used to define the element. The net result is a very intuitive procedure for assigning weights to each node. The problem is that the hash-marked areas at the ends are not included within the elements. A possible approach is to lump the mass represented by the hash-marked area with the adjacent node.

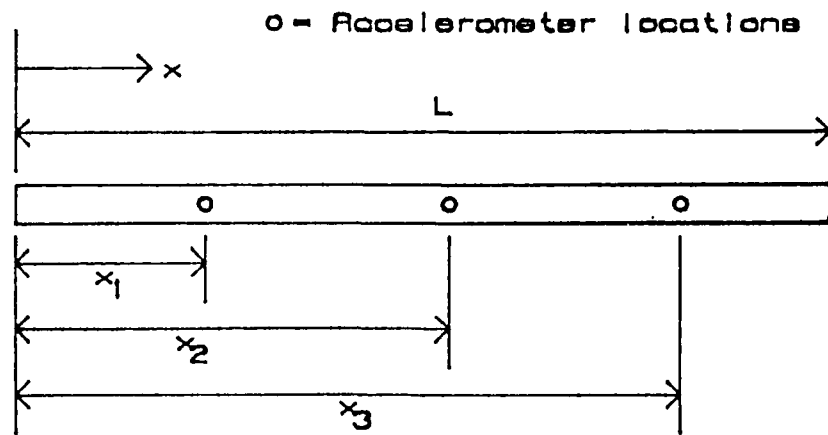
An engineering rule of thumb in finite element analysis is that $2m$ nodes are required to accurately represent m mode shapes. It is to be expected that lumping masses based directly on finite elements rather than on mode shapes can only provide accurate predictions for a limited number of frequency components in the result for the forcing function. Examples given in a later section tend to support this hypothesis.

5.3 Application of the Finite Element Method to Beams.

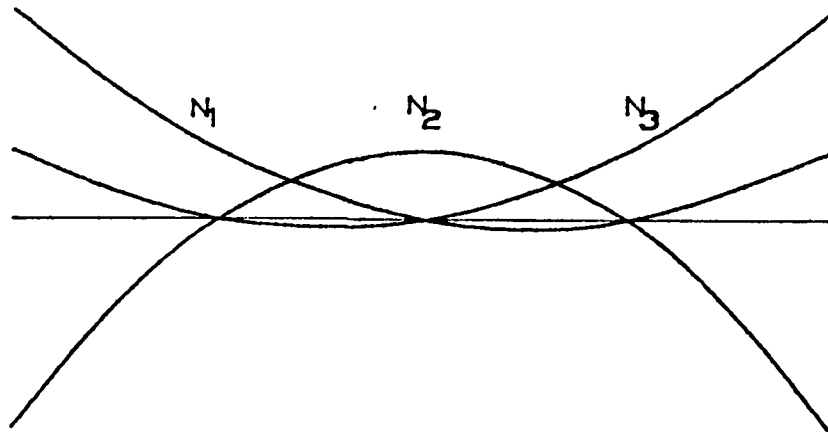
For elementary Euler-Bernouilli beam theory, an element can be defined in which two degrees of freedom are associated with each node. If the first degree of freedom corresponds to translation and the second to rotation, then the consistent element mass matrix is

$$[M] = \frac{M^e}{420} \begin{bmatrix} 156 & 22h & 54 & -13h \\ 22h & 4h^2 & 13h & -3h^2 \\ 54 & 13h & 156 & -22h \\ -13h & -3h^2 & -22h & 4h^2 \end{bmatrix} \quad (5.43)$$

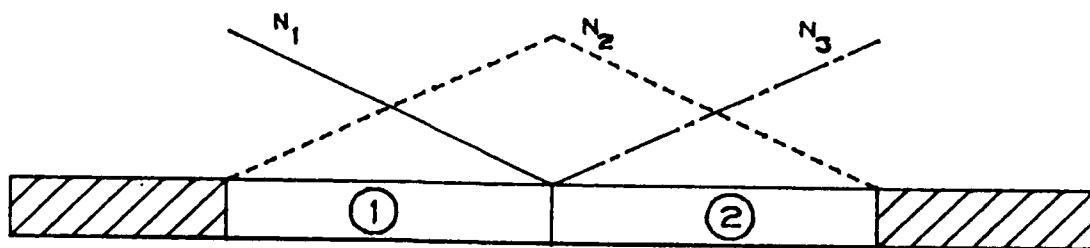
in which M^e denotes the element, and h the length. Now both rigid body translation and rotation are possible. However, normally transverse forces are of primary interest, rather than applied moments, so the appropriate rigid body mode to use in the matrix equation of motion is



(a) Bar with Three Accelerometers.



(b) Sketch of Lagrange Polynomials as Nodal Basis Functions.



○ = Element Number

(c) Nodal Basis Functions for C^0 Elements.

Figure 5.1. Nodal Basis Functions for a Bar.

that of rigid body translation in which results similar to those of the previous section continue to hold. In particular, the vector defining rigid body translation for an element is

$$\langle R \rangle = \langle 1, 0, 1, 0 \rangle \quad (5.44)$$

and the element weight factors become

$$\langle R \rangle [M] = \frac{M^e}{420} \langle 210, 35h, 210, -35h \rangle \quad (5.45)$$

The translational terms are the first and third components in this vector, which indicates that the result is a simple assignment of one-half the mass of an element to each translational degree of freedom. Again, any excess mass at the ends of the beam not defined within an element would have to be lumped at the appropriate nodes. Similar results can be derived for elements used to model other structural members. Sample results for beams and plates are given in the next section.

5.4 Experimental Results.

Effective weights, determined by the mode shape and finite element approaches discussed in the previous sections, for a free-free beam of two different acceleration configurations were used to predict input forces. These forces of random and impact loadings were compared by plots with the measured forces. A third case used a free-free plate where the effective weights were determined by the finite element

approach.

The first case is that of a free-free steel beam with the five accelerometers placed at the nodes of the fourth vibrational mode (See Figure 5.2). This is considered to be a strategic placement of the gauges (Priddy et al. (1988)). From Equations (5.16) two of the five equations for this setup come from rigid body translation and rotation. The other three equations involve the first three vibrational modes. This forms the set of equations

$$\begin{bmatrix} 1.0 & 1.0 & 1.0 & 1.0 & 1.0 \\ 34.48 & 18.01 & 0.0 & 18.01 & -34.48 \\ 1.323 & -0.392 & -1.216 & 0.392 & 1.323 \\ 0.861 & -1.282 & 0.0 & 1.282 & -0.861 \\ 0.423 & -1.043 & 1.422 & 1.043 & 0.423 \end{bmatrix} \begin{Bmatrix} w_1 \\ w_2 \\ w_3 \\ w_4 \\ w_5 \end{Bmatrix} = \begin{Bmatrix} 11.36 \\ 0.0 \\ 0.0 \\ 0.0 \\ 0.0 \end{Bmatrix} \quad (5.46)$$

where 11.36 lb_m is the mass of the beam. The effective weights from Equations (5.46) are tabulated in Table 1 as effective weights determined from the mode shapes.

A second set of effective weights for this beam setup were determined from the finite element approach (See Table 5.1). For this beam, case 1, the two different sets of effective weights were very close. The difference between random and impact loadings determined from both sets of effective weights to the measured forces was small (See Figures 5.3, 5.4, 5.5, and 5.6).

The second case is for the same beam and same number of accelerometers with the gauges moved to a reasonable location, but where the modal shape approach yielded a negative effective weight (See Figure

Table 5.1. Effective Weights for Each Case.

Case Number	Effective weights determined from mode shapes.	Effective weights determined from finite elements.
Case 1	$w_1 = w_5 = 1.91 \text{ lb}$	$w_1 = w_5 = 1.99 \text{ lb}$
Free-Free Beam	$w_2 = w_4 = 2.50 \text{ lb}$	$w_2 = w_4 = 2.43 \text{ lb}$
(See Figure 5.2)	$w_3 = 2.54 \text{ lb}$	$w_3 = 2.53 \text{ lb}$
Case 2	$w_1 = w_5 = 4.34 \text{ lb}$	$w_1 = w_5 = 2.83 \text{ lb}$
Free-Free Beam	$w_2 = w_4 = -1.46 \text{ lb}$	$w_2 = w_4 = 1.93 \text{ lb}$
(See Figure 5.7)	$w_3 = 5.60 \text{ lb}$	$w_3 = 1.84 \text{ lb}$
Case 3		$w_1 = w_2 = w_3 = w_4 =$
Plate		$w_5 = w_6 = 1.84 \text{ lb}$
(See Figure 5.1')		

All Dimensions in Inches.

Mass = 11.38 lb.

○ - Location of an accelerometer.

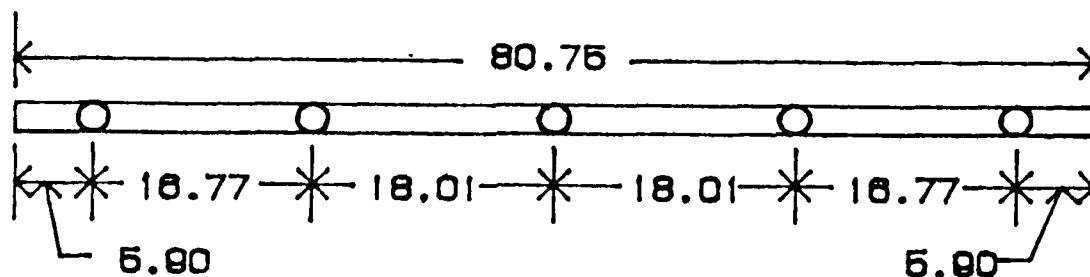


Figure 5.2. Case 1 - Free-Free Beam Configuration of Accelerometers (A Strategic Location).

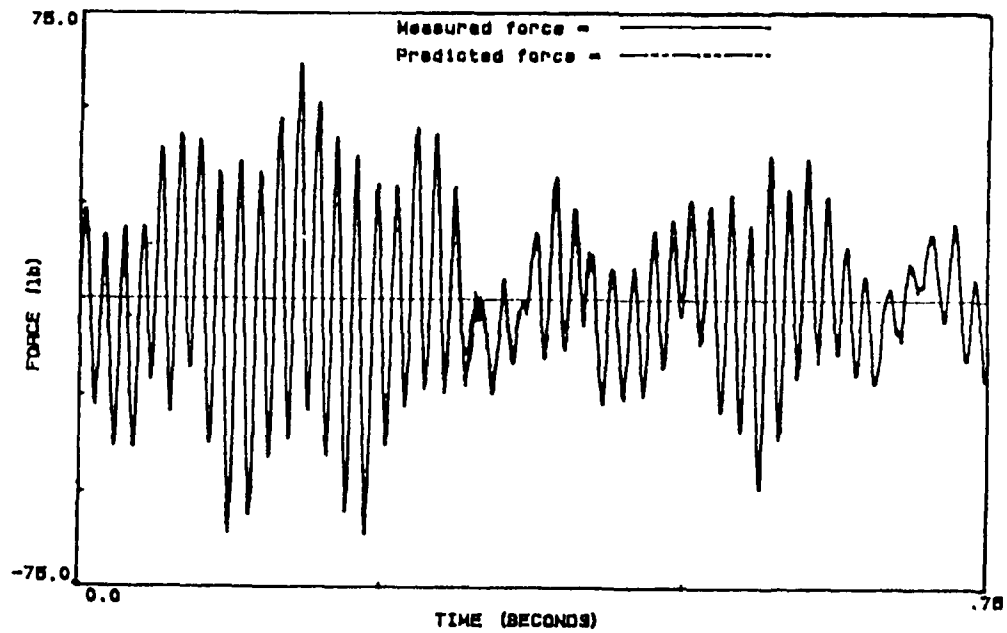


Figure 5.3. Case 1 - Free-Free Beam. Predicted Force Calculated from the Effective Weights Determined from the Mode Shape Approach.

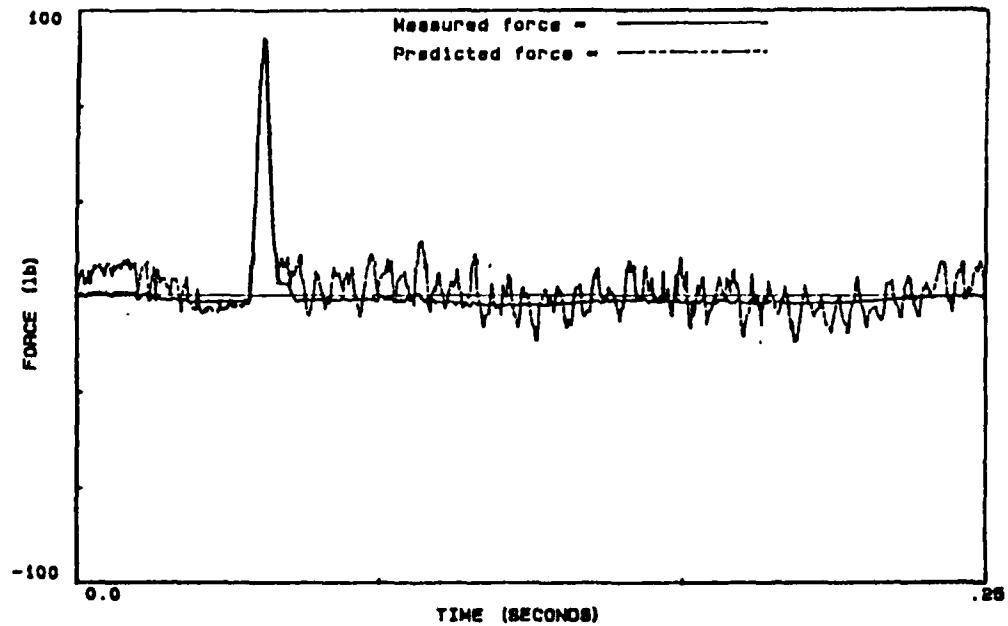


Figure 5.4. Case 1 - Free-Free Beam. Predicted Force Calculated from the Effective Weights Determined from the Mode Shape Approach.

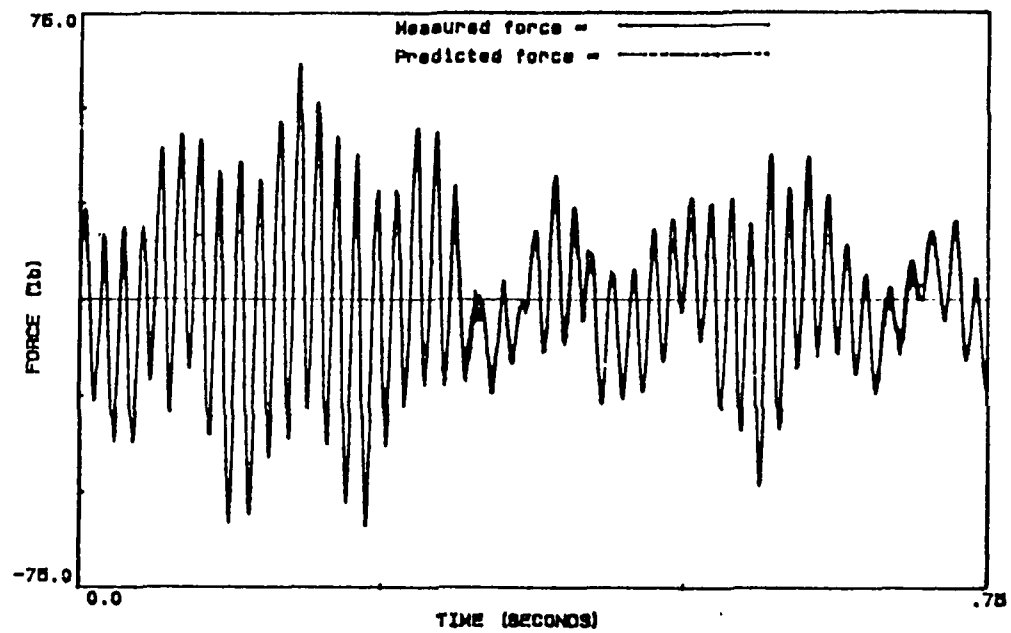


Figure 5.5. Case 1 - Free-Free Beam. Predicted Force Calculated from the Effective Weights Determined from the Finite Element Approach.

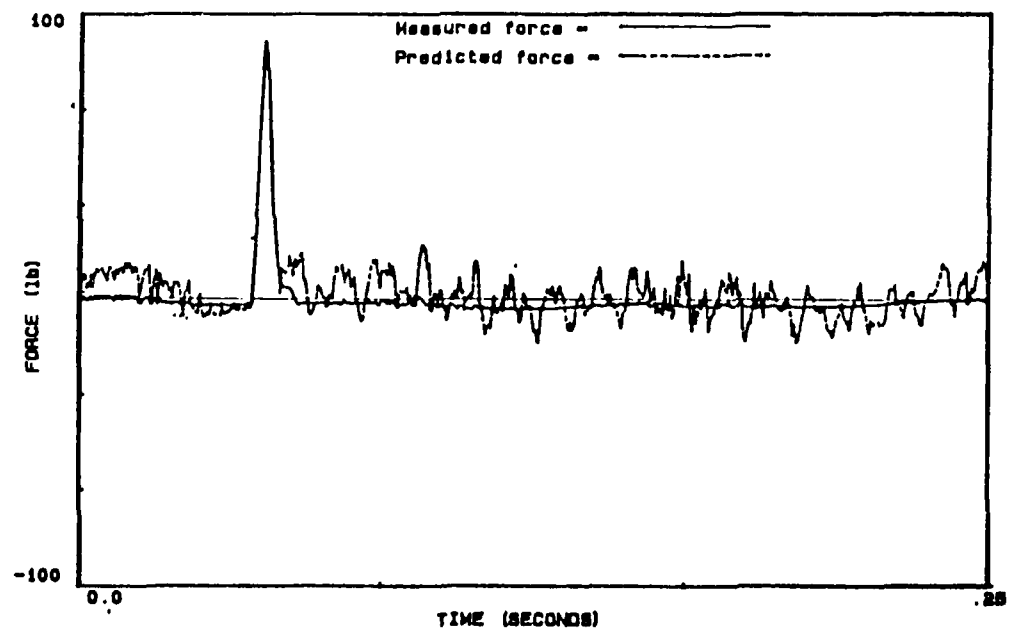


Figure 5.6. Case 1 - Free-Free Beam. Predicted Force Calculated from the Effective Weights Determined from the Finite Element Approach.

5.7). The results of using Equation (5.16) in this case is

$$\begin{bmatrix} 1.0 & 1.0 & 1.0 & 1.0 & 1.0 \\ 27.37 & 13.08 & 0.0 & -13.08 & -27.37 \\ 0.527 & -0.766 & -1.216 & -0.766 & 0.527 \\ -0.371 & -1.287 & 0.0 & 1.287 & 0.371 \\ -1.008 & -0.270 & 1.422 & -0.270 & -0.008 \end{bmatrix} \begin{Bmatrix} w_1 \\ w_2 \\ w_3 \\ w_4 \\ w_5 \end{Bmatrix} = \begin{Bmatrix} 11.36 \\ 0.0 \\ 0.0 \\ 0.0 \\ 0.0 \end{Bmatrix} \quad (5.47)$$

The effective weights determined by the mode and finite element approach are much different (See Table 5.1). This was expected because, for the finite element approach, the effective weights are always positive. The results comparing the random input to this beam show small difference between the predicted and the measured force (See Figures 5.8 and 5.10). The impact loading showed high amplitude oscillation after the removal of the load for both sets of predicted forces (See Figures 5.12 and 5.14). The impact loading has a higher bandwidth of frequencies.

The third case is that of an aluminum plate (See Figure 5.12). Only the finite element approach was used to determine the effective weights. These weights and the response accelerations were used to predict an impact loading which is compared with the measured loading in Figure 5.13.

All Dimensions in Inches.

Mass = 11.36 lb.

○ - Location of an accelerometer.

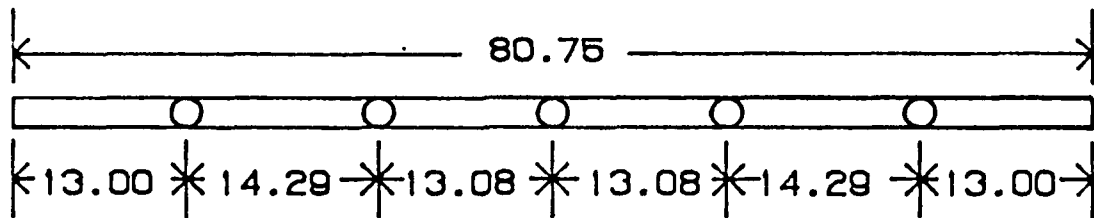


Figure 5.7. Case 2 - Free-Free Beam Configuration of Accelerometers (A Routine Location).

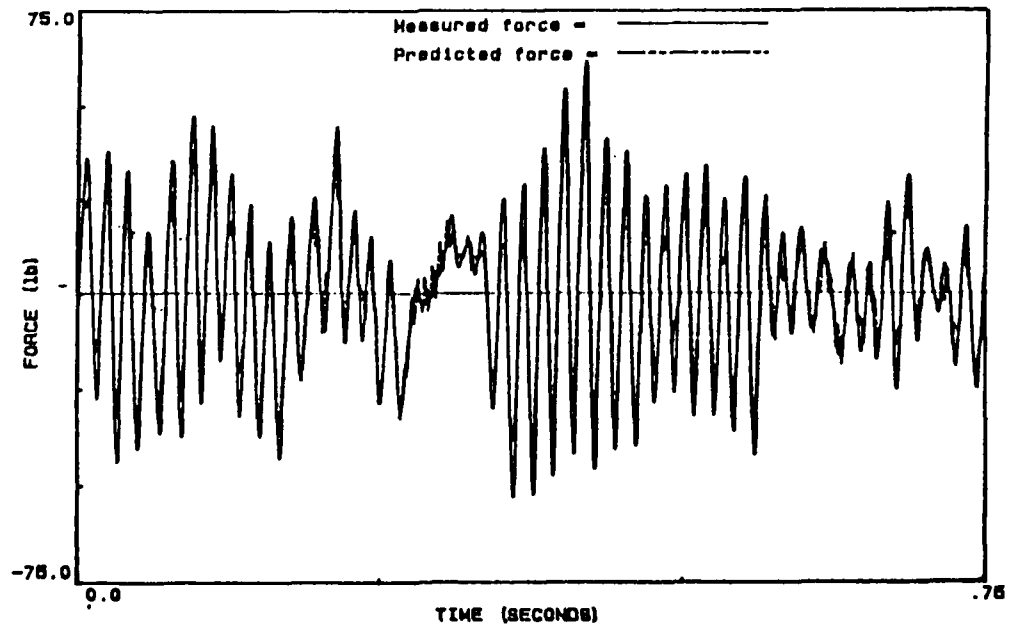


Figure 5.8. Case 2 - Free-Free Beam. Predicted Force Calculated from the Effective Weights Determined from the Mode Shape Approach.

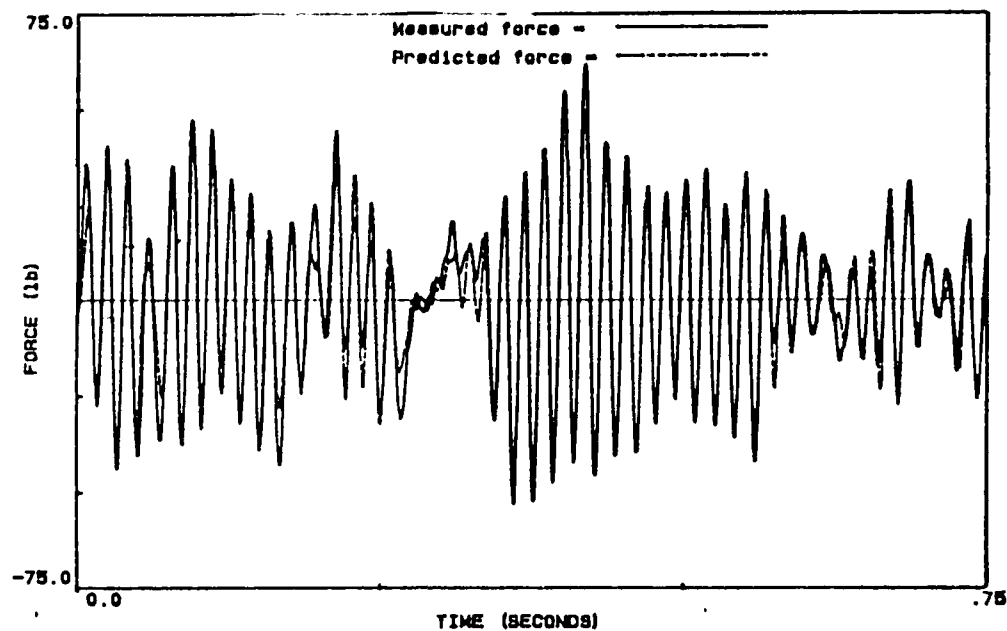


Figure 5.9. Case 2 - Free-Free Beam. Predicted Force Calculated from the Effective Weights Determined from the Finite Element Approach.

All Dimensions in Inches.

Mass = 11.08 lb.

o = Location of an Accelerometer.

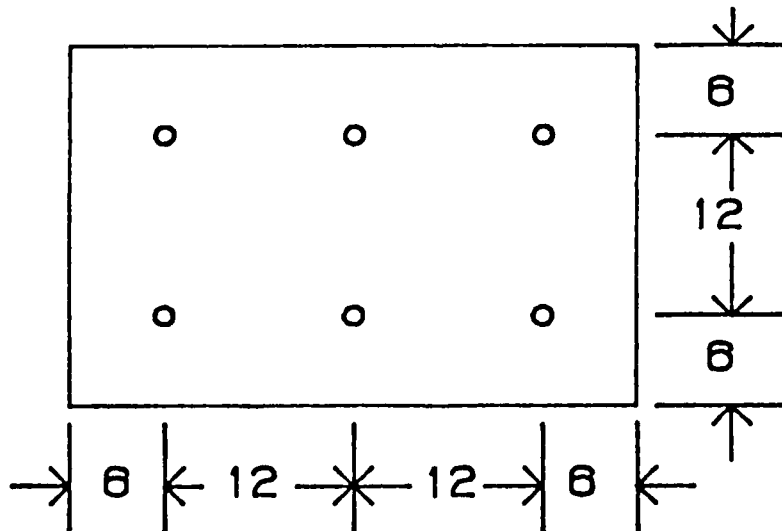


Figure 5.10. Case 3 - Plate Configuration.

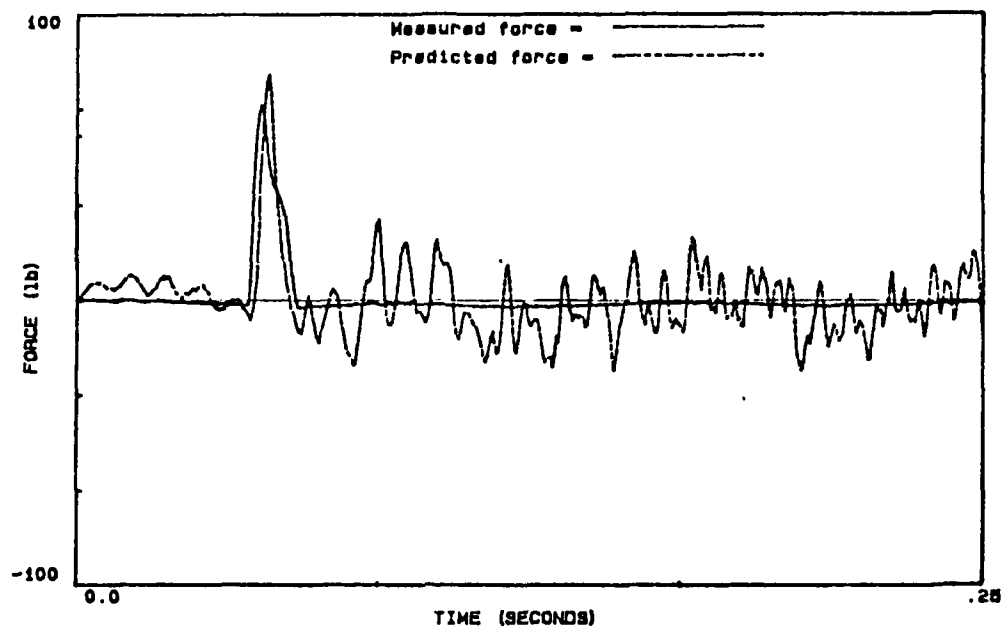


Figure 5.11. Case 3 - Predicted and Measured Forces for the Plate.

CHAPTER 6.

PROCEDURES AND INSTRUMENTATION FOR DYNAMIC TESTING

6.0. Introduction.

A dynamic laboratory provides a facility to simulate a specific vibrational environment and it normally has tighter control of the parameters. A dynamic test of excites a structure and measures indirectly the applied forces and responses to a structure. This seemingly simple test process can be tedious, and the downfall for an overall dynamic analysis. To prevent this problem, a microcomputer was incorporated into a University of New Mexico vibration system.

Besides providing a means to transfer testing procedure information by checklists and programming of manual tasks the microcomputer made possible, by analog-to-digital and digital-to-analog converters, a method for controlling random vibrations. An electrodynamic shaker created the random vibration using a driving signal calculated from the microcomputer. Each driving signal for a desired response is derived using a frequency response function which is estimated as test runs are performed. The desired simulated random vibration is produced internally by randomizing the phase angles of a sine or cosine series.

For damageable specimens, this method prevents inadvertently damaging the structure by accidentally overexciting the specimen. The vibration from the shaker converges quickly to the desired excitation.

6.1. Description of Equipment.

The incorporation of the microcomputer as the controlling component essentially developed a new alternative, a cost effective vibration

system (See Figure 6.1). The microcomputer generates and modifies the driving signal for the shaker. The microcomputer contains 64k main memory with 256k extended memory. The extended memory provided storage of signals between processing. Analog-to-digital, A-D, converters; digital-to-analog, D-A, converters; and clocks were installed in the microcomputer. The converters used 12 bit binary numbers. This provides a resolution of the signals from 0 to 4095. The setup allowed

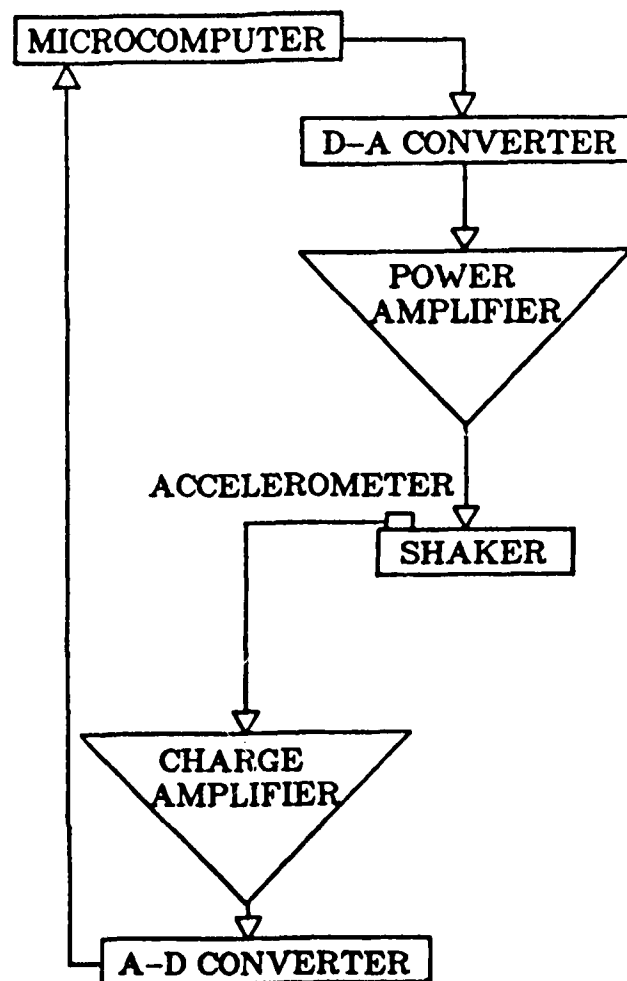


Figure 6.1. Vibration System with Microcomputer

a D-A and an A-D conversion during the same scan. This configuration can digitally convert up to 10,000 samples per second; however, only 2,000 samples per second were used.

Low pass filters were used, at both the output and input to the converters, to prevent aliasing in the digital data. In this application a cutoff frequency of 500 Hz was used.

The output driving signal was sent to an electromagnetic shaker through a power amplifier whose frequency range is from 5 cps to 5,000 cps. The shaker operates in a 5-cps to 4,000-cps range and has a rated force of 1,500 pounds.

The response was measured by piezoelectric accelerometer with power supply and charge amplifier. The accelerometer was mounted on the same platform as a test specimen.

6.2 Methodology and Testing Procedures.

For a linear single-degree-of-freedom structure, the response can be determine in the frequency domain as

$$Y(\omega) = H(\omega) X(\omega), \quad (6.1)$$

where $Y(\omega)$ is the response, $X(\omega)$ is the input, and $H(\omega)$ is the response function. If $H(\omega)$ is known, then, an input could be determined for a desired response; that is

$$X^I(\omega) = [H(\omega)]^{-1} X^D(\omega), \quad (6.2)$$

where $X^I(\omega)$ is the input and $X^D(\omega)$ is the desired response. This

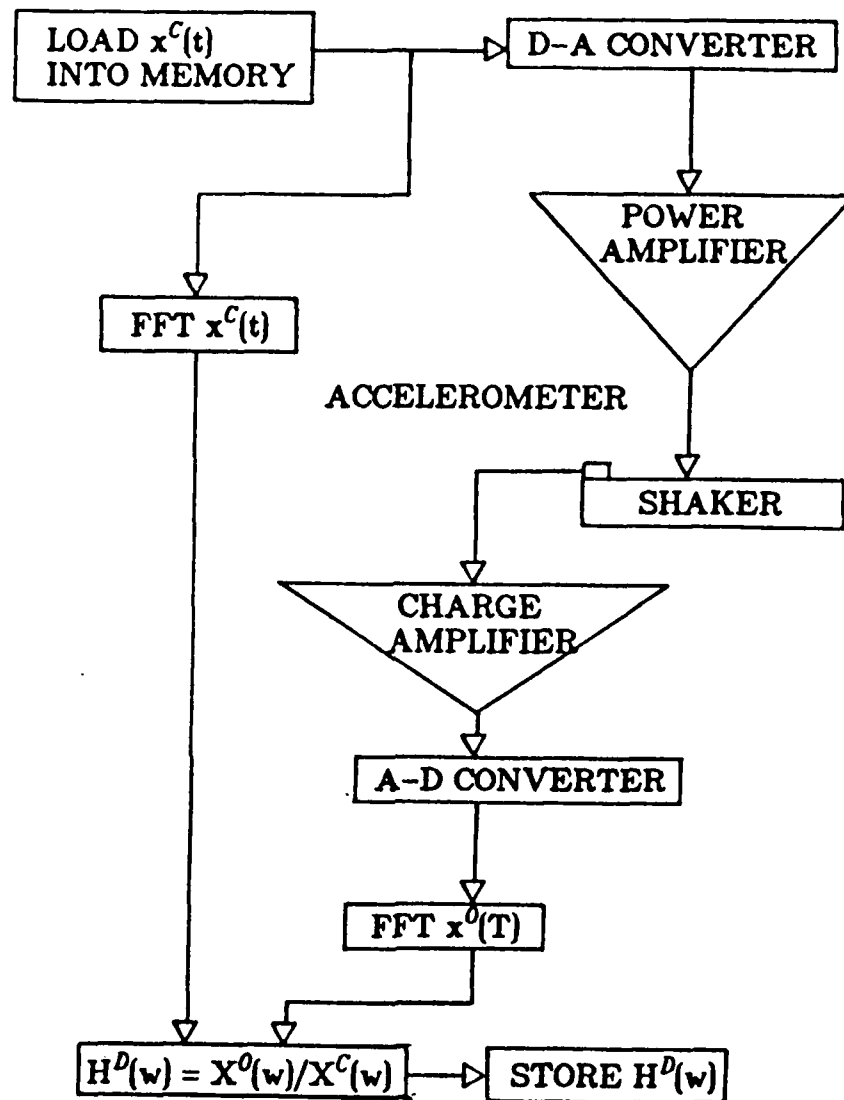


Figure 6.2. Step 1 to Determine $H(w)$.

determination (Equation (6.2)) provides the basis for controlling the shaking table by using the microcomputer.

For a driving signal to be calculated for a specific desired response, the response function must be determined at least in the frequency range of the desired response. The determination of $H(w)$

falls into two categories: first where the test specimen assumes no damage and second where the test specimen damages as the testing progresses.

The estimation of the response function takes advantage of the improved method proposed by Mitchell (1982). This estimation takes an average of the common estimator of $H(\omega)$ shown in Bendat (1986) and a second estimator of $H(\omega)$. Following the nomenclature of Mitchell (1982), Bendat showed that the first estimator (common estimator),

$$H_1(\omega) = \frac{G_{xy}}{G_{xx}} \quad (6.3)$$

is less than or equal to the true transfer function. G is the auto-spectrum or cross-spectrum of one or two signals respectively.

The second estimator, following the above nomenclature,

$$H^2(\omega) = \frac{G_{yy}}{G_{yx}} \quad (6.4)$$

was shown to be greater than or equal to the true transfer function.

The transfer function used in deriving the driving signal is the average of $H_1(\omega)$ and $H^2(\omega)$,

$$H(\omega) = \frac{H_1(\omega) + H^2(\omega)}{2} \quad (6.5)$$

For the first category, the test specimen is assumed to be unchanged and the transfer function remains constant. The driving signal is

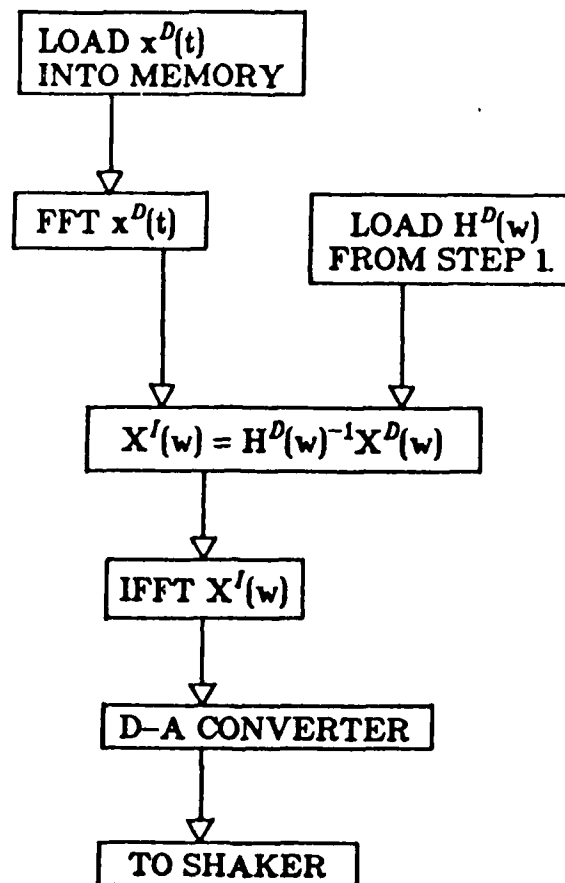


Figure 6.3. Step 2, Determine Input Signal for a Desired Response.

calculated from

$$D^n(\omega) = [H(\omega)]^{-1} X^n(\omega) \quad (6.6)$$

where $D^n(\omega)$ is the driving signal to produce the desired excitation,

$X^n(\omega)$. The estimation of $H(\omega)$ is upgraded after each test with a new average. Using these assumptions, the following procedures are used for this category of test specimens (see Figure 6.2.).

1. A reference signal, $x^n(t)$, is generated and loaded in the computer memory.

2. The fft of $x^n(t)$ is computed and the driving signal, $D^n(\omega)$, is computed by Equation 6.6.

3. The driving signal is transformed to the time domain and fed to the shaker system through the D-A converter.

4. The response is measured and used to compute $H_1^n(\omega)$ and $H_2^n(\omega)$.

5. An average of $H^n(\omega)$ is computed after each test run and stored for future test runs.

6. Step 1-5 is repeated for each test run.

The second category of testing is for damageable specimens. Initially a low input $x^1(t)$ is applied to estimate the first $H(\omega)$. This prevents damaging the specimen. Second, as the specimen damages, the $H(\omega)$ changes; therefore, a weighted average of $H(\omega)$ is implemented as the test runs are performed. The procedures are similar to the first category (see Figure 6.3).

6.3 Simulation of Digital Random Signal.

A computer generated waveform simulates a random process. The waveform is stored as a digital signal that is transformed into an analog signal by a digital-to-analog converter. The waveform is created for a specific stationary random process by correlating with its spectral density function, which allows applications for physical phenomena of stationary and special cases of nonstationary random

processes.

A random process is classified by probability properties as stationary or nonstationary (Bendat, 1986 and Newland, 1976). Two properties, necessary in this report to classify the random processes, are the mean value and the autocorrelation function.

For an ensemble of sample function, $x_j(t)$, (see Figure 6.4) the mean value, $\mu_x(t_n)$, is computed by taking the value of each $x_j(t)$ at time t_n , summing the values, and dividing by the number of sample functions, N . The autocorrelation function, $R_{xx}(t_n, t_n + \tau)$ can be computed by taking the ensemble average of the product of values at two times, t_n and $t_n + \tau$. In equation form, these two properties are

$$\mu_x(t_n) = \lim_{N \rightarrow \infty} \frac{1}{N} \sum_{k=1}^N x_k(t_n) \quad (6.7)$$

$$R_{xx}(t_n, t_n + \tau) = \lim_{N \rightarrow \infty} \frac{1}{N} \sum_{k=1}^N x_k(t_n) x_k(t_n + \tau) \quad (6.8)$$

where x_k corresponds to a sample function and N is the number of sample functions.

If either the mean square or the autocorrelation function vary as t_n varies, the random process is said to be nonstationary. If these two properties do not vary with time, the process is called stationary or weakly stationary. The random process is called strongly stationary, if all probability moments are time invariant. Stationary random processes are further divided into ergodic and nonergodic. The process is ergodic if the mean value and autocorrelation function along any one sample function are equal to the

ensemble average. If the random process is not ergodic, it is called nonergodic.

Pseudo or periodic random data simulate ergodic random processes by correlating to its spectral density function. The spectral density function, $S(\omega)$, is the Fourier transform of the autocorrelation function. Assuming only stationary random processes, $S(\omega)$ is always positive and symmetrical around the y-axis. Many individual sample functions, $x_n(t)$, correspond to one spectral density function.

The spectral density function shows a picture of the frequency

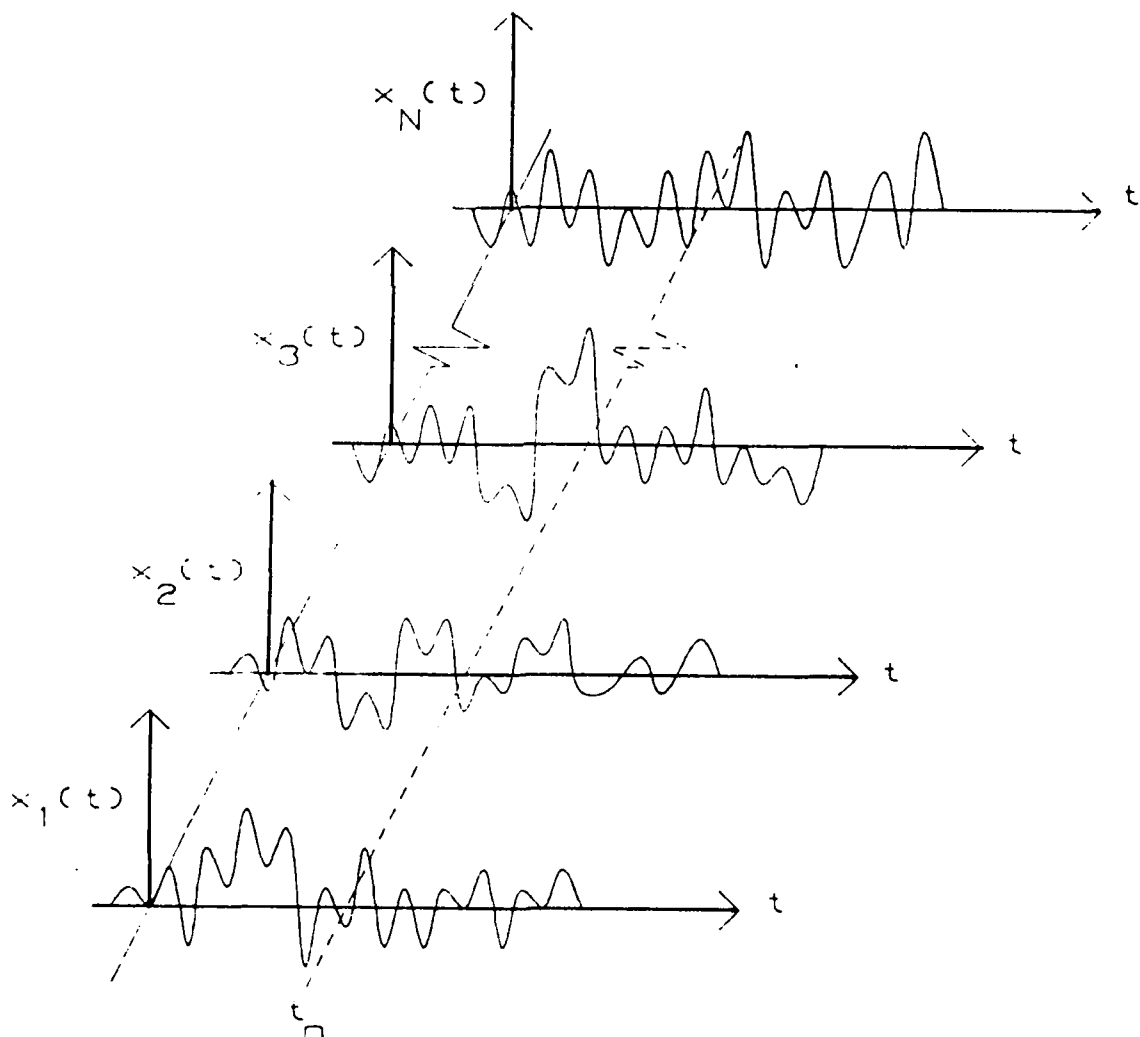


Figure 6.4. Ensemble of Sample Function for a Random Process.

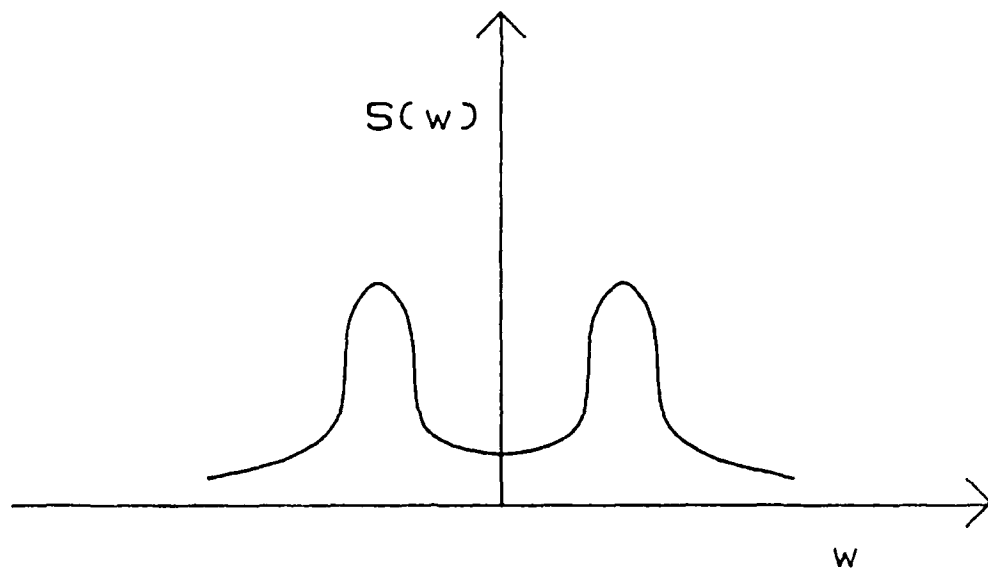


Figure 6.5. Typical Narrow-Banded Spectra Density Curve.

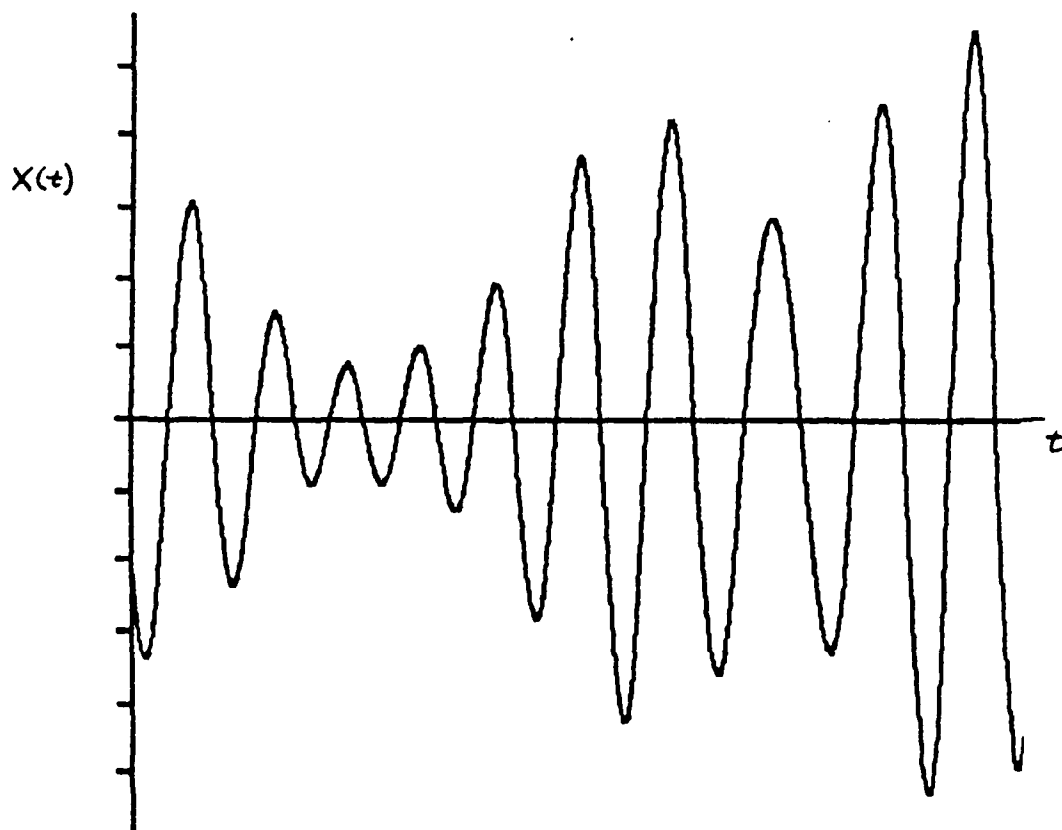


Figure 6.6. Narrow-Band Random Vibration Signal

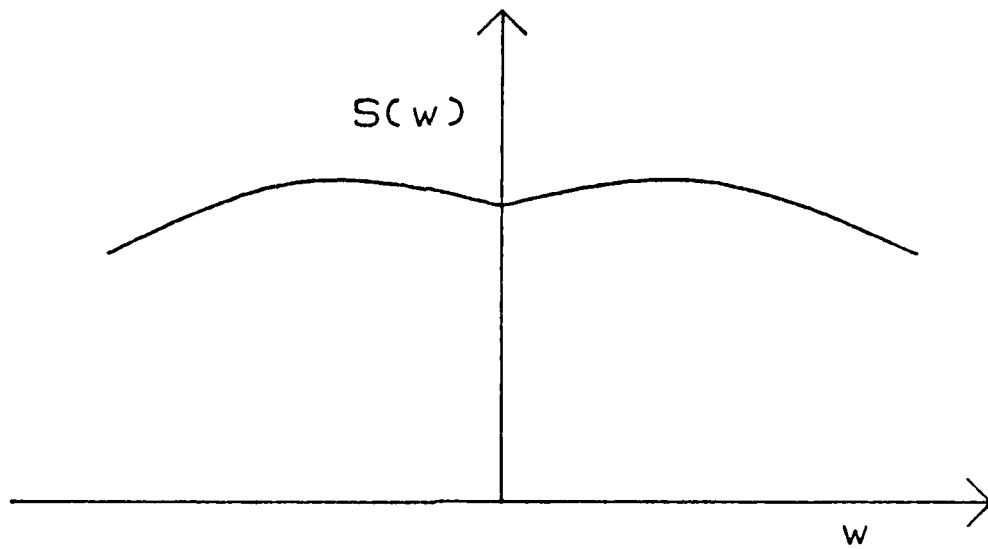


Figure 6.7. Typical Wide-Banded Spectral Density Curve.

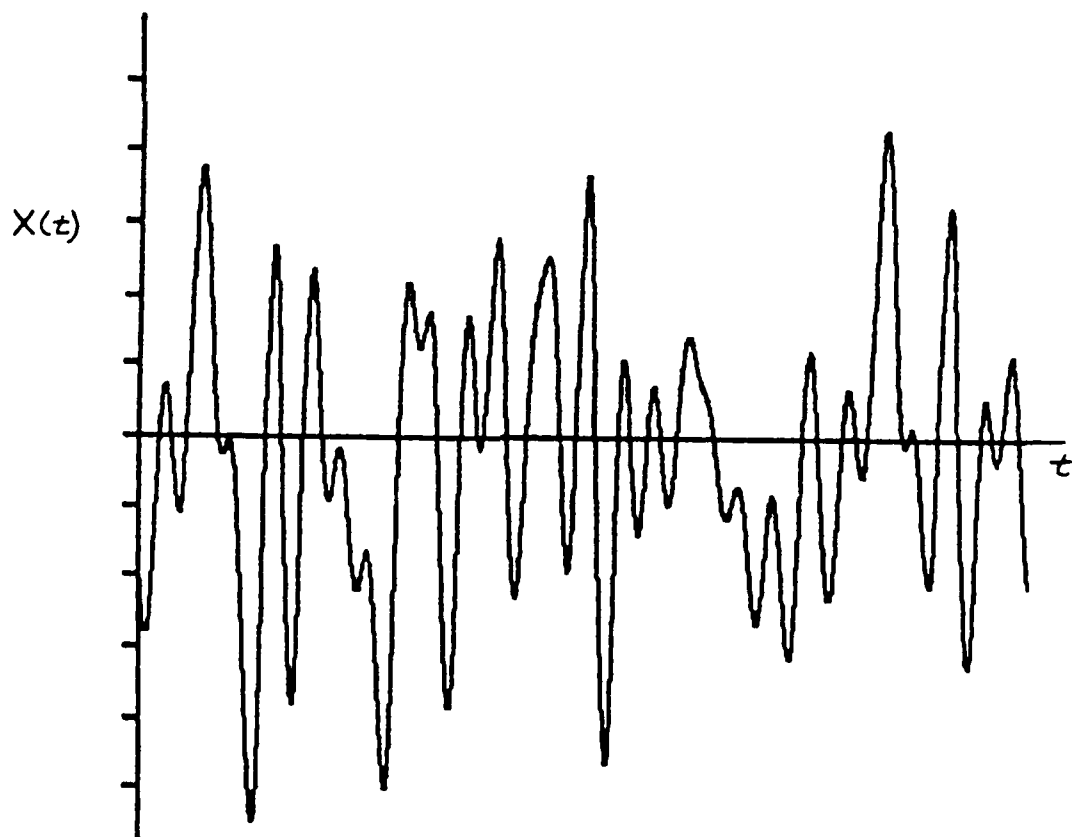


Figure 6.8. Wide-Band Random Vibration Signal.

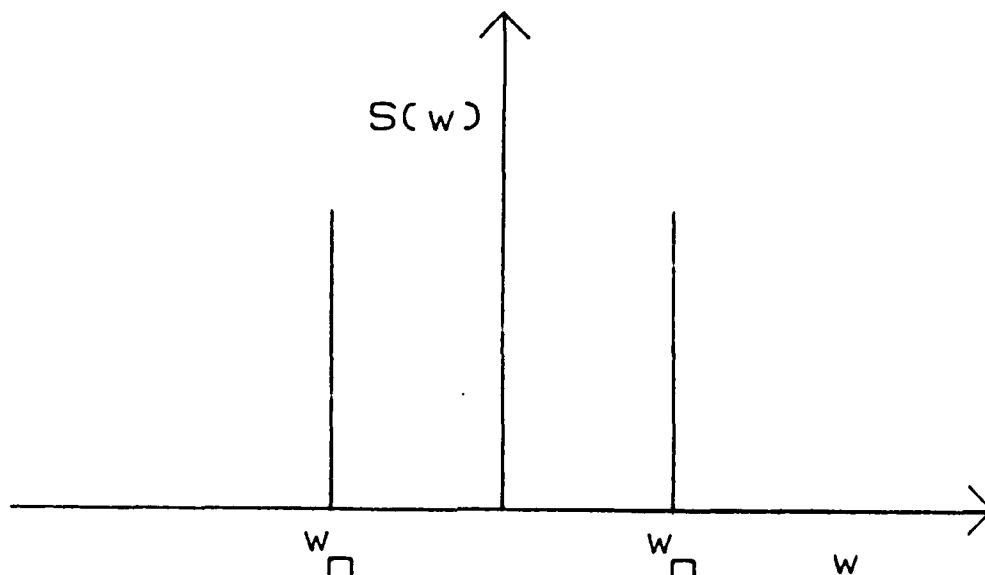


Figure 6.9. Sine Waveform Spectral Density Curve.

content of a random process. Figure 6.5 shows a typical narrow-banded spectral density function. The frequencies are concentrated in a small area which indicates a time domain sample of the form shown in Figure 6.6. A wide-banded spectral density (see Figure 6.7) has a wide range of frequencies. Its corresponding time domain signals become more erratic (see Figure 6.8).

The spectral density function of a sine wave has a value at one point (see Figure 6.9). Using the spectral density function as the reference for a random process, a combination of sine or cosine waveforms will simulate the random process for experimental purposes. In particular, one group of cosine waveforms is

$$x(t) = \sum_{j=1}^n C_j \cos(\omega_j t + \varphi_j) \quad (6.9)$$

where ω_j , $j=1, \dots, n$, are the band of frequencies, φ_j , $j=1, \dots, n$, are chosen to be uniformly distributed random variable on the interval $(0, 2\pi)$ and C_j , $j=1, \dots, n$, are equal to $2\sqrt{S(\omega_j)\Delta\omega}$.

The values of C_j , $j=1, \dots, n$, are derived by taking the $R_{xx}(\tau)$ of Equation (6.9) (The notation, $R_{xx}(\tau)$, replaces $R_{xx}(t_n, t_n + \tau)$ for ergodic random processes.). The substitution of time variable t_0 and t_1 yields

$$R_{xx}(\tau) = \frac{1}{4\pi^2} \int_{-\pi}^{\pi} d\varphi_i \int_{-\pi}^{\pi} d\varphi_j \sum_{i=1}^n \sum_{j=1}^n C_i C_j \cos(\omega_i t_0 - \varphi_i) \cos(\omega_j t_1 - \varphi_j). \quad (6.10)$$

Now consider when $j \neq i$.

$$\frac{C_i C_j}{4\pi^2} \int_{-\pi}^{\pi} d\varphi_i \int_{-\pi}^{\pi} d\varphi_j \cos(\omega_i t_0 - \varphi_i) \cos(\omega_j t_1 - \varphi_j) = 0$$

Second consider when $j=i$.

$$\frac{C_i^2}{4\pi^2} \int_{-\pi}^{\pi} d\varphi_i \int_{-\pi}^{\pi} d\varphi_i \cos(\omega_i t_0 - \varphi_i) \cos(\omega_i t_1 - \varphi_i) = 2\pi^2 \cos(\omega_i(t_0 - t_1))$$

From Equation (6.10) and the above results

$$R_{xx}(\tau) = \sum_{i=1}^n \frac{C_i^2}{2} \cos(\omega_i(t_0 - t_1)) = \sum_{i=1}^n \frac{C_i^2}{2} \cos(\omega_i(\tau)). \quad (6.11)$$

As stated before, $S(\omega)$ is defined to be the Fourier transform of the autocorrelation function.

$$S(\omega) = \frac{1}{2\pi} \int_{-\infty}^{\infty} R_{xx}(\tau) e^{-i\omega\tau} d\tau \quad (6.12)$$

Consider substituting Equation (6.11) with limits of T into Equation (6.12). First,

$$\int_{-T}^T R_{xx}(\tau) e^{-i\omega\tau} d\tau = \sum_{i=1}^n \frac{C_i^2}{2} \int_{-T}^T \cos(\omega_i(\tau)) e^{-i\omega\tau} d\tau \quad (6.13)$$

The integral in Equation (6.13) is

$$\int_{-T}^T \cos(\omega_i(\tau)) e^{-i\omega\tau} d\tau = \frac{\sin(\omega_i - \omega)T}{\omega_i - \omega} + \frac{\sin(\omega_i + \omega)T}{\omega_i + \omega}. \quad (6.14)$$

Also,

$$\int_{-\infty}^{\infty} \frac{\sin(\omega T)}{\omega} d\omega = \pi. \quad (6.15)$$

From Equations (6.13), (6.14), (6.15) and $T \rightarrow \infty$,

$$\int_{-\infty}^{\infty} \cos(\omega_i(\tau)) e^{-i\omega\tau} d\tau = \pi [\delta(\omega_i + \omega) + \delta(\omega_i - \omega)] \quad (6.16)$$

where $\delta(\omega)$ is the delta function defined as

$$\delta(\omega) = \begin{cases} 1 & \omega=0 \\ 0 & \text{elsewhere} \end{cases} \quad (6.17)$$

Finally, substituting the results of Equation (6.16) into Equation (6.13) yields

$$S(\omega) = \frac{1}{4} \sum_{i=1}^n C_i^2 [\delta(\omega_i + \omega) + \delta(\omega_i - \omega)] \quad (6.18)$$

From Equation (6.18), C_i , $i=1, \dots, n$, are determined to be $C_i = 2 \sqrt{S(\omega_i) \Delta\omega}$ which was specified at the beginning as

$$x(t) = \sum_{i=1}^n 2 \sqrt{S(\omega_i) \Delta\omega} \cos(\omega_i t + \varphi_i) \quad (6.19)$$

where φ_j , $j=1, \dots, n$, is random distributed on the interval $(0, 2\pi)$, $S(\omega)$ is the value at ω_j and $\Delta\omega$ is the bandwidth of the dividing interval for the specific spectral density function (see Figure 6.10).

6.4. Experimental Tests.

In the specimen shown in Figure 11, the first and second mode of vibration was 8 Hz and 58 Hz respectively. This specimen was being tested for force identification. It was desired to excite predominantly

the first mode of vibration. A spectral density function (see Figure 6.12) with bandwidth of 5 to 30 Hz was proposed for generating an excitation signal. Using Equation (6.19), a random signal was produced in the microcomputer. This became the desired response $x^D(t)$ (see Figure 6.13). In this test, the first run was done at the normal levels, because the specimen was assumed to be undamaged after each run. Figure 6.14 shows the modulus of $H^1(\omega)$. In the region of concern the curve is smooth, but outside this region this not true; however, the values are not important in determining the input signal to obtain the desired response.

Figure 6.15 shows the calculated signal to produce the desired response. The desired and measured response are compared in Figure 6.13. The goal for this test run was to excite the first mode of vibration. The modulus for the acceleration at mass 2 (see Figure 6.16) shows that the first mode of vibration was excited.

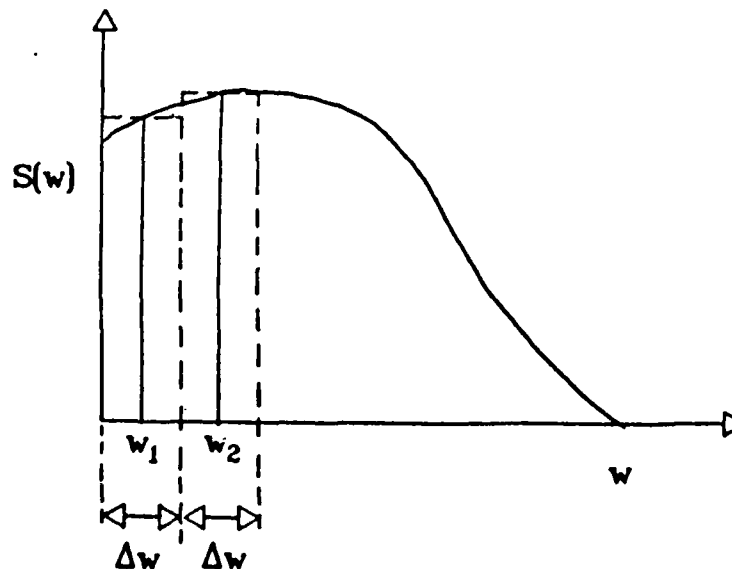


Figure 6.10. Spectral Density Notation Used in Equation (6.19).

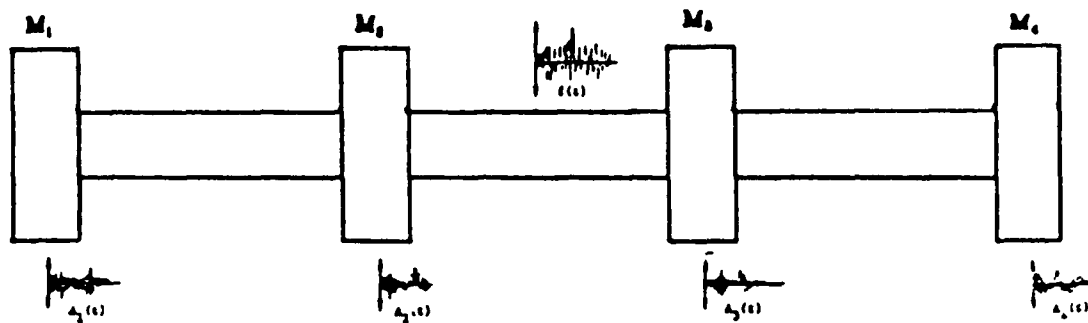


Figure 6.11. Force Identification Specimen.

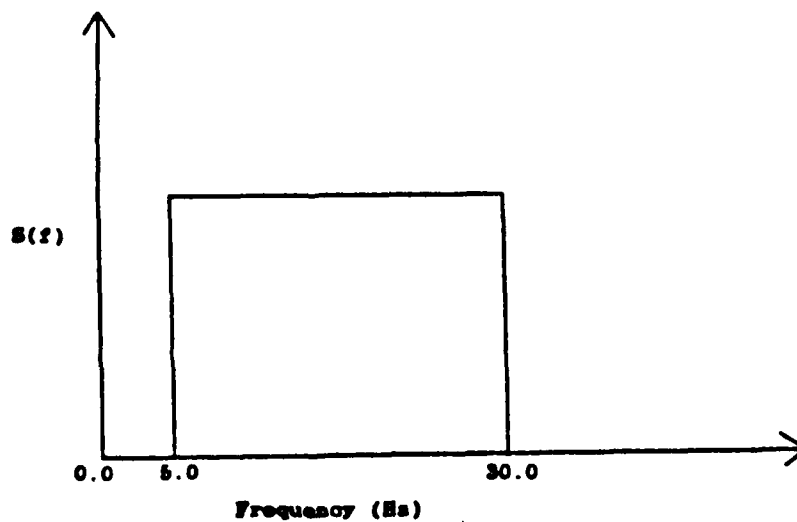


Figure 6.12. Spectral Density Curve with Bandwidth of 5 to 30 Hz.

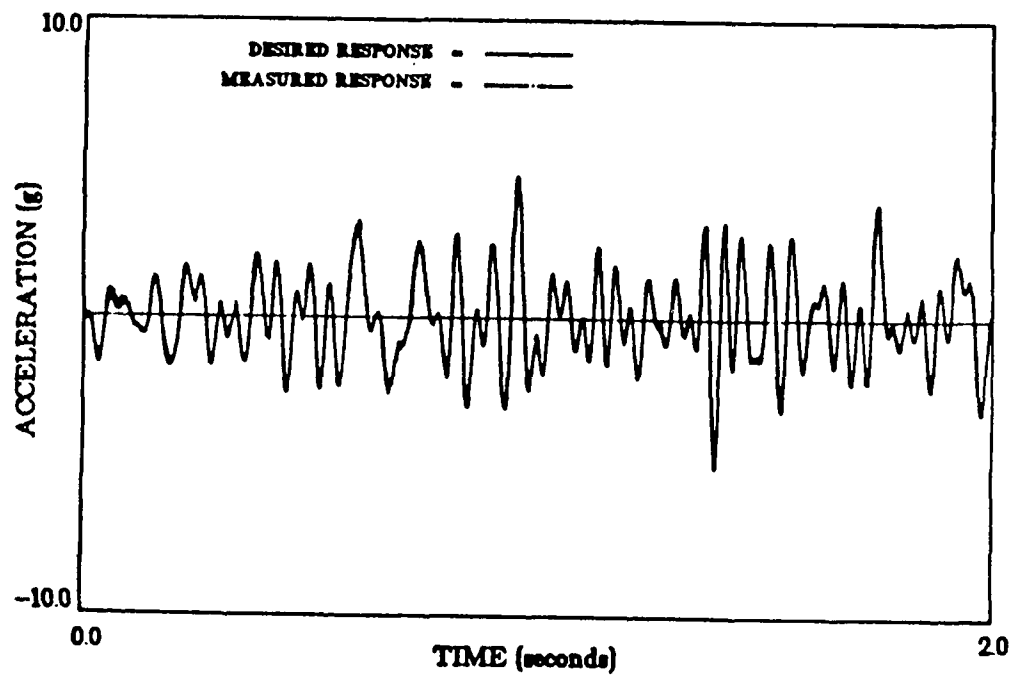


Figure 6.13. Desired and Measured Response.

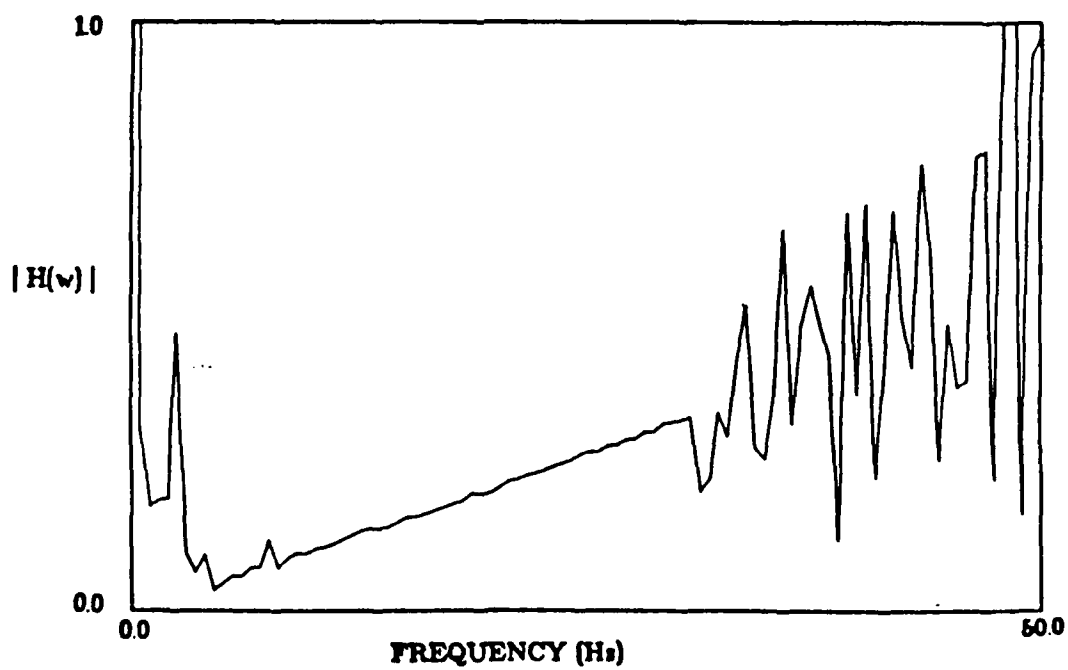


Figure 6.14. Modulus of $H^1(\omega)$ for Force Identification Setup.

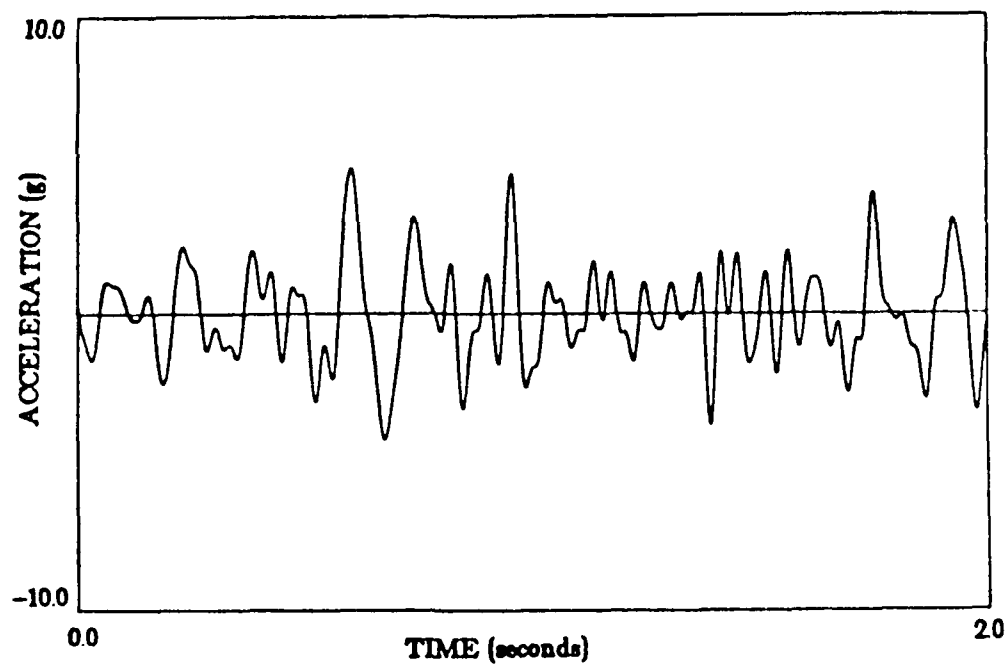


Figure 6.15. Input Signal for Desired Signal of Figure 6.12.

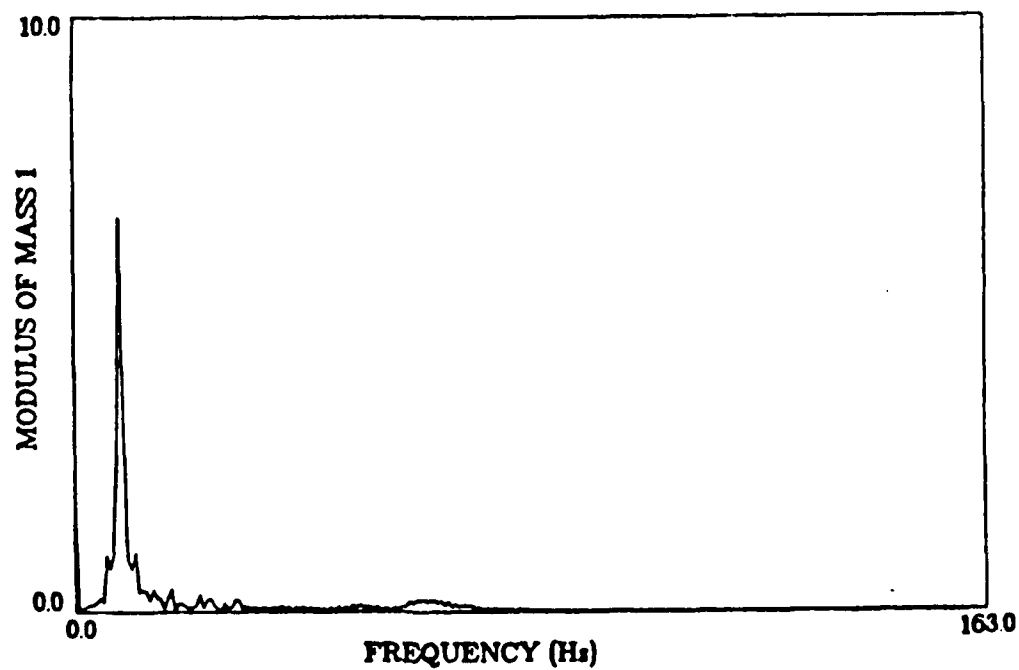


Figure 6.16. Modulus of Acceleration for Mass 2.

CHAPTER 7.

SUMMARY AND CONCLUSION

7.0. Summary.

The main objective of this research was to develop an alternate method to determine input forces to a structure. This method was the sum of weighted acceleration technique, SWAT. The work which was conducted for this research explored the assumption that SWAT can accurately estimate forces that are applied to multi-degree-of-freedom structures. The main discussion of the report focused on methods to determine the effective weights of the following SWAT equation.

$$F_R = \sum_{i=1}^n w_i a_i \quad (7.1)$$

A time domain approach and a frequency domain approach to determine the effective weights were presented in chapter 2. Both of these approaches used experimental data. This was an input-output data formulation where the input data were forces that excited the structure and the output data were the measurements of acceleration at specific points along the structure. The frequency domain approach was less sensitive to noise contained in the experimental data, but both methods provided effective weights which produced favorable results. These two approaches were first utilized with lumped mass systems that were excited with a random force. In all cases when the input force was plotted against the force that was calculated from SWAT, the comparison was almost perfect.

In chapter 3, these two experimental approaches were applied to continuous systems. In addition to the random excitation, impact loadings were applied to the structures. The random excitation experiments duplicated the results of the lumped mass systems. The impact loading tests showed a trend of SWAT to be "band-limited." Band-limited in this case, means that the content of the input force in the frequency domain has power at a specific range of frequencies. The force history record which was calculated from SWAT predicted the main events. In the regions after the main events, the results showed that the higher vibration modes continued to vibrate without the effective weights cancelling the resulting force.

SWAT accurately predicted the forces for nonlinear structures. The nonlinearity for the test specimens in this research were graphed by a force-mapping technique.

The above approaches required experimental data to determine the effective weights for a structure. Two methods not requiring experimental data were developed using the mode shape of a structure and finite elements. The use of these approaches opens avenues for more applications where experimental excitation of a structure is virtually impossible. The mode shapes of a structure may be determined from a number of different methods such as finite elements or finite difference. Applications and results of these methods are shown in Chapter 5.

7.1. Conclusions.

SWAT was developed to provide an alternate means of calculating the input forces to a structure. Conclusions from this research are as

follows:

1. SWAT is a simple and powerful approach to determine input forces for multi-degree-of-freedom structures. The method requires only measured accelerations and effective weights for the structure to determine the input force.

2. The band-width of the input forces is important when considering the number of effective weights to use. In general, the more locations to measure the accelerations used in SWAT, the wider the bandwidth for a specific set of effective weights.

3. SWAT predicts input forces for both linear and nonlinear structures.

4. The use of methods such as the mode shape approach and finite element approach allow the use of SWAT without using experimental data to determine the effective weights. This is especially important for large structures.

APPENDIX 1.

DATA RECORDS FOR LUMPED MASS SYSTEMS

A1.0 Introduction.

In Chapter 2, symmetric (see Figure 2.2) and antisymmetric (see Figure 2.3) test specimens were used to represent a lump mass system. Seven test runs of different bandwidth of random excitation were performed on each specimen. Test runs 1, 3, and 5 were used to determine the effective weights. The other runs were used for comparing the predicted force, which was determined using SWAT, to the measured force. This appendix contains plots of the experiment data records for each of the specimens for test runs 1, 3, and 5.

A1.1 Symmetric Records.

TABLE A1.1 Symmetric Lump Mass Specimen's Reference for Plots of Test Runs 1, 3, and 5.

Test Run #	1	3	5
Bandwidth of Excitation	0-50 Hz	110-200 Hz	0-200 Hz
Acceleration Record of Mass 1	Figure A1.1	Figure A1.7	Figure A1.13
Modulus of Acceleration Record of Mass 1	Figure A1.2	Figure A1.8	Figure A1.14
Acceleration Record of Mass 2	Figure A1.3	Figure A1.9	Figure A1.15
Modulus of Acceleration Record of Mass 2	Figure A1.4	Figure A1.10	Figure A1.16
Force Record	Figure A1.5	Figure A1.11	Figure A1.17
Modulus of Force Record	Figure A1.6	Figure A1.12	Figure A1.18

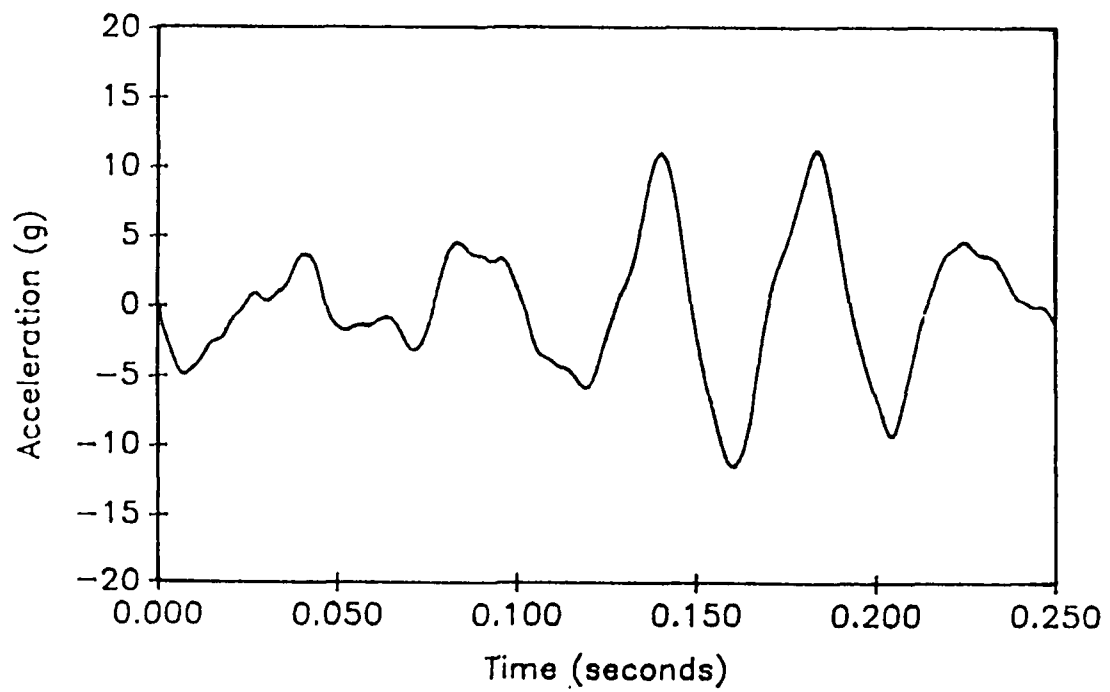


Figure A1.1. Acceleration Record of Mass 1 for Symmetric Test Specimen of Test Run 1.

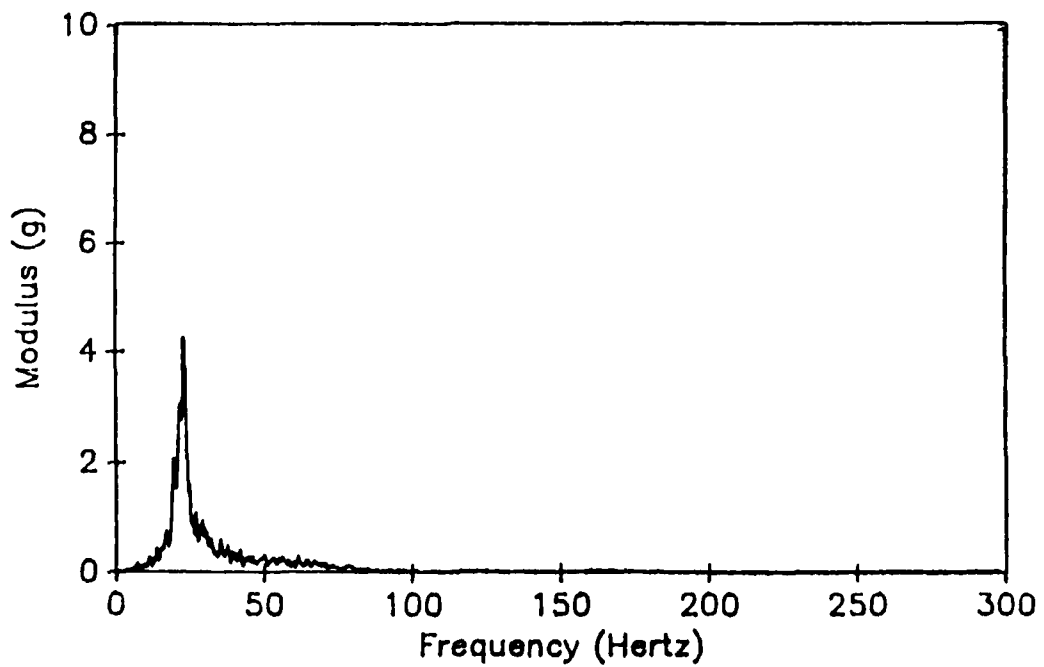


Figure A1.2. Modulus of Acceleration Record of Mass 1 for Symmetric Test Specimen of Test Run 1.

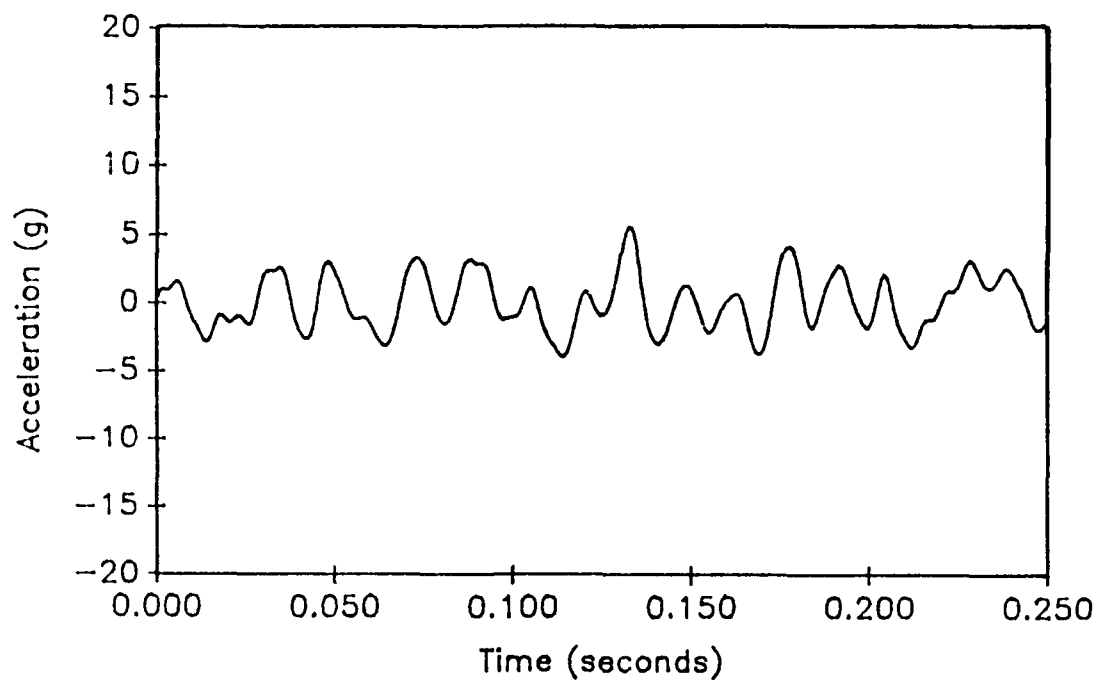


Figure A1.3. Acceleration Record of Mass 2 for Symmetric Test Specimen of Test Run 1.

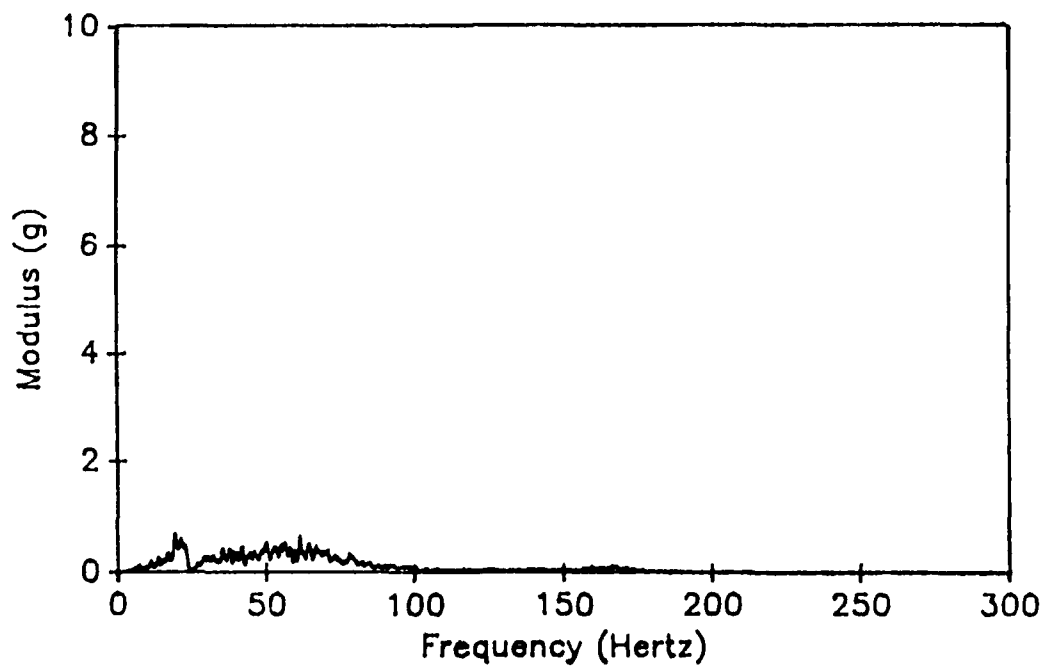


Figure A1.4. Modulus of Acceleration Record of Mass 2 for Symmetric Test Specimen of Test Run 1.

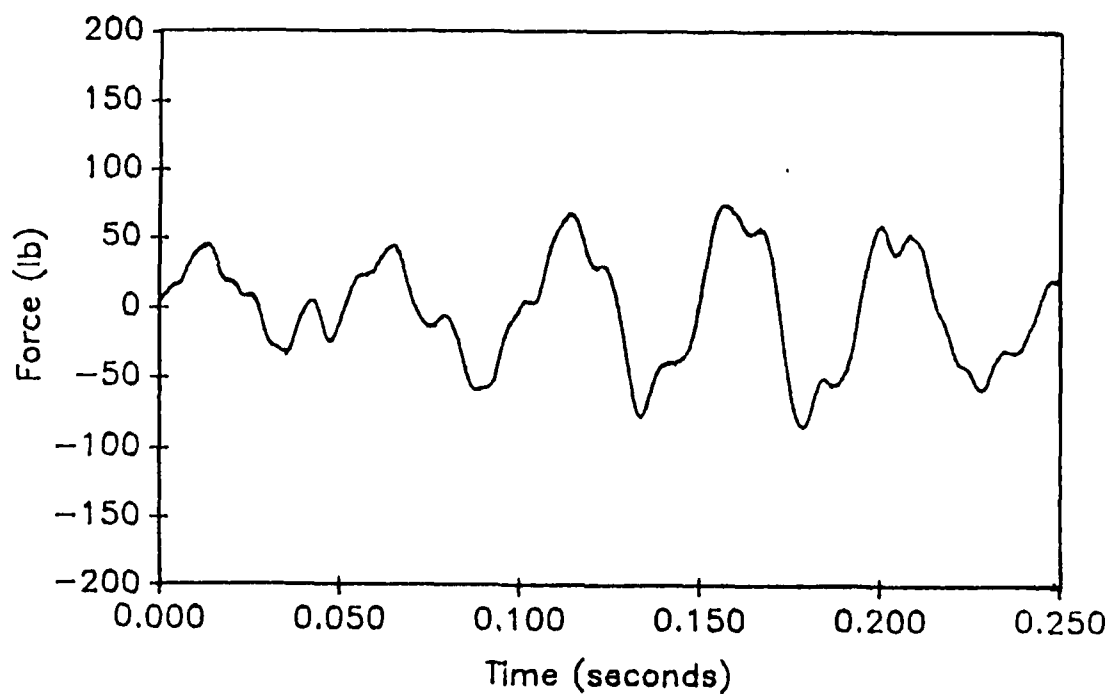


Figure A1.5. Force Record for Symmetric Test Specimen of Test Run 1.

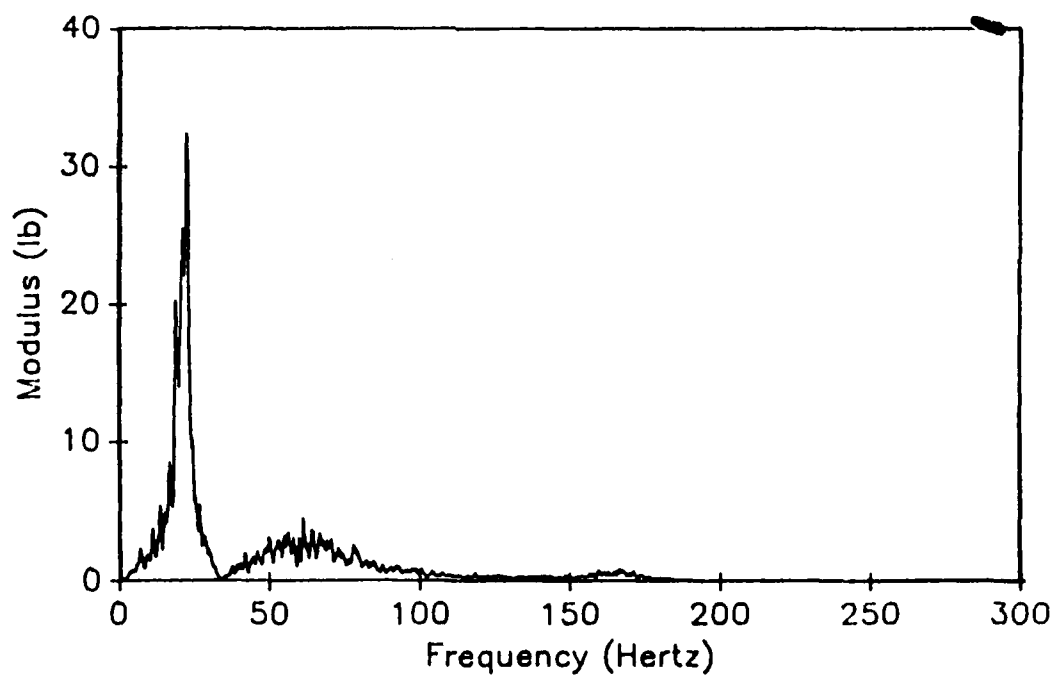


Figure A1.6. Modulus of Force Record for Symmetric Test Specimen of Test Run 1.

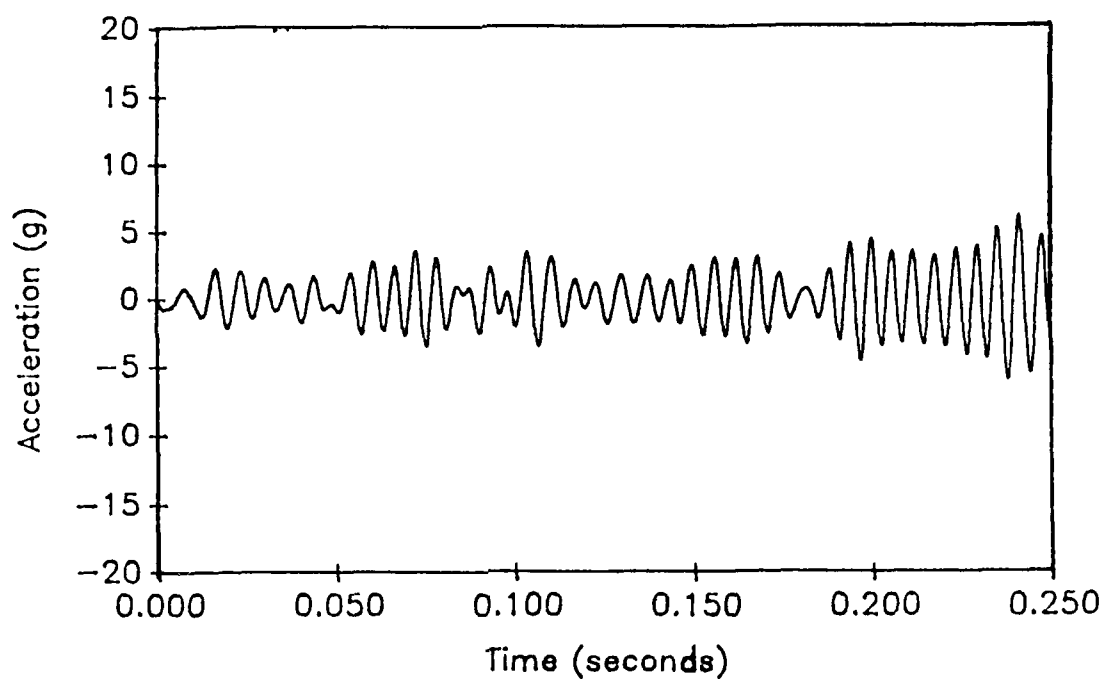


Figure A1.7. Acceleration Record of Mass 1 for Symmetric Test Specimen of Test Run 3.

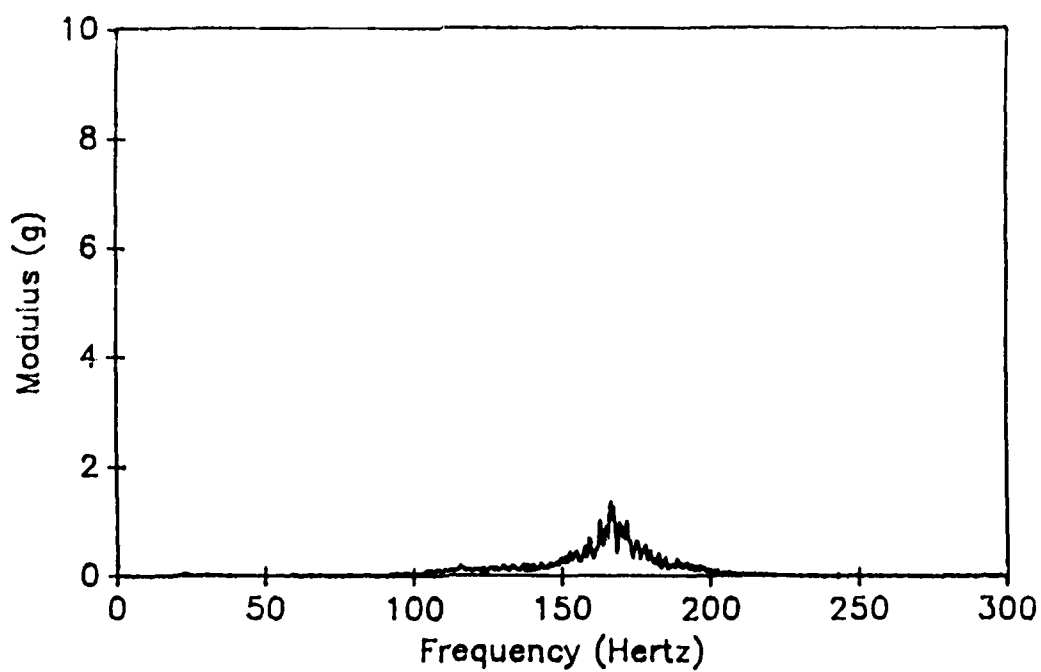


Figure A1.8. Modulus of Acceleration Record of Mass 1 for Symmetric Test Specimen of Test Run 3.

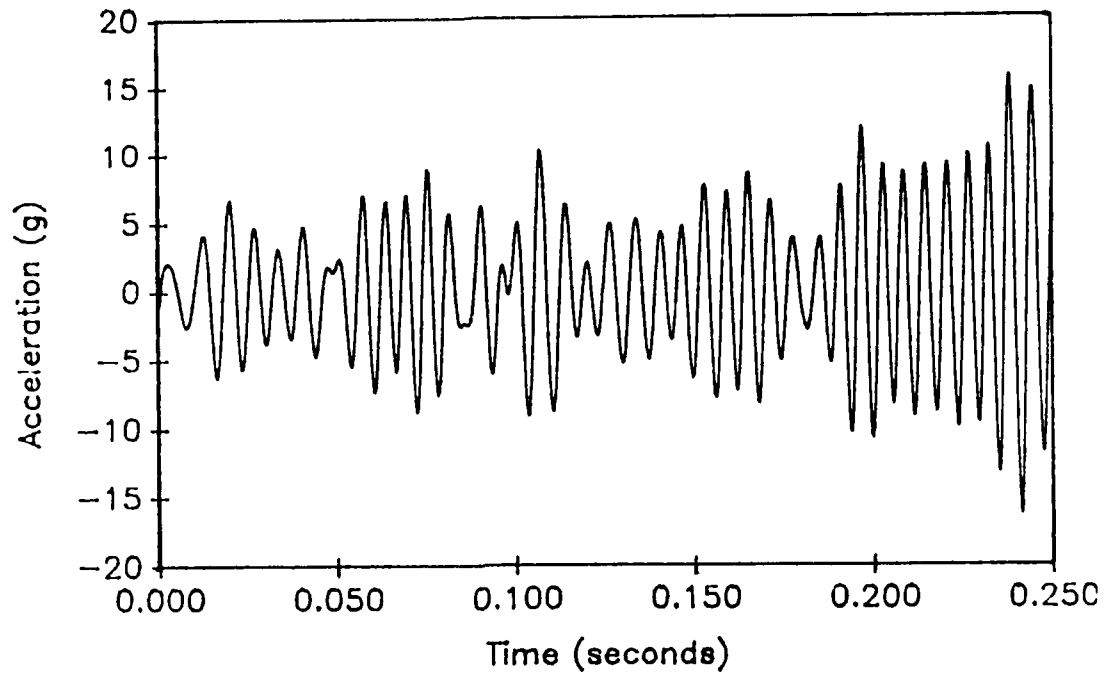


Figure A1.9. Acceleration Record of Mass 2 for Symmetric Test Specimen of Test Run 3.

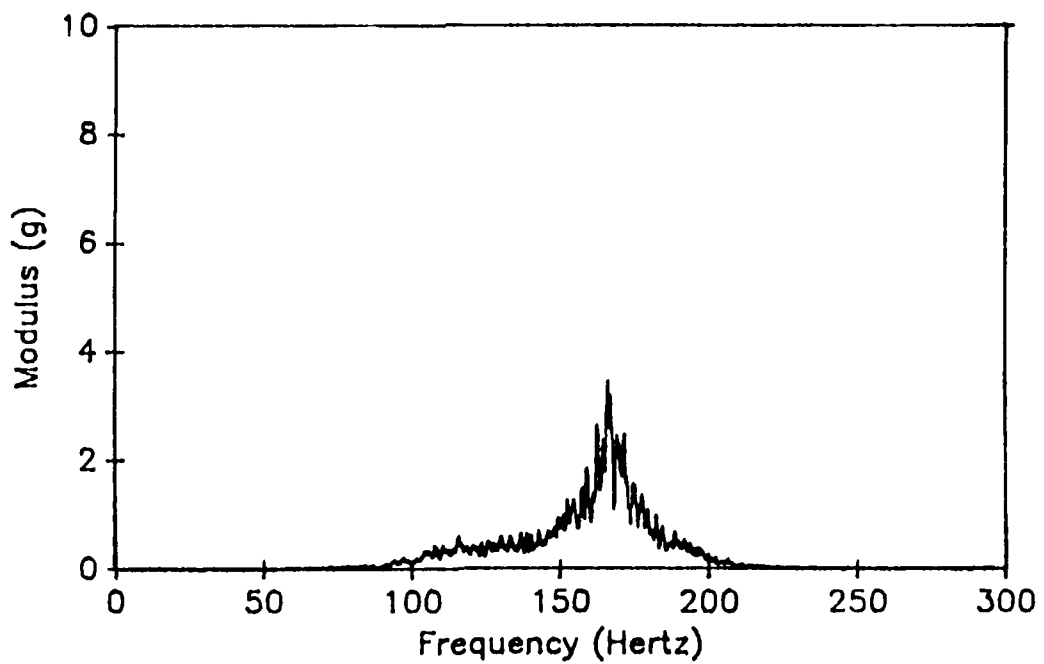


Figure A1.10. Modulus of Acceleration Record of Mass 2 for Symmetric Test Specimen of Test Run 3.

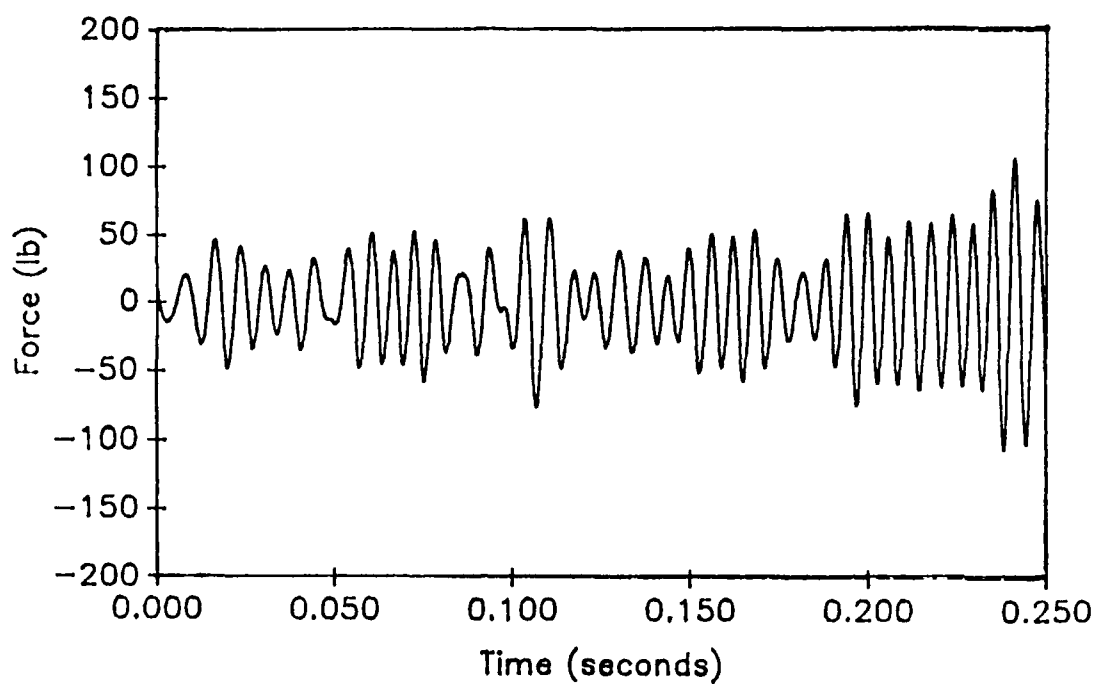


Figure A1.11. Force Record for Symmetric Test Specimen of Test Run 3.

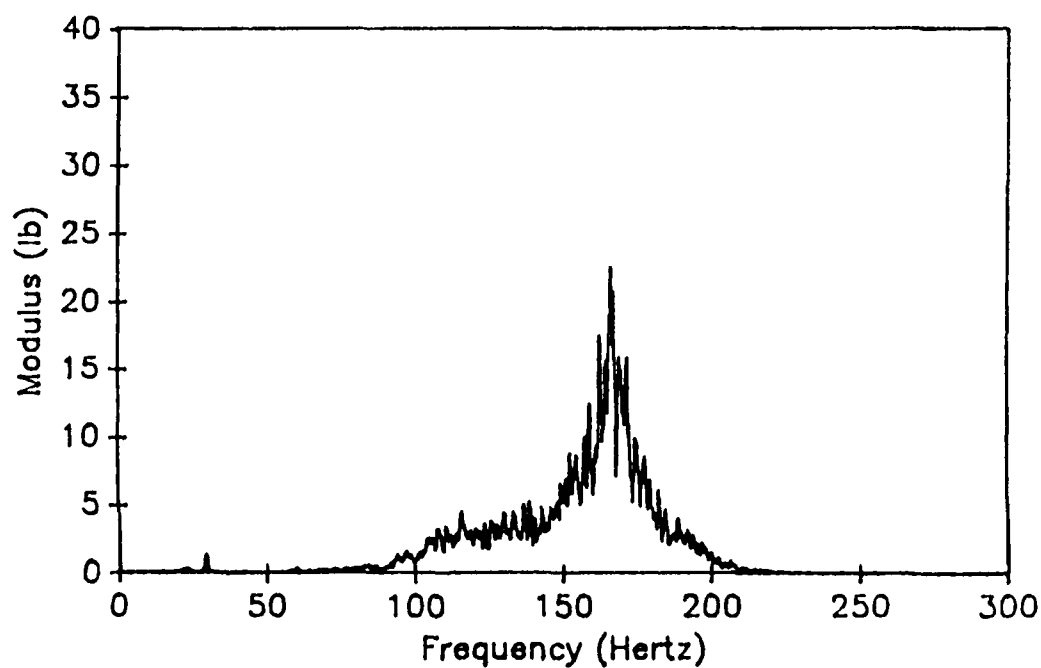


Figure A1.12. Modulus of Force Record for Symmetric Test Specimen of Test Run 3.

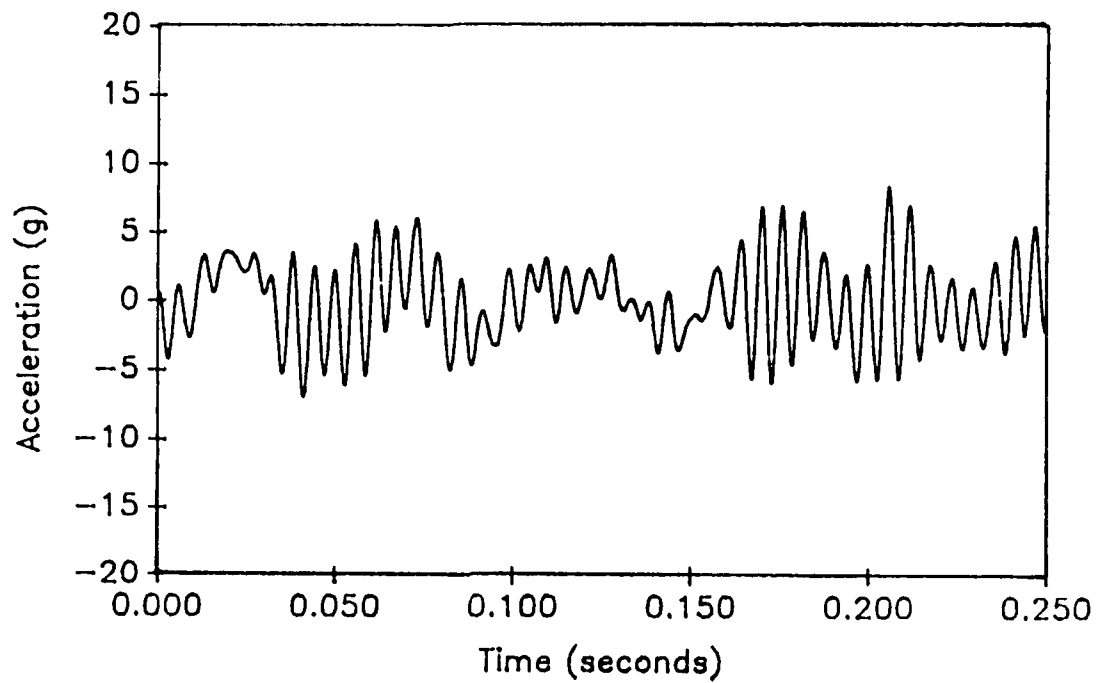


Figure A1.13. Acceleration Record of Mass 1 for Symmetric Test Specimen of Test Run 5.

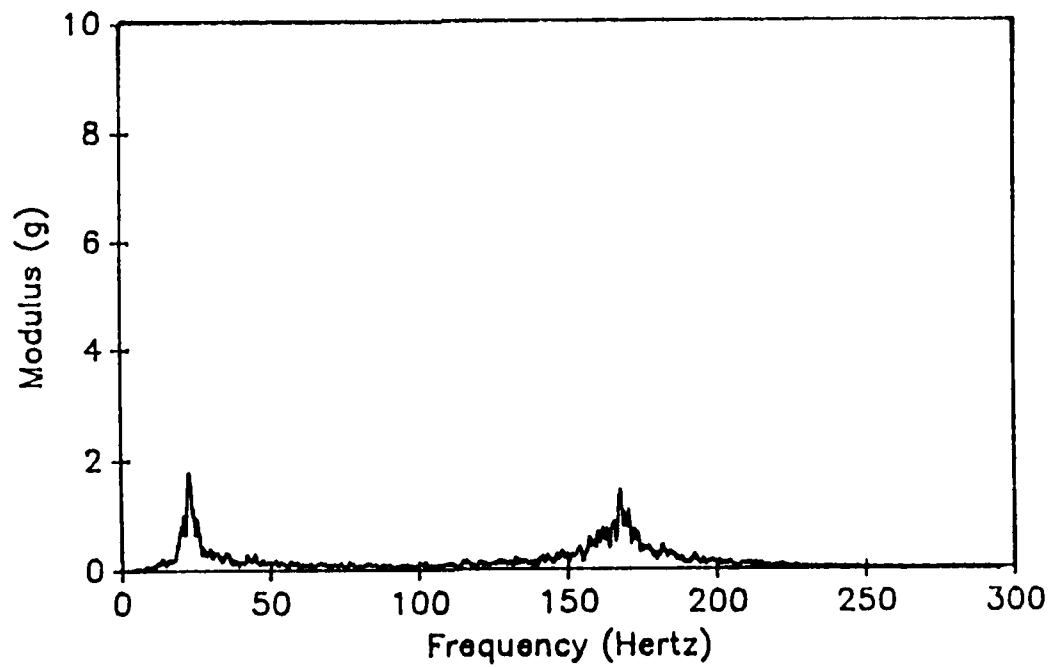


Figure A1.14. Modulus of Acceleration Record of Mass 1 for Symmetric Test Specimen of Test Run 5.

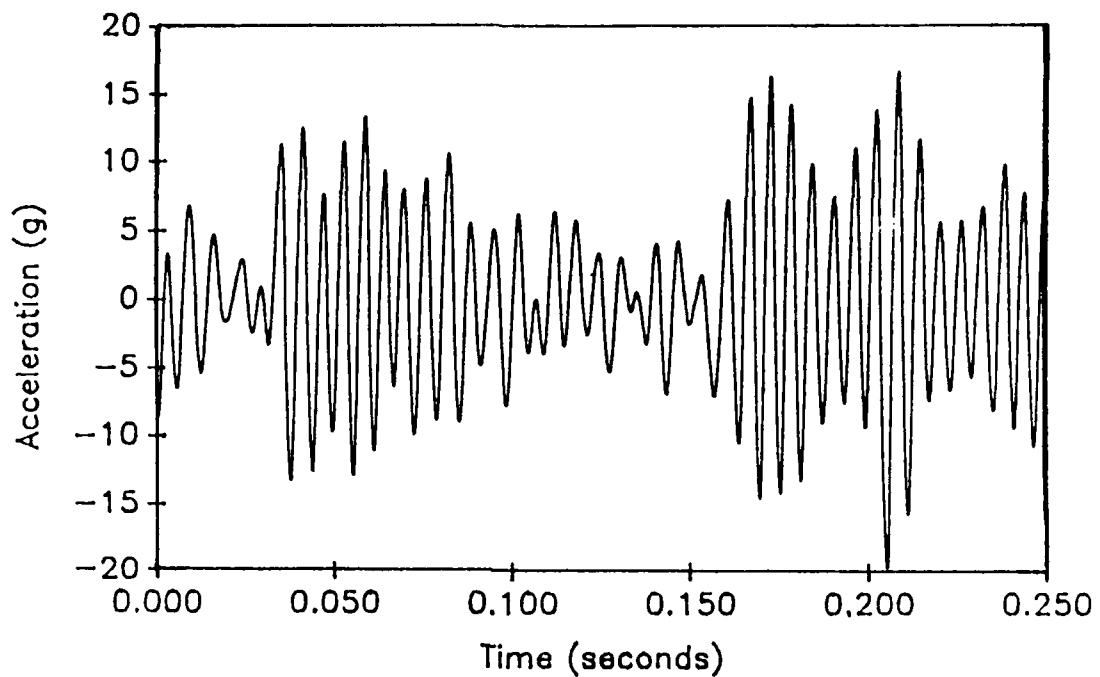


Figure A1.15. Acceleration Record of Mass 2 for Symmetric Test Specimen of Test Run 5.

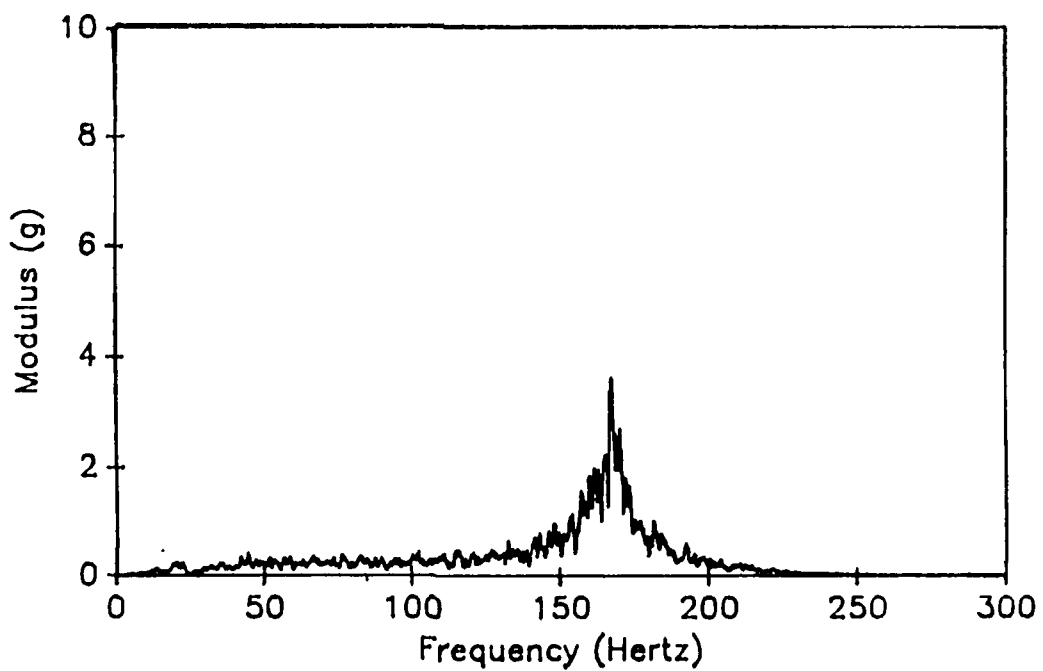


Figure A1.16. Modulus of Acceleration Record of Mass 2 for Symmetric Test Specimen of Test Run 5.

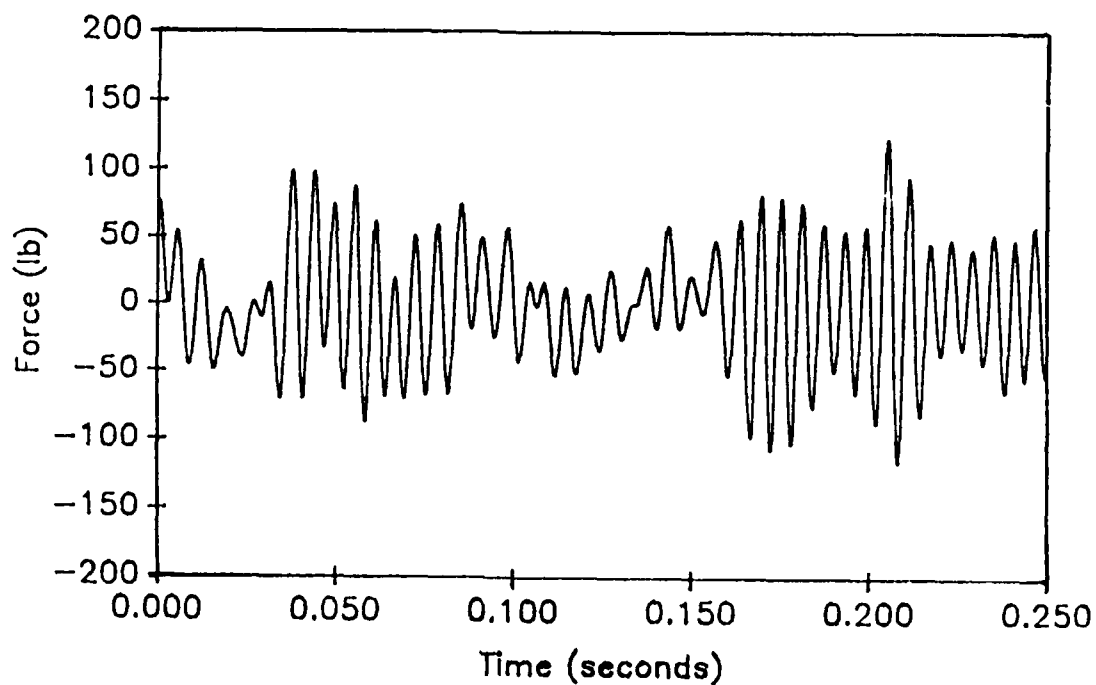


Figure A1.17. Force Record for Symmetric Test Specimen of Test Run 5.

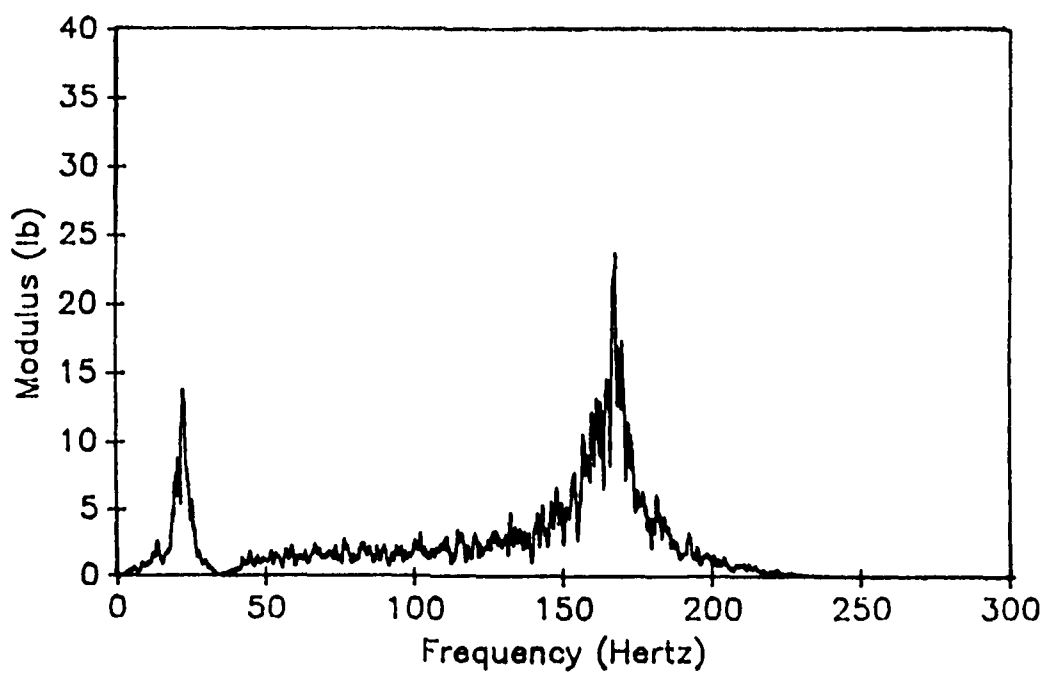


Figure A1.18. Modulus of Force Record for Symmetric Test Specimen of Test Run 5.

A1.2 Antisymmetric Records.

TABLE A1.2 Antisymmetric Lump Mass Specimen's Reference for Plots of the Test Runs 1, 3, and 5.

Test Run #	1	3	5
Bandwidth of Excitation	0-50 Hz	110-200 Hz	0-200 Hz
Acceleration Record of Mass 1	Figure A1.19	Figure A1.29	Figure A1.39
Modulus of Acceleration Record of Mass 1	Figure A1.20	Figure A1.30	Figure A1.40
Acceleration Record of Mass 2	Figure A1.21	Figure A1.31	Figure A1.41
Modulus of Acceleration Record of Mass 2	Figure A1.22	Figure A1.32	Figure A1.42
Acceleration Record of Mass 3	Figure A1.23	Figure A1.33	Figure A1.43
Modulus of Acceleration Record of Mass 3	Figure A1.24	Figure A1.34	Figure A1.44
Acceleration Record of Mass 4	Figure A1.25	Figure A1.35	Figure A1.45
Modulus of Acceleration Record of Mass 4	Figure A1.26	Figure A1.36	Figure A1.46
Force Record	Figure A1.27	Figure A1.37	Figure A1.47
Modulus of Force Record	Figure A1.28	Figure A1.38	Figure A1.48

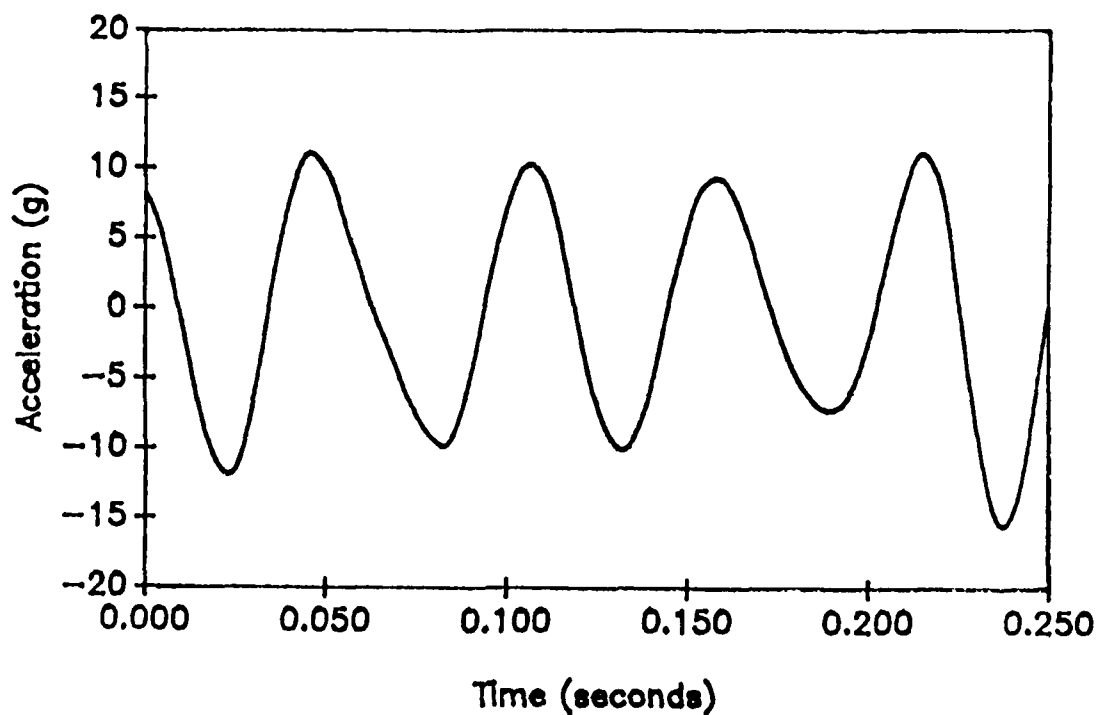


Figure A1.19. Acceleration Record of Mass 1 for Antisymmetric Test Specimen of Test Run 1.

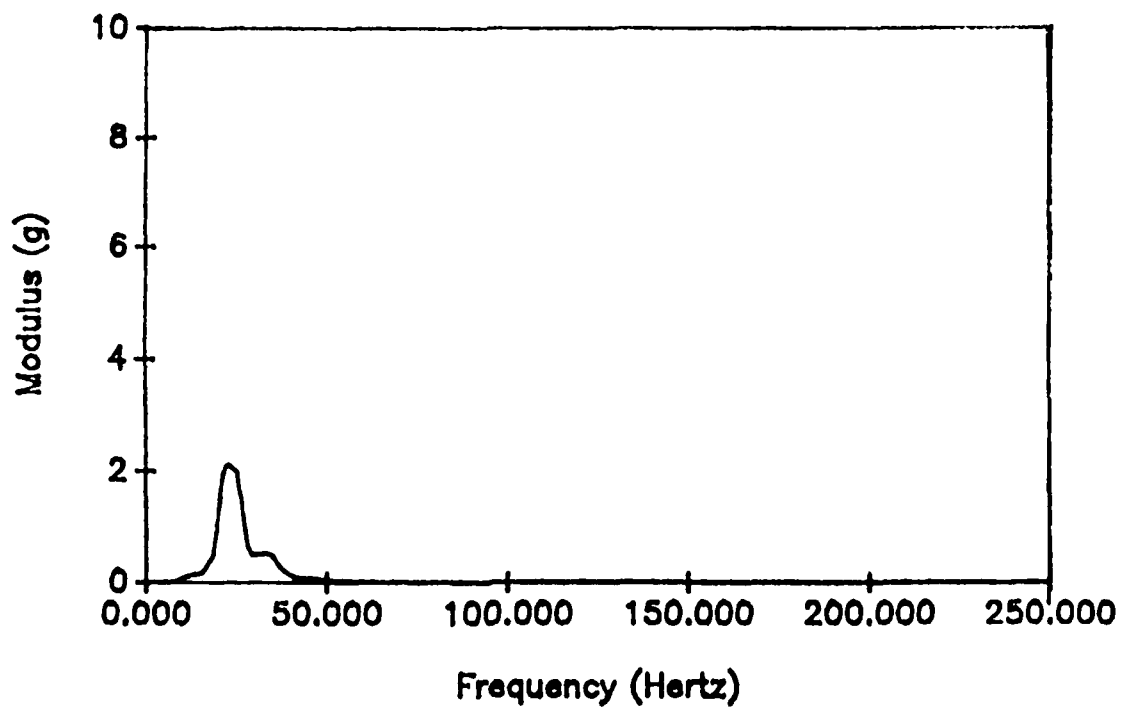


Figure A1.20. Modulus of Acceleration Record of Mass 1 for Antisymmetric Test Specimen of Test Run 1.

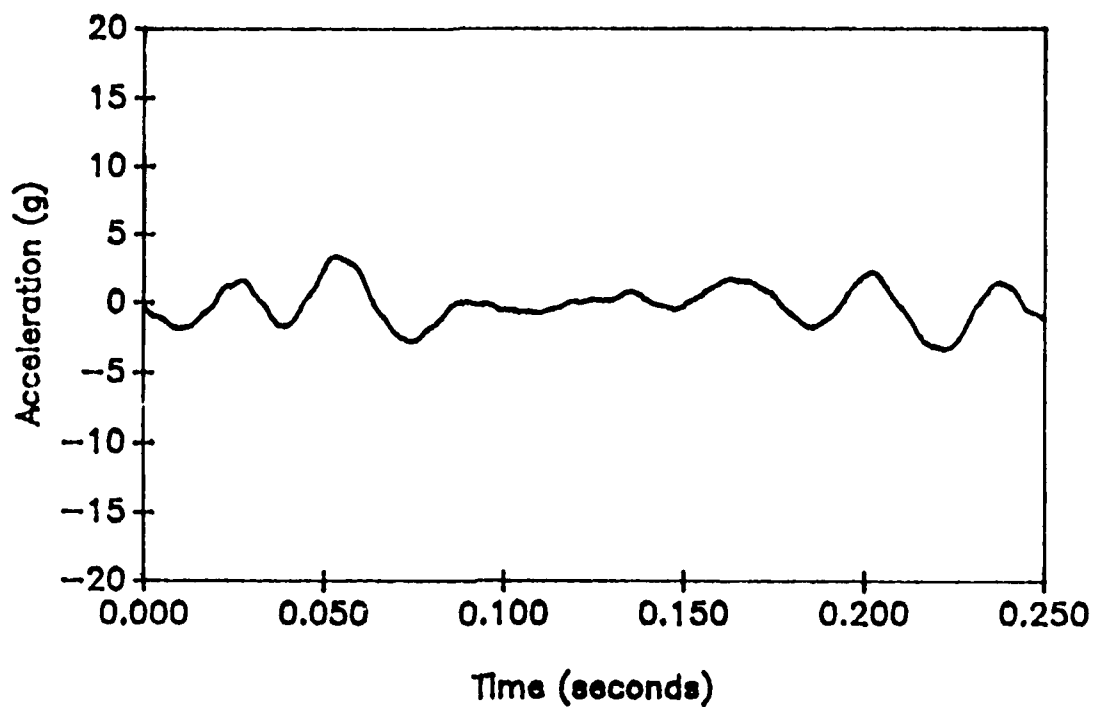


Figure A1.21. Acceleration Record of Mass 2 for Antisymmetric Test Specimen of Test Run 1.

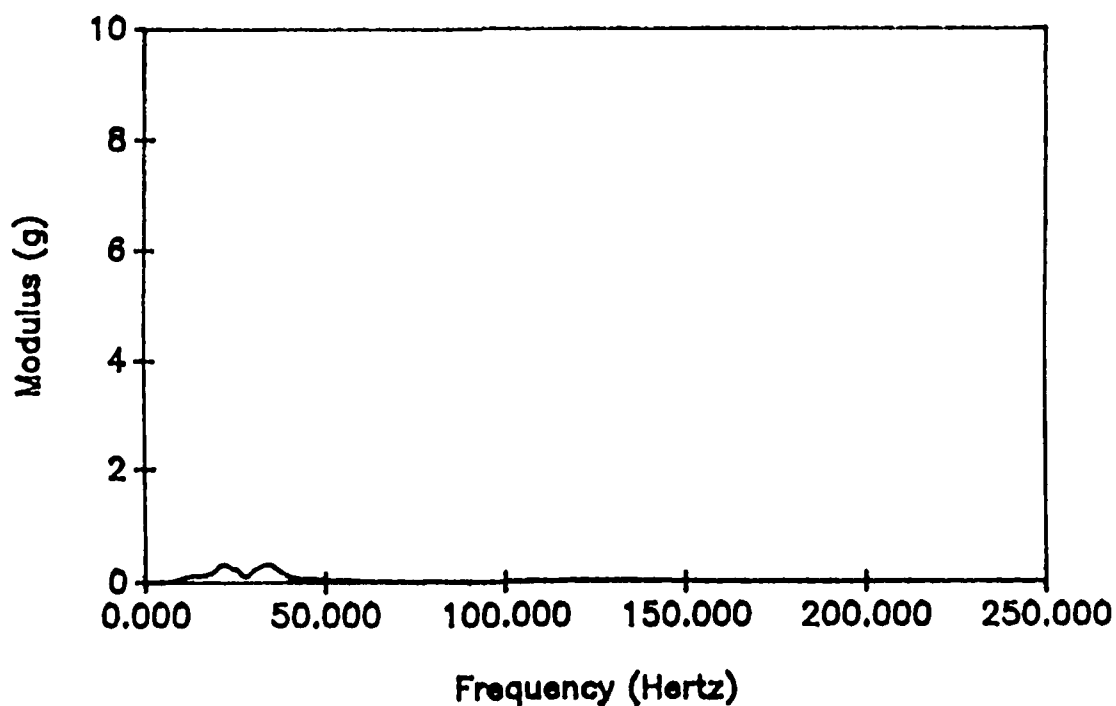


Figure A1.22. Modulus of Acceleration Record of Mass 2 for Antisymmetric Test Specimen of Test Run 1.

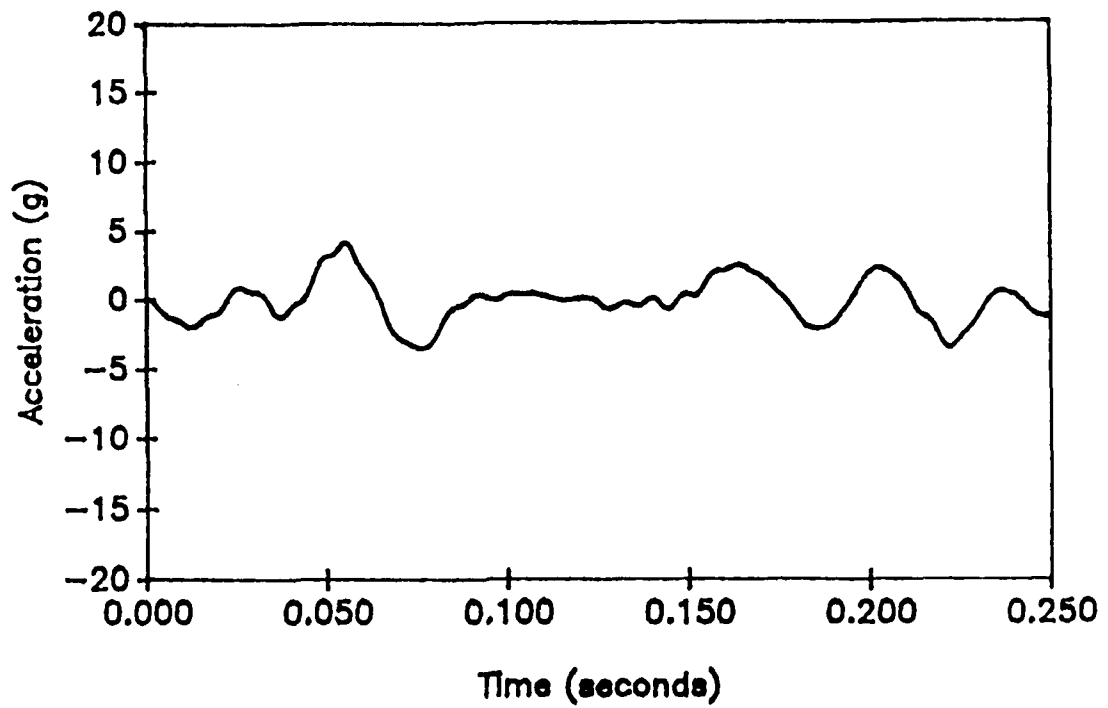


Figure A1.23. Acceleration Record of Mass 3 for Antisymmetric Test Specimen of Test Run 1.

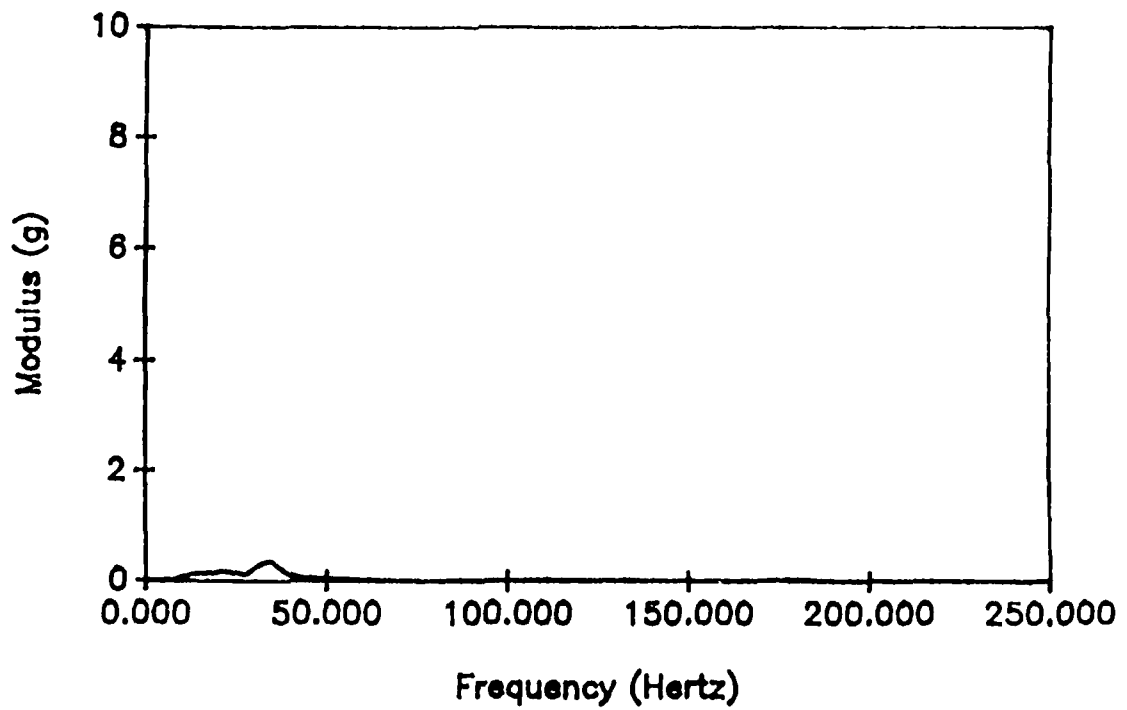


Figure A1.24. Modulus of Acceleration Record of Mass 3 for Antisymmetric Test Specimen of Test Run 1.

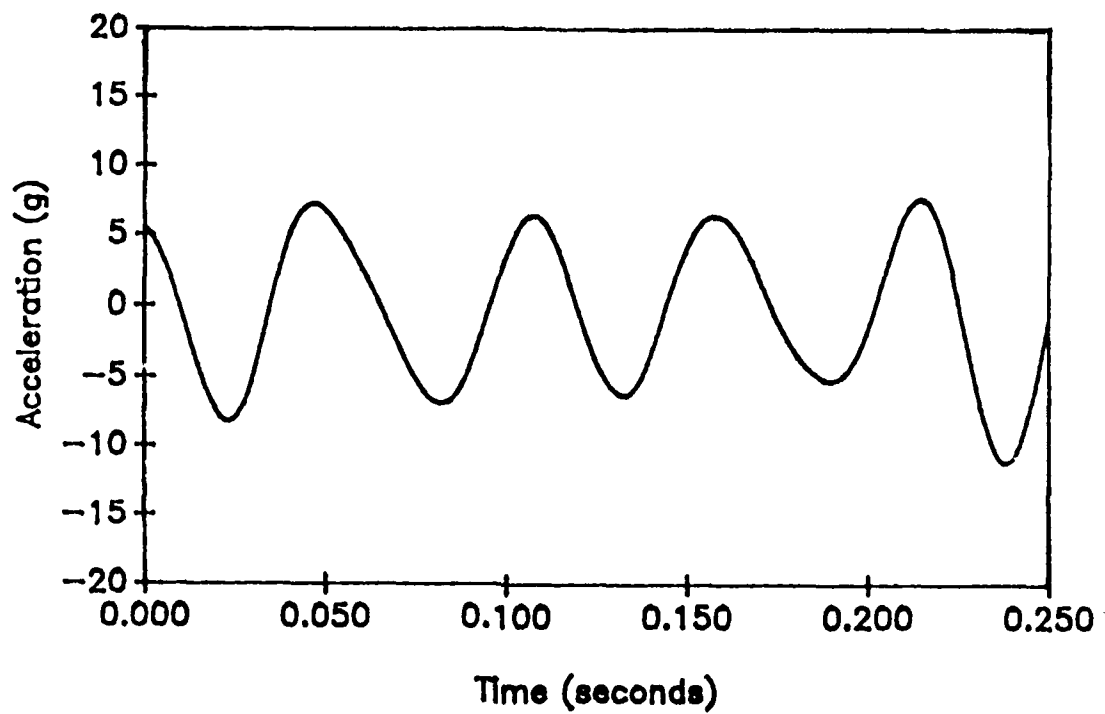


Figure A1.25. Acceleration Record of Mass 4 for Antisymmetric Test Specimen of Test Run 1.

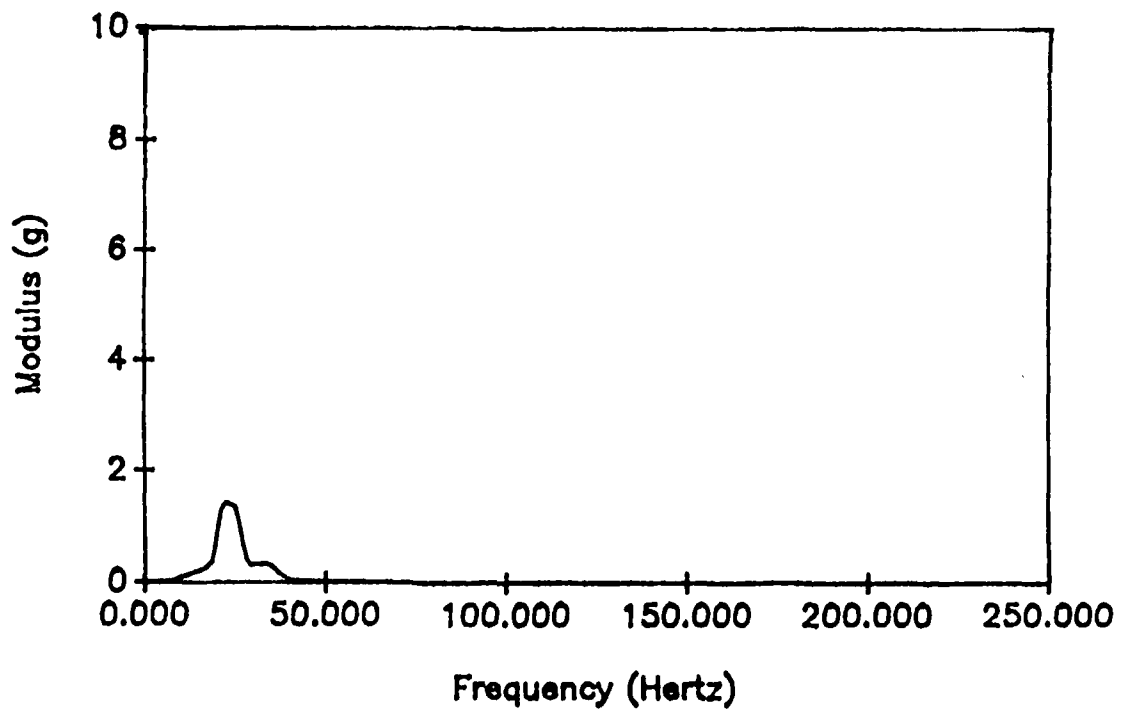


Figure A1.26. Modulus of Acceleration Record of Mass 4 for Antisymmetric Test Specimen of Test Run 1.

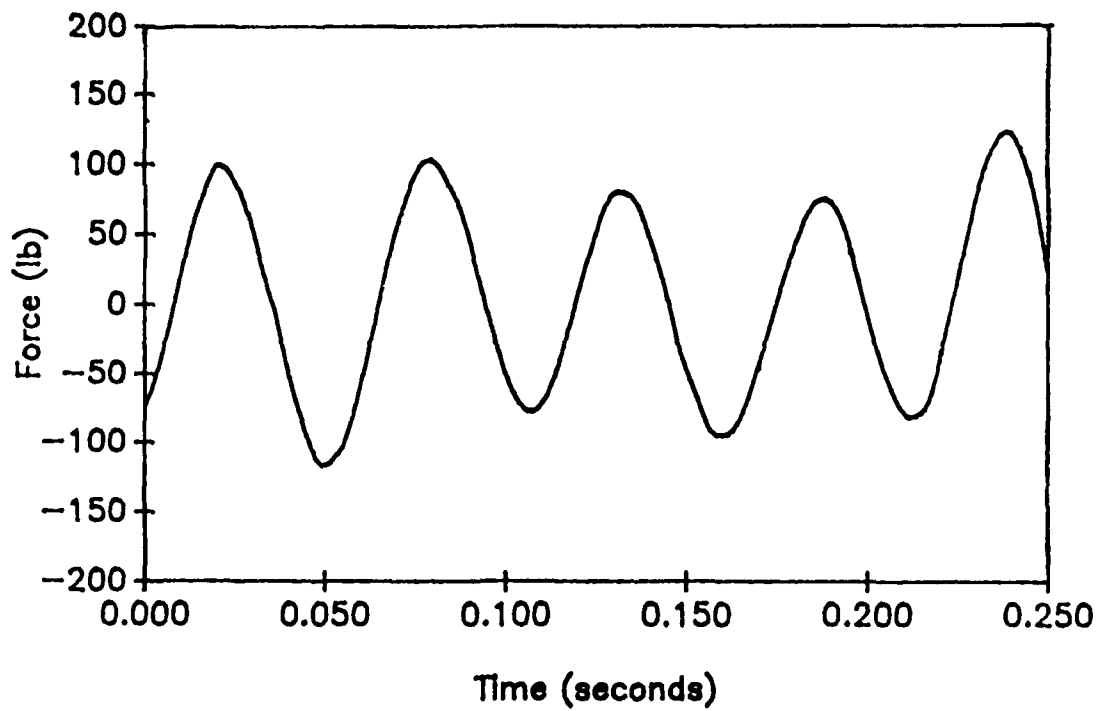


Figure A1.27. Force Record for Antisymmetric Test Specimen of Test Run 1.

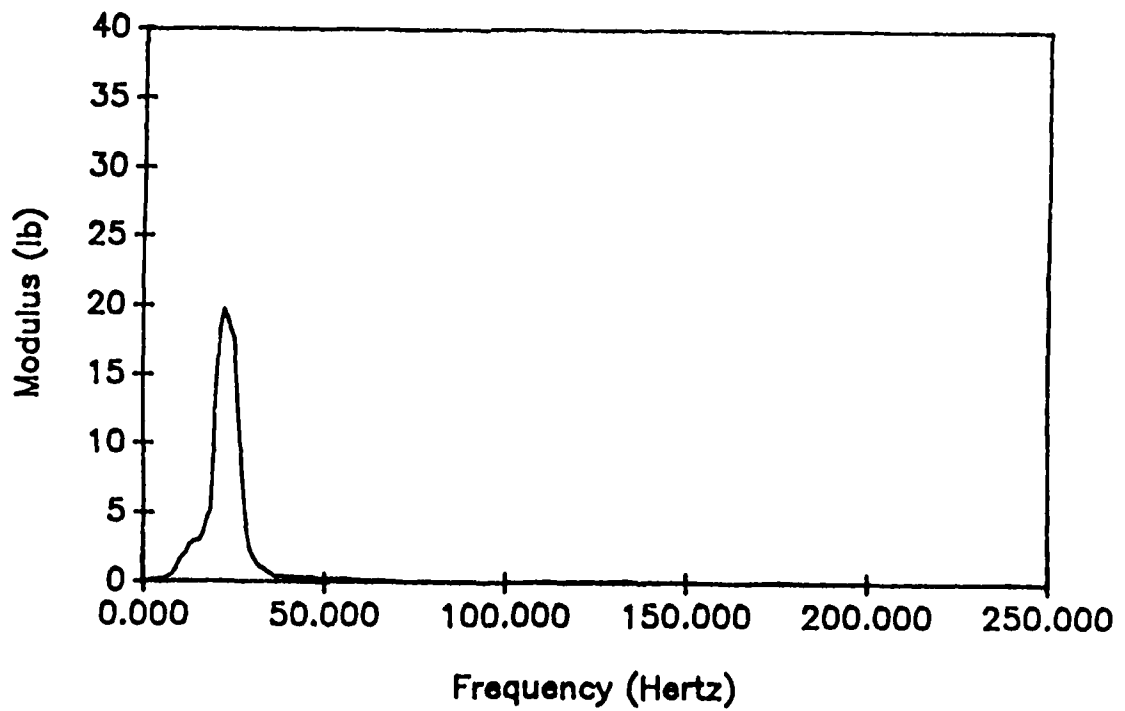


Figure A1.28. Modulus of Force Record for Antisymmetric Test Specimen of Test Run 1.

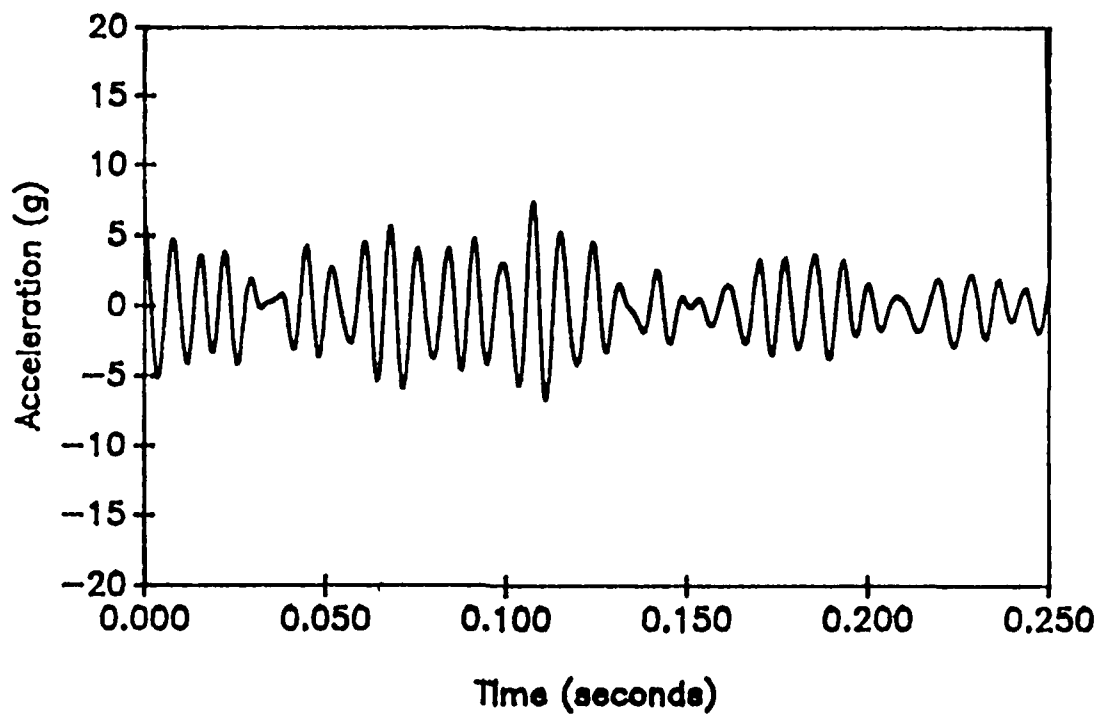


Figure A1.29. Acceleration Record of Mass 1 for Antisymmetric Test Specimen of Test Run 3.

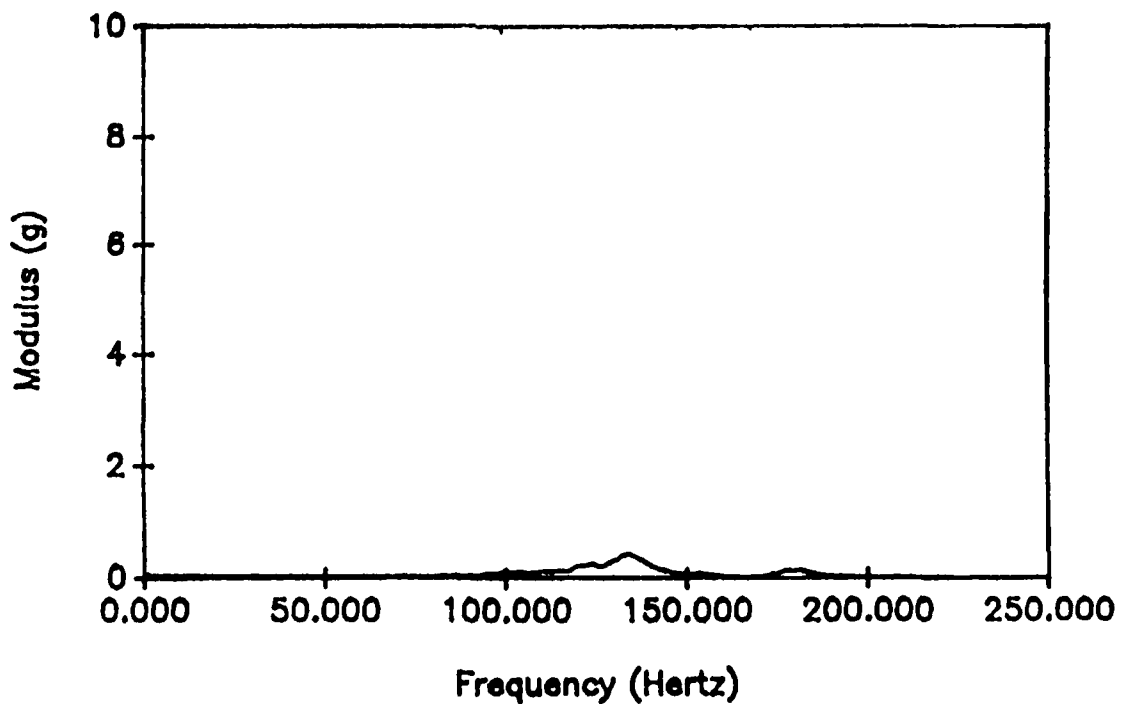


Figure A1.30. Modulus of Acceleration Record of Mass 1 for Antisymmetric Test Specimen of Test Run 3.

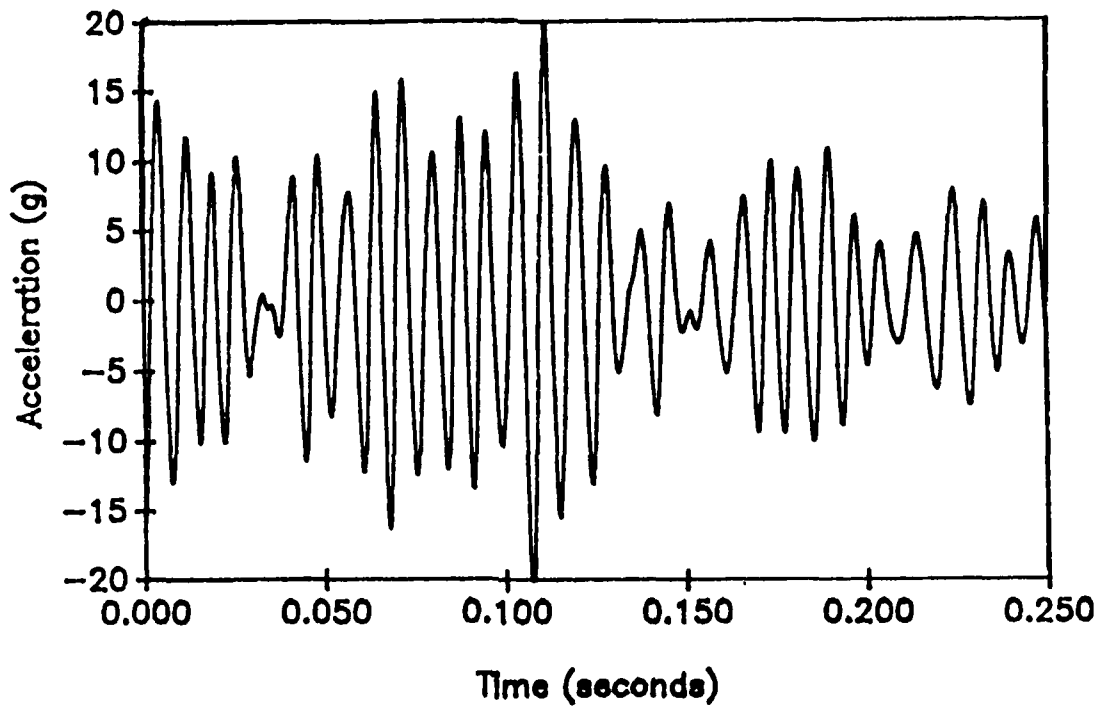


Figure A1.31. Acceleration Record of Mass 2 for Antisymmetric Test Specimen of Test Run 3.

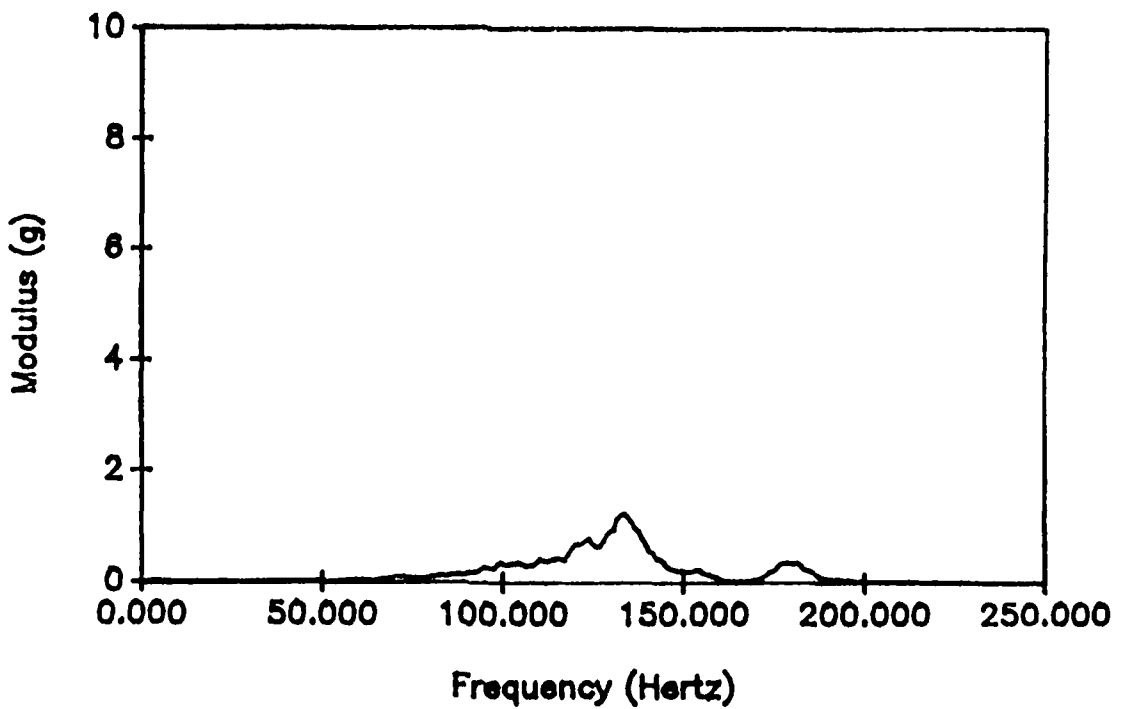


Figure A1.32. Modulus of Acceleration Record of Mass 2 for Antisymmetric Test Specimen of Test Run 3.

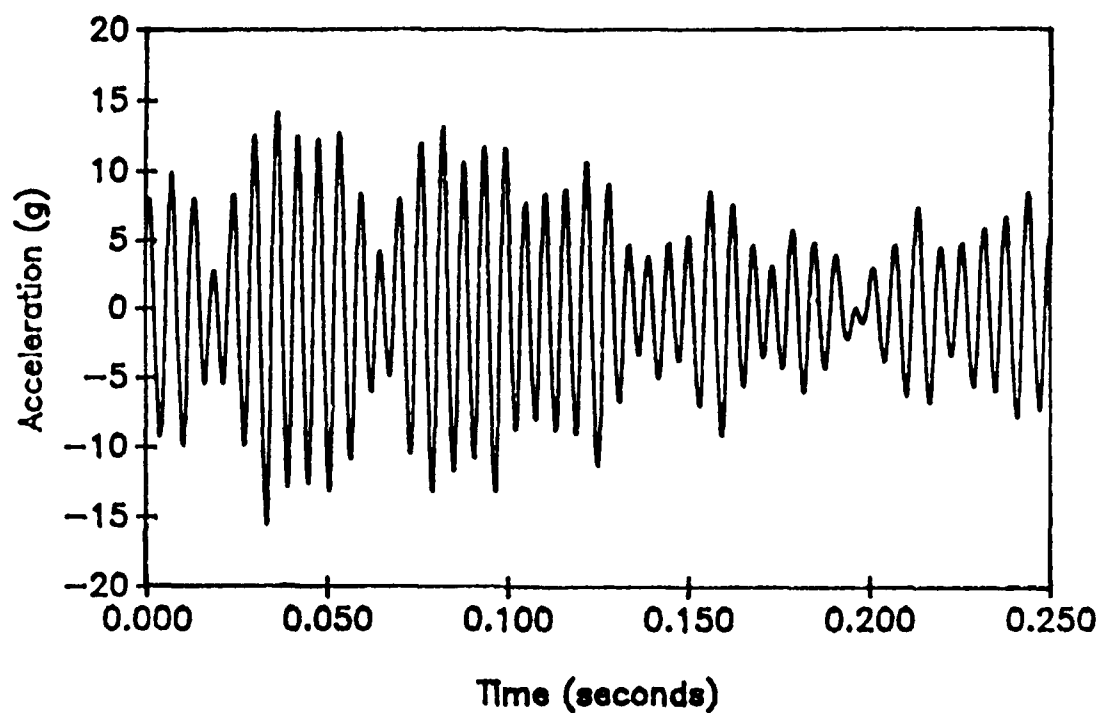


Figure A1.33. Acceleration Record of Mass 3 for Antisymmetric Test Specimen of Test Run 3.

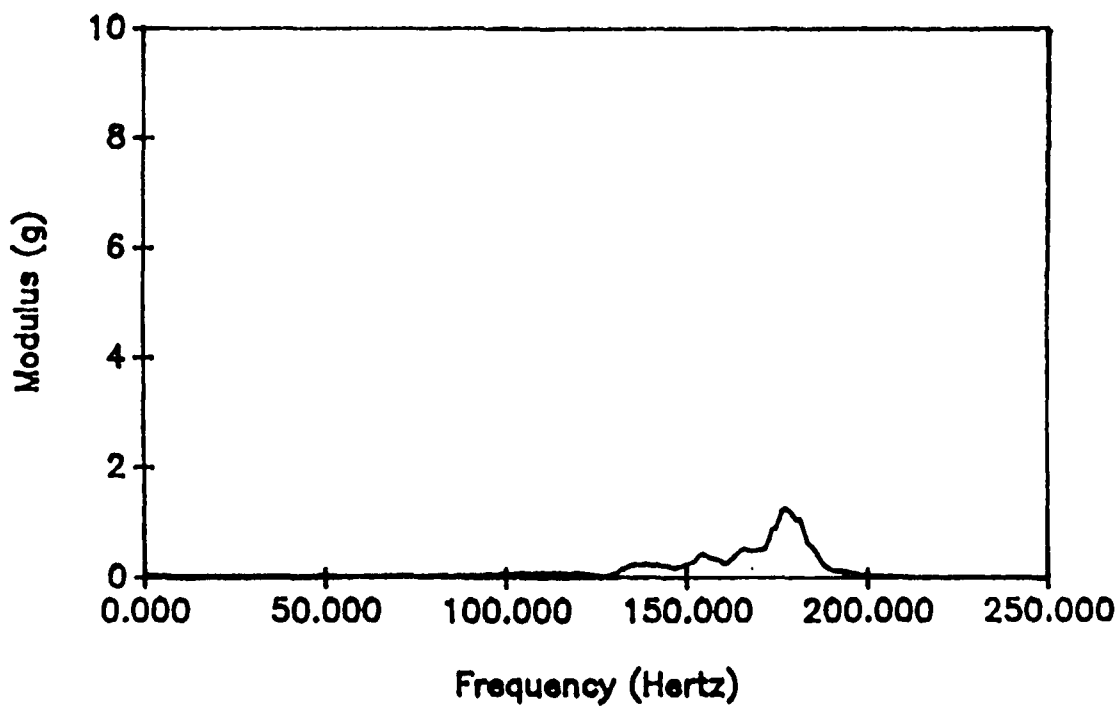


Figure A1.34. Modulus of Acceleration Record of Mass 3 for Antisymmetric Test Specimen of Test Run 3.

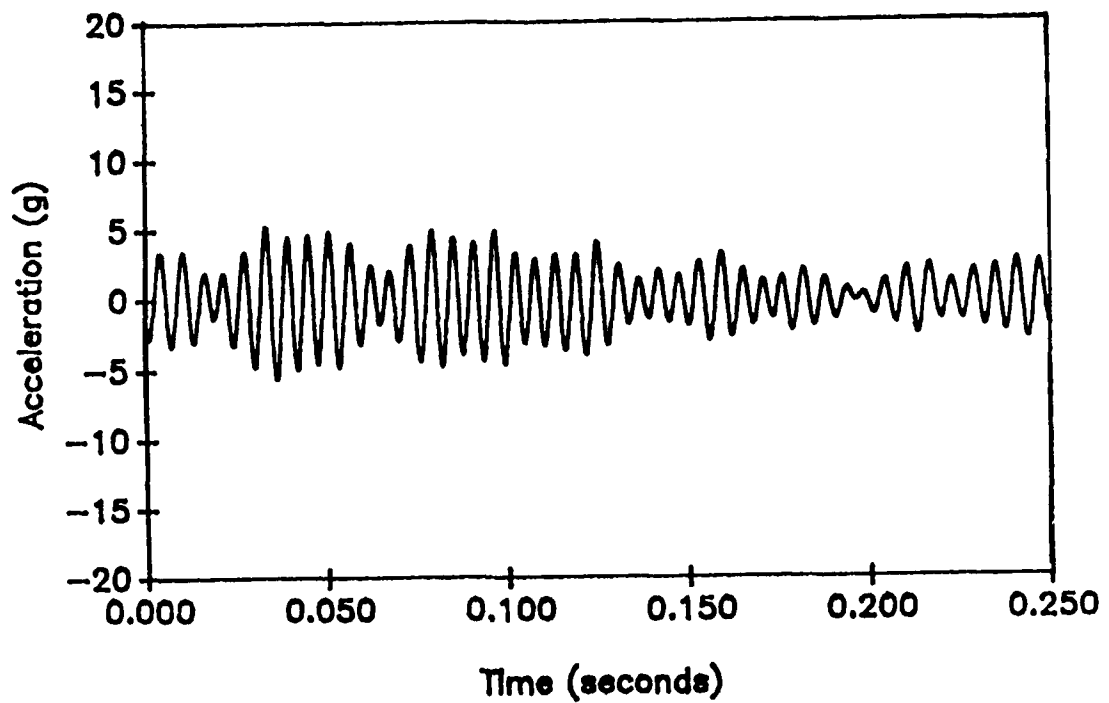


Figure A1.35. Acceleration Record of Mass 4 for Antisymmetric Test Specimen of Test Run 3.

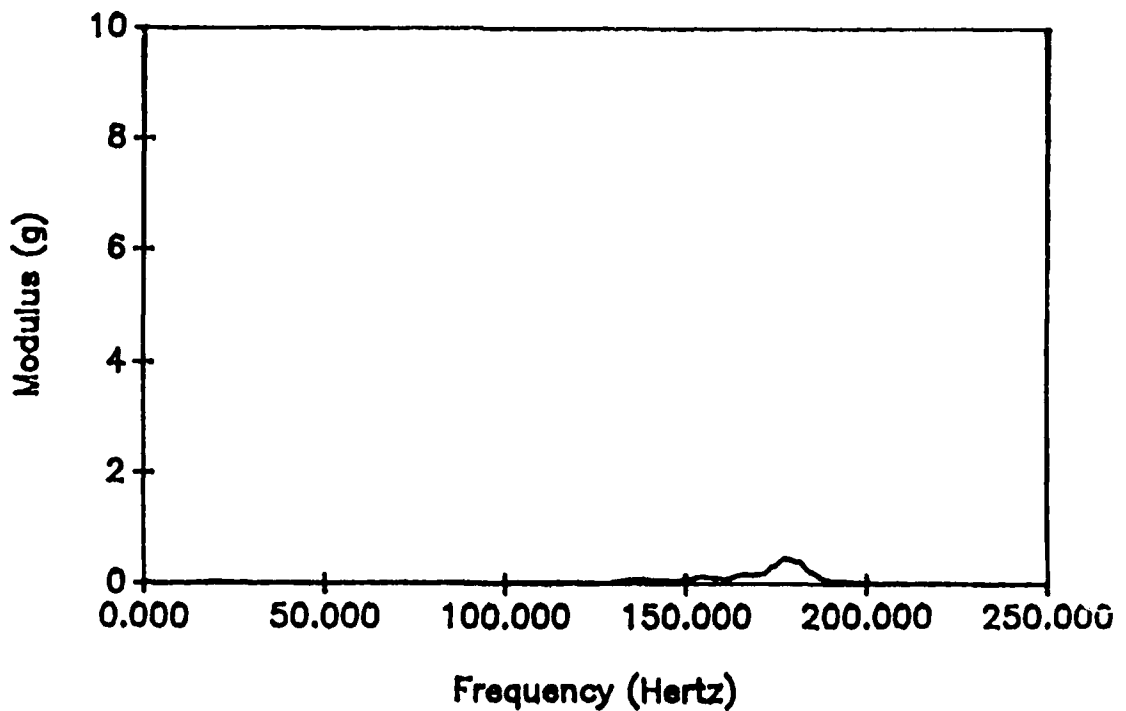


Figure A1.36. Modulus of Acceleration Record of Mass 4 for Antisymmetric Test Specimen of Test Run 3.

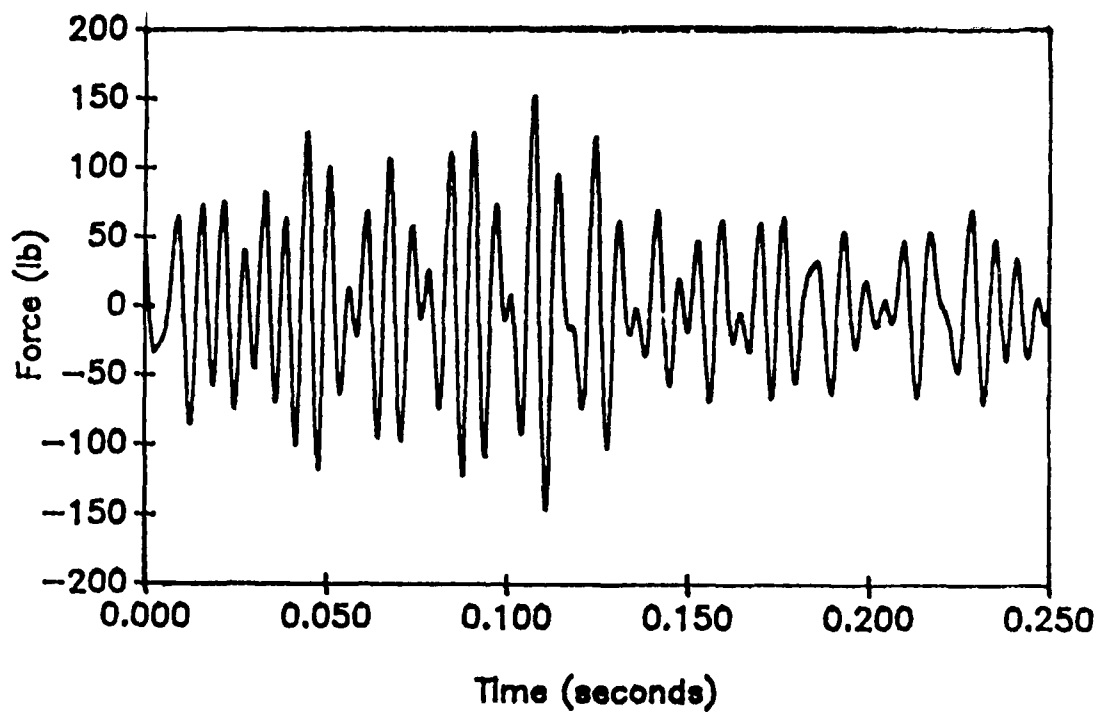


Figure A1.37. Force Record for Antisymmetric Test Specimen of Test Run 3.

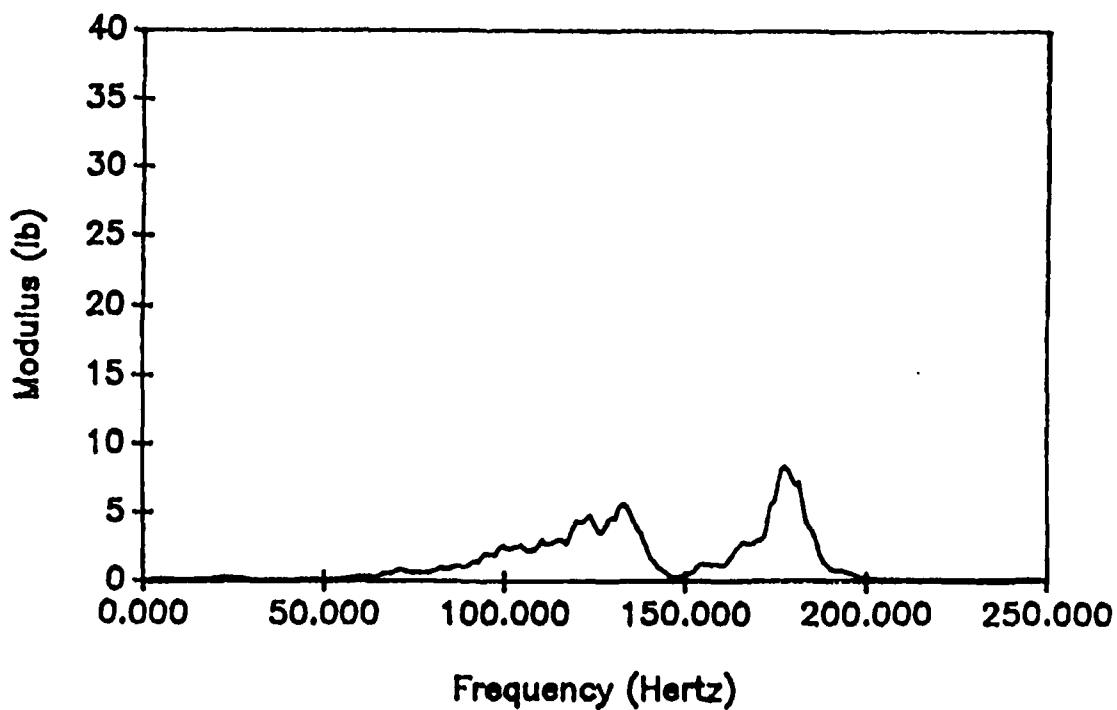


Figure A1.38. Modulus of Force Record for Antisymmetric Test Specimen of Test Run 3.

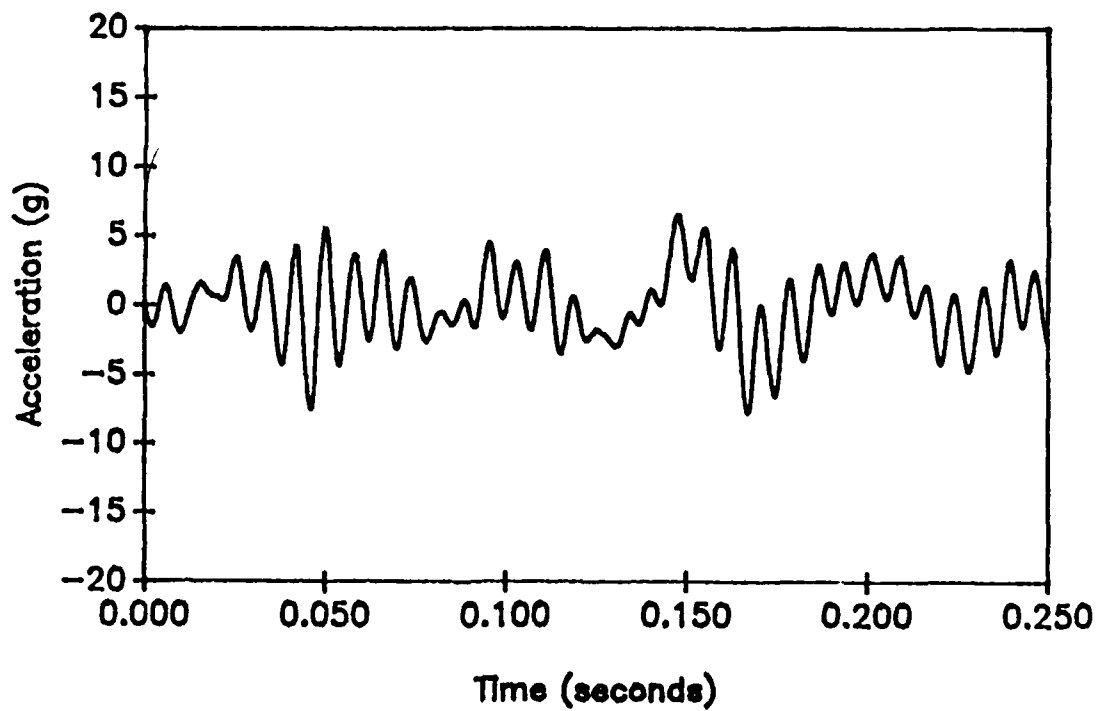


Figure A1.39. Acceleration Record of Mass 1 for Antisymmetric Test Specimen of Test Run 5.

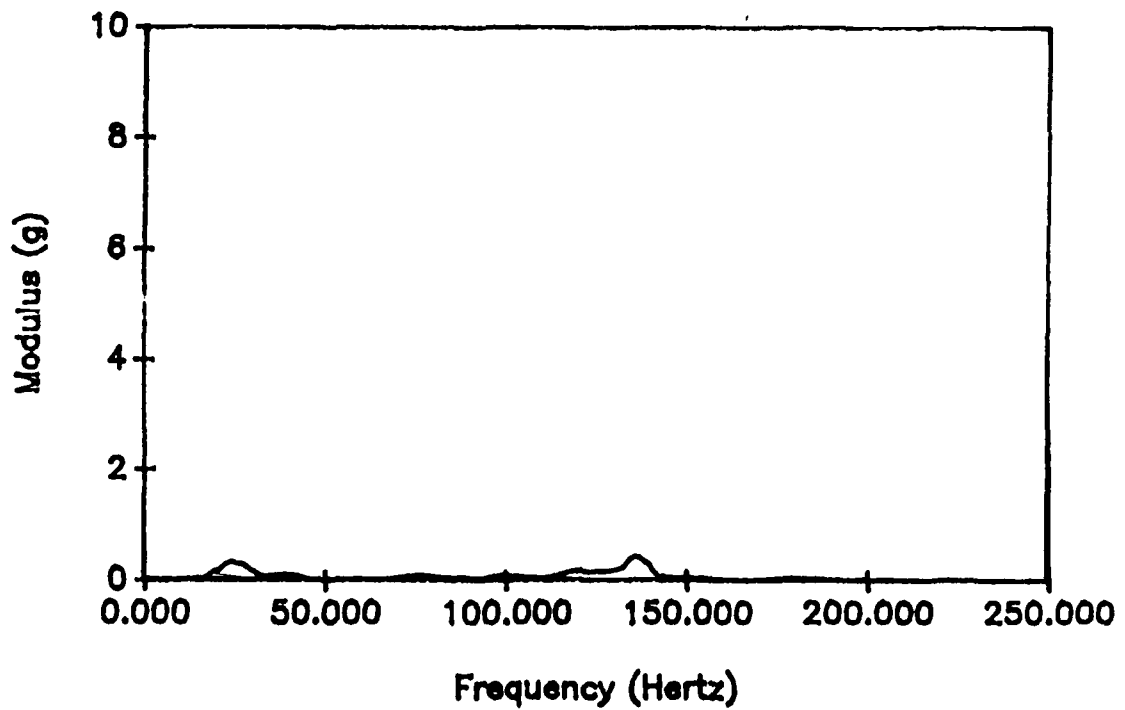


Figure A1.40. Modulus of Acceleration Record of Mass 1 for Antisymmetric Test Specimen of Test Run 5.

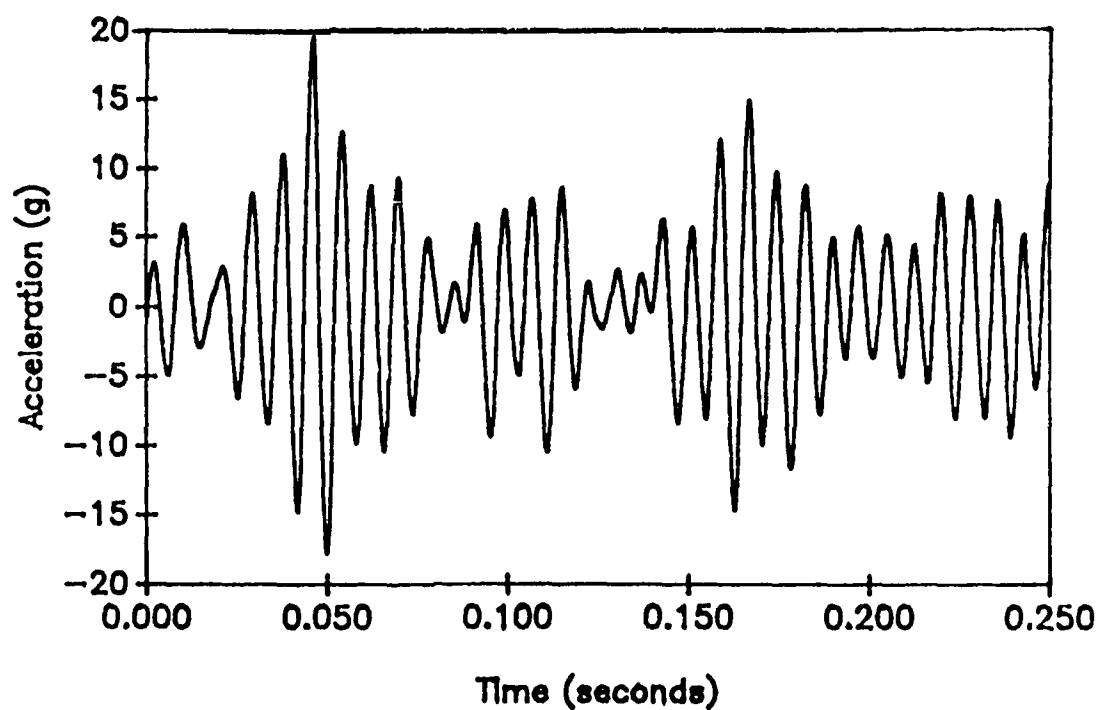


Figure A1.41. Acceleration Record of Mass 2 for Antisymmetric Test Specimen of Test Run 5.

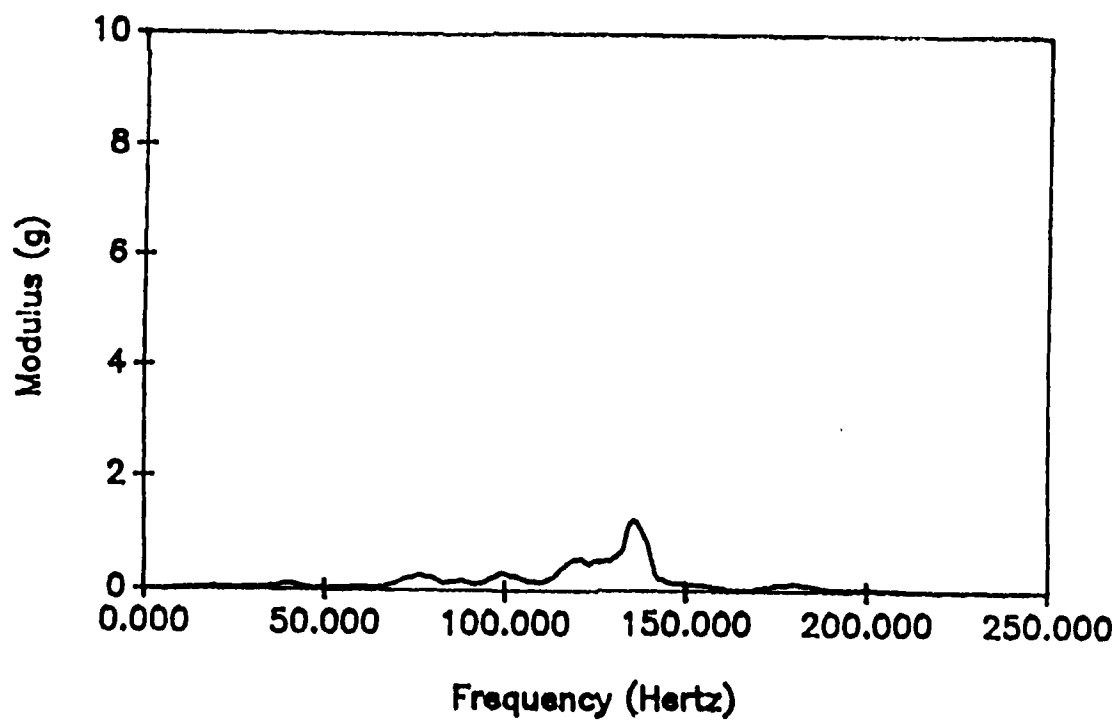


Figure A1.42. Modulus of Acceleration Record of Mass 2 for Antisymmetric Test Specimen of Test Run 5.

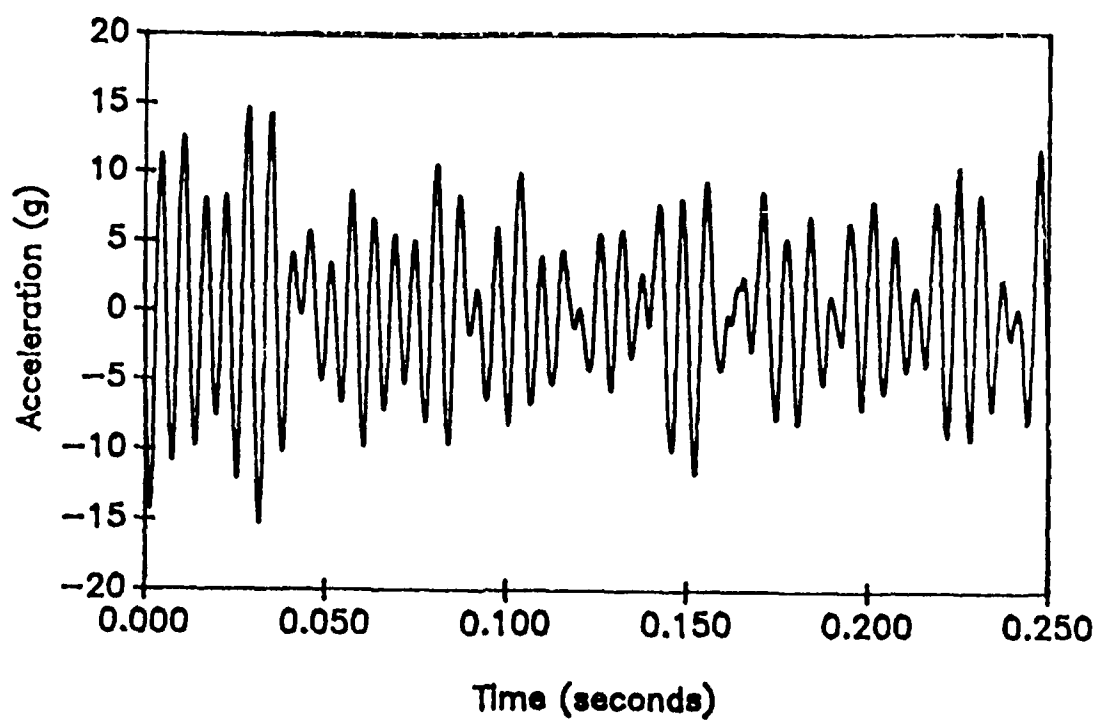


Figure A1.43. Acceleration Record of Mass 3 for Antisymmetric Test Specimen of Test Run 5.

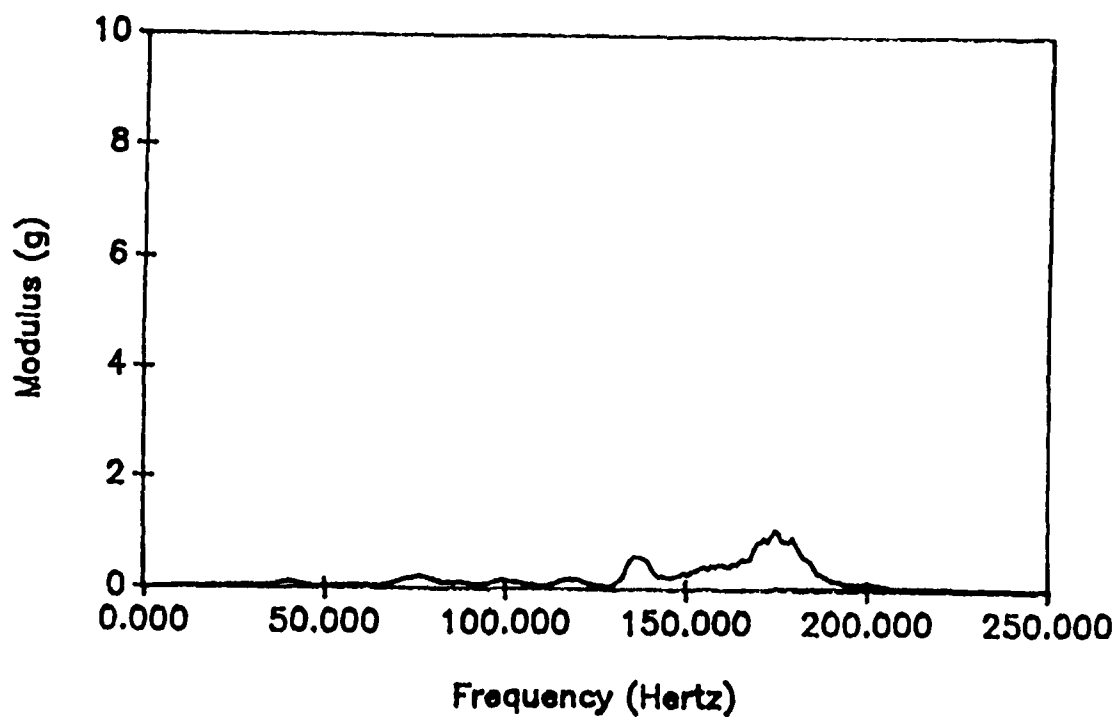


Figure A1.44. Modulus of Acceleration Record of Mass 3 for Antisymmetric Test Specimen of Test Run 5.

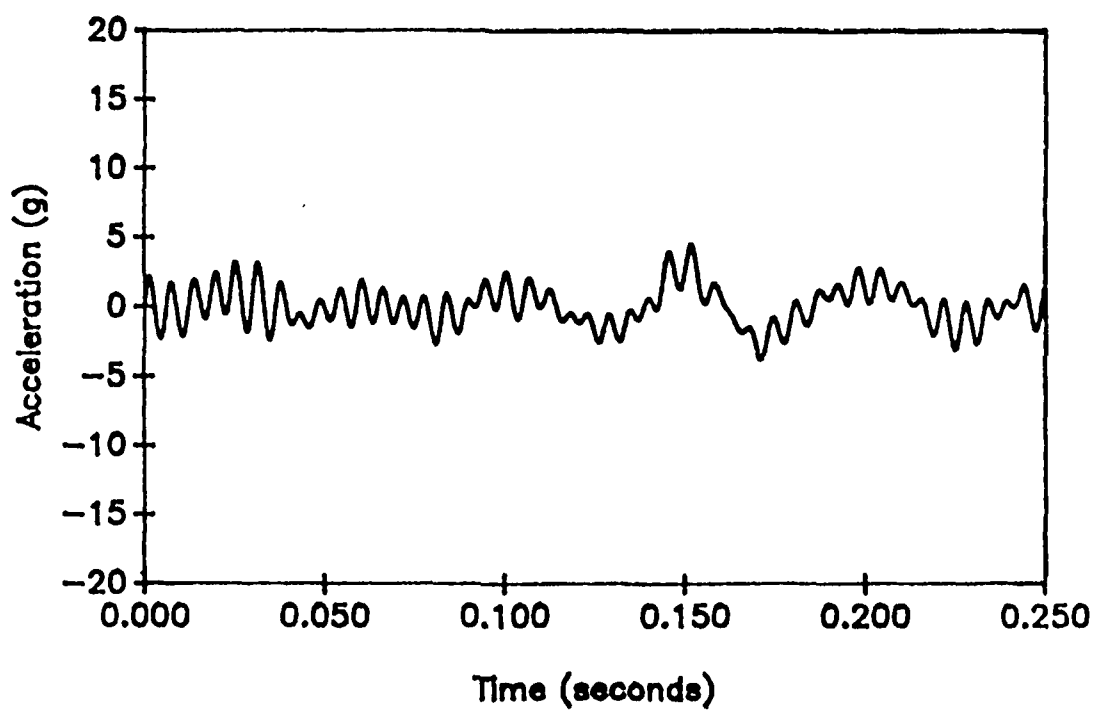


Figure A1.45. Acceleration Record of Mass 4 for Antisymmetric Test Specimen of Test Run 5.

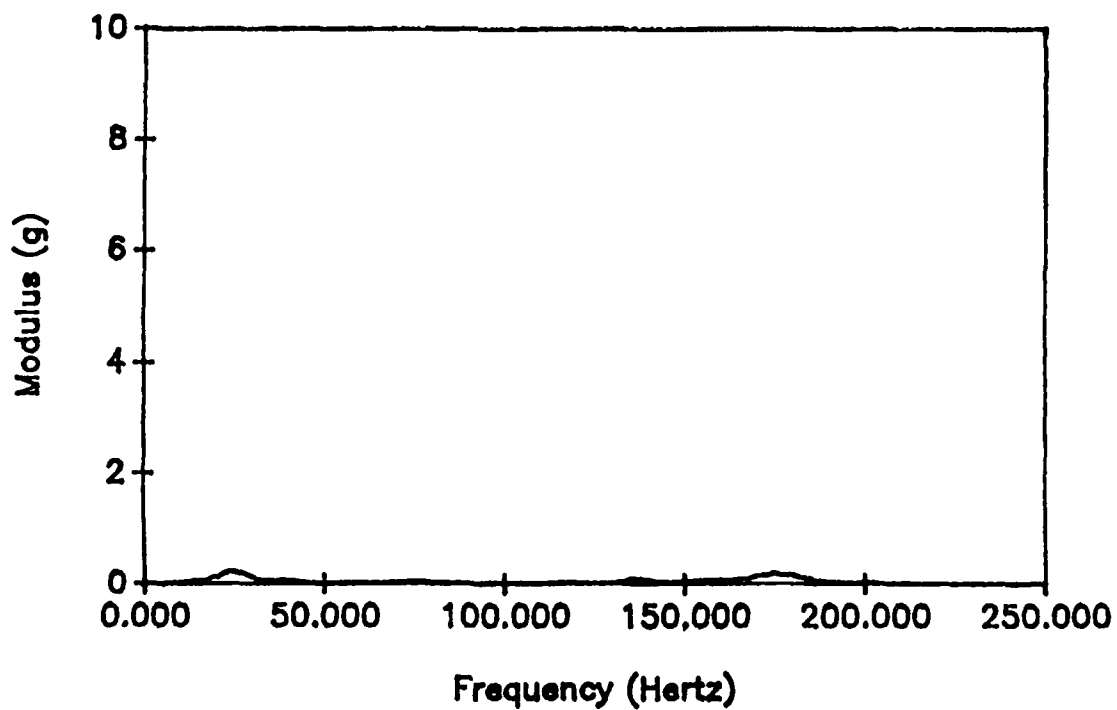


Figure A1.46. Modulus of Acceleration Record of Mass 4 for Antisymmetric Test Specimen of Test Run 5.

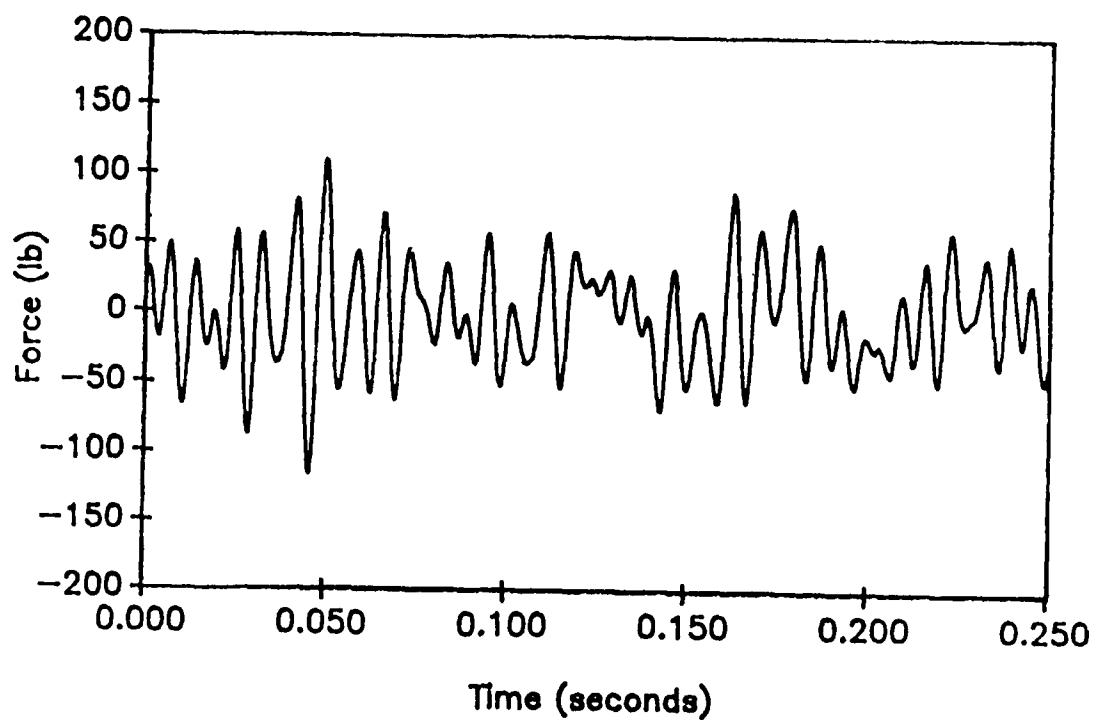


Figure A1.47. Force Record for Antisymmetric Test Specimen of Test Run 5.

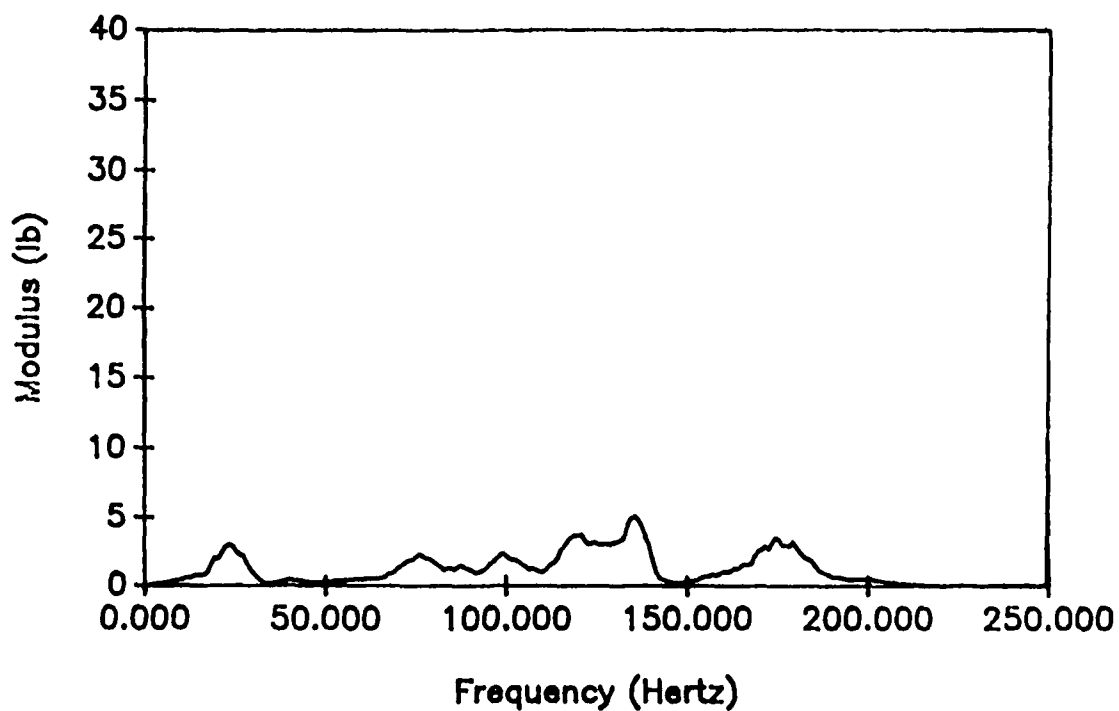


Figure A1.48. Modulus of Force Record for Antisymmetric Test Specimen of Test Run 5.

APPENDIX 2.

RECURSIVE LEAST SQUARE ALGORITHM

```

C
C THIS IS THE MAIN PROGRAM FOR TIME DOMAIN
C SYSTEM IDENTIFICATION
C
C THIS PROGRAM IS FOR 1 TO 5 PARAMETER TO IDENTIFY.
C
  REAL*8 AA(5),FS,GN(5,5),GX(5),GP(5,5)
  REAL*8 XT(5),TP(5)
  REAL*8 RS,PA(5,5),PT(5,5),ALPHA
  INTEGER ANS,L,M
  CHARACTER*10 NAME(5),NAMEF,OUTPUT,INTT
  DATA LDA /5/
C
C   SET THE DIMENSION OF THE SUBROUTINES
C
  GO TO 20
  9  WRITE (6,10)
 10  FORMAT ('*****',
1/'*****MENU*****',
1/'*****',
1/'          1.CHANGE VALUES.',
1/'          2.I.D. PARAMETERS.',
1/'          3.STOP.',
1/'  INPUT A NUMBER (1-3)',
1/'*****')
  READ (5,*) ANS
  IF (ANS.EQ.1) GOTO 20
  IF (ANS.EQ.2) GOTO 30
  IF (ANS.EQ.3) GOTO 40
  GO TO 9
 20  write(6,*)'INPUT THE NUM.OF I.D. PARAMETERS (1-5)'
  READ (5,*) L
  IF(L.LT.1.OR.L.GT.5)GOTO 20
  write(6,*)'INPUT ALPHA. (INITI.VALUE FOR PA MATRIX)'
  READ (5,*) ALPHA
  write(6,*)'INUT THE NUMBER OF POINTS TO DELETE AS BEGINNING'
  READ(5,*)ND
  write(6,*)'INPUT TOTAL PTS'
  READ (5,*) N
  write(6,*)'INPUT NAME OF AA (INITI.VECTOR FOR I.D. 10 CHAR.)'
  READ(5,21)INTT
  write(6,*)'INPUT THE FILE NAMES OF THE COLUMN OF MATRIX A'
  DO 19 I=1,L
    write(6,*)'INPUT THE FILE FOR COLUMN ',I
    READ(5,21)NAME(I)
 19  CONTINUE
 21  FORMAT (A10)
  write(6,*)'INPUT NAME OF FORCE FILE.(10 CHAR.)'
  READ (5,21) NAMEF

```

```

write(6,*)'INPUT NAME OF OUTPUT I.D.PARAMETER.(10 CHAR) '
READ (5,21) OUTPUT
C
WRITE (6,22) L,ALPHA,ND,N,INTT,(NAME(I),I=1,5),NAMEF,OUTPUT
22  FORMAT (1X,T3,'L              = ',I4,
1/,T3,'ALPHA              = ',D19.12,
1/,T3,'DELETE PTS        = ',I10,
1/,T3,'TOTAL PTS         = ',I10,
1/,T3,'INITI. VECOTRS    = ',A10,
1/,T3,'COLUMN VECTORS    = ',A10,
1/,T3,'                  = ',A10,
1/,T3,'                  = ',A10,
1/,T3,'                  = ',A10,
1/,T3,'                  = ',A10,
1/,T3,'FORCE FILE       = ',A10,
1/,T3,'I.D. PARAM.FILE = ',A10)
GO TO 9
30  CLOSE (5)
      DO 31 I=1,L
      II=6+I
      OPEN (UNIT=II,FILE=NAME(I),STATUS='OLD')
31  CONTINUE
      OPEN(UNIT=1,FILE=NAMEF,STATUS='OLD')
      OPEN (UNIT=2,FILE=OUTPUT,STATUS='NEW')
      OPEN (UNIT=3,FILE=INTT,STATUS='OLD')
      WRITE (2,22) L,ALPHA,ND,N,INTT,(NAME(I),I=1,5),NAMEF,OUTPUT
      write(6,*)'*****PROCEED``G*****'
      DO 50 I=1,L
      READ (3,*) AA(I)
50  CONTINUE
      DO 300 I=1,L
      II=6+I
      DO 300 J=1,ND
      READ(II,*)GAR
300  CONTINUE
      IF(ND.LT.1)GOTO 311
      DO 310 I=1,ND
      READ(1,*)GAR
310  CONTINUE
311  DO 60 I=1,L
      DO 60 J=1,L
      PA(I,J)=0.
60  CONTINUE
      DO 61 I=1,L
      PA(I,I)=ALPHA
61  CONTINUE
      DO 70 I=1,N
      DO 80 J=1,L
      II=6+J
      READ(II,*)XT(J)
80  CONTINUE
      CALL MULRM (LDA,XT,L,PA,L,TP)
      CALL MULRC (TP,L,XT,GA)
      GAM=1./(1.+GA)

```

```

      DO 81 J=1,L
        DO 81 K=1,L
          GN(J,K)=GAM*PA(J,K)
81      CONTINUE
        CALL MULMC (LDA,GN,L,L,XT,GX)
        CALL MULCR (LDA,GX,L,TP,GP)
        CALL MULRC (XT,L,AA,TA)
        read(1,*)fs
        DO 85 J=1,L
          AA(J)=AA(J)+GX(J)*(FS-TA)
          DO 85 K=1,L
            PA(J,K)=PA(J,K)-GP(J,K)
85      CONTINUE
95      CONTINUE
70      CONTINUE
        DO 200 J=1,L
          WRITE(2,*)AA(J)
200     CONTINUE
40      continue
      STOP
      END

```

REFERENCES

1. Åström, K. J. and P. Eykhoff, (1971). "System Identification - A Survey." *Automatica*, Vol. 7, pp. 123-162.
2. Bateman, V. I., and O. M. Solomon, Jr., (1987). "Reconstruction of Dynamic Structural Inputs in the Presence of Noise." *Proceedings of the 1987 SEM Spring Conference*, June.
3. Barker, H. ... , R. W. Davy, (1970). "2nd - Order Volterra Kernel Measurement using Pseudorandom Ternary Signals and Discrete Fourier Transform." May 1970.
4. Barrett, J. F., (1980), "Formula for Output Autocorrelation and Spectrum of a Volterra System with Stationary Gaussian Input." *IEE PROC.*, Vol. 127, Pt. D, No. 6, November.
5. Beck, James L., and Paul C. Jennings, (1980). "Structural Identification using Linear Models and Earthquake Records." *Earthquake Engineering and Structural Dynamics*, Vol. 8., 145-160.
6. Bekey, George A., (1970). "System Identification - an Introduction and a Survey", *Simulation Councils, Inc.*, Oct.
7. Bekey, G. A., and Sardis, (1982). *Identification and System Parameter Estimation*. IFAC, Pergamon Press, 1982.
8. Bendat, J. S., (1976). "System Identification from Multiple Input/Output Data." *Journal of Sound and Vibration* (1976) 49(3), 293-308.
9. Bendat, J. S. and Piersol, A. G., (1986). *Random Data: Analysis and Measurements Procedures*, 2nd Edit., Wiley-Interscience, New York.
10. Billings, S. A., (1980). "Identification of Nonlinear Systems - A Survey." *IEE Proc.*, Vol. 126, No. 5, May.
11. Bishop, R. E. D., and G. M. L. Gladwell, (1963). "An Investigation into the Theory of Resonance Testing." *Phil. Trans. of the Royal Society of London*, Vol. 255, January 1963.
12. Caravani, P., M. L. Watson, and W. T. Thomson, (1971). "Recursive Least-Squares Time Domain Identification of Structural Parameters." *Journal of Applied Mechanics*, March.
13. Caravani, P., and W. T. Thomson, (1974). "Identification of Damping Coefficients in Multidimensional Linear Systems." *Journal of Applied Mechanics*, June 1974.
14. Chung, C. and W. Sachse, (1985). "Analysis of Elastic Wave Signals from an Extended Source in a Plate." *J. Acoust. Soc. Am.*, Vol. 77, No. 4, 1985, pp. 1335-1341.

15. Chouychai, Thanu, and Tuong Vinh, (1986). "Analysis of Non-Linear Structure by Programmed Impact Testing and Higher Order Transfer Function." *Proceedings of the 4th IMAC*, Feb. 1986.
16. Collins, Jon. D., Gary C. Hart, T. K. Hasselman, and Bruce Kennedy, (1974). "Statistical Identification of Structures." *AIAA Journal*, February 1974.
17. Craig, Roy R., and Mark A. Blair, (1985). "A Generalized Multiple-Input, Multiple-Output Modal Parameter Estimation Algorithm." *AIAA Journal*, Vol. 23, No. 6, June 1985.
18. Crawley, Edward F., and Allan C. Aubert, (1986a). "Identification of Nonlinear Structural Elements by Force-State Mapping." *AIAA Journal*, Vol. 24, No. 1, January 1986.
19. Crawley, Edward F., and Kevin J. O'Donnell, (1986b). "Identification of Nonlinear System Parameters in Joints using the Force-State Mapping Technique." *AIAA Journal*, Vol. 24. No. 1. Jan 1986.
20. Distefano, Nestor, and Amitav Rath, (1975). "System Identification in Nonlinear Structural Seismic Dynamics." *Computer Methods in Applied Mechanics and Engineering*, 5 (1975) 353-372.
21. Distefano, Nestor, and Bonifacio Pena-Pardo, (1976). "System Identification of Frames under Seismic Loads." *Journal of the Engineering Mechanics Division*, ASCE Vol. 102, EM2, April 1976.
22. Doyle, J. F., (1984a). "An Experimental Method for Determining the Dynamic Contact Law." *Experimental Mechanics*, March 1984.
23. Doyle, J. F., (1984b). "Further Developments in Determining the Dynamic Contact Law." *Experimental Mechanics*, December 1984.
24. Doyle, James F., (1987). "An Experimental Method for Determining the Location and Time of Initiation of an Unknown Dispersing Pulse." *Experimental Mechanics*, September 1987.
25. Elliott, K. B., J. N. Juang, and J. Robinson, (1988). "Force Prediction using Singular-Value Decomposition." *Proceedings of the 6th IMAC*, Kissimmee, Florida, 1988.
26. Ewins, D. J., (1984). *Modal Testing: Theory and Practice*, Research Studies Press Ltd., 1984.
27. Eykoff, P., (1974). *System Identification - Parameter and State Estimation*, John Wiley and Sons, Inc., New York, 1974.
28. Eykhoff, Pieter, (1981). *Trends and Progress in System Identification*. IFAC, Pergamon Press, 1981.

29. Fabunmi, James A., (1985). "Modal Constraints on Structural Dynamic Force Determination." *Journal of the American Helicopter Society*, October 1985.
30. Fabunmi, J. A., (1986). "Effects of Structural Modes on Vibratory Force Determination by the Pseudoinverse Technique." *AIAA Journal*, Vol. 24, Number 3, March 1986.
31. Fabunmi, James A., (1987). "Feasibility of Dynamic Load Determination from Measured Mobilities." *Proceedings of the 1987 SEM Spring Conference*, June.
32. Fakhouri, S. Y., (1980). "Identification of the Volterra Kernels of Nonlinear Systems." *IEE PROC.*, Vol. 127, Pt. D, No. 6, November.
33. Gersch, W., N. N. Nielsen, and H. Alaike, (1973). "Maximum Likelihood Estimation of Structural Parameters from Random Vibration Data." *Journal of Sound and Vibration* (1973) 31(3), 295-308.
34. Gersch W., (1974a). "On the Achievable Accuracy of Structural System Parameter Estimates." *Journal of Sound and Vibration*, (1974) 34(1), 63-79.
35. Gersch, Will, and Douglas Foutch, (1974b). "Least Squares Estimates of Structural System Parameters Using Covariance Function Data." *IEEE Transactions on Automatic Control*, Vol. AC-19, No. 6, December 1974.
36. Gregory, Dan, Ron Coleman and Tom Priddy, (1985). "Measurement of Dynamic Forces Acting on Non-Rigid Bodies," Vibration Test Division 7542, Sandia National Laboratories, Albuquerque, NM.
37. Gregory, D. L., T. G. Priddy, and D. O. Smallwood, (1986). "Experimental Determination of the Dynamic Forces Acting on Non-Rigid Bodies," *SAE Technical Paper* 861791, Aerospace Technology Conference, Long Beach, CA.
38. Hanson, Richard J., (1986). "Linear Least Squares with Bounds and Linear Constraints." *Siam J. Sci. Stat. Comput.*, Vol. 7, No. 3, July.
39. Hart, Gary C., and J. T. P. Yao, (1977). "System Identification in Structural Dyamics." *Journal of Engineering Mechanics Division*, Vol. 103, No. EM6, ASCE pp. 1089-1104.
40. Hillary, B., and D. J. Ewins, (1984). "The Use of Strain Gauges in Force Determination and Frequency Response Function Measurements." *Proceedings of the 2th IMAC, Orlando, Florida, 1984.*

41. Hu, Yuxian, (1980). "Input Identification from Structural Vibration Response." Report No. UCB/EERC-80/26, Earthquake Engineering Research Center, University of California, Berkeley, 1980.
42. Hunter, Norman F., and Thomas L. Paez, (1988). "Experimental Identification of Nonlinear Structural Models." Proceedings of the 6th IMAC, Kissimmee, Florida, 1988.
43. Hsia, T. C., (1977). *System Identification, Least - Square Methods*. D. C. Heath and Company.
44. Ibáñez, P., (1973). "Identification of Dynamic Parameters of Linear and Non-Linear Structural Models from Experimental Data." *Nuclear Engineering and Design* 25. 30-41.
45. Ibáñez, P., (1974). "Methods for the Identification of Dynamic Parameters of Mathematical Structural Models from Experimental Data." *Nuclear Engineering and Design* 27. 209-219.
46. Imregun, M., and D. J. Ewins, (1987). "An Investigation into the Equivalent Force Determination from Structural Response." Proceedings of the 1987 SEM Spring Conference. June.
47. Jordan, R. W. and G. S. Whitson, (1984). "Remote Impact Analysis by Use of Propagated Acceleration Signals, II: Comparison between Theory and Experiment." *J. Sound and Vibration*, Vol. 97, No. 1, 1984, pp. 53-63.
48. Juang, Jer-Nan and R. S. Pappa, (1987). "A Comparative Overview of Modal Testing and System Identification for Control of Structure", *Proceedings of the 1987 SEM Spring Conference*, June.
49. Kennedy, Charles C., and C.D. P. Pancu, (1947). "Use of Vectors in Vibration Measurement and Analysis." *Journal of the Aeronautical Sciences*, Vol. 14, No. 11, November 1947.
50. Kozin, F., and H. G. Natike, (1986). "System Identification Techniques." *Structural Safety*, 3, 269-316. Elsevier Science Publisher B. V., Amsterdam.
51. Kreitinger, Timothy J., and Ming L. Wang, (1988). "Force Identification from Nonlinear Structure Response." Proceedings of the 6th International Modal Analysis Conference, Kissimmee, Florida.
52. Lawrence, P. J., (1981). "Estimation of the Volterra Functional Series of a Nonlinear System using Frequency-Response Data." *IEE PROC.*, Vol. 128, Pt. D, No. 5, Sept.
53. Ljung, Lennart, and Keith Glover, (1981). "Frequency Domain Versus Time Domain Methods in System Identification." *Automatica*, Vol. 17, No. 1, 71-86.

54. Luk, Y. W., and L. D. Mitchell, (1983). "System Identification via Modal Analysis." *AMD-Vol. 59*, ASME, November 1983.
55. Maine, Richard E. and Kenneth W. Iliff, (1981). "Formulation and Implementation of a Practical Algorithm for Parameter Estimation with Process and Measurement Noise." *SIAM J. Appl. Math.*, Vol 41, No. 3, Dec.
56. Masri, S. F., G. A. Bekey, H. Sassi, and T. K. Caughey, (1982). "Non-Parametric Identification of a Class of Non-Linear Multidegree Dynamic Systems." *Earthquake Engineering and Structural Dynamics*, Vol. 10, 1-30.
57. McVerry, Graeme H., (1980). "Structural Identification in the Frequency Domain from Earthquake Records." *Earthquake Engineering and Structural Dynamics*, Vol. 8, 161-180.
58. Mertens, M., H. Van der Auweraer, P. Vanherck, and R. Snoeys, (1986). "Detection of Nonlinear Dynamic Behaviour of Mechanical Structures." *Proceedings of the 4th IMAC*, Los Angeles, CA, 1986.
59. Michaels, J. E., and Pao, Y. H., (1985). "The Inverse Source Problem for an Oblique Force on an Elastic Plate." *J. Acoust. Soc. Am.*, Vol. 77, No. 6, 1985, pp. 2005-2011.
60. Michaels, J. E., and Pao, Y. H., (1986). "Determination of Dynamic Forces from Wave Motion Measurements." *J. Applied Mechanics*, March 1986, pp. 61-68.
61. Mitchell, L. D., (1982). "Improved Methods for the Fast Fourier Transform (FFT) Calculation of the Frequency Response Function," *Trans. ASME, J. Mech. Des.*, 104, 277-279 April.
62. Natke, H. G., (1987). "Input and Damping Identification within the Frequency Domain." *Journal of Modal Analysis*, April 1987.
63. Natke, H. G., J. N. Juang, and W. Gaawronski, (1988). "A Brief Review on the Identification of Nonlinear Mechanical Systems." *Proceedings of the 6th IMAC*, Kissimmee, Florida, 1988.
64. Newland, D. E., (1976). *An Introduction to Random Vibration And Spectral Analysis*, Longman Publishing, 1976.
65. Paez, Thomas L., Ming-Liang Wang, and Frederick D. Ju, (1982). "Diagnosis of Damage in SDF Structures." *The Bureau of Engineering Research*, The University of New Mexico, Albuquerque, NM, March 1982.
66. Paez, Thomas L., (1987). "Nonlinear Structural System Modelling." *28th Structures, Structural Dynamics, and Materials Conference*, Monterey, CA, April 1987.

67. Priddy, Tom G., Dan L. Gregory, and Ron G. Coleman, (1988). "Strategic Placement of Accelerometers to Measure Forces by the Sum of Weighted Accelerations." *Proceedings of the 6th International Modal Analysis Conference*, Kissimmee, Florida.
68. Rodeman, R. and J. T. P. Yao, (1973). "Structural Identification Literature Review", *Report CE-STR-73-3*, Purdue University, December.
69. Simonian, S. S., (1981a). "Inverse Problems in Structural Dynamics - I. Theory." *Inter. Journal for Numerical Methods In Engineering*.17 357-365.
70. Simonian, S. S., (1981b). "Inverse Problems in Structural Dynamics - II. Applications." *Inter. Journal for Numerical Methods In Engineering*.17 367-386.
71. Singh, Y. P., and S. Subramanian, (1980). "Frequency-Response Identification of Structure of Nonlinear Systems." *IEE Proceedings*, Vol. 127, Pt. D, No. 3, May 1980
72. Shinozuka, M., C. B. Yun, and H. Imani, (1982). "Identification of Linear Structural Dynamic Systems." *J. Eng. Mechanics*, Proc. ASCE, Vol. 108, No. EM6, 1982, pp. 1371-1390.
73. Smallwood, D. O. and D. L. Gregory, "Experimental Determination of the Mass Matrix Using a Constrained Least Squares Solution," *AIAA, 28th SDM Conference Paper*, 1987.
74. Stephens, Jerry E., and James T. P. Yao, (1985). "Data Processing of Earthquake Acceleration Records." *Report CE-STR-85-5*, Purdue University.
75. Stevens, K. K., (1987). "Force Identification Problems-An Overview", *Proceedings of the 1987 Sem Spring Conference*, June.
76. Subbayyan, R., and R. Nagarajan, (1978). "A Discrete-Time Identification Algorithm with an Improved Convergence." *IEEE Transaction on Automatic Control*, Vol. AC-23, No. 4, August 1978.
77. Tomlinson, G. R., (1986). "Detection, Identification and Quantification of Nonlinearity in Modal Analysis - A Review." *Proceedings of the 4th IMAC*, Union College, Feb.
78. Trujillo, D. M., (1978). "Application of Dynamic Programming to the General Inverse Problem." *International Journal for Numerical Methods in Engineering*, Vol. 12, 613-624.
79. Trujillo, D. M., and A. L. Carter, (1982). "A New Approach to the Integration of Accelerometer Data", *Earthquake Engineering and Structural Dynamics*, Vol. 10. 1982.

80. Wang, Ming-Liang, Paez, Thomas L., and Frederick D. Ju, (1982). "Mathematical Models for Damageable Structures." The Bureau of Engineering Research, Technical Report CE-64(83)AFOSR-993-1, The University of New Mexico, Albuquerque, NM, March 1982.
81. Wang, Ming-Liang, Thomas L. Paez, and Frederick D. Ju, (1983). "Identification of Damage in Hysteretic Structures." The Bureau of Engineering Research, Report No. CE-72(84) AFOSR-933-1, The University of New Mexico, Albuquerque, NM, March 1982.
82. Wang, M. L., T. L. Paez, and F. D. Ju, (1983). "Models for Damage Diagnosis in SDF Structures." *Proceedings of the Symposium on the Interaction of Non-Nuclear Munitions with Structures*, pp. 159-165, Colorado Springs, Col 1983.
83. Wang, M. L., T. J. Kreitinger, and H. L. Luo, (1987). "Force Identification from Structural Responses", *Proceedings of the 1987 SEM Spring Conference on Experimental Mechanics*, Houston, Texas.
84. Wellstead, Peter E., (1981). "Non-Parametric Methods of System Identification." *Automatica*, Vol. 17, No. 1, pp. 55-69, 1981.
85. Whitson, G. S., (1984). "Remote Impact Analysis by Use of Propagated Acceleration Signals, I: Theoretical Methods." *J. Sound and Vibration*, Vol. 97, No. 1, 1984, pp. 35-51.
86. Yoshikawa, Tsuneo, and Toshiharu Sugie, (1981). "Inverse Systems for Reproducing Linear Functions of Inputs." *Automatica*, Vol. 17, No. 5, pp. 763-769, 1981.

VITA

Timothy J. Kreitinger [REDACTED] North Dakota

[REDACTED] He attended grade and high school in North Dakota. He obtained a Bachelor of Science degree in Civil Engineering from North Dakota State University in 1980. From 1980 to 1984, he worked for the United States Air Force. He attended the University of New Mexico from 1984 to the present. He received a Master of Science degree in Civil Engineering in 1986. He is sponsored by the United States Air Force to work toward a Ph. D. degree in Structural Engineering.